

# TURBULENCE, FLOWS AND MAGNETIC FIELD GENERATION IN PLASMAS USING A MAGNETOHYDRODYNAMIC MODEL

*By*

RUPAK MUKHERJEE

PHYS06201404004

Institute for Plasma Research, Gandhinagar

*A thesis submitted to the*

*Board of Studies in Physical Sciences*

*In partial fulfillment of requirements*

*for the Degree of*

DOCTOR OF PHILOSOPHY

*of*

HOMI BHABHA NATIONAL INSTITUTE



June, 2019

# Homi Bhabha National Institute

## Recommendations of the Viva Voce Committee

As members of the Viva Voce Committee, we certify that we have read the dissertation prepared by **Rupak Mukherjee** entitled "TURBULENCE, FLOWS AND MAGNETIC FIELD GENERATION IN PLASMAS USING A MAGNETOHYDRODYNAMIC MODEL" and recommend that it may be accepted as fulfilling the dissertation requirement for the award of Degree of Doctor of Philosophy.

Abhijit Date: 18/09/2019  
Chairman - Prof. Abhijit Sen

Rajaraman Date: 18/09/2019  
Guide/Convener - Prof. Rajaraman Ganesh

Arnab Rai Choudhuri Date: 18/09/2019  
Examiner - Prof. Arnab Rai Choudhuri

R Date: 18/09/2019  
Member - Prof. Radhakrishnan Srinivasan

Daniel Date: 18/09/2019  
Member - Dr. Daniel Raju

Final approval and acceptance of this dissertation is contingent upon the candidate's submission of the final copies of the thesis to HBNI.

I hereby certify that I have read this dissertation prepared under my direction and recommend that it may be accepted as fulfilling the thesis requirement.

Date: 18/09/2019

Place: Grandhinagar, Gujarat

Rajaraman  
Prof Rajaraman Ganesh

Guide

## STATEMENT BY AUTHOR

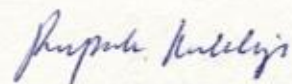
This dissertation has been submitted in partial fulfillment of requirements for an advanced degree at Homi Bhabha National Institute (HBNI) and is deposited in the Library to be made available to borrowers under rules of the HBNI.

Brief quotations from this dissertation are allowable without special permission, provided that accurate acknowledgement of source is made. Requests for permission for extended quotation from or reproduction of this manuscript in whole or in part may be granted by the Competent Authority of HBNI when in his or her judgement the proposed use of the material is in the interests of scholarship. In all other instances, however, permission must be obtained from the author.

  
Rupak Mukherjee

## DECLARATION

I, hereby declare that the investigation presented in the thesis has been carried out by me. The work is original and has not been submitted earlier as a whole or in part for a degree / diploma at this or any other Institution / University.



Rupak Mukherjee



## List of publications arising from the Thesis

1. *Recurrence in three dimensional magnetohydrodynamic plasma*  
Rupak Mukherjee, Rajaraman Ganesh and Abhijit Sen  
*Physics of Plasmas*, **26**, 022101, (2019)
2. *Coherent nonlinear oscillations in magnetohydrodynamic plasma*  
Rupak Mukherjee, Rajaraman Ganesh and Abhijit Sen  
*Physics of Plasmas* **26**, 042121, (2019)
3. *Three Dimensional Pseudo-Spectral Compressible Magnetohydrodynamic GPU Code for Astrophysical Plasma Simulation*  
Rupak Mukherjee, Rajaraman Ganesh, Vinod Saini, Udaya Maurya, Nagavi-jayalakshmi Vydyanathan, Bharatkumar Sharma  
*IEEE Conference Proceedings of 25th International Conference on High Performance Computing Workshops (HiPCW)*, (2018)
4. *Numerical relaxation of a 3D MHD Taylor - Woltjer state subject to abrupt expansion*  
Rupak Mukherjee and Rajaraman Ganesh  
*Conference Proceedings of 27th IAEA Fusion Energy Conference*, 476, (2018)
5. *Study of dynamo action in three dimensional magnetohydrodynamic plasma with Arnold-Beltrami-Childress flow*  
Rupak Mukherjee, Rajaraman Ganesh and Abhijit Sen  
Manuscript under preparation, arXiv: 1901.09610

  
Rupak Mukherjee

## DEDICATIONS

*To my parents and teachers.*

## ACKNOWLEDGEMENTS

*'I have had my invitation to this world's festival, and thus my life has been blessed.  
My eyes have seen and my ears have heard.*

*It was my part at this feast to play upon my instrument, and I have done all I  
could.*

*Now, I ask, has the time come at last when I may go in and see thy face and offer  
thee my silent salutation?'*

*- Song Offerings (Gitanjali), Rabindranath Tagore.*

At the very outset, I convey my deepest regards to my parents Mr. Dipak Kumar Mukherjee and Mrs. Rupali Mukherjee to allow me to pursue my dream in general Science (specifically in Mathematics and Physics) when all my 'true' well-wishers wanted me to be an Engineer or a Doctor after my '*brilliant performance*' (read as *high percentage of marks*) in school. Had my parents had not given me the chance to risk my future (and so theirs), I would have never been able to write this acknowledgement of my PhD Thesis. The temperament I cherish in my heart, mostly took birth from the music I learnt to listen from my father - my favourite - Rabindra-sangeet and the story books of world literature my father used to bring for me when I was in school. These weaved the utopian dreams within me that dragged me into this life.

Talking about my PhD tenure, I am endlessly grateful to my thesis supervisor (read as - *guru* and not *boss*) Ganesh (Prof. Rajaraman Ganesh)! His friendly and spirited support and guidance from the initial phase of work (which was completely different from my today's Thesis) until this day of writing my Thesis have been the source of inspiration for me. I am thankful to him for providing me the incredible independence in my work (read as - *switching between completely different fields*), which went a long way in arriving at this shape. The care and the way in which he nurtured (read as - *brainwashed!*) me during the long journey - turning me from a purely analytically oriented student to a computational physicist - I will never forget. The discussions at literally any time of the day however busy he was in his administrative duties, were always inspiring and motivating. I have learnt countless things from him apart from the obvious plasma physics and numerical techniques - for example how to read a scientific paper, how to present a work to the community and how to remain calm in untoward situations. I would like to thank him for his

incessant encouragement when everything went against me and for being patient with me throughout those periods when I was absolutely unproductive for a very long time during the development of my code. His assiduous carefulness at all times from the initial simulation days in his W-6 office to writing research articles and this thesis, has been a great teaching tool.

I gratefully acknowledge *Sen Sir* (Prof. Abhijit Sen), my Chairman Doctoral Committee / my friend philosopher and (*if not*) guide, who has a significant contribution into this thesis. By his careful analysis of my numerical results, he enlightened me about ‘how to look at a problem’. He taught me deciphering the physics from my simulation data, giving talks and seminars, writing papers and how to be truthful and correct in scientific statements. Besides the discussion about the PhD project, he taught me various concepts of nonlinear dynamics and plasma physics. Discussion with him always stretched the horizon of my knowledge and I could feel the broader spectrum of the subject. All of these together, gradually turned me from a student to a researcher.

I am obliged to Dr. Radhakrishnan Srinivasan and Dr. Daniel Raju for consenting to be my Doctoral Committee members. It was a privilege to have them in the committee. The insightful comments and content recommendation from my Doctoral Committee in my yearly reviews helped me to finish my PhD in time.

I would like to thank Prof. Sudip Sengupta, Dr. Mrityunjay Kundu, Dr. Ashwin Joy, Dr. Devendra Sharma, Dr. Santanu Karkari, Dr. Joydeep Ghosh, Dr. Prabal Chattopadhyay and staff at FCIPT & VIDHATA for their endurance while teaching us during the first year course work. Prof. Subroto Mukherjee, Prof. Sudip Sengupta, Dr. Mainak Bandyopadhyay, and Dr. Pintu Bandyopadhyay have been of continuous support and advice in Academic affairs.

I would also take the opportunity to thank Mr. Udaya Maurya and Mr. Vinod Saini for their numerous help during the tough periods in my numerical work as well as the difficult moments of my life. The thesis would have been incomplete without the help from Dr. Naga Vijayalakshmi Vydyanathan, Dr. Shivakumar Malapaka and Dr. Samriddhi Shankar Ray, in various aspects of parallel computing architectures and computer algorithms. My simulation runs would never be finished without the help from Deepak, Hemant-ji, Arvind-ji and Prashant-ji from Computer center.

The library staff, computer centre staff and administrative staff of IPR, have always remained cooperative. I convey my thanks to Mr. Arvind M Singh, Mr. Hemant Joshi, Mr. Deepak Aggarwal, Mr. Gaurav Garg, Mr. Prashant Kumar, Mr. Govind



Lokhande, Mr. Sharad Jash, Mr. Saroj Das, Mr. Shravan Kumar, Ms. Smita Parmar, Mrs. Shilpa Khandker, Mr. H.C. Khanduri, Mr. Pinakin Devluk, Mr. Aditya Panchasara, Mr. Hitesh Mehta, Mr. Dinesh Nair, Mr. M H Vartak, Mr. H. C. Chamunde, Mr. Silel Shah, Ms. Shirin Bhesania for their help and advice on numerous occasions. I thank Joydeep sir, Mani sir, Mr. H. C. Chamunde, Mr. M. H. Vartak, Soumen and Harshita who made my additional responsibility of student representative quite easy.

The stay in IPR Hostel was made eventful and pleasant by the welcoming team of seniors - Maya, Vikrant, Rameswar, Gurudatt, Sayak, Manjit, Soumen, Roopendra, Bhishu, Niraj, Akanksha, Vidhi, Harish, Sonu, Meghraj, Arghya, Debraj, Umesh, Surabhi, Bhumika, Narayan, Ratan, Sagar, Jervis, Alam, Prabhakar, Atul, Sandeep, Pallavi, Meenakshee, Harshita and others and fellow students - Avnish, Shivam, Jana (Subrata), Arun, Gaurav, Tirthendu and Anirban. My two batchmates, Jana (Subrata) and Arun were of really great support for me when I had hard times, through their advices and numerous help. The hostel life was made cheerful by the juniors - Srimanta, Neeraj, Arnab, Piyush, Debrup, Garima, Dipshikha, Priti, Chinmoy, Rohit, Hari, Satadal, Nidhi, Ayushi, Devshree, Pawandeep, Swapnali, Soumen, Sanjeev, Jagannath, Prince, Shishir, Suman, Anjan, Rosh and others. I am sincerely grateful to my colleagues with whom I shared the office place for a very long time. Paras, Nitin, Rajanikant, Chinmoy, Arnab, Akanksha, Bibhu in Admin Annex office and Pawandeep, Nidhi, Devshree, Ayushi, Vidhi, Avnish, Satadal, Jay and Prince in FF-13 office gifted me a quiet and comfortable work space where I could concentrate and work day and night and saved me from several technical glitches I faced in my everyday life. The healthy (*though sometimes bland*) food of Jeeva bhai had really saved a lot of time of mine which otherwise I would have to spend in cooking.

It is my pleasure to thank Manish, Rakesh, Abhishek, Kali, Srijit, Debashis, Hardik, Prasad, Arvind, Bondhu-bhai (Jagabandhu), Rohit, Ratnesh, Udaya, Ravi, Sunil, Abhishek, Vinod, Aritra, Shivam, Swati and others for their cheerful company. For sure, I could have never finished the three trekkings at the foothills of Himalaya without the encouragement from Hardik, Rohit and Ratnesh.

I am immensely indebted to some of the teachers who taught me in University, College and School days - Prof. Parthasarathi Majumdar, Prof. Somendra Mohan Bhattacharjee, Prof. Mahan Mj, Dr. Sayantani Bhattacharyya, Dr. Bobby Ezhuthachan, Prof. Siddhartha Sen, Dr. Ashik Iqbal, Dr. Abhijit Bandyopadhyay, Dr. Sobhan K. Sounda, Dr. Parthasarathi Mukhopadhyay, Dr. Soumen

Mondal, Prof. Dipanjan Rai Chaudhuri, Late Prof. Subash Roy - who have been a source of impeccable motivation and continuous support to choose research as my career, to say the least.

Lastly I must admit, I owe to the revered monks of several monastic organisations who gave me the lessons of life, that filled 'my heart with joy unspeakable'!

*'Thou hast made me endless, such is thy pleasure. This frail vessel thou emptiest  
again and again, and fillest it ever with fresh life.*

*This little flute of a reed thou hast carried over hills and dales, and hast breathed  
through it melodies eternally new.*

*At the immortal touch of thy hands my little heart loses its limits in joy and gives  
birth to utterance ineffable*

*Thy infinite gifts come to me only on these very small hands of mine. Ages pass,  
and still thou pourest, and still there is room to fill.'*

*- Song Offerings (Gitanjali), Rabindranath Tagore.*

# Contents

Abstract . . . . .	14
List of Figures . . . . .	26
<b>1 Introduction</b>	<b>39</b>
1.1 General properties of plasma: . . . . .	40
1.2 Theoretical models of plasma: . . . . .	41
1.3 MagnetoHydroDynamic model of plasma: . . . . .	42
1.4 Basic problems addressed in this thesis: . . . . .	43
1.5 Motivation for a new code: . . . . .	45
<b>2 Numerical Technique</b>	<b>51</b>
2.1 Motivation . . . . .	51
2.2 Code G-MHD3D . . . . .	54
2.3 Governing equations . . . . .	55
2.3.1 Normalisation of the MHD equations . . . . .	59
2.4 Two dimensional numerical tests . . . . .	61
2.4.1 Incompressible hydrodynamic flow . . . . .	62
2.4.2 Weakly compressible hydrodynamic flow . . . . .	63
2.4.3 Weakly compressible magnetohydrodynamic flow . . . . .	66
2.5 Three dimensional numerical tests . . . . .	69

2.5.1	For hydrodynamic flow . . . . .	71
2.5.2	For magnetohydrodynamic flow . . . . .	72
2.6	Tracer Particles . . . . .	80
2.6.1	Interpolation Scheme for Test Particle Transport . . . . .	81
2.6.2	Particle Pusher Scheme . . . . .	83
2.7	GPU Acceleration . . . . .	84
2.7.1	OpenACC Acceleration of MHD3D . . . . .	85
2.7.2	cuFFT Library . . . . .	86
2.7.3	Out-of-core Processing . . . . .	87
2.7.4	Performance Results . . . . .	90
2.8	Future Scope . . . . .	92
2.9	Acknowledgements . . . . .	92
<b>3</b>	<b>Nonlinear Coherent Oscillation</b>	<b>95</b>
3.1	Introduction . . . . .	95
3.2	Governing Equations . . . . .	99
3.3	Parameter Details . . . . .	100
3.4	Simulation Results . . . . .	101
3.4.1	Results for Decaying 2D Orszag-Tang Flow . . . . .	101
3.4.2	Results for Decaying 2D Cat's Eye Flow . . . . .	102
3.4.3	Results for Forced 2D Orszag-Tang Flow . . . . .	102
3.4.4	Results for Decaying 3D Roberts Flow . . . . .	104
3.4.5	Results for Decaying 3D Cat's Eye Flow . . . . .	105
3.4.6	Results for Decaying 3D ABC Flow . . . . .	106
3.4.7	Analysis of Decaying 3D ABC Flow . . . . .	107
3.4.8	Results for Forced ABC Flow . . . . .	112



3.5	Galerkin Representation in Two dimensions . . . . .	113
3.6	Summary and Future Work . . . . .	118
<b>4</b>	<b>Recurrence</b>	<b>121</b>
4.1	Introduction . . . . .	121
4.2	Governing Equations . . . . .	125
4.3	Initial and boundary conditions . . . . .	126
4.3.1	Parameter details . . . . .	126
4.4	3D DNS Results from G-MHD3D . . . . .	127
4.4.1	Taylor-Green flow . . . . .	128
4.4.2	Roberts flow . . . . .	132
4.4.3	Arnold-Beltrami-Childress flow . . . . .	136
4.4.4	Cats Eye flow . . . . .	140
4.5	Analytical description of DNS results . . . . .	141
4.6	Summary and conclusion . . . . .	145
<b>5</b>	<b>Self Consistent Dynamo</b>	<b>151</b>
5.1	Introduction . . . . .	151
5.2	Governing Equations . . . . .	160
5.3	Parameter Details . . . . .	161
5.4	Simulation Results . . . . .	162
5.4.1	Initial Profile of Density, Velocity and Magnetic Field . . . . .	162
5.4.2	Transition to Self-Consistent Dynamo: Initial value problem . . . . .	163
5.4.3	Kinematic Dynamo: Driven velocity field . . . . .	164
5.4.4	Dynamo with Back-Reaction or Self-Consistent Dynamo . . . . .	170
5.5	Summary and Future Works . . . . .	178

<b>6</b>	<b>Conclusion</b>	<b>181</b>
6.1	Introduction . . . . .	181
6.2	Summary . . . . .	182
6.3	Future Work . . . . .	185

## Abstract

Understanding plasma turbulence is key to control the disruption of plasma in experimental devices thereby improving the confinement of plasma as well as predicting extreme events occurring in astrophysical objects and stellar matter. One of the best suited models to explain various large or intermediate scale events in plasma is magnetohydrodynamics (MHD). The magnetic field-lines coupled with the plasma flow offer completely new dynamics and energy transfer mechanism between modes. To understand such new mechanism “direct numerical simulation” (DNS) study of MHD equation is very necessary.

In order to carefully observe the energy cascades through different modes, I have developed an MPI parallel three dimensional pseudo-spectral DNS code from scratch that governs the dynamics of plasma within the framework of single fluid MHD. In collaboration with NVIDIA, India, the code has been GPU parallelised [Rupak Mukherjee *et. al.* IEEE Conference Proceedings of 25th International Conference on High Performance Computing Workshops (HiPCW), 2018 ] and multi-GPU parallelisation using NVLink has recently been achieved. The code is operated at different parameter regimes to explore the energy exchange through new pathways. Three such novel features are identified out of the present study.

In the presence of weak resistivity, the MHD model is known to predict irreversible conversion of magnetic energy into fluid kinetic energy (i.e. reconnection) as well as conversion of kinetic energy into mean large scale magnetic field (i.e. dynamo) [Rupak Mukherjee, Rajaraman Ganesh, Conference Proceedings of 27th IAEA Fusion Energy Conference, 476, (2018)]. Therefore it is interesting to ask oneself, for a given fluid type and magnetic field strength, are there fluid flow profiles which do neither - that is, neither does the flow generate mean magnetic field nor the magnetic field energy is converted to flow energy; instead there are nearly “reversible” coherent nonlinear oscillations. From our DNS results from the code G-MHD3D, I have shown that both in two and three dimensions, coherent nonlinear oscillation persists for a wide range of initial flow speeds or Alfvén Mach number. A finite mode Galerkin representation of the two dimensional MHD equations in analytically carried out to verify the possibility of such energy exchange phenomena and I found good agreement between our analytical and DNS results. [Rupak Mukherjee, Rajaraman Ganesh, Abhijit Sen; Physics of Plasmas, **26**, 042121 (2019)]

For three dimensional chaotic flows at Alfven resonance, I perform detailed DNS study using G-MHD3D and find that for two different initial conditions, one flow reconstructs the initial fluid and magnetic flow profile and the other does not. I call the phenomena as “Recurrence” and provide a possible explanation of the event, by checking the boundedness of Rayleigh quotient which measures the effective number of active degrees of freedom in a high dimensional system. Though “Recurrence” has been observed in many hydrodynamic systems earlier, the cause of recurrence in MHD system is completely different. Unlike hydrodynamic systems, in MHD system, the energy oscillates between kinetic and magnetic modes thereby periodically destroying and reconstructing back the structures of the field variables. Such effects can have wide applications in short time predictions of plasma profiles in experimental devices where real time plasma imaging can be performed. [Rupak Mukherjee, Rajaraman Ganesh, Abhijit Sen; Physics of Plasmas, **26**, 022101 (2019)]

Finally I study the driven dissipative systems at very high Alfven Mach number leading to self-consistent stretch-twist-fold (STF) dynamo effect showing short scale magnetic field generation from kinetic energy. Starting with Arnold-Beltrami-Childress (ABC) driven flow I find the dynamo effect to take place and optimal parameters for “fast” dynamo is obtained. For self consistent evolution of the set of 3D MHD equations the kinetic energy spectra is found to have a  $-5/3$  scaling showing a fully developed Kolmogorov type of turbulence even though the plasma dynamics significantly differ from that of the hydrodynamic one. From extensive DNS study using G-MHD3D I also distinguish the optimal parameter set to obtain “fast” dynamo for ABC flows. [Rupak Mukherjee, Rajaraman Ganesh, Abhijit Sen, arXiv:1901.09610]

Combining all the above results I have obtained, it is learnt that, the single fluid MHD description of plasma do offer new energy cascading pathways through kinetic as well as magnetic field variables thereby altering the nature of turbulence generally observed in well-studied hydrodynamic cases. Thus it can be stressed that in order to study the plasma turbulence occurring in fusion devices or in astrophysical objects the fundamental energy cascading pathways play a crucial role and needs to be analysed carefully.



# **SYNOPSIS**

Plasmas are known as the fourth state of visible matter (as opposed to “dark” matter). When a gas is heated, the neutral atoms constituting the gas, get excited and thereby ionised. Thus the electrons and the ions of such a medium very often form a plasma that shows collective behaviour. The origin of such behaviour is the partial shielding of the one species of charged particles by the another [1]. Thus plasmas can be identified as a charged medium having quasi-neutrality in space and showing the property of collective oscillations in response to any external perturbation [1]. There are laboratory and astro-plasmas which are non-neutral as well [2]. Our focus is on quasi-neutral plasmas.

Because of strong thermal radiation, the neutral atoms get ionised and form an ionised gas maintaining a quasi-neutrality in space. Thus the state of matter that constitutes the structure of a young star primarily dominated by its thermal energy, is the plasma state [3]. Such plasmas are found in stellar atmosphere. Also, very hot ionised gases in the form of plasma, forms the accretion disks around a black hole or a neutron star. The electrons and ions of the excited gas of the hot magnetised medium having very high kinetic energy, collide with each-other and undergo nuclear fusion process through quantum tunnelling effect, thereby releasing the binding energy of the nucleus in the form of thermal radiation. This thermal radiation pressure keeps the star burning, thus overpowering the gravitational pull that tries to quench the star. Once the star runs out of the thermal energy emitted from fusion process, because of the gravitational pull, turns into a white dwarf [4] or a neutron star / black hole [5, 6] depending on the *irreducible mass* of the star [7].

In different laboratories around the globe, there are several plasma reactor experiments being carried out to mimic the thermo-nuclear fusion process in violent

plasmas taking place in stars. However the nature of plasma-confinement in the stars and the fusion reactors are completely different. In astrophysical plasmas, the confinement is through the gravitational pull that holds the plasma which is ready to expand, otherwise, within the volume of the star [8]. On the other hand in terrestrial reactors, it is the magnetic field that prevents the plasma loss to the walls of the reactor vessels [9]. Even though the confinement techniques are different, the fundamental motive of such experiments is to harness the binding energy of atoms and transform it, to the form of daily usable electricity for the service of the mankind. At present huge efforts in terms of human resource and finance are being given by several governments of different countries to ‘bring the Sun to the Earth’. Some examples of such experimental devices are ADITYA [10] & SST-1 [11] India, ITER [12] and WEST [13] at France, JET [14] at UK, NSTX [15] and DIII-D [16] at USA, EAST [17] at China etc.

In astrophysical plasmas, because of very high kinetic energy, the fast motion of any charged particle, generate a magnetic field which in turn crucially governs the dynamics of the particle itself as well as the other particles in the vicinity. Since plasma is a charged gas, it can be modelled as a fluid on which electromagnetic body forces act [18]. In case of large number of particles having very high degrees of freedom, a spatially averaged model called ‘*fluid model*’ has been found to be very efficient to predict the behaviour of the plasma [19]. The model follows the dynamics of *fluid elements* constituting of a large number of particles collisional enough to neglect the fluctuations arising due to finite number of the particles.

The motion of the charged-fluid element in presence of self-generated magnetic field, gets primarily governed by the Maxwell’s equations coupled with the equations of *hydro-dynamics* [20]. The subject that studies the self-consistent evolution

of such a magnetised plasma-fluid is known as Magneto-Hydro-Dynamics (MHD) [18]. The theory of MHD is one of the well studied models to analyse the three dimensional magnetised plasma turbulence which is very crucial to understand the fundamental behaviour of astro-plasmas present in the Sun or other young stars as well as for the careful operation of complicated fusion reactors, for example Stellarators or Tokamaks.

Paradoxically, MHD model has also been found to hold good in the study of cores of tokamak where large angle Coulomb collisions are absent or nearly absent [9]. Thus MHD is one of the most successful theories that explains fluid like processes of fusion plasmas well. However, the long time prediction of any state of such plasma by analytical means, is very hard to obtain within this model. It is because of the nature of the set of nonlinearly coupled equations describing the MHD model, which are very hard to solve analytically [21]. The magnetised fluid model in the continuum limit poses a very challenging question in anticipating the future, starting from any given initial state [22]. Thesis addresses this question and have found an answer of this problem within very restricted parameter sets. Because of the extra dimensionality introduced by the magnetic variables, within the premise of the MHD model, the magnetic field coupled with the fluid variables offer energy to get exchanged between the fluid and the magnetic modes. The energy exchange opens up a new pathway for forward and inverse cascades of energy amongst different length-scales [23]. One such phenomena which is extensively studied in this Thesis, is the nonlinear coherent oscillations of energy between the kinetic and magnetic scales thereby periodically destroying and re-constructing the fluid and magnetic flow profiles with time [24, 25]. Such periodical reconstruction helps in predicting the long time behaviour of the plasma under the MHD approximations. Thus the extra dimensionality of the problem helps trapping in phase-space of the system and offers completely new physics results full of surprises within the premise of MHD

model.

Plasmas - both in hot stars as well as in fusion devices, are often in turbulent state. In case of a fully developed turbulent plasma medium, the nonlinear interactions between the distant length scales allow the energy to cascade through various modes. The nature of kinetic energy cascade for different initial spectrum has been a longstanding challenge in the field of fluid dynamics. Starting from relativistic jets [26] to angular momentum transport in accretion disks [27] - all need a thorough understanding of the plasma turbulence amongst different scales. Thus understanding plasma turbulence is a key to control the disruption of plasma in such experimental devices thereby improving the confinement of plasma for fusion to take place as well as predicting extreme events occurring in astrophysical objects and stellar matter. In addition, the magnetic field-lines coupled with such plasma flow offer completely new dynamics and energy transfer mechanism within the plasma. Because of the strong coupling between flow and magnetic variables, the dynamics of a fully developed turbulent plasma present in stellar objects needs a separate careful treatment. The inherent features of this plasma turbulence are needed to be understood and properly analysed to predict any surprising event taking place in our nearest star “The Sun” or in the fusion reactors running over the several laboratories.

The large [28] and small [29] scale magnetic field generation from flow fields is generally called “Dynamo”. This phenomena is often seen in the Sun as well as in accretion disks [30, 31, 32] around any compact object (for example a neutron star or a black hole). One of the most successful theory that explains the dynamo phenomenon was given by Eugene Newman Parker [28]. Large or intermediate scale magnetic field generated out of the kinetic energy primarily governs the dynamics of the charged fluid (plasma) through a time dependent Lorentz force term added in

the Navier-Stokes equation, thereby self-consistently affecting the dynamics of the fluid flow. This bifurcates the study of plasma from the already known and well-explored subject “fluid dynamics”. Thus the nature of turbulence in a MHD plasma is primarily different than that of the hydrodynamic one. A turbulent plasma has been shown to produce large amplitude of short-scale magnetic field - a phenomenon called “fluctuation dynamo” [29]. The quest for the fast growth of magnetic field - both large and short scale - in astrophysical objects is still on and is one of the most interesting topic of research currently [33]. In this Thesis the simulation starts with a three dimensional chaotic flow and find out optimal parameter set to generate “fast” dynamo - whose growth rate remains finite as the magnetic Reynolds number is sufficiently large..

In general, it is very difficult to solve the set of coupled nonlinear MHD equations analytically. Thus powerful numerical solvers are needed to capture the physics issues happening in plasma. Of late, direct numerical simulation (DNS) [34] techniques are available that captures the time evolution of the full set of Navier-Stokes equation coupled with Maxwell’s equations and resolves spatial and temporal scales till the smallest dissipative and resistive limits without resorting to any turbulence model. Addressing some of these issues of magnetic field generation and plasma dynamics require well resolved, long time simulation having low phase or dispersion error. Such calculation requires efficient, well parallelized numerical solver capable of handling compressible MHD physics as well as numerical complexities. In order to simulate such a physical process, the finite difference DNS schemes falls short to cope up with the requirement of the high speed performance of the code. Pseudo-spectral technique is observed to be much more accurate and faster method than finite difference methods [35]. A three dimensional compressible MHD solver G-MHD3D is developed, which considers continuity, momentum and energy equations for fluid and magnetic variables with a thermodynamic closure for pressure

[36]. G-MHD3D uses conservative form using pseudo-spectral method in cartesian coordinates with GPU parallelization. The numerical solver that has been developed captures similar Dynamo Effect for chaotic plasma flows. The code is expected to contribute even more for better understanding of such turbulent phenomena in cosmos. In the present Thesis, DNS results are obtained from the code, operated at different parameter regimes identifying several novel nonlinear phenomena that addresses nonlinear energy cascades between the non-local length-scales of kinetic and magnetic variables.

This thesis is divided into 6 chapters. **Chapter - 1** provides an introduction to plasma and the different theoretical models to study plasma. Validity of such models are described explicitly after describing the individual models. Next, an introduction to the MHD model, qualitatively mentioning the governing equations of the model, is provided. Single fluid MHD model is introduced specifically for identifying the regime of application of such model into fusion studies and in astrophysical objects. The shortcomings of the MHD model are also highlighted. Finally, the fundamental new results obtained in this PhD thesis are described in brief and comments are made for their experimental feasibility in laboratory devices. Some applications of this study in real world are provided in the conclusion.

**Chapter - 2** describes the development of an MPI [37] parallel three dimensional pseudo-spectral DNS code from scratch that governs the dynamics of plasma within the framework of single fluid MHD. In collaboration with NVIDIA, India, the code has been GPU parallelised [36] and multi-GPU parallelisation using NVLink [38] has recently been achieved. Extensive physics benchmarking studies as well as numerical scaling studies of the code G-MHD3D is presented in this chapter along with GPU [39] parallelization, scalability and numerical as well as physics details. It is

envisaged that this new code with its extensive physics diagnostics and GPU scalability should be able to address some of the fundamental physics issues in different areas such as reconnection (a phenomena of transforming back the magnetic energy to kinetic energy of the plasma), dynamos as well as MHD turbulence. The code is operated at different parameter regimes to explore the energy exchange through new pathways. Three such novel features are identified out of the present study and described in the following chapters.

**Chapter - 3** describes one of the most exclusive examples of such nonlinear energy exchange between kinetic and magnetic modes of single fluid MHD description of plasma. In the presence of weak resistivity, the MHD model is known to predict irreversible conversion of magnetic energy into fluid kinetic energy (i.e. reconnection) [40, 41, 42, 43, 44, 45] as well as conversion of kinetic energy into mean large scale magnetic field (i.e. dynamo) [30, 31, 32, 46, 28, 29]. Therefore it is interesting to ask oneself, for a given fluid type and magnetic field strength, are there fluid flow profiles which do neither - that is, neither does the flow generate mean magnetic field nor the magnetic field energy is converted to flow energy; instead there are nearly “reversible” coherent nonlinear oscillations because of generation of nonlinear non-dispersive Alfvén waves. From the DNS results from the code G-MHD3D it has been shown that both in two and three dimensions, coherent nonlinear oscillation persists for a wide range of initial flow speeds or Alfvén Mach number. A finite mode Galerkin representation of the two dimensional MHD equations is analytically carried out to verify the possibility of such energy exchange phenomena and it is found that DNS results are in good agreement with our analytical speculations [23].

**Chapter - 4** describes detailed DNS study of single fluid MHD equations using G-MHD3D, for three dimensional chaotic flows at Alfvén resonance and find that for

two different initial conditions, one flow reconstructs the initial fluid and magnetic flow profile and the other does not. The phenomena is called as "Recurrence". Furthermore, an explanation of the event checking boundedness of Rayleigh quotient is delineated, which measures the effective number of active degrees of freedom in a high dimensional system. Though "Recurrence" has been observed in many hydrodynamic systems earlier [47, 48, 49, 50], the cause of recurrence in MHD system is completely different. Unlike hydrodynamic systems, in MHD system, the energy oscillates between kinetic and magnetic modes thereby periodically destroying and reconstructing back the structures of the field variables. Such effects can have wide applications in short time predictions of plasma profiles in experimental devices where real time plasma imaging can be performed [24].

**Chapter - 5**, elucidates studies of driven dissipative systems at very high Alfvén Mach number leading to self-consistent stretch-twist-fold (STF) dynamo [51, 52, 53] effect showing short scale magnetic field generation from kinetic energy. Starting with Arnold-Beltrami-Childress (ABC) driven flow, Alfvén Mach number is raised at the identical parameter space described in Chapter - 3 and the dynamo effect is found to take place and optimal parameters for "fast" dynamo is obtained. For self consistent evolution of the set of 3D MHD equations, the kinetic energy spectra is found to have a  $-5/3$  scaling showing a fully developed Kolmogorov type of turbulence [54] even though the plasma dynamics significantly differ from that of the hydrodynamic one. From extensive DNS study using G-MHD3D, the optimal parameter set to obtain "fast" dynamo for ABC flows [55] are also distinguished.

Finally, **Chapter - 6** consolidates the work and enumerate the major tasks that can be undertaken for further research in this field. Combining all the above results that have been obtained, it becomes evident that, the single fluid MHD description



of plasma offers new energy cascading pathways through kinetic as well as magnetic field variables thereby altering the nature of turbulence generally observed in well-studied hydrodynamic cases. Thus it can be stressed that in order to study the plasma turbulence occurring in fusion devices or in astrophysical objects the fundamental energy cascading pathways play a crucial role and needs to be analysed carefully.



# List of Figures

2.1	Initial velocity profile of K-H instability. . . . .	63
2.2	Snapshot of vorticity profile of K-H instability for $K_x = 3$ at time $t = 21.9$ with grid resolution $N_x = N_y = 256$ , $L_x = L_y = 2\pi$ , $\nu = 10^{-4}$ , $dt = 10^{-3}$ , $\omega_0 = 2$ , $d = \frac{3\pi}{128}$ and $M = 0$ . . . . .	64
2.3	Comparison of kinetic energy in y-direction of K-H instability for $k_x = 3$ with AGSpect [56] for $M = 0.05$ . . . . .	64
2.4	Growth rate ( $2\gamma$ ) of K-H instability is plotted with mode number ( $k_x$ ) of excitation. The red solid line is evaluated from the analytical expression obtained by Drazin. The blue line with 'X' sign represents the growth rate from earlier code in vorticity formalism and the magenta line with symbol 'O' represents the same from velocity formalism code with Mach number ( $M$ ) = 0.05. . . . .	65
2.5	Time evolution of y-directional kinetic energy (see Fig. 2.1) at the perpendicular to the flow direction is evaluated with time. Fig 2 of Keppens et al [57] reproduced by my code for the identical parameters with Mach Number ( $M$ ) = 0.5. The value of growth rate ( $\gamma = 1.7$ ) is found to be in good agreement with the value obtained from Table 1 ( $\gamma = 1.728$ ) by Keppens et al [57]. Fig 2 of Keppens et al [57] with Mach Number ( $M$ ) = 0.5. . . . .	66
2.6	The change of growth rate ( $\frac{\gamma a}{V_0}$ ) with the mode number of excitation ( $k_x a$ ). . . . .	67
2.7	Comparison of natural frequency and its harmonics as well as its beats of my code with its harmonics with AGSpect [56] for $M = 0.5$ . . . . .	67
2.8	Time evolution of the prearranged vortex merger with $M = 0.5$ with grid size $256^2$ . . . . .	68
2.9	The x-component of magnetic field ( $B_x(x, y)$ ) profile at time $t = 10$ . The grid resolution I use is $128^2$ and time-step width $10^{-3}$ . . . . .	69
2.10	The y-component of magnetic field ( $B_y(x, y)$ ) profile at time $t = 10$ . The grid resolution I use is $128^2$ and time-step width $10^{-3}$ . . . . .	69

2.11	The change of growth rate with the mode number of excitation. The red dashed line indicates the hydrodynamic case and the blue dot-dashed line indicates the uniform magnetohydrodynamic case. The magenta solid line indicates the growth of magnetic energy with time.	70
2.12	The change of growth rate ( $\frac{\gamma a}{V_0}$ ) with the mode number of excitation ( $k_x a$ ) for hydrodynamic (red dotted) as well as magneto-hydrodynamic (blue starred) cases. The growth rate for Magnetohydrodynamic flows at higher wave numbers is found to be higher than that of the Hydrodynamic one as previously identified by Keppens <i>et al</i> [57].	70
2.13	Conservation of divergence of $\vec{B}$ and divergence of $\vec{V}$ . $\vec{\nabla} \cdot \vec{B} \sim \mathcal{O}(10^{-32})$ implies a strict conservation of the divergence of magnetic field till the machine precision. However, even though sonic Mach number is 0.1 indicating an incompressible regime, governing equations allow the density to fluctuate and hence, the $\vec{\nabla} \cdot \vec{V}$ is $\sim \mathcal{O}(10^{-11})$ but not as good as that of $\vec{B}$ .	71
2.14	The time evolution of kinetic energy [ $= \sum_{x,y,z} u^2(x, y, z, t)$ ] per grid with $k_0 = 1, 2, 4, 8$ .	72
2.15	A zoomed view of Fig. 2.14. The amplitude of fluctuation is found to decrease as $k_0$ increases.	72
2.16	A zoomed view of Fig. 2.14. The amplitude of fluctuation is found to decrease as $k_0$ increases.	73
2.17	Profile of RMS of velocity divergence ( $\theta'$ ) with time for $k_0 = 8$ and $M = 0.1$	73
2.18	Growth of magnetic energy [ $= \sum_{x,y,z} B^2(x, y, z, t)$ ] in the form of kinematic dynamo benchmarked with Galloway and Frisch [58] with $R_m = 120$ . Figure reproduced from Galloway and Frisch [58] with $R_m = 120$ . The initial time evolution and the star-up of dynamo action is different in the two figures because of the difference between the initial random number seeds used in the simulation.	74
2.19	Growth of magnetic energy [ $= \sum_{x,y,z} B^2(x, y, z, t)$ ] in the form of kinematic dynamo benchmarked with Galloway and Frisch [58] with $R_m = 200$ . Figure reproduced from Galloway and Frisch [58] with $R_m = 200$ . The initial time evolution and the star-up of dynamo action is different in the two figures because of the difference between the initial random number seeds used in the simulation.	74

2.20	Growth of magnetic energy [= $\sum_{x,y,z} B^2(x, y, z, t)$ ] in the form of kinematic dynamo benchmarked with Galloway and Frisch [58] with $R_m = 450$ . Figure reproduced from Galloway and Frisch [58] with $R_m = 450$ . The initial time evolution and the star-up of dynamo action is different in the two figures because of the difference between the initial random number seeds used in the simulation. . . . .	75
2.21	x-component of magnetic field ( $B_x(x, y, 0)$ ) at time $t = 300$ at identical parameter of Galloway and Frisch [58] with $R_m = 450$ . . . . .	75
2.22	y-component of magnetic field ( $B_y(x, y, 0)$ ) at time $t = 300$ at identical parameter of Galloway and Frisch [58] with $R_m = 450$ . . . . .	76
2.23	z-component of magnetic field ( $B_z(x, y, 0)$ ) at time $t = 300$ at identical parameter of Galloway and Frisch [58] with $R_m = 450$ . . . . .	76
2.24	Multiple frequencies observed in the magnetic energy [= $B^2(t)$ ] of the MHD version of the DNS of decaying hydrodynamic turbulence earlier observed by Samtaney <i>et al.</i> [59] . . . . .	77
2.25	Conservation of shifted total energy [ $\delta TE = \sum_{x,y,z} u^2(x, y, z, t) - \sum_{x,y,z} u^2(x, y, z, 0) + \sum_{x,y,z} B^2(x, y, z, t) - \sum_{x,y,z} B^2(x, y, z, 0)$ ] and time evolution of shifted kinetic [ $\delta KE = \sum_{x,y,z} u^2(x, y, z, t) - \sum_{x,y,z} u^2(x, y, z, 0)$ ] and shifted magnetic [ $\delta ME = B^2(t) - B^2(0)$ ] energy for Arnold-Beltrami-Childress flow with $M_A = 1$ and $M = 0.1$ and $Re = Rm = 450$ with $k_0 = 1$ . . . . .	78
2.26	Time evolution of shifted kinetic [ $\delta KE = \sum_{x,y,z} u^2(x, y, z, t) - \sum_{x,y,z} u^2(x, y, z, 0)$ ] and shifted magnetic [ $\delta ME = \sum_{x,y,z} B^2(x, y, z, t) - \sum_{x,y,z} B^2(x, y, z, 0)$ ] energy for Taylor-Green flow with $M_A = 1$ and $M = 0.1$ and $Re = Rm = 450$ with $k_0 = 1$ . . . . .	78
2.27	Time evolution of shifted kinetic [ $\delta KE = \sum_{x,y,z} u^2(x, y, z, t) - \sum_{x,y,z} u^2(x, y, z, 0)$ ] and shifted magnetic [ $\delta ME = \sum_{x,y,z} B^2(x, y, z, t) - \sum_{x,y,z} B^2(x, y, z, 0)$ ] energy for Roberts flow with $M_A = 1$ and $M = 0.1$ and $Re = Rm = 450$ with $k_0 = 1$ . . . . .	79
2.28	Time evolution of shifted kinetic [ $\delta KE = \sum_{x,y,z} u^2(x, y, z, t) - \sum_{x,y,z} u^2(x, y, z, 0)$ ] and shifted magnetic [ $\delta ME = \sum_{x,y,z} B^2(x, y, z, t) - \sum_{x,y,z} B^2(x, y, z, 0)$ ] energy for Cat's Eye flow with $M_A = 1$ and $M = 0.1$ and $Re = Rm = 450$ with $k_0 = 1$ . . . . .	79

2.29	CIC scheme for volume weighting for the evaluation of magnetic fields on the location of the tracer particles. The tracer particle (yellow filled circle) is located within the unit shell. It divides the unit shell into 8 subshells, one of them are shown in dark colors with blue circles at the edges. The magnetic field at the tracer particle location ( $\vec{B}_p$ ) is interpolated from the grid magnetic field ( $\vec{B}_g$ ) of the outer corner grids (black hollow circles). The weights of interpolation is given in Eq. 2.20 . . . . .	82
2.30	Mapping of OpenMP loops in MHD3D to OpenACC parallel loops in G-MHD3D. . . . .	86
2.31	OpenACC Compilation of G-MHD3D. . . . .	87
2.32	Steps to call cuFFT routines in G-MHD3D. . . . .	87
2.33	Calling cuFFT routines through C wrapper modules in G-MHD3D. . . . .	88
2.34	Calling cuFFT routines through C wrapper modules in G-MHD3D. . . . .	88
3.1	Time evolution of shifted kinetic [ $\delta KE = u^2(t) - u^2(0)$ ], magnetic [ $\delta ME = B^2(t) - B^2(0)$ ] and total [ $\delta TE = u^2(t) - u^2(0) + B^2(t) - B^2(0)$ ] energy per grid for two dimensional Orszag-Tang flow with $N = 128^2$ , $U_0 = 1$ , $k_0 = 1$ , $M_s = 0.01$ , $M_A = 1$ and $Re = Rm = 10^{-4}$ in the absence of external forcing. The energy keeps on switching between kinetic and magnetic modes keeping the total energy conserved. It is found that the time period of oscillation is $T = 2.971$ . . . . .	102
3.2	Time evolution of shifted kinetic [ $\delta KE = u^2(t) - u^2(0)$ ], magnetic [ $\delta ME = B^2(t) - B^2(0)$ ] and total energy [ $\delta TE = u^2(t) - u^2(0) + B^2(t) - B^2(0)$ ] per grid for two dimensional Cat's Eye flow with $N = 128^2$ , $U_0 = 1$ , $A = 0.5$ , $k_0 = 1$ , $M_s = 0.01$ , $M_A = 1$ and $Re = Rm = 10^{-4}$ in the absence of external forcing. The energy keeps on switching between kinetic and magnetic modes keeping the total energy conserved. The decay of total energy can be detrended by the multiplying the data by $\exp(-2Dt)$ implying that it is solely due to viscous and resistive effects. The shift denotes the initial values of the kinetic and magnetic energies (at time $t = 0$ ) are subtracted from the time evolution data of the corresponding variables. The time period of oscillation is $T = 1.659$ . . . . .	103

3.3 Time evolution of shifted kinetic [ $\delta KE = u^2(t) - u^2(0)$ ], magnetic [ $\delta ME = B^2(t) - B^2(0)$ ] and total energy [ $\delta TE = u^2(t) - u^2(0) + B^2(t) - B^2(0)$ ] per grid for two dimensional Orszag-Tang flow with  $N = 128^2$ ,  $U_0 = 1$ ,  $k_0 = 1$ ,  $M_s = 0.01$ ,  $M_A = 1$  and  $Re = Rm = 10^{-4}$  in the presence of external forcing. The energy keeps on switching between kinetic and magnetic modes. The total energy also oscillates around the same frequency and the whole system acts as a forced-relaxed system. The shift denotes the initial values of the kinetic and magnetic energies (at time  $t = 0$ ) are subtracted from the time evolution data of the corresponding variables. . . . . 104

3.4 Time evolution of shifted kinetic [ $\delta KE = u^2(t) - u^2(0)$ ], magnetic [ $\delta ME = B^2(t) - B^2(0)$ ] and total energy [ $\delta TE = u^2(t) - u^2(0) + B^2(t) - B^2(0)$ ] per grid for three dimensional Roberts flow with  $N = 64^3$ ,  $U_0 = 0.1$ ,  $A = B = C = 1$ ,  $k_0 = 1$ ,  $M_s = 0.1$ ,  $M_A = 1$  and  $Re = Rm = 450$  in the absence of external forcing. The energy keeps on switching between kinetic and magnetic modes keeping the total energy conserved. The decay of total energy can be detrended by the multiplying the data by  $\exp(-2Dt)$  implying that it is solely due to viscous and resistive effects. The shift denotes the initial values of the kinetic and magnetic energies (at time  $t = 0$ ) are subtracted from the time evolution data of the corresponding variables. The time period of oscillation is  $T = 30.680$  . . . . . 105

3.5 Time evolution of shifted kinetic [ $\delta KE = u^2(t) - u^2(0)$ ], magnetic [ $\delta ME = B^2(t) - B^2(0)$ ] and total energy [ $\delta TE = u^2(t) - u^2(0) + B^2(t) - B^2(0)$ ] per grid for three dimensional Cat's Eye flow with  $N = 64^3$ ,  $U_0 = 0.1$ ,  $A = \sqrt{\frac{3}{5}}$ ,  $B = 2A$ ,  $k_0 = 1$ ,  $M_s = 0.1$ ,  $M_A = 1$  and  $Re = Rm = 450$  in the absence of external forcing. The energy keeps on switching between kinetic and magnetic modes keeping the total energy conserved. The decay of total energy can be detrended by the multiplying the data by  $\exp(-2Dt)$  implying that it is solely due to viscous and resistive effects. The shift denotes the initial values of the kinetic and magnetic energies (at time  $t = 0$ ) are subtracted from the time evolution data of the corresponding variables. The time period of oscillation is  $T = 30.510$  . . . . . 106

- 3.6 Time evolution of shifted kinetic [ $\delta KE = u^2(t) - u^2(0)$ ], magnetic [ $\delta ME = B^2(t) - B^2(0)$ ] and total energy [ $\delta TE = u^2(t) - u^2(0) + B^2(t) - B^2(0)$ ] per grid for three dimensional Arnold-Beltrami-Childress flow with  $N = 64^3$ ,  $U_0 = 0.1$ ,  $A = B = C = 1$ ,  $k_0 = 1$ ,  $M_s = 0.1$ ,  $M_A = 1$  and  $Re = Rm = 450$  in the absence of external forcing. The energy keeps on switching between kinetic and magnetic modes keeping the total energy conserved. The decay of total energy can be detrended by the multiplying the data by  $\exp(-2Dt)$  implying that it is solely due to viscous and resistive effects. The shift denotes the initial values of the kinetic and magnetic energies (at time  $t = 0$ ) are subtracted from the time evolution data of the corresponding variables. The time period of oscillation is  $T = 30.171$  107
- 3.7 Time evolution of shifted kinetic (solid) [ $\delta KE = u^2(t) - u^2(0)$ ], magnetic (dashed) [ $\delta ME = B^2(t) - B^2(0)$ ] and total (dotted) [ $\delta TE = u^2(t) - u^2(0) + B^2(t) - B^2(0)$ ] energy per grid for three dimensional Arnold-Beltrami-Childress flow with  $N = 64^3$ ,  $U_0 = 0.1$ ,  $A = B = C = 1$ ,  $k_0 = 1$  (red), 2 (blue), 4 (magenta),  $M_s = 0.1$ ,  $M_A = 1$  and  $Re = Rm = 450$  in the absence of external forcing. Drag forces are found to affect the kinetic modes more than the magnetic modes as expected and explained in the text. The shift denotes the initial values of the kinetic and magnetic energies (at time  $t = 0$ ) are subtracted from the time evolution data of the corresponding variables. . . . . 108
- 3.8 Time evolution of shifted kinetic (solid) [ $\delta KE = u^2(t) - u^2(0)$ ], magnetic (dashed) [ $\delta ME = B^2(t) - B^2(0)$ ] and total (dotted) [ $\delta TE = u^2(t) - u^2(0) + B^2(t) - B^2(0)$ ] energy per grid for three dimensional Arnold-Beltrami-Childress flow with  $N = 64^3$ ,  $U_0 = 0.1$ ,  $A = B = C = 1$ ,  $k_0 = 8$  (red), 16 (blue),  $M_s = 0.1$ ,  $M_A = 1$  and  $Re = Rm = 450$  in the absence of external forcing. Drag forces are found to affect the kinetic modes more than the magnetic modes as expected and explained in the text. The shift denotes the initial values of the kinetic and magnetic energies (at time  $t = 0$ ) are subtracted from the time evolution data of the corresponding variables. 109
- 3.9 Variation of time period of oscillation ( $T$ ) of kinetic and magnetic energy with  $k_0$ . [see Table 3.1] . . . . . 109
- 3.10 Time evolution of shifted kinetic energy [ $\delta KE = u^2(t) - u^2(0)$ ] per grid for three dimensional Arnold-Beltrami-Childress flow with  $N = 64^3$ ,  $U_0 = 0.1$ ,  $A = B = C = 1$ ,  $k_0 = 1$ ,  $M_s = 0.1$ ,  $M_A = 0.1$  (red), 0.2 (green), 0.3 (blue), 0.4 (magenta), 0.5 (black) and  $Re = Rm = 450$  in the absence of external forcing. The frequency of oscillation decreases with the increase of  $M_A$ . The shift denotes the initial values of the kinetic and magnetic energies (at time  $t = 0$ ) are subtracted from the time evolution data of the corresponding variables. . . . . 110



3.11	Time evolution of shifted kinetic energy $[\delta KE = u^2(t) - u^2(0)]$ per grid for three dimensional Arnold-Beltrami-Childress flow with $N = 64^3$ , $U_0 = 0.1$ , $A = B = C = 1$ , $k_0 = 1$ , $M_s = 0.1$ , $M_A = 0.5$ (red), 1 (blue), 1.5 (magenta) and $Re = Rm = 450$ in the absence of external forcing. The frequency of oscillation decreases with the increase of $M_A$ . The shift denotes the initial values of the kinetic and magnetic energies (at time $t = 0$ ) are subtracted from the time evolution data of the corresponding variables. . . . .	111
3.12	Variation of time period of oscillation ( $T$ ) of kinetic and magnetic energy with $M_A$ . [see Table 3.2] . . . . .	111
3.13	Saturation of magnetic energy with higher values of $M_A$ indicating “dynamo effect”. . . . .	112
3.14	Time evolution of shifted kinetic $[\delta KE = u^2(t) - u^2(0)]$ , magnetic $[\delta ME = B^2(t) - B^2(0)]$ and total energy $[\delta TE = u^2(t) - u^2(0) + B^2(t) - B^2(0)]$ per grid for three dimensional Arnold-Beltrami-Childress flow with $N = 64^3$ , $U_0 = 0.1$ , $A = B = C = 1$ , $k_0 = 1$ , $M_s = 0.1$ , $M_A = 1$ and $Re = Rm = 450$ in the presence of external forcing. The energy keeps on switching between kinetic and magnetic modes. The total energy also oscillates around the same frequency and the whole system acts as a forced-relaxed system. The shift denotes the initial values of the kinetic and magnetic energies (at time $t = 0$ ) are subtracted from the time evolution data of the corresponding variables. . . . .	113
3.15	Initial time evolution obtained from Fig. 3.14. . . . .	114
3.16	Intermediate time evolution obtained from Fig. 3.14. . . . .	114
3.17	Late time evolution obtained from Fig. 3.14. . . . .	115
3.18	Time evolution of kinetic and magnetic energy per grid for three dimensional Arnold-Beltrami-Childress flow with $N = 64^3$ , $U_0 = 0.1$ , $A = B = C = 1$ , $k_0 = 1$ , $M_s = 0.1$ , $M_A = 0.1$ and $Re = Rm = 450$ in the presence of external forcing. The shift denotes the initial values of the kinetic and magnetic energies (at time $t = 0$ ) are subtracted from the time evolution data of the corresponding variables. . . . .	115
3.19	Galerkin truncated two dimensional MHD equations representing similar nonlinear coherent oscillations observed in DNS results with $k = 1$ .	117
3.20	Galerkin truncated two dimensional MHD equations representing similar nonlinear coherent oscillations observed in DNS results with $k = 2$ .	117
3.21	Galerkin truncated two dimensional MHD equations representing similar nonlinear coherent oscillations observed in DNS results with $k = 4$ .	118

4.1	Conservation of magnetic (red solid) and fluid (blue dotted) helicity over a long time for Taylor - Green flow. . . . .	128
4.2	The shifted kinetic $[\delta KE = \frac{1}{2} \iiint_V \vec{u}^2(x, y, z, t) - \frac{1}{2} \iiint_V \vec{u}^2(x, y, z, 0)]$ (red solid) and magnetic $[\delta ME = \frac{1}{2} \iiint_V \vec{B}^2(x, y, z, t) - \frac{1}{2} \iiint_V \vec{B}^2(x, y, z, 0)]$ (blue dotted) energies of Taylor - Green flow oscillate with time exchanging energy between their respective modes. The shift is measured by the removal of the initial magnitude of kinetic and magnetic energy respectively. . . . .	129
4.3	The kinetic energy spectra $[E_k(= \sum \frac{u_k^2}{2})$ vs $k]$ from long time evolution of the Taylor-Green velocity profile. Even after several recurrence cycles, the energies are found to be contained in the large spatial scales only. The oscillation of the first five modes with time indicates a recurrence phenomena. The difference of energy in the fundamental mode oscillates with a magnitude of two orders of magnitude. . . . .	130
4.4	The magnetic energy spectra $[B_k(= \sum \frac{B_k^2}{2})$ vs $k]$ from long time evolution of the Taylor-Green velocity profile. Even after several recurrence cycles, the energies are found to be contained in the large spatial scales only. The oscillation of the first five modes with time indicates a recurrence phenomena. The difference of energy in the fundamental mode oscillates with a magnitude of two orders of magnitude. . . . .	130
4.5	The time evolution of kinetic and magnetic energy contained in fundamental mode for the Taylor-Green velocity profile. Energy is continuously exchanged between kinetic and magnetic variables for several cycles. . . . .	131
4.6	The time evolution of kinetic and magnetic energy contained in first five modes for the Taylor-Green velocity profile. All the five modes efficiently exchange energy between kinetic and magnetic variables leading to the happening of recurrence phenomena. . . . .	131
4.7	Conservation of magnetic (red solid) and fluid (blue dotted) helicity over a long time for Roberts flow. . . . .	133
4.8	The shifted kinetic $[\delta KE = \frac{1}{2} \iiint_V \vec{u}^2(x, y, z, t) - \frac{1}{2} \iiint_V \vec{u}^2(x, y, z, 0)]$ (red solid) and magnetic $[\delta ME = \frac{1}{2} \iiint_V \vec{B}^2(x, y, z, t) - \frac{1}{2} \iiint_V \vec{B}^2(x, y, z, 0)]$ (blue dotted) energies of Roberts flow oscillate with time exchanging energy between their respective modes. The shift is measured by the removal of the initial magnitude of kinetic and magnetic energy respectively. . . . .	133
4.9	The kinetic and magnetic energy spectra from long time evolution of the Roberts velocity profile. Even after several recurrence cycles, the energies are found to be contained in the large spatial scales only. . .	134

4.10	The kinetic and magnetic energy spectra from long time evolution of the Roberts velocity profile. Even after several recurrence cycles, the energies are found to be contained in the large spatial scales only. . .	134
4.11	The kinetic and magnetic energy spectra from long time evolution of the Roberts velocity profile. Even after several recurrence cycles, the energies are found to be contained in the large spatial scales only. . .	135
4.12	The kinetic and magnetic energy spectra from long time evolution of the Roberts velocity profile. Even after several recurrence cycles, the energies are found to be contained in the large spatial scales only. . .	135
4.13	Time evolution of magnetic (red solid), fluid (blue dotted) and total (magenta dashed) helicity over a long time for Arnold-Beltrami-Childress flow. . . . .	136
4.14	The shifted kinetic $[\delta KE = \frac{1}{2} \iiint_V \vec{u}^2(x, y, z, t) - \frac{1}{2} \iiint_V \vec{u}^2(x, y, z, 0)]$ (red solid) and magnetic $[\delta ME = \frac{1}{2} \iiint_V \vec{B}^2(x, y, z, t) - \frac{1}{2} \iiint_V \vec{B}^2(x, y, z, 0)]$ (blue dotted) energies for Arnold-Beltrami-Childress flow oscillate with time exchanging energy between their respective modes. The shift is measured by the removal of the initial magnitude of kinetic and magnetic energy respectively. . . . .	137
4.15	The kinetic and magnetic energy spectra from long time evolution of the Arnold-Beltrami-Childress velocity profile. Even after several recurrence cycles, the energies are found to be contained in the large spatial scales only. . . . .	138
4.16	The kinetic and magnetic energy spectra from long time evolution of the Arnold-Beltrami-Childress velocity profile. Even after several recurrence cycles, the energies are found to be contained in the large spatial scales only. . . . .	138
4.17	The kinetic and magnetic energy spectra from long time evolution of the Arnold-Beltrami-Childress velocity profile. Even after several recurrence cycles, the energies are found to be contained in the large spatial scales only. . . . .	139
4.18	The kinetic and magnetic energy spectra from long time evolution of the Arnold-Beltrami-Childress velocity profile. Even after several recurrence cycles, the energies are found to be contained in the large spatial scales only. . . . .	139
4.19	Time evolution of magnetic (red solid), fluid (blue dotted) and total (magenta dashed) helicity over a long time for Cat's Eye flow. . . . .	140

4.20	The shifted kinetic $[\delta KE = \frac{1}{2} \iiint_V \vec{u}^2(x, y, z, t) - \frac{1}{2} \iiint_V \vec{u}^2(x, y, z, 0)]$ (red solid) and magnetic $[\delta ME = \frac{1}{2} \iiint_V \vec{B}^2(x, y, z, t) - \frac{1}{2} \iiint_V \vec{B}^2(x, y, z, 0)]$ (blue dotted) energies for Cat's Eye flow oscillate with time exchanging energy between their respective modes. The shift is measured by the removal of the initial magnitude of kinetic and magnetic energy respectively. . . . .	141
4.21	The kinetic and magnetic energy spectra from long time evolution of the Cat's Eye velocity profile. Even after several recurrence cycles, the energies are found to be contained in the large spatial scales only.	142
4.22	The kinetic and magnetic energy spectra from long time evolution of the Cat's Eye velocity profile. Even after several recurrence cycles, the energies are found to be contained in the large spatial scales only.	142
4.23	The kinetic and magnetic energy spectra from long time evolution of the Cat's Eye velocity profile. Even after several recurrence cycles, the energies are found to be contained in the large spatial scales only.	143
4.24	The kinetic and magnetic energy spectra from long time evolution of the Cat's Eye velocity profile. Even after several recurrence cycles, the energies are found to be contained in the large spatial scales only.	143
4.25	The time evolution of Rayleigh Quotient $[Q(t)]$ for Taylor-Green (TG) and Arnold-Beltrami-Childress (ABC) flow. . . . .	144
4.26	Recurrence of velocity isosurfaces for Taylor-Green flow [Eq. 4.5] for the magnitudes 0.001, 0.05, 0.01. . . . .	146
4.27	Recurrence of magnetic field isosurfaces for Taylor-Green flow for the magnitudes 0.13, 0.16, 0.2. . . . .	147
4.28	Time evolution of velocity isosurfaces for Arnold-Beltrami-Childress flow [Eq.4.8] for the magnitudes 0.03, 0.05, 0.08, 0.1. . . . .	148
4.29	Time evolution of magnetic field isosurfaces for Arnold-Beltrami-Childress flow for the magnitudes 0.1, 0.133, 0.166, 0.2. . . . .	149
5.1	(Color online) Transition to dynamo like regime with the increase of $M_A$ from coherent nonlinear oscillation regime. $B^2(t)/B^2(0)$ shows the normalised magnetic energy as the Alfvén velocity changes with variation of $M_A$ . Thus a growth in normalised magnetic energy indicates a dynamo like phenomena to occur. However, at large $M_A$ , a saturation is found. . . . .	163

5.2	Kinematic Dynamo effect reproduced using the identical parameter regime ( $A = B = C = 1$ , $k_f = 1$ ) by Galloway <i>et al</i> [58]. The grid resolution is $64^3$ which is close to the value $60^3$ that was taken by Galloway <i>et al</i> [58]. The growth rates of magnetic energy $\left(\sum_V \frac{B^2(x,y,z)}{2}\right)$ of kinematic dynamo are found to increase as $Rm$ is increased. The oscillation frequency of the magnetic energy is also found to be similar as Galloway <i>et al</i> [58] . . . . .	166
5.3	Magnetic energy spectra at different times for ABC flow with the identical parameter described in Fig. (5.2) with $Rm = 450$ . The energy content in the large scales at late times shows that the short scales are equally important for a kinematic dynamo obtained from ABC flow. . . . .	166
5.4	Kinematic Dynamo effect for different driving frequency ( $k_f$ ). The magnetic energy is normalised with the initial magnitude at time $t = 0$ . The parameters chosen are $A = B = C = 1$ and $Re = Rm = 450$ with $U_0 = 1$ and $M_A = 1000$ . The initial growth rates are found to grow as $k_f$ is increased. . . . .	168
5.5	Kinematic Dynamo effect for different driving frequency ( $k_f$ ). The normalised magnetic energy is defined as $\left(\sum_V \frac{B^2(x,y,z,t)}{2} - \sum_V \frac{B^2(x,y,z,0)}{2}\right)$ . The parameters chosen are $A = B = C = 1$ and $Re = Rm = 450$ with $U_0 = 0.1$ and $M_A = 1000$ . The initial growth rates are found to grow and saturate as the $k_f$ is increased. . . . .	168
5.6	Kinematic Dynamo effect for different driving frequency ( $M_A$ ). The parameters chosen are $A = B = C = 1$ and $Re = Rm = 450$ with $U_0 = 1$ . The growth rates are found to be identical for different $M_A$ values. . . . .	169
5.7	Kinematic Dynamo effect for different driving frequency ( $M_A$ ). The parameters chosen are $A = B = C = 1$ and $Re = Rm = 450$ with $U_0 = 0.1$ . The growth rates are found to be identical for different $M_A$ values. . . . .	169
5.8	Self-consistent dynamo growth of kinetic $\left(\sum_V \frac{U^2(x,y,z)}{2}\right)$ and magnetic $\left(\sum_V \frac{B^2(x,y,z)}{2}\right)$ energy for ABC flow with $M_A = 1000$ and $k_f = 1$ for a long time with initial flow profile as ABC flow. . . . .	170
5.9	Self-consistent dynamo growth of kinetic and magnetic energy for two different initial conditions with $M_A = 1000$ and $k_f = 1$ . The initial growth rate of magnetic energy for ABC initial flow profile is found to be identical with that of random field profile. . . . .	171

---

5.10	Self-Consistent dynamo growth of kinetic and magnetic energy for five different initial velocities viz. $U_0 = 0.1, 0.2, 0.3, 0.4, 0.5$ , with $M_A = 1000$ , $A = B = C = 0.1$ and $k_f = 1$ . The initial growth rate of magnetic energy for ABC initial flow profile is found to be identical for all initial magnitude of velocities. . . . .	173
5.11	Self-Consistent dynamo growth of kinetic and magnetic energy for three different forcing magnitudes $A = 0.1, 0.2, 0.3$ having $A = B = C$ , with $M_A = 1000$ and $k_f = 1$ . The initial growth rate of magnetic energy for ABC initial flow profile is found to increase with the increment of magnitude of forcing. . . . .	173
5.12	Self-Consistent dynamo growth of kinetic and magnetic energy for $k_f = 1, 2, 4, 8, 16$ with $M_A = 1000$ . The growth rate of magnetic energy is found to be steeper with the increase of $k_f$ . The growth rate of kinetic energy due to external forcing decreases as $k_f$ is increased. .	174
5.13	Self-Consistent dynamo growth of kinetic and magnetic energy for $M_A = 1, 100, 1000$ . The back-reaction of magnetic field on velocity field is found to affect the growth rate and dynamics of velocity field. This effect is captured in the time evolution of kinetic energy for different $M_A$ . . . . .	176
5.14	Kinetic energy spectra for self-consistent dynamo with $U_0 = 0.1$ , $A = B = C = 0.1$ , $k_f = 1$ , $M_A = 1000$ , $Re = Rm = 450$ . . . . .	177
5.15	Kinetic energy spectra for self-consistent dynamo with $U_0 = 0.1$ , $A = B = C = 0.1$ , $k_f = 1$ , $M_A = 1000$ , $Re = Rm = 450$ . . . . .	177
5.16	Growth of kinetic and magnetic energy for $M_s = 0.1, 0.2, 0.3, 0.4, 0.5$ at $M_A = 100$ . The growth rate does not get much affected with the change of compressibility. . . . .	178

# Chapter 1

## Introduction

Plasma - a quasineutral composition of oppositely charged particles and neutrals exhibiting collective behaviour - appears in nature with a wide variety of lengths and time scales. The plasma in galaxies and stars spans a length scale of light-years and survives for several billion years [3]. On the other hand in terrestrial experiments plasmas cover a length scale of a few meters and the confinement time is around millisecond to at best tens of seconds for a single experimental shot [10]. However, one very appealing fact is that, the underlying fundamental physical laws that govern the dynamics of plasma occurring in burning stars as well as laboratory experiments are identical [60]. Hence, the basic equations governing the dynamics of such plasmas at both astrophysical and terrestrial devices are the same. The only difference lies in the magnitude and scales of the fields and hence the parameters involved into the equations. This striking similarity of the equations holding in the two different limits of length and time scales is because of the invariance of the fundamental equations over the spatial and temporal scales [61].

In laboratory devices, a very small fraction of ionisation of the neutral gas takes place due to thermal ionization. The degree of ionisation in such devices was first

estimated by Meghnad Saha by his Saha ionisation formula [62, 63]. The strong bias between the opposite electrodes for capacitively coupled discharges or the induced current for inductively coupled discharges, accelerates the electrons and the ions followed by an avalanche process of breakdown of the medium [64, 1]. On the contrary, because of the nuclear fusion process taking place at the core of a star, the strong thermal radiation coming out of the core, ionises the neutral atoms and forms a soup of ionised gas [8]. The strong gravitational force confines the plasma in the star and the convective flows facilitate the fusion process to continue. The electrons and ions of the hot plasma at the core of the star having very high kinetic energy, collide with one another and undergo nuclear fusion process through a quantum tunnelling process thereby releasing the binding energy of the nucleus in the form of thermal radiation. This thermal radiation pressure keeps the star burning, overpowering the gravitational pull that tries to quench the star. Once the star runs out of the thermal energy emitted from fusion process, it turns into a white dwarf [4] or a neutron star / black hole [5, 6] depending on the *irreducible mass* of the star [7]. In laboratories around the globe, several plasma reactor experiments are being carried out to mimic the fusion process occurring in stars [10, 15, 17, 14, 12, 16, 13]. Though the magnetic confinement used in terrestrial fusion reactors is fundamentally different from the gravitational confinement that holds the plasma in stars, the fundamental motive of such experiments is to harness the binding energy of atoms and transform it to the form of daily usable electricity for the service of mankind.

## 1.1 General properties of plasma:

In general, a plasma even though being an outcome of the ionized states of the neutral atoms, always tries to find equilibrium and thus abhors any gradient. In order to prevent a charge gradient in space, electrons having much higher mobility than ions very often shield the ions forming a Boltzmann distribution around the ions



and thereby maintain a quasi-neutrality in space [65]. Similarly in order to smooth out any spatial gradient, plasma responds with collective mode to any external perturbations. These properties primarily distinct a plasma from any general ionised gas [65]. In general, typically plasmas show the following three properties.

1. The number of charged particles within a sphere (called the Debye sphere whose radius is called as Debye screening length) surrounding a given charged particle, is high enough to shield the electrostatic interaction of the particles outside of the sphere.
2. Debye screening length (as defined above) is much short compared to the physical length scale the plasma spans.
3. The electron plasma frequency (measuring plasma oscillations of the electrons in the background of immobile ions) is large compared to the frequency of collisions between electrons and neutral particles (also called electron-neutral collision frequency).

## 1.2 Theoretical models of plasma:

There are several theoretical models that help to explain the behaviours observed in plasmas. It is important to note that none of the models explain all the phenomena observed, but each of them has certain regime of validity [66]. The high temperature fusion grade plasma is normally explained through kinetic theory, while the low temperature large scale behaviour of a plasma is modelled through a space-time averaged description such as a fluid model [66]. In kinetic theory, the distribution function of the particles is time evolved using Fokker-Planck or Vlasov-Maxwell equations and the motion of each particle can be studied [67]. In fluid theory, a fluid element is considered, within which there are sufficient particles having high enough

collisions that thermalise the fluctuations within the fluid element and thus help to maintain the physical measurable quantities identical throughout each of such elements [19]. Thus the collision mean-free path of each particle is much smaller than the length scale of the fluid element, which essentially means that a particle once entered a fluid element undergoes large number of collisions before leaving the same fluid element. Navier-Stokes equation is known to be a very successful model to explain the dynamics of fluid elements at different length and time scales.

### 1.3 MagnetoHydroDynamic model of plasma:

In case of a charged fluid, such as plasma, the motion of charged particles generates a magnetic field which in turn crucially governs the dynamics of the particle itself. Thus the Lorentz force term needs to be added to the Navier-Stokes equation. Also in order to track the time evolution of the magnetic field associated with each fluid element, I need to simultaneously solve all the Maxwell's equations self-consistently [18].

Thus the motion of the charged-fluid element in presence of self-generated magnetic field, gets primarily governed by the Maxwell's equations coupled with the Navier-Stokes equation which now includes a Lorentz force term. The subject that studies the self-consistent evolution of such a magnetised plasma-fluid is known as Magneto-Hydro-Dynamics (MHD) [18]. The theory of MHD is found to well-explain the phenomena observed in the astrophysical plasmas present in the Sun [68] or other young stars as well as in the fusion reactors, for example stellarators or tokamaks [8]. In fusion reactors, for example tokamaks, the core is nearly collisionless [9]. Along the field lines, even though the collisions (large angle Coulomb collisions) are nearly absent, the nonlinear MHD studies seem to work well [9]. Thus MHD theory

has been found to hold good even beyond its regime of validity.

Arguably, understanding plasma dynamics is the key to control the disruption of self-sustained plasma in fusion devices to improve the plasma-confinement time - an essential parameter for fusion to take place as well as prediction of plasma eruption, frequently occurring in the Sun that affects the magnetic field lines of the Earth quite heavily. The magnetic field-lines coupled with such plasma flow offer completely new dynamics and energy transfer mechanism within the plasma. Because of the strong coupling, the MHD fluid comes in a widely different variety and the dynamics of a fully developed turbulent magnetised plasma needs a separate careful treatment [20]. The inherent features of such plasma turbulence are needed to be understood and properly analysed to predict any extreme event taking place in our nearest star “The Sun” or to carefully operate the fusion reactors in the terrestrial laboratories.

## 1.4 Basic problems addressed in this thesis:

In case of a fully developed neutral fluid turbulence in three dimensions, typically the energy input occurs at the large scale lengths and then the kinetic energy cascades to the shorter length scales until viscous effects drag the energy out of the system [69]. The single fluid MHD model adds a new dimension to this problem. The single fluid model of MHD is primarily motivated from the wide difference of time scale of oscillation of electrons and the ions present in the plasma medium. The gyration frequency of the electrons being quite higher than that of the ions, the electrons always shields the ions, wherever the ions move. Thus the quasi-neutrality is maintained throughout the plasma and the plasma beyond its shielding length-scale, can be treated as a single fluid [18]. This treatment reduces the complexity of the governing equations as well as the computational cost of the simulation. Thus

long time evolution of any phenomena in the nonlinear regime can be well examined. In case of a single fluid MHD turbulence, even if the energy input happens at large scales of kinetic mode, the energy gets an alternate path to flow through the magnetic modes [23]. This opens up a possibility of energy exchange through forward and inverse cascades of energy, amongst different length-scales. Thus in some cases, the energy contained at the large scales keeps switching between the two modes [23]. One such phenomenon is nonlinear coherent oscillations of energy between the kinetic and magnetic scales thereby periodically destroying and re-constructing the fluid and magnetic flow profiles with time [24, 25]. Thus the extra dimension in the problem introduced through the magnetic variables, offers new interesting results full of surprises within the ambit of MHD model.

In this thesis I ask the question as to what happens to the fluid and magnetic field structures when the energy oscillates between these two modes. I find the frequency of this energy oscillation to scale linearly with Alfven speed. The variation of the frequency of oscillation with initial wave number is also analysed. I delineate a study of an analytical finite mode approximated incompressible MHD equations and explain such oscillations from the Galerkin truncated equations. For both two dimensional as well as three dimensional externally driven flows, I find that the MHD plasma system acts as a forced relaxed medium [23]. Further I find that for some typical chaotic flows in three dimensions, the initial velocity and magnetic field profile re-constructs back with time, but for some other profiles they do not do so. I extend an analytical approach used earlier by Thyagaraja [70] and explain the phenomena in the light of “effective degrees of freedom”. If the effective degrees of freedom is less, then the motion can be bounded and the system comes back to its initial profile over and over again - a recursion phenomenon - first identified by George David Birkhoff in 1927 [71]. Thus the phase space of ideal MHD system even though has very high degrees of freedom, consists of trapping region where, once the system starts its

motion continues to evolve and infinitely many times come arbitrarily close to the initial condition within the trapping region. Though counter-intuitive, such phenomena is observed in the present work for several different chaotic flows [24].

If the energy content of the magnetic modes is much lesser than the kinetic mode, the kinetic energy at large scales can directly channel to the magnetic scales through an external drive and accumulate in large [28] as well as short [29] scale magnetic energy. Such process is very common in astrophysical and geophysical systems and has been a crucial point of study from the middle of the twentieth century. The large and short scale magnetic field generation in the Sun [46] as well as in accretion disks [30, 31, 32] around any compact object (for example a neutron star or a black hole) is called “Dynamo Effect”. One of the most successful theoretical model to explain such effect was first identified by Eugene Newman Parker [28]. This large or intermediate scale magnetic field generated at the cost of kinetic energy primarily governs the dynamics of the charged fluid (plasma) through a time dependent Lorentz force term added in the Navier-Stokes equation, thereby adding an extra dimension to the already known and well-explored subject “fluid dynamics” [45]. In this thesis I explore the parameter regime for the fastest growth of magnetic energy when different amplitudes of drive are turned on in the flow. I study the cases where different initial wave-numbers are excited in the flow [55] using new computer simulation code with modest spectral spread.

## 1.5 Motivation for a new code:

Addressing some of these issues of magnetic field generation and plasma dynamics requires, efficient, well parallelized numerical solver capable of handling compressible MHD physics as well as numerical complexities. In order to simulate such a physical

process, the finite difference method based direct numerical simulation (DNS) [34] schemes require comparatively much larger time than the pseudo-spectral method [35]. In pseudo-spectral method, I take the spatial derivatives in the spectral space by taking the Fourier transform of the equations and the algebraic operations of the spatial variables are performed in the real space. Pseudo-spectral technique is observed to be much more accurate and faster method in the context of the performance of the code [35]. I have developed a three dimensional compressible MHD solver G-MHD3D, which considers continuity, momentum and energy equations for fluid and magnetic variables with a thermodynamic closure for pressure [36]. G-MHD3D uses conservative form in cartesian coordinates with GPU parallelization. The numerical solver I have developed captures Dynamo Effect for chaotic plasma flows at modest spectral resolution. The code is expected to contribute even more for better understanding of such turbulent phenomena in Cosmos. In the present thesis, DNS results are obtained from the code, operated at different parameter regimes identifying several novel nonlinear phenomena that addresses nonlinear energy cascades between the non-local length-scales of kinetic and magnetic variables.

This Thesis is divided into 6 chapters.

In **Chapter 2**, I describe the development of an MPI [72] parallel three dimensional pseudo-spectral DNS [34] code from scratch that governs the dynamics of plasma within the framework of single fluid MHD. In collaboration with NVIDIA, India, the code has been ported to GPU [36] and multi-GPU parallelisation using NVLink has recently been achieved. Pseudo-spectral technique is used to achieve better accuracy and faster performance over finite difference schemes [35]. In order to evaluate the Fourier transforms accurately and at low time cost, MPI parallel FFTW [73] routine is used extensively. For single GPU code, cuFFT [74] routine is

used alongwith openACC [75] parallelisation (shared memory architechture similar to OpenMP [37] parallelisation) while for multi-GPU code AccFFT [76] routine is used alongwith underlying MPI [72] parallelisation. The time solvers of the code are explicit for the ease of porting to GPU cards [39]. I provide the performance results at different GPU cards connected with NVLink [38]. Extensive physics benchmarking studies as well as numerical scaling studies of the code G-MHD3D is presented in this chapter along with GPU parallelization procedure, scalability and numerical as well as physics details. Alongwith the time evolution of the fluid elements I add some passive tracer particles in the MHD fluid and continuously notice the trajectory of these particles. These provide the spatial correlation between several fluid elements over time. It is envisaged that this new code with its extensive physics diagnostics and GPU scalability is able to address some of the fundamental physics issues in areas such as reconnection (a phenomenon of transforming back the magnetic energy to kinetic energy of the plasma), dynamos as well as MHD turbulence. The code is operated at different parameter regimes to explore the energy exchange through new pathways. Three such novel features are identified out of the present study and described in the following chapters.

**Chapter 3**, describes one of the most exclusive examples of such nonlinear energy exchange between kinetic and magnetic modes of single fluid MHD description of plasma. In the presence of weak resistivity, the MHD model is known to predict irreversible conversion of magnetic energy into fluid kinetic energy (i.e. reconnection) [45, 40, 41, 42, 43, 44] as well as conversion of kinetic energy into mean large-scale magnetic field (i.e. dynamo) [28, 29, 46, 30, 31, 32]. Therefore it is interesting to ask, for a given fluid type and magnetic field strength, are there fluid flow profiles for which, neither does the flow generate mean magnetic field nor the magnetic field energy is converted to flow energy; instead there are nearly “reversible” coherent nonlinear oscillations? From my DNS results from the code G-MHD3D I have

shown that both in two dimensions and three dimensions, the energy coherently oscillates between the large length scales of velocity and magnetic field variables until viscous and resistive effects drain the energy from the system. I also find that the coherent nonlinear oscillation persists for a wide range of initial flow speeds or Alfvén Mach number. A finite mode Galerkin representation of the two dimensional MHD equations is analytically carried out to verify the possibility of such energy exchange phenomena and I have found good agreement between my analytical and DNS results [23]. I also delineate the regime of validity of the analytical model and show departure of the results from the analytical model as I move in parameter space. Further effect of this frequency of oscillation is analysed on the initial wave number that is excited in the flow. Finally I study the driven dissipative systems under the action of the identical flows and find that plasma acts as a forced-relaxed system both in two and three spatial dimensions.

In **Chapter 4**, I perform detailed DNS study of single fluid MHD equations using G-MHD3D, for three dimensional chaotic flows at Alfvén resonance and find that for two different initial conditions, one flow reconstructs the initial fluid and magnetic flow profile and the other does not. I call this phenomena as “Recurrence”. In single dimension, recurrence was first observed in a chain of oscillators and this process is famously known as FPUT (Fermi-Pasta-Ulam-Tsingou) problem [77, 78]. The cause of such phenomenon was explained by Kruskal and Zabusky [79] introducing the idea of “solitons”. For hydrodynamic systems, in two spatial dimensions, reconstruction of initial data was first numerically observed by Yuen and Ferguson [80]. Thyagaraja [70] explained existence of such phenomena in nonlinear Schrodinger equation based on the analytical bound on Rayleigh Quotient which measures the effective number of active degrees of freedom of a system. The first ever statement on the possibility of recurrence came from Birkhoff in 1927, in his book Dynamical Systems [71]. Later, in another paper, Thyagaraja [81] commented on the difficulty of the exten-



sion of such approach to higher dimensional systems. In oceanographical references [48] and in the case of sand dunes [49] there are indications of observation of such recurrence and it is found that, this process critically depends on the initial condition of the system. To the best of my knowledge, recurrence has never been found in three dimensional MHD system. I delineate an explanation of my observation of recurrence in three dimensional MHD system by numerically checking boundedness of Rayleigh Quotient in a high dimensional system. Though “Recurrence” has been observed in many hydrodynamic systems earlier [47, 50], the cause of recurrence in MHD system is fundamentally different. As mentioned in the previous chapter, unlike hydrodynamic systems, in MHD system, the energy can oscillate between kinetic and magnetic modes thereby periodically destroying and reconstructing back the structures of the field variables - a phenomenon that gives birth to recurrence. Such effects can have wide applications in short time prediction of plasma disrupts in devices where magnetic confinement of plasma takes place and where real time plasma imaging can be performed. [24]

In **Chapter 5**, first I study the Alfven Mach scaling of the “Nonlinear coherent oscillation” observed in Chapter 3. I find that, as the Alfven Mach number ( $M_A$ ) is increased from unity, initially the frequency of oscillation scales linearly but slowly several other frequencies start generating, thereby breaking down the simple oscillation. It is believed to be due to excitation of short scales in the system as  $M_A$  is increased. The linear finite mode Galerkin expansion falls short to explain such phenomena and distant scales start to interact thereby complicating the energy flow mechanism. Finally I notice tendency to occur “dynamo” like phenomena in such system for increasing values of  $M_A$ . Next, I study the driven dissipative systems at very large Alfven Mach number ( $M_A$ ) leading to self-consistent stretch-twist-fold (STF) dynamo [51, 52] effect showing short-scale magnetic field generation from kinetic energy. The magnetic field lines are first stretched through the fluid flows,

then twisted and then again folded back [53]. This way, it generates short scales in the magnetic field variables. Arnold-Beltrami-Childress (ABC) flow is known to produce fastest kinematic dynamo effect [33]. However, in tokamak plasmas and in astrophysical plasmas, the back reaction of the magnetic field to the velocity field through the Lorentz force term is not negligible [9]. I report a saturation of such self-consistent dynamos where the back-reaction affects the flows unlike the kinematic counterpart. The saturation is expected because of the deviation of the flow profile from the ABC one, due to continuous back-reaction of magnetic variables to the fluid variables. Starting with ABC driven flow I find the dynamo effect to take place and optimal parameters for “fast” dynamo are obtained. For self-consistent evolution of the set of 3D MHD equations, the kinetic energy spectra is found to have a  $-5/3^{rd}$  scaling showing a fully developed Kolmogorov type of turbulence [54] even though the plasma dynamics significantly differs from that of the hydrodynamic one. From DNS study using G-MHD3D I also distinguish the optimal parameter set to obtain “fast” dynamo for ABC flows [55] at another spectral resolution.

Finally in **Chapter 6**, I consolidate my work and enumerate the major tasks that can be undertaken for further research in this field. Combining all the above results I have obtained, it becomes evident that, the single fluid MHD description of plasma offers new energy cascading pathways through kinetic as well as magnetic field variables thereby altering the nature of turbulence generally observed in well-studied hydrodynamic cases. Thus it can be stressed that in the study of plasma turbulence occurring in fusion devices or in astrophysical objects the fundamental energy cascading pathways play a crucial role and this needs to be analysed carefully.

# Chapter 2

## Numerical Technique

### 2.1 Motivation

A variety of plasmas - both in laboratory and in astrophysical conditions - sustain turbulence, which is often accompanied by large scale flows and self generated magnetic fields which in turn control the turbulence and regulate the plasma dynamics. Some of the examples are accretion disc formation, generation of large scale magnetic field via the dynamo process etc [82]. Analytical techniques work well in linear approximations of the governing equations of such plasma. However, in the longer time scales, because of the nonlinear interaction of several scales, analytical methods often fail to explain behaviours observed. In general, in order to understand such open problems, direct numerical simulation of the plasma becomes very necessary. Thus, it is very important to develop numerical solvers that simulate the basic governing equation of plasma at some specific limits accurately. The performance of the solver should also be fast enough to cater to the need of the physics problem. Keeping in mind the above requirements, as a part of the current Thesis, development of one such numerical solver from scratch has been attempted and physics result coming out of this solver is the main physics focus of this Thesis work.

As explained in Chapter 1, in this Thesis work, a MHD code G-MHD3D has been developed to simulate the three dimensional magneto-hydrodynamic plasma dynamics in a periodic domain and the code is applied to understand the fundamental physics of plasma dynamics including plasma turbulence with a better clarity.

The basic governing equations of this study are the continuity equation, momentum equation, induction equation and a proper equation of state or equivalent energy equation to attain the closure issue of fluid dynamics. The choice of equation for pressure is considered according to the physics problems of interest. It can be modified according to the need of the physical situation I need to handle.

The heart of the code is a pseudo-spectral technique which is computationally very fast [35] and accurate as compared to finite-difference methods. In this technique, the derivatives of any quantity is taken in its spectral space (Fourier transform of the quantity) and the time evolution is performed in the real space. Time integration schemes used are Runge-Kutta 4, Predictor-corrector method and Adam-Bashforth algorithms and the convergence of each of the methods are checked. Finally Adam-Bashforth algorithm is selected which suits my purpose the best because of the better performance of the method.

Due to their mass difference, the timescale of response for the two different species of plasma viz. electrons and ions, are quite disparate and hence the theoretical models describing the equations are taken as single fluid magnetohydrodynamic (MHD) equations. The single fluid MHD description of a plasma is quite approximated but has been found to serve aptly to explain many phenomena observed in laboratory and astrophysical systems [9]. Thus under certain criteria (described in Chapter

1), the plasma dynamics is believed to be well modelled through single fluid MHD equations. The two different charge species (electrons and ions) are assumed to form a single fluid because of the negligible mass of the electrons. A fluid element is assumed to be much larger than the length scale of separation between the two different charge species. Also the timescale at which the phenomena are observed are quite longer than the gyrofrequency of each of the charge species. Thus no large scale electric field is produced due to charge separation in the timescale of interest. This does not discard the inductive electric field generation due to the time dependent currents and the corresponding time dependent magnetic fields. This separation of force scales greatly reduces the computational cost of the code.

In order to speed-up the performance of the code, initially the OpenMP architecture is used and then MPI parallelisation is implemented into the CPU-code. However, for further improvement, the shared memory architecture used is OpenACC [75] which shares the memory of a Graphics Processing Unit (GPU) among different “threads” each having its own “thread memory”, together with a CPU. To further reduce the computation time, I finally use a distributed memory architecture called Message Passing Interface (MPI) together with the shared GPU parallelisation. Thus the code, in its present form, simultaneously runs on multiple GPU cards (“device”), on each card having a shared memory computation mentioned previously. The input and output of the code are copied from and to the CPUs (“host”). The details of the GPU computation, its code-lets and compilation procedure are documented in Section 2.7 of this Chapter. Thus, inspite of several well developed code for example, PENCIL and PLUTO etc., the development of my own code from scratch and its GPU parallelisation helped to reduce the computation time since the CPU computing is resource intensive and this has greatly helped me to perform the runs I have reported specially in Chapter 5.

The development of the code G-MHD3D also strengthens the numerical proficiency in working in several directions in future. The parallelised CPU as well as the GPU code is expected to be a fundamental tool to study varied problems in the magnetohydrodynamic plasma turbulence both in fusion devices as well as in modelling of several new astrophysical phenomena.

## 2.2 Code G-MHD3D

As discussed above, G-MHD3D is an OpenACC [75] parallel three dimensional weakly compressible, viscous, resistive magnetohydrodynamic GPU code. It is based on pseudo-spectral technique to address spontaneous magnetic field generation and related problems. The pseudo-spectral technique uses the cuFFT libraries which are considered as one of the fastest Fourier Transform GPU libraries available [74]. Pseudo-spectral technique is applied to calculate the spatial derivatives and to evaluate the non-linear terms involved in the basic underlying equations. The time derivative is solved using multiple time solvers viz. Adams-Bashforth, Runge-Kutta 4 and Predictor-Corrector algorithms and all the solvers has been checked to provide identical results with each-other. The velocity and the magnetic field strength has been normalised with the sound speed and the Alfvén speed in the system. The salient features of the OpenMP parallel CPU code - MHD3D and G-MHD3D are listed in Table 2.1.

G-MHD3D is capable of handling weakly compressible fluids, that uses pseudo-spectral technique for spatial discretisation with a standard de-aliasing by 2/3 truncation rule to simulate the set of single fluid MHD equations. The equations are evaluated in three dimensions with periodic boundary conditions in cartesian coordinates. I use the multi-dimensional FFTW libraries to evaluate the fourier transforms, whenever needed.

In the following, I provide the specifications of the basic details and the salient features of my 3D MHD code both for CPU and GPU versions.

Type of equations	Compressible Navier-Stokes + Maxwell's Equations
Dimensionality	2D & 3D
Spatial Derivative Solver	Pseudo-Spectral
Time update	Adams-Bashforth, Runge-Kutta 4, Predictor-Corrector
Computer architecture	CPU, GPU (NVIDIA)
Parallelization	OpenMP, MPI, OpenACC
External Libraries	FFTW, cuFFT
Precision	Double
Language	Fortran 95

Table 2.1: Features of MHD3D and G-MHD3D.

## 2.3 Governing equations

The basic equations that are evolved in G-MHD3D with different specific initial conditions are as follows:

$$\text{Mass density: } \frac{\partial \rho}{\partial t} + \vec{\nabla} \cdot (\rho \vec{u}) = 0 \quad (2.1)$$

$$\begin{aligned} \text{Momentum equation: } \frac{\partial(\rho \vec{u})}{\partial t} + \vec{\nabla} \cdot [\rho \vec{u} \otimes \vec{u}] &= \frac{\vec{J} \times \vec{B}}{c} - \vec{\nabla} P \\ &+ \vec{\nabla} \cdot (2\nu \rho \vec{\bar{S}}) + \rho \vec{F} \end{aligned} \quad (2.2)$$

$$\text{Shear viscosity:} \quad S_{ij} = \frac{1}{2}(\partial_i u_j + \partial_j u_i) - \frac{1}{3}\delta_{ij}\theta \quad (2.3)$$

$$\text{Dilation:} \quad \theta = \vec{\nabla} \cdot \vec{u} \quad (2.4)$$

$$\text{Equation of state:} \quad P = \gamma\rho KT = C_s^2\rho \quad (2.5)$$

$$\text{Non relativistic Ampere's law:} \quad \vec{J} = \frac{c}{4\pi}\vec{\nabla} \times \vec{B} \quad (2.6)$$

$$\text{Faraday's law:} \quad \frac{\partial \vec{B}}{\partial t} = -c\vec{\nabla} \times \vec{E} \quad (2.7)$$

$$\text{Ohm's law:} \quad \vec{E} + \frac{\vec{u} \times \vec{B}}{c} = \frac{1}{\sigma}\vec{J} \quad (2.8)$$

$$\text{No magnetic monopole:} \quad \vec{\nabla} \cdot \vec{B} = 0 \quad (2.9)$$

In this system of equations,  $\rho$ ,  $\vec{u}$ ,  $P$  and  $\vec{B}$  are the density, velocity, kinetic pressure and magnetic field of a fluid element respectively.  $C_s$  is assumed as constant. The coefficient of kinematic viscosity, magnetic resistivity and charge density are denoted as  $\mu$ ,  $\eta$   $\sigma$  and it is assumed that all of these are constants over space and time. The symbol “ $\otimes$ ” represents the dyadic between two vector quantities.

The kinetic Reynolds number ( $Re$ ) and magnetic Reynolds number ( $Rm$ ) are defined as  $Re = \frac{U_0 L}{\mu}$  and  $Rm = \frac{U_0 L}{\eta}$  where  $U_0$  is the maximum velocity of the fluid system to start with and  $L$  is the system length.

I also define the sound speed of the fluid as  $C_s = \frac{U_0}{M_s}$ , where,  $M_s$  is the sonic Mach number of the fluid. The Alfven speed is determined from  $V_A = \frac{U_0}{M_A}$  where  $M_A$  is the Alfven Mach number of the plasma. The initial magnetic field present in the plasma is determined from the relation  $B_0 = V_A \sqrt{\rho_0}$ , where,  $\rho_0$  is the initial density value of the fluid.

Substituting 2.6 into 2.2, I obtain,

$$\frac{\partial(\rho\vec{u})}{\partial t} + \vec{\nabla} \cdot \left[ \rho\vec{u} \otimes \vec{u} + \left( P + \frac{1}{8\pi}|\vec{B}|^2 \right) \mathbf{I} - \frac{1}{4\pi}\vec{B} \otimes \vec{B} \right] = \vec{\nabla} \cdot (2\nu\rho\vec{S}) + \rho\vec{F}$$



Substituting 2.8 into 2.7 and using 2.6 & 2.9, I obtain,

$$\begin{aligned}
 \frac{\partial \vec{B}}{\partial t} &= -c \vec{\nabla} \times \left[ -\frac{\vec{u} \times \vec{B}}{c} + \frac{1}{\sigma} \vec{J} \right] = \vec{\nabla} \times \vec{u} \times \vec{B} - \frac{c}{4\pi\sigma} \vec{\nabla} \times \vec{\nabla} \times \vec{B} \\
 &= \vec{\nabla} \times \vec{u} \times \vec{B} + \frac{c}{4\pi\sigma} \nabla^2 \vec{B} \\
 \Rightarrow \quad \frac{\partial \vec{B}}{\partial t} + \vec{\nabla} \cdot (\vec{u} \otimes \vec{B} - \vec{B} \otimes \vec{u}) &= \frac{c}{4\pi\sigma} \nabla^2 \vec{B} \\
 \Rightarrow \quad \frac{\partial \vec{B}}{\partial t} + \vec{\nabla} \cdot (\vec{u} \otimes \vec{B} - \vec{B} \otimes \vec{u}) &= \eta \nabla^2 \vec{B}, \quad \text{where, } \eta = \frac{c}{4\pi\sigma}
 \end{aligned}$$

The internal energy ( $E$ ) is evaluated by the time evolution of the following equation:

$$\frac{\partial E}{\partial t} + \vec{\nabla} \cdot \left[ (E + P_{tot}) \vec{u} - \frac{1}{4\pi} \vec{u} \cdot (\vec{B} \otimes \vec{B}) - 2\nu\rho\vec{u} \cdot \vec{\bar{S}} - \frac{\eta}{4\pi} \vec{B} \times (\vec{\nabla} \times \vec{B}) \right] = 0$$

where  $E = \rho\epsilon_{int} + \frac{1}{2}\rho|\vec{u}|^2 + \frac{1}{8\pi}|\vec{B}|^2$  and  $P_{tot} = P + \frac{1}{8\pi}|\vec{B}|^2$ .

Thus the complete set of MHD equations in conservative form are

$$\frac{\partial \rho}{\partial t} + \vec{\nabla} \cdot (\rho\vec{u}) = 0 \tag{2.10}$$

$$\frac{\partial(\rho\vec{u})}{\partial t} + \vec{\nabla} \cdot \left[ \rho\vec{u} \otimes \vec{u} + \left( P + \frac{1}{8\pi}|\vec{B}|^2 \right) \mathbf{I} - \frac{1}{4\pi} \vec{B} \otimes \vec{B} \right] = \vec{\nabla} \cdot (2\nu\rho\vec{\bar{S}}) + \rho\vec{F} \tag{2.11}$$

$$\frac{\partial E}{\partial t} + \vec{\nabla} \cdot \left[ (E + P_{tot}) \vec{u} - \frac{1}{4\pi} \vec{u} \cdot (\vec{B} \otimes \vec{B}) - 2\nu\rho\vec{u} \cdot \vec{\bar{S}} - \frac{\eta}{4\pi} \vec{B} \times (\vec{\nabla} \times \vec{B}) \right] = 0 \tag{2.12}$$

$$\frac{\partial \vec{B}}{\partial t} + \vec{\nabla} \cdot (\vec{u} \otimes \vec{B} - \vec{B} \otimes \vec{u}) = \eta \nabla^2 \vec{B} \tag{2.13}$$

Thus equation 2.10, 2.13 denote the continuity, momentum, energy and induction equation for a magnetised plasma. The complete set of equations in component form for a three dimensional plasma becomes,

$$\frac{\partial \rho}{\partial t} + \frac{\partial}{\partial x}(\rho u_x) + \frac{\partial}{\partial y}(\rho u_y) + \frac{\partial}{\partial z}(\rho u_z) = 0$$

$$\begin{aligned}
 \frac{\partial(\rho u_x)}{\partial t} + \frac{\partial}{\partial x} \left[ \rho u_x u_x + P_{tot} - \frac{1}{4\pi} B_x B_x - 2\nu\rho S_{xx} \right] \\
 + \frac{\partial}{\partial y} \left[ \rho u_x u_y - \frac{1}{4\pi} B_x B_y - 2\nu\rho S_{xy} \right] + \frac{\partial}{\partial z} \left[ \rho u_x u_z - \frac{1}{4\pi} B_x B_z - 2\nu\rho S_{xz} \right] &= \rho F_x \\
 \frac{\partial(\rho u_y)}{\partial t} + \frac{\partial}{\partial x} \left[ \rho u_y u_x - \frac{1}{4\pi} B_y B_x - 2\nu\rho S_{yx} \right] \\
 + \frac{\partial}{\partial y} \left[ \rho u_y u_y + P_{tot} - \frac{1}{4\pi} B_y B_y - 2\nu\rho S_{yy} \right] + \frac{\partial}{\partial z} \left[ \rho u_y u_z - \frac{1}{4\pi} B_y B_z - 2\nu\rho S_{yz} \right] &= \rho F_y \\
 \frac{\partial(\rho u_z)}{\partial t} + \frac{\partial}{\partial x} \left[ \rho u_z u_x - \frac{1}{4\pi} B_z B_x - 2\nu\rho S_{zx} \right] \\
 + \frac{\partial}{\partial y} \left[ \rho u_z u_y - \frac{1}{4\pi} B_z B_y - 2\nu\rho S_{zy} \right] + \frac{\partial}{\partial z} \left[ \rho u_z u_z + P_{tot} - \frac{1}{4\pi} B_z B_z - 2\nu\rho S_{zz} \right] &= \rho F_z
 \end{aligned}$$

$$\begin{aligned}
 \frac{\partial E}{\partial t} + \frac{\partial}{\partial x} \left[ (E + P_{tot}) u_x - \frac{1}{4\pi} (u_x B_x B_x + u_y B_x B_y + u_z B_x B_z) \right. \\
 \left. - 2\nu\rho (u_x S_{xx} + u_y S_{xy} + u_z S_{xz}) \right. \\
 \left. - \frac{\eta}{4\pi} \left\{ B_y \left( \frac{\partial B_y}{\partial x} - \frac{\partial B_x}{\partial y} \right) + B_z \left( \frac{\partial B_z}{\partial x} - \frac{\partial B_x}{\partial z} \right) \right\} \right] \\
 + \frac{\partial}{\partial y} \left[ (E + P_{tot}) u_y - \frac{1}{4\pi} (u_x B_y B_x + u_y B_y B_y + u_z B_y B_z) \right. \\
 \left. - 2\nu\rho (u_x S_{yx} + u_y S_{yy} + u_z S_{yz}) \right. \\
 \left. + \frac{\eta}{4\pi} \left\{ B_x \left( \frac{\partial B_y}{\partial x} - \frac{\partial B_x}{\partial y} \right) - B_z \left( \frac{\partial B_z}{\partial y} - \frac{\partial B_y}{\partial z} \right) \right\} \right] \\
 + \frac{\partial}{\partial z} \left[ (E + P_{tot}) u_z - \frac{1}{4\pi} (u_x B_z B_x + u_y B_z B_y + u_z B_z B_z) \right. \\
 \left. - 2\nu\rho (u_x S_{zx} + u_y S_{zy} + u_z S_{zz}) \right. \\
 \left. + \frac{\eta}{4\pi} \left\{ B_x \left( \frac{\partial B_z}{\partial x} - \frac{\partial B_x}{\partial z} \right) + B_y \left( \frac{\partial B_z}{\partial y} - \frac{\partial B_y}{\partial z} \right) \right\} \right] = 0
 \end{aligned}$$

$$\begin{aligned}
 \frac{\partial B_x}{\partial t} - \left[ \frac{\partial}{\partial y} (u_x B_y - u_y B_x) + \frac{\partial}{\partial z} (u_x B_z - u_z B_x) \right] &= \eta \left( \frac{\partial^2 B_x}{\partial x^2} + \frac{\partial^2 B_x}{\partial y^2} + \frac{\partial^2 B_x}{\partial z^2} \right) \\
 \frac{\partial B_y}{\partial t} + \left[ \frac{\partial}{\partial x} (u_x B_y - u_y B_x) - \frac{\partial}{\partial z} (u_y B_z - u_z B_y) \right] &= \eta \left( \frac{\partial^2 B_y}{\partial x^2} + \frac{\partial^2 B_y}{\partial y^2} + \frac{\partial^2 B_y}{\partial z^2} \right) \\
 \frac{\partial B_z}{\partial t} + \left[ \frac{\partial}{\partial x} (u_x B_z - u_z B_x) + \frac{\partial}{\partial y} (u_y B_z - u_z B_y) \right] &= \eta \left( \frac{\partial^2 B_z}{\partial x^2} + \frac{\partial^2 B_z}{\partial y^2} + \frac{\partial^2 B_z}{\partial z^2} \right)
 \end{aligned}$$

$$\begin{aligned}
 P_{tot} &= P_{th} + \frac{1}{8\pi}(B_x^2 + B_y^2 + B_z^2); \quad P_{th} = C_s^2 \rho \\
 S_{xx} &= \frac{du_x}{dx} - \frac{1}{3} \left( \frac{du_x}{dx} + \frac{du_y}{dy} + \frac{du_z}{dz} \right); \quad S_{xy} = \frac{1}{2} \left( \frac{du_y}{dx} + \frac{du_x}{dy} \right); \quad S_{xz} = \frac{1}{2} \left( \frac{du_z}{dx} + \frac{du_x}{dz} \right) \\
 S_{yx} &= \frac{1}{2} \left( \frac{du_x}{dy} + \frac{du_y}{dx} \right); \quad S_{yy} = \frac{du_y}{dy} - \frac{1}{3} \left( \frac{du_x}{dx} + \frac{du_y}{dy} + \frac{du_z}{dz} \right); \quad S_{yz} = \frac{1}{2} \left( \frac{du_z}{dy} + \frac{du_y}{dz} \right) \\
 S_{zx} &= \frac{1}{2} \left( \frac{du_x}{dz} + \frac{du_z}{dx} \right); \quad S_{zy} = \frac{1}{2} \left( \frac{du_y}{dz} + \frac{du_z}{dy} \right); \quad S_{zz} = \frac{du_z}{dz} - \frac{1}{3} \left( \frac{du_x}{dx} + \frac{du_y}{dy} + \frac{du_z}{dz} \right)
 \end{aligned}$$

The forcing determines a spatial averaged velocity of the system ( $\langle |\vec{U}(x, y, z, t)| \rangle_{x,y,z}$ ) in the presence of uniform dissipation ( $\nu \neq 0$ ). A reference scale for pressure ( $P_{ref}$ ) and density ( $\rho_{ref}$ ) is fixed to determine the reference sound speed ( $C_{s_{ref}}$ ). This provides a sonic Mach Number at steady state ( $M_s = \frac{\langle |\vec{U}(x,y,z,t)| \rangle_{x,y,z}}{C_{s_{ref}}}$ ). I also evaluate a dynamic sound speed,  $C_s(t) = \sqrt{\frac{\gamma \langle P(x,y,z,t) \rangle_{x,y,z}}{\langle \rho(x,y,z,t) \rangle_{x,y,z}}}$ . The dynamic Alfven speed is determined by  $V_A(t) = \frac{\langle |\vec{B}(x,y,z,t)| \rangle_{x,y,z}}{4\pi \sqrt{\langle \rho(x,y,z,t) \rangle_{x,y,z}}}$ . Thus one can evaluate the dynamic Alfven Mach number as  $M_A(t) = \frac{\langle |\vec{U}(x,y,z,t)| \rangle_{x,y,z}}{V_A(t)}$ .

### 2.3.1 Normalisation of the MHD equations

The normalisation of MHD equations used in the work are provided below. The equation of state is considered as  $P = C_s^2 \rho$ . Here the equations of unforced turbulence are dealt by setting  $F = 0$ . For simplicity, it is also assumed that, the off-diagonal components of the viscosity terms are zero. For the sake of elucidation, only for the following discussion, the Lorentz force term ( $\vec{J} \times \vec{B}$ ) is considered to be absent in the momentum equation. Then the reduced set of equations are

$$\frac{\partial \rho}{\partial t} + \vec{\nabla} \cdot (\rho \vec{u}) = 0 \quad (2.14)$$

$$\frac{\partial \vec{u}}{\partial t} + (\vec{u} \cdot \vec{\nabla}) \vec{u} = -C_s^2 \frac{\vec{\nabla} \rho}{\rho} + \frac{\nu}{\rho} \nabla^2 \vec{u} \quad (2.15)$$

$$\frac{\partial \vec{B}}{\partial t} + \vec{\nabla} \times \vec{u} \times \vec{B} = \eta \nabla^2 \vec{B} \quad (2.16)$$

Let us define  $\rho = \rho_0 \tilde{\rho}$ ,  $t = t_0 \tilde{t}$  and  $\vec{r} = L \vec{\tilde{r}}$  where,  $\rho_0$  be the initial density value of the fluid,  $L$  be the characteristic length-scale and  $t_0$  be a characteristic timescale.

Eq. 2.14 can be written as

$$\frac{\rho_0}{t_0} \frac{\partial \tilde{\rho}}{\partial \tilde{t}} + \frac{\rho_0 u_0}{L} \vec{\nabla} \cdot (\tilde{\rho} \vec{\tilde{u}}) = 0$$

Defining,  $u_0 = \frac{L}{t_0}$ , I obtain,

$$\frac{\partial \tilde{\rho}}{\partial \tilde{t}} + \vec{\nabla} \cdot (\tilde{\rho} \vec{\tilde{u}}) = 0$$

Eq. 2.15 can be written as,

$$\begin{aligned} \frac{L}{t_0^2} \frac{\partial \vec{\tilde{u}}}{\partial \tilde{t}} + \frac{L}{t_0^2} \left( \vec{\tilde{u}} \cdot \vec{\nabla} \right) \vec{\tilde{u}} &= -\frac{C_s^2}{L} \frac{\vec{\nabla} \tilde{\rho}}{\tilde{\rho}} + \frac{\nu}{\rho_0 L t_0} \frac{\vec{\nabla}^2 \vec{\tilde{u}}}{\tilde{\rho}} \\ \Rightarrow \frac{\partial \vec{\tilde{u}}}{\partial \tilde{t}} + \left( \vec{\tilde{u}} \cdot \vec{\nabla} \right) \vec{\tilde{u}} &= -\frac{C_s^2}{u_0^2} \frac{\vec{\nabla} \tilde{\rho}}{\tilde{\rho}} + \frac{\nu}{\rho_0 L u_0} \frac{\vec{\nabla}^2 \vec{\tilde{u}}}{\tilde{\rho}} \\ \Rightarrow \frac{\partial \vec{\tilde{u}}}{\partial \tilde{t}} + \left( \vec{\tilde{u}} \cdot \vec{\nabla} \right) \vec{\tilde{u}} &= -\frac{1}{M_s^2} \frac{\vec{\nabla} \tilde{\rho}}{\tilde{\rho}} + \frac{1}{Re} \frac{\vec{\nabla}^2 \vec{\tilde{u}}}{\tilde{\rho}} \end{aligned}$$

where,  $M_s = \frac{u_0}{C_s}$  and  $Re = \frac{\rho_0 u_0 L}{\nu}$

Eq. 2.16 can be written as

$$\begin{aligned} \frac{B_0}{t_0} \frac{\partial \vec{\tilde{B}}}{\partial \tilde{t}} + \frac{B_0}{t_0} \vec{\nabla} \times \vec{\tilde{u}} \times \vec{\tilde{B}} &= \frac{\eta B_0}{L^2} \vec{\nabla}^2 \vec{\tilde{B}} \\ \Rightarrow \frac{\partial \vec{\tilde{B}}}{\partial \tilde{t}} + \vec{\nabla} \times \vec{\tilde{u}} \times \vec{\tilde{B}} &= \frac{\eta t_0}{L^2} \vec{\nabla}^2 \vec{\tilde{B}} \\ \Rightarrow \frac{\partial \vec{\tilde{B}}}{\partial \tilde{t}} + \vec{\nabla} \times \vec{\tilde{u}} \times \vec{\tilde{B}} &= \frac{\eta}{L u_0} \vec{\nabla}^2 \vec{\tilde{B}} \\ \Rightarrow \frac{\partial \vec{\tilde{B}}}{\partial \tilde{t}} + \vec{\nabla} \times \vec{\tilde{u}} \times \vec{\tilde{B}} &= \frac{1}{R_m} \vec{\nabla}^2 \vec{\tilde{B}} \end{aligned}$$

where,  $R_m = \frac{Lu_0}{\eta}$ .

Removing the tilde-sign (“~”) from the variables, I write the equations as:

$$\begin{aligned}\frac{\partial \rho}{\partial t} + \vec{\nabla} \cdot (\rho \vec{u}) &= 0 \\ \frac{\partial \vec{u}}{\partial t} + (\vec{u} \cdot \vec{\nabla}) \vec{u} &= -\frac{1}{M_s^2} \frac{\vec{\nabla} \rho}{\rho} + \frac{1}{Re} \frac{\nabla^2 \vec{u}}{\rho} \\ \frac{\partial \vec{B}}{\partial t} + \vec{\nabla} \times \vec{u} \times \vec{B} &= \frac{1}{R_m} \nabla^2 \vec{B}\end{aligned}$$

This normalisation is followed throughout the code G-MHD3D which of-course includes the  $\vec{J} \times \vec{B}$  term as well.

In order to check the accuracy of the numerical solver developed, first several two dimensional basic numerical tests are performed, and then the three dimensional numerical tests are described.

## 2.4 Two dimensional numerical tests

To begin with, two dimensional numerical checks of my code at hydrodynamic as well as magnetohydrodynamic limits are performed. The numerical tests indicate several details of such technique learnt and are discussed at length in the following Sections.

### 2.4.1 Incompressible hydrodynamic flow

In two dimensions, the Navier-Stokes equation in velocity variables with compressibility effects become,

$$\begin{aligned}\frac{\partial \rho}{\partial t} + \vec{\nabla} \cdot (\rho \vec{u}) &= 0 \\ \frac{\partial \vec{u}}{\partial t} + (\vec{u} \cdot \vec{\nabla}) \vec{u} &= \frac{\mu}{\rho} \nabla^2 \vec{u} - \frac{C_s^2}{\rho} \vec{\nabla} \rho\end{aligned}$$

For incompressible fluid, the Navier-Stokes equation in vorticity and stream-function variables become,

$$\begin{aligned}\frac{\partial \vec{\omega}}{\partial t} + \vec{u} \cdot \vec{\nabla} \vec{\omega} &= \nu \nabla^2 \vec{\omega} \\ \vec{\omega} &= \vec{\nabla} \times \vec{u}\end{aligned}$$

Another pseudo-spectral code is developed that simulates the above equations and its results for some typical initial flow profiles are checked with the present code at the appropriate incompressible limit.

In order to simulate the two dimensional hydrodynamic fluid, the equations in velocity variables are time evolved and the growth rate of Kelvin-Helmholtz instability is reproduced for a broken jet in the incompressible limit analytically calculated earlier by Drazin [83]. The analytical formula obtained by Drazin [83] in my notation becomes,

$$\begin{aligned}\gamma &= \frac{k_x U_0}{3} \left[ \sqrt{3} - 2 \frac{k_x}{R_E} - 2 \left\{ \left( \frac{k_x}{R_E} \right)^2 + 2 \sqrt{3} \frac{k_x}{R_E} \right\}^{\frac{1}{2}} \right] \\ R_E &= \frac{U_0 d}{\nu}\end{aligned}$$

where  $\gamma$  is growth rate,  $k_x$  is the mode number of perturbation,  $R_E$  is the Reynolds

number,  $U_0$  is the maximum fluid velocity,  $d$  is the shear width and  $\nu$  is the coefficient of viscosity. I run my simulation with parameters  $N_x = N_y = 512$ ;  $L_x = L_y = 2\pi$ ;  $\omega_0 = 25$ ;  $d = \frac{3\pi}{128}$ ;  $\nu = 1.5 \times 10^{-3}$ . The initial velocity profile is obtained from the vorticity profile given by  $\omega = \frac{\omega_0}{\cosh^2\left(\frac{y-3L_y/4}{d}\right)} - \frac{\omega_0}{\cosh^2\left(\frac{y-L_y/4}{d}\right)}$ . The identical growth rate from this code with  $M = 0.05$  is obtained and checked with another code that simulates the Navier-Stokes equation in vorticity formalism (mentioned earlier) with  $M = 0$  [Fig 2.3]. The same growth rate from another existing, well-benchmarked code AG-Spect [56] at the limit of negligible visco-elasticity ( $\tau_m = 10^{-4}$ ) [Fig 2.4] is also obtained. For this benchmarking the initial condition that have been used is  $\omega = \frac{\omega_0}{\cosh^2\left(\frac{y+L_y/4}{d}\right)} - \frac{\omega_0}{\cosh^2\left(\frac{y-L_y/4}{d}\right)} + \frac{\omega_0}{\cosh^2\left(\frac{y-3L_y/4}{d}\right)} - \frac{\omega_0}{\cosh^2\left(\frac{y+3L_y/4}{d}\right)}$  with  $\omega_0 = 2$  and  $k_x = 3$ . The Kelvin-Helmholtz instability with a velocity gradient is also reproduced and the same growth rate given by Ray [84] is found.

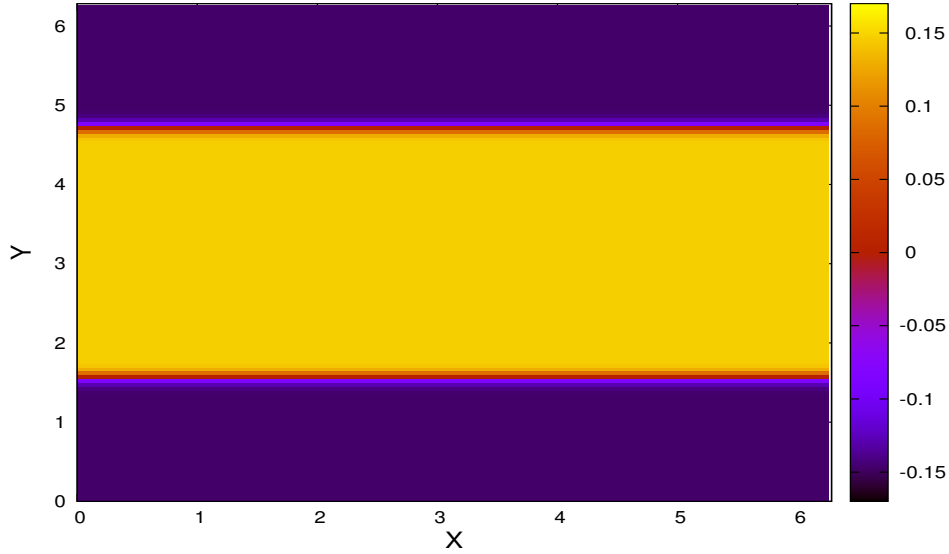


Figure 2.1: Initial velocity profile of K-H instability.

### 2.4.2 Weakly compressible hydrodynamic flow

In order to check the code in the compressible regime, identical growth rates are reproduced for the hydrodynamic limit as numerically obtained by Keppens et al [57]

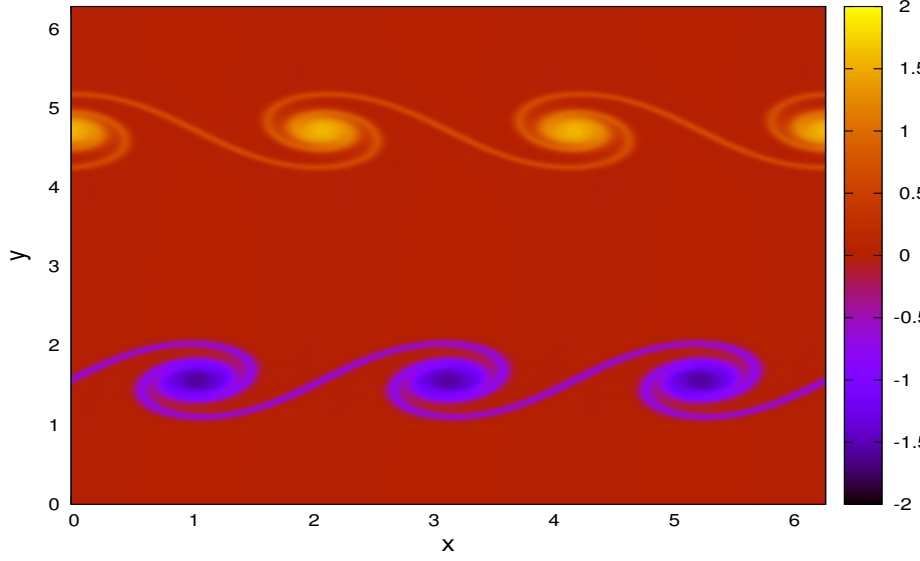


Figure 2.2: Snapshot of vorticity profile of K-H instability for  $K_x = 3$  at time  $t = 21.9$  with grid resolution  $N_x = N_y = 256$ ,  $L_x = L_y = 2\pi$ ,  $\nu = 10^{-4}$ ,  $dt = 10^{-3}$ ,  $\omega_0 = 2$ ,  $d = \frac{3\pi}{128}$  and  $M = 0$ .

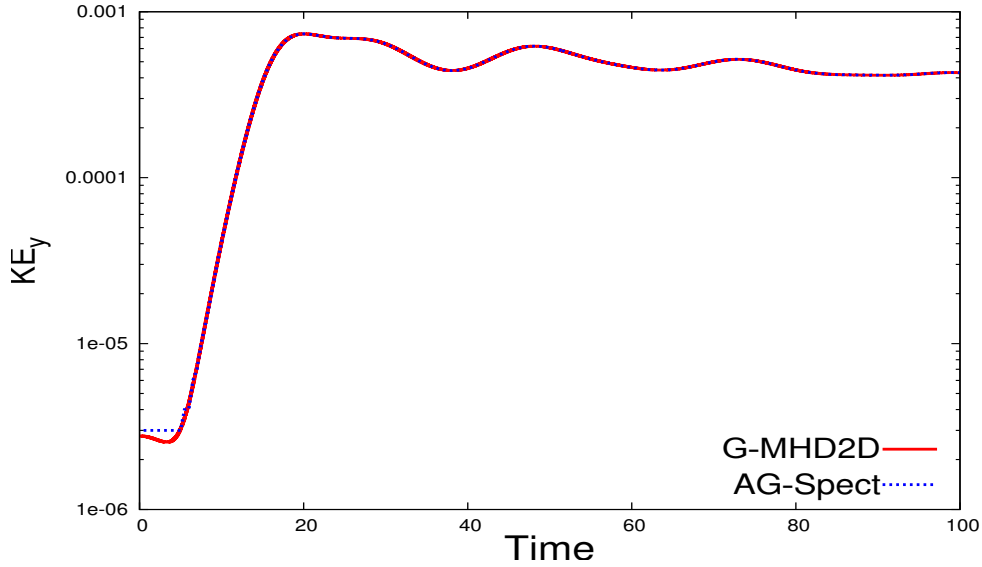


Figure 2.3: Comparison of kinetic energy in y-direction of K-H instability for  $k_x = 3$  with AGSpect [56] for  $M = 0.05$

for a compressible K-H flow [Fig 2.5]. Following Keppens et al [57], a velocity profile  $u_x = U_0 \left[ \tanh\left(\frac{y-L_y/3}{a}\right) - \tanh\left(\frac{y-L_y/3}{a}\right) - 1 \right]$  is chosen with a shear width  $a = 0.05$  and a sinusoidal perturbation in perpendicular direction to the initial flow velocity  $u_y = u_{y0} \sin(kx) \exp\left[-\frac{(y-L_y/3)^2}{\sigma^2}\right] + u_{y0} \sin(kx) \exp\left[-\frac{(y-2L_y/3)^2}{\sigma^2}\right]$  with  $U_0 = 0.645$ ,  $u_{y0} = 10^{-4}$ ,  $k_x = 2\pi$  and  $\sigma = 4a$  is excited.  $\gamma = \frac{5}{3}$ ,  $P_0 = 1 = \rho_0$ ,  $L_x = 1$  and



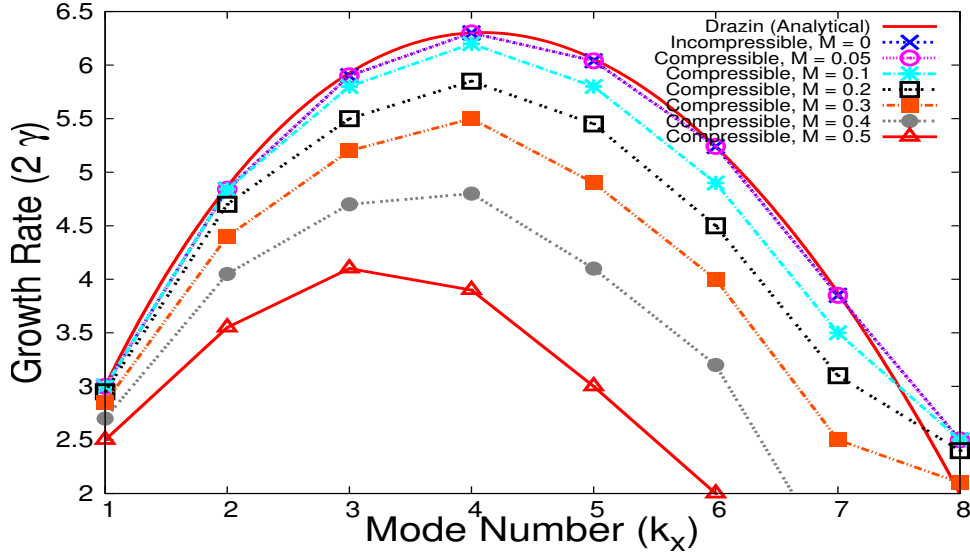


Figure 2.4: Growth rate ( $2\gamma$ ) of K-H instability is plotted with mode number ( $k_x$ ) of excitation. The red solid line is evaluated from the analytical expression obtained by Drazin. The blue line with 'X' sign represents the growth rate from earlier code in vorticity formalism and the magenta line with symbol 'O' represents the same from velocity formalism code with Mach number ( $M$ ) = 0.05.

$L_y = 2$  with  $N_x = N_y = 128$  and Mach number  $M = 0.5$ . Using this parameter similar to Keppens et al [57] the growth rate of the Kelvin - Helmholtz instability is exactly reproduced as in Keppens et al [57]. Next, the mode number of excitation ( $k_x = 1, 2, 2.5, 3, 4$ ) is changed and the growth rate is found to follow the similar values of Keppens et al [57] (Fig 2.9). Also the similar growth rates are obtained for different Mach numbers for a fixed mode number of excitation as obtained by Keppens et al [57].

For further check in nonlinear regime with weak compressibility I time evolve a circular arrangement of  $N_{pv} = 5$  point vortices ( $\omega_{point} = 10$ ) with radius ( $d_{pv} = 0.032\frac{L}{2}$ ) at a distance of  $R_{point} = 0.4L$  from the center of a circular patch vortex ( $\omega_{patch} = 1$ ) with radius  $R_{patch} = 0.3L$ , with  $\nu = 2 \times 10^{-4}$ ,  $M = 0.5$ ;  $L = 2\pi$ ;  $N_x = N_y = 256$  and obtain the frequencies in the total energy from this code as well as AGSpect code [56], another pseudo-spectral code that is capable of simulating the visco-elastic fluids with periodic boundary condition. I find the natural frequency, its

harmonics and its beats with the harmonics to be in quite good agreement (Fig.2.5) with the AGSpect code [56] at appropriate limit (i.e. for negligible viscoelasticity [ $\tau_m = 10^{-4}$ ]).

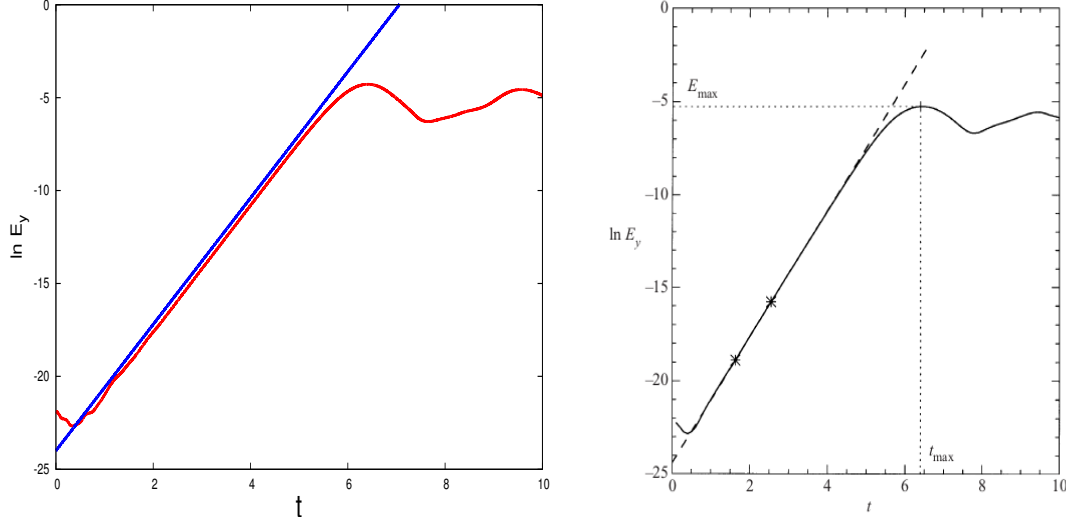


Figure 2.5: Time evolution of y-directional kinetic energy (see Fig. 2.1) at the perpendicular to the flow direction is evaluated with time. Fig 2 of Keppens et al [57] reproduced by my code for the identical parameters with Mach Number ( $M$ ) = 0.5. The value of growth rate ( $\gamma = 1.7$ ) is found to be in good agreement with the value obtained from Table 1 ( $\gamma = 1.728$ ) by Keppens et al [57]. Fig 2 of Keppens et al [57] with Mach Number ( $M$ ) = 0.5.

Following a snapshot of vortex mergers with above parameter values at different times is provided [Fig. 2.8] [85, 86].

### 2.4.3 Weakly compressible magnetohydrodynamic flow

In order to simulate the weakly compressible magnetohydrodynamic fluid I time evolve the following set of equations. The physical system I simulate is identical to that described in Section 2.4.2 with a uniform magnetic field in one direction.

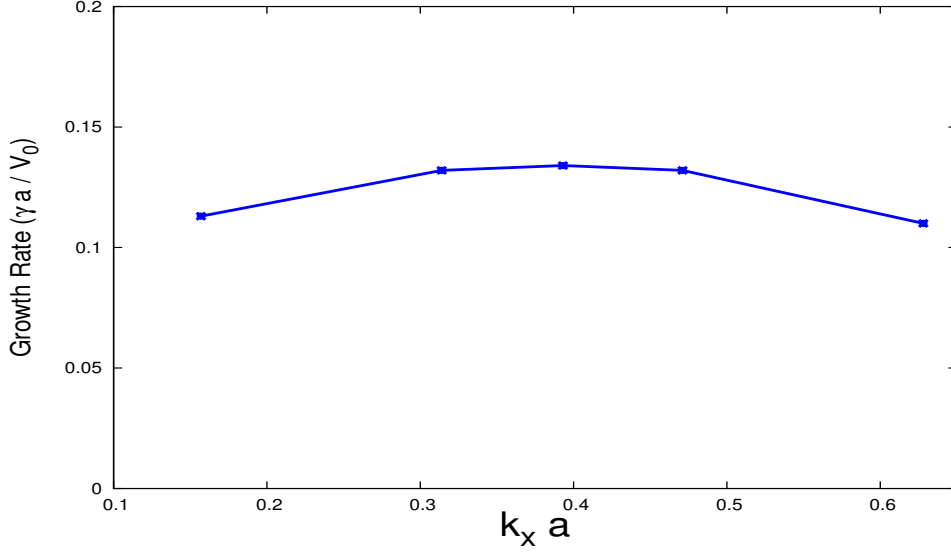


Figure 2.6: The change of growth rate ( $\frac{\gamma a}{V_0}$ ) with the mode number of excitation ( $k_x a$ ).

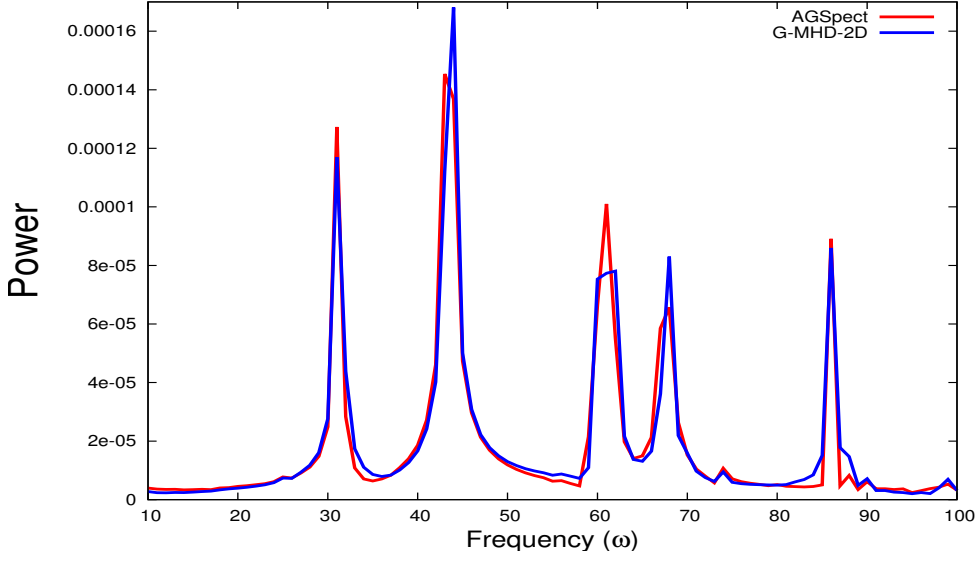


Figure 2.7: Comparison of natural frequency and its harmonics as well as its beats of my code with its harmonics with AGSpect [56] for  $M = 0.5$ .

$$\begin{aligned}
 \frac{\partial \rho}{\partial t} + \vec{\nabla} \cdot (\rho \vec{u}) &= 0 \\
 \frac{\partial (\rho \vec{u})}{\partial t} + \vec{\nabla} \cdot \left[ \rho \vec{u} \otimes \vec{u} + \left( P + \frac{B^2}{2} \right) \mathbf{I} - \vec{B} \otimes \vec{B} \right] &= \mu \nabla^2 \vec{u} \\
 \frac{\partial E}{\partial t} + \vec{\nabla} \cdot \left[ \left( E + P + \frac{B^2}{2} \right) \vec{u} - \vec{u} \cdot (\vec{B} \otimes \vec{B}) - \eta \vec{B} \times (\vec{\nabla} \times \vec{B}) \right] &= \mu (\vec{\nabla} \cdot \vec{u})^2 \\
 \frac{\partial \vec{B}}{\partial t} + \vec{\nabla} \cdot (\vec{u} \otimes \vec{B} - \vec{B} \otimes \vec{u}) &= \eta \nabla^2 \vec{B}
 \end{aligned}$$

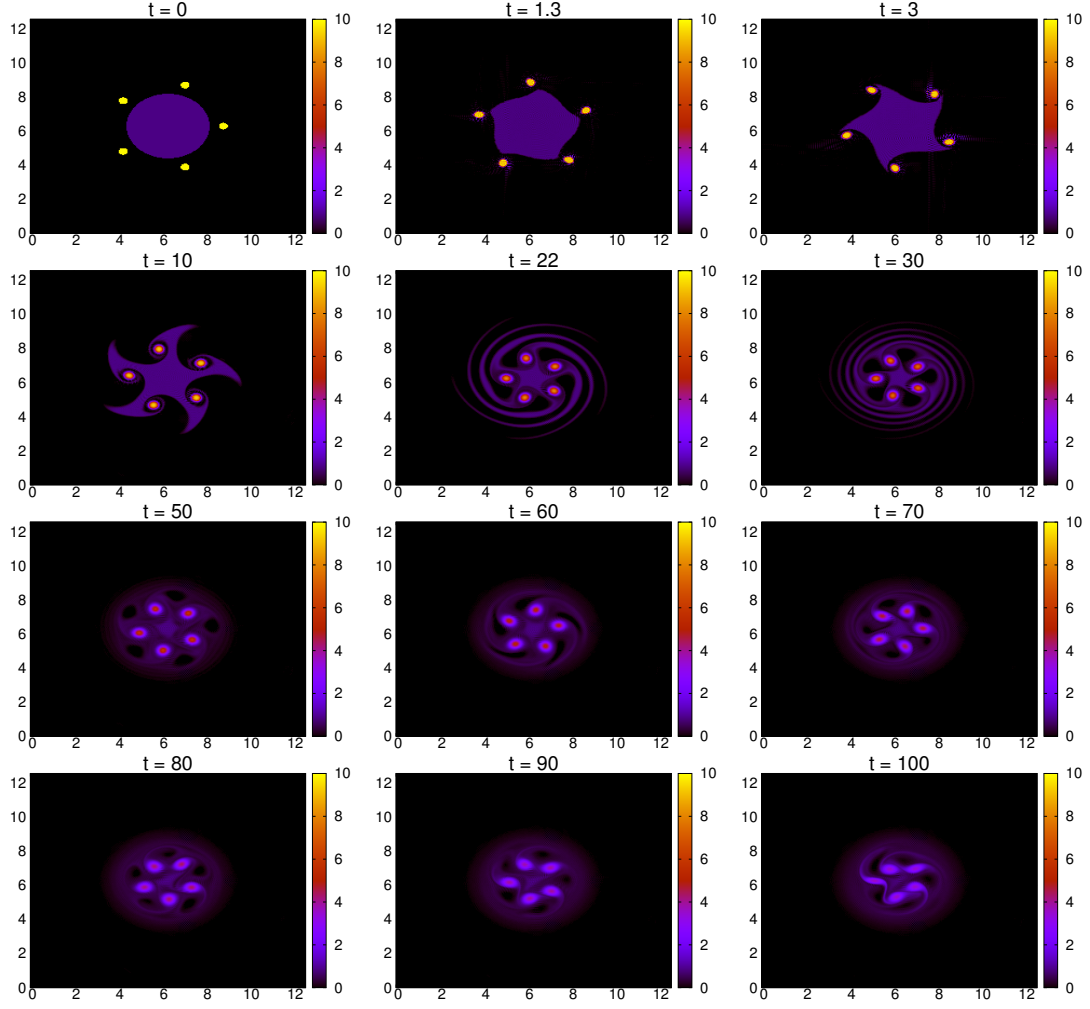


Figure 2.8: Time evolution of the prearranged vortex merger with  $M = 0.5$  with grid size  $256^2$ .

The earlier results by Keppens et al [57] have shown a slightly higher growth rate compared to the hydrodynamic one at higher mode numbers of excitation for the Kelvin-Helmholtz instability in presence of a uniform magnetic field [Fig. 2.11]. Keeping the fluid velocity profile identical as mentioned in the previous section, I add a magnetic field with spatial profile  $B_0 \hat{x}$  at time  $t = 0$  with  $M_A = 5$  and  $B_0 = 0.129$ . All the numerical parameters are kept identical to that mentioned in Section 2.4.2. With this parameter, I get the identical growth rate as Keppens as shown in Fig 2.11.

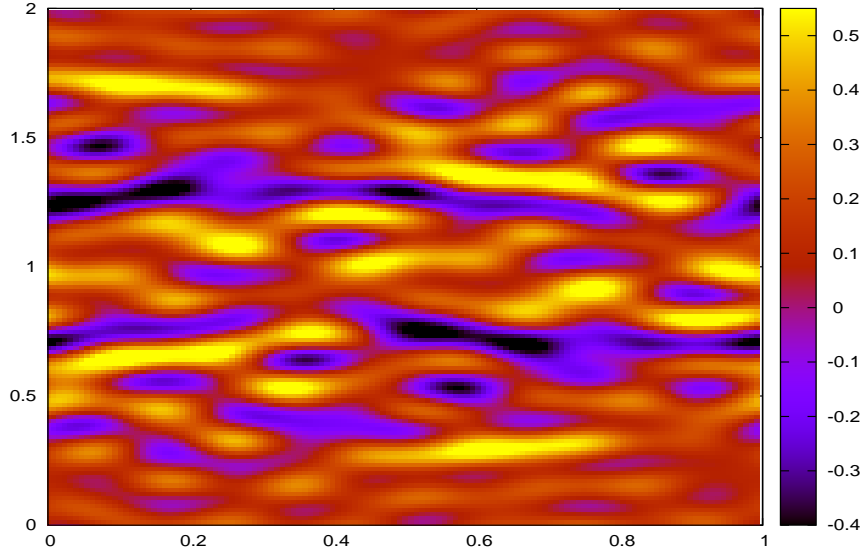


Figure 2.9: The x-component of magnetic field ( $B_x(x, y)$ ) profile at time  $t = 10$ . The grid resolution I use is  $128^2$  and time-step width  $10^{-3}$ .

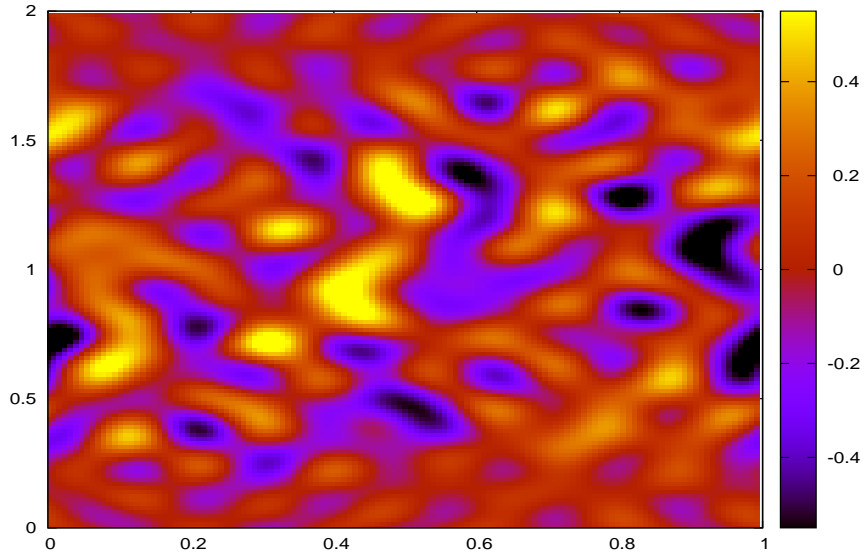


Figure 2.10: The y-component of magnetic field ( $B_y(x, y)$ ) profile at time  $t = 10$ . The grid resolution I use is  $128^2$  and time-step width  $10^{-3}$ .

## 2.5 Three dimensional numerical tests

In three dimensions I time evolve the following set of equations

$$\frac{\partial \rho}{\partial t} + \vec{\nabla} \cdot (\rho \vec{u}) = 0 \quad (2.17)$$

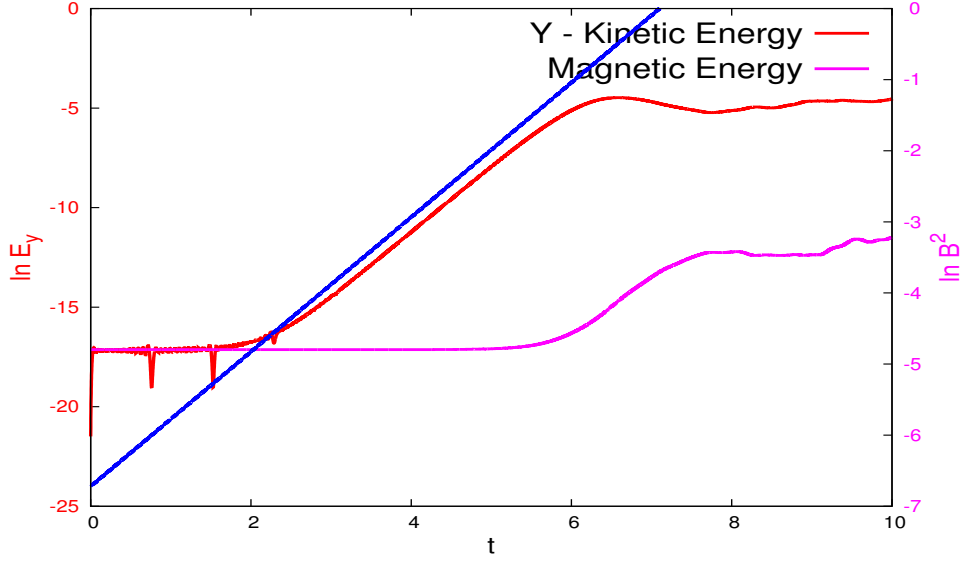


Figure 2.11: The change of growth rate with the mode number of excitation. The red dashed line indicates the hydrodynamic case and the blue dot-dashed line indicates the uniform magnetohydrodynamic case. The magenta solid line indicates the growth of magnetic energy with time.

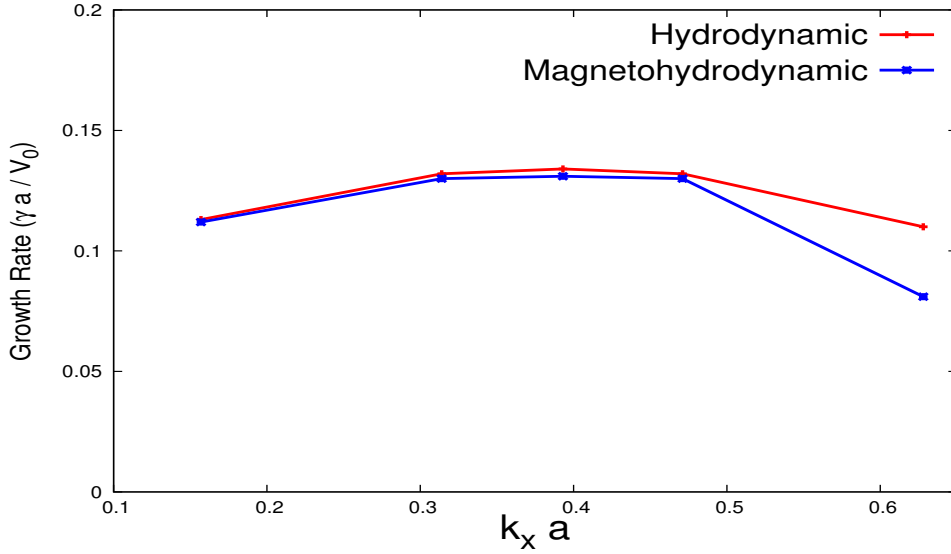


Figure 2.12: The change of growth rate ( $\frac{\gamma a}{V_0}$ ) with the mode number of excitation ( $k_x a$ ) for hydrodynamic (red dotted) as well as magneto-hydrodynamic (blue starred) cases. The growth rate for Magneto-hydrodynamic flows at higher wave numbers is found to be higher than that of the Hydrodynamic one as previously identified by Keppens *et al* [57].

$$\begin{aligned} \frac{\partial(\rho \vec{u})}{\partial t} + \vec{\nabla} \cdot \left[ \rho \vec{u} \otimes \vec{u} + \left( P + \frac{B^2}{2} \right) \mathbf{I} - \vec{B} \otimes \vec{B} \right] \\ = \mu \nabla^2 \vec{u} + \rho \vec{f}; \quad P = C_s^2 \rho \end{aligned} \quad (2.18)$$

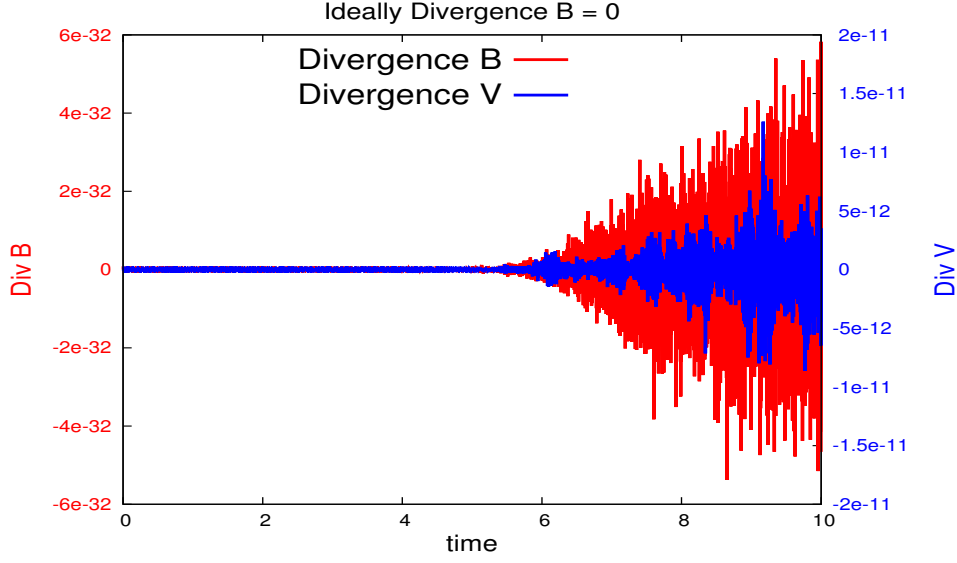


Figure 2.13: Conservation of divergence of  $\vec{B}$  and divergence of  $\vec{V}$ .  $\vec{\nabla} \cdot \vec{B} \sim \mathcal{O}(10^{-32})$  implies a strict conservation of the divergence of magnetic field till the machine precision. However, even though sonic Mach number is 0.1 indicating an incompressible regime, governing equations allow the density to fluctuate and hence, the  $\vec{\nabla} \cdot \vec{V}$  is  $\sim \mathcal{O}(10^{-11})$  but not as good as that of  $\vec{B}$ .

$$\frac{\partial \vec{B}}{\partial t} + \vec{\nabla} \cdot (\vec{u} \otimes \vec{B} - \vec{B} \otimes \vec{u}) = \eta \nabla^2 \vec{B} \quad (2.19)$$

### 2.5.1 For hydrodynamic flow

In order to simulate hydrodynamic flows Eq. 5.3 is turned off in the above set of equations. The initial profile is chosen as  $E(k) = Ak^4 \exp(-2k^2/k_0^2)$ . The RMS (root-mean-square) of the velocity divergence is defined as  $\theta' = \langle (\partial u_i / \partial x_i)^2 \rangle^{1/2}$  and the Skewness is defined as  $S_3 \equiv \frac{\langle (\partial u_1 / \partial x_1)^3 \rangle}{\langle (\partial u_1 / \partial x_1)^2 \rangle^{3/2}}$ .  $\theta'$  implies the tendency of divergence of velocity field while  $S_3$  measures the deviation from the Gaussian nature of the flow profile. The time evolution of  $\theta'$  and  $S_3$  as previously obtained by Samtaney et al [59] is reproduced.

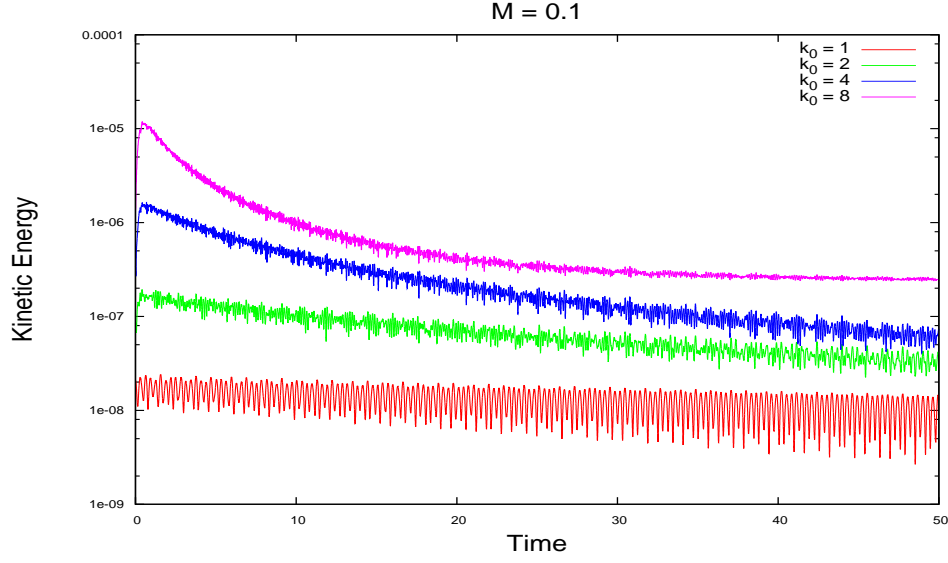


Figure 2.14: The time evolution of kinetic energy  $[= \sum_{x,y,z} u^2(x,y,z,t)]$  per grid with  $k_0 = 1, 2, 4, 8$ .

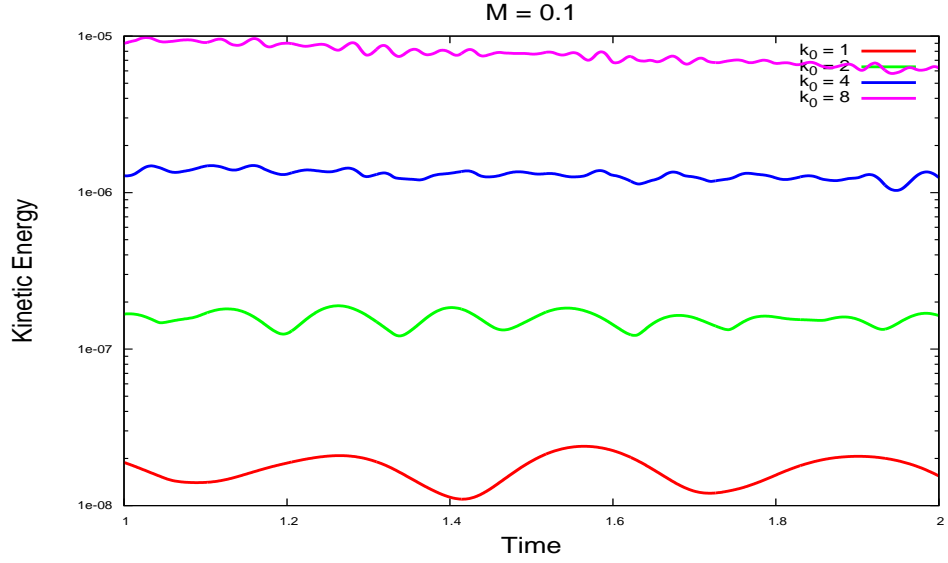


Figure 2.15: A zoomed view of Fig. 2.14. The amplitude of fluctuation is found to decrease as  $k_0$  increases.

### 2.5.2 For magnetohydrodynamic flow

First I turn off Eq. 5.1 and 5.2 and start with the initial condition  $\rho = \rho_0$  as a uniform density fluid, the initial velocity profile as  $u_x = U_0[A \sin(k_0 z) + C \cos(k_0 y)]$ ,  $u_y = U_0[B \sin(k_0 x) + A \cos(k_0 z)]$ ,  $u_z = U_0[C \sin(k_0 y) + B \cos(k_0 x)]$  and the initial magnetic field as  $B_x = B_y = B_z = B_0$ . I choose,  $\rho_0 = 1$ ,  $U_0 = 1$ ,  $k_0 = 1$  and



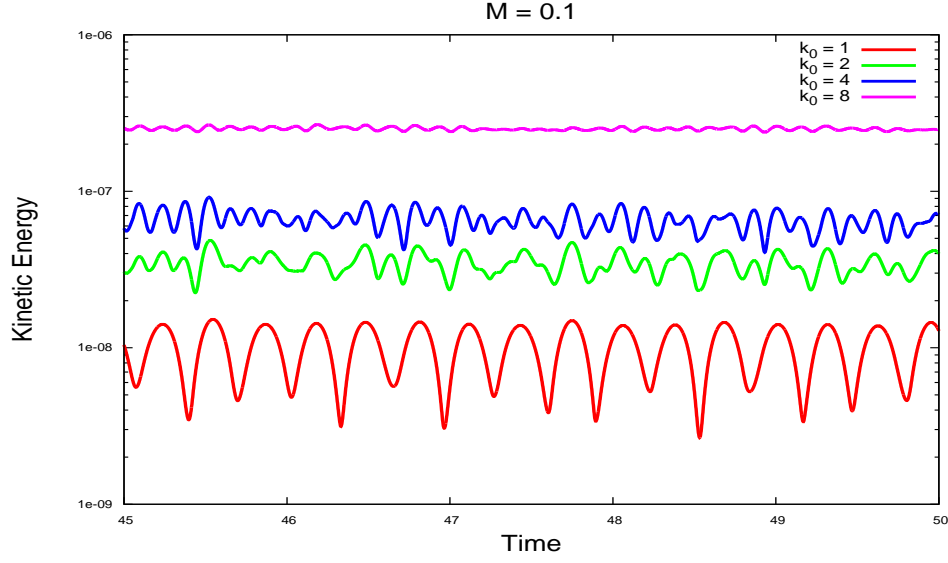


Figure 2.16: A zoomed view of Fig. 2.14. The amplitude of fluctuation is found to decrease as  $k_0$  increases.

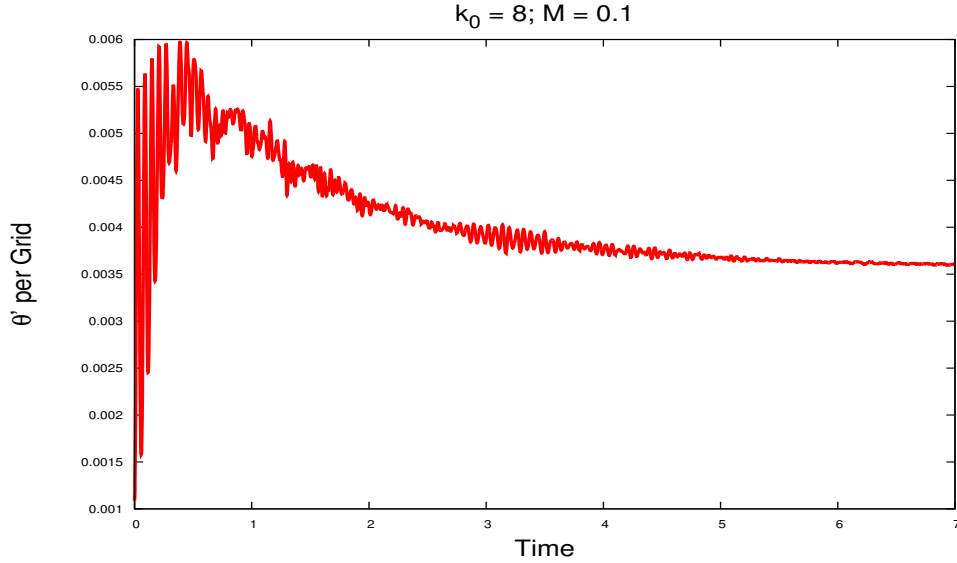


Figure 2.17: Profile of RMS of velocity divergence ( $\theta'$ ) with time for  $k_0 = 8$  and  $M = 0.1$

$A = B = C = 1$  as previously taken by Galloway et al [58]. I reproduce the growth rate of the magnetic energy for the specified ABC flow for Reynolds numbers [Fig. 2.18, 2.19, 2.20]  $Re = 120, 200$  and  $450$ . The exponential growth of magnetic energy of several orders of magnitude is known as “dynamo effect”.

Next, I time evolve all the terms viz. Eq. 5.1, 5.2 and 5.3, in addition with an

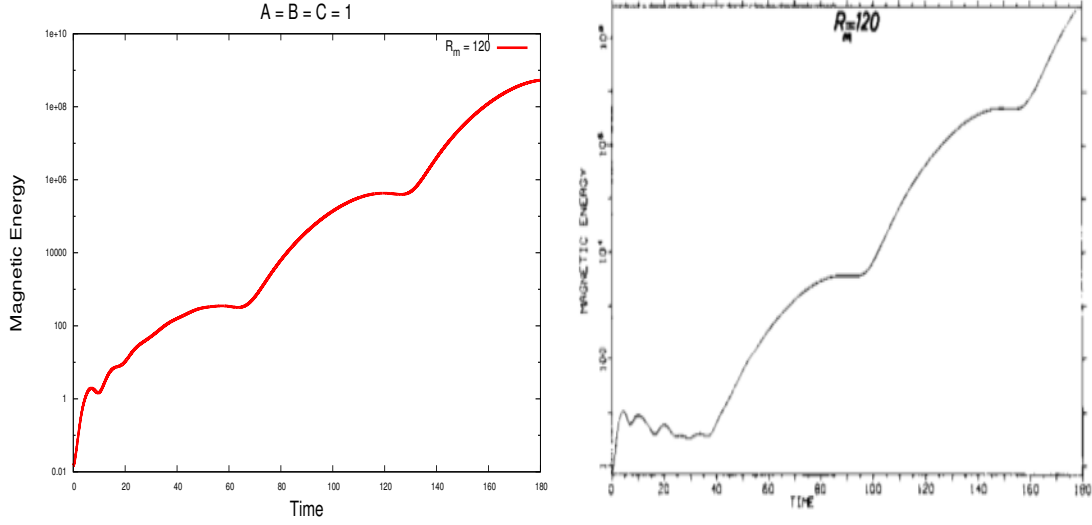


Figure 2.18: Growth of magnetic energy  $[= \sum_{x,y,z} B^2(x,y,z,t)]$  in the form of kinematic dynamo benchmarked with Galloway and Frisch [58] with  $R_m = 120$ . Figure reproduced from Galloway and Frisch [58] with  $R_m = 120$ . The initial time evolution and the star-up of dynamo action is different in the two figures because of the difference between the initial random number seeds used in the simulation.

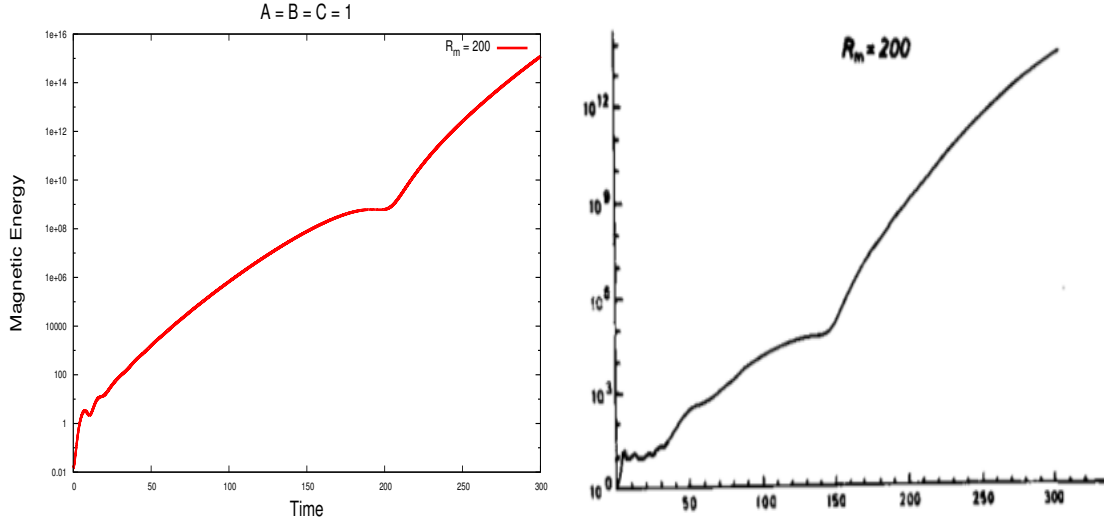


Figure 2.19: Growth of magnetic energy  $[= \sum_{x,y,z} B^2(x,y,z,t)]$  in the form of kinematic dynamo benchmarked with Galloway and Frisch [58] with  $R_m = 200$ . Figure reproduced from Galloway and Frisch [58] with  $R_m = 200$ . The initial time evolution and the star-up of dynamo action is different in the two figures because of the difference between the initial random number seeds used in the simulation.

external forcing defined as:

$$\vec{f} = \begin{pmatrix} A \sin(k_f z) + C \cos(k_f y) \\ B \sin(k_f x) + A \cos(k_f z) \\ C \sin(k_f y) + B \cos(k_f x) \end{pmatrix}$$

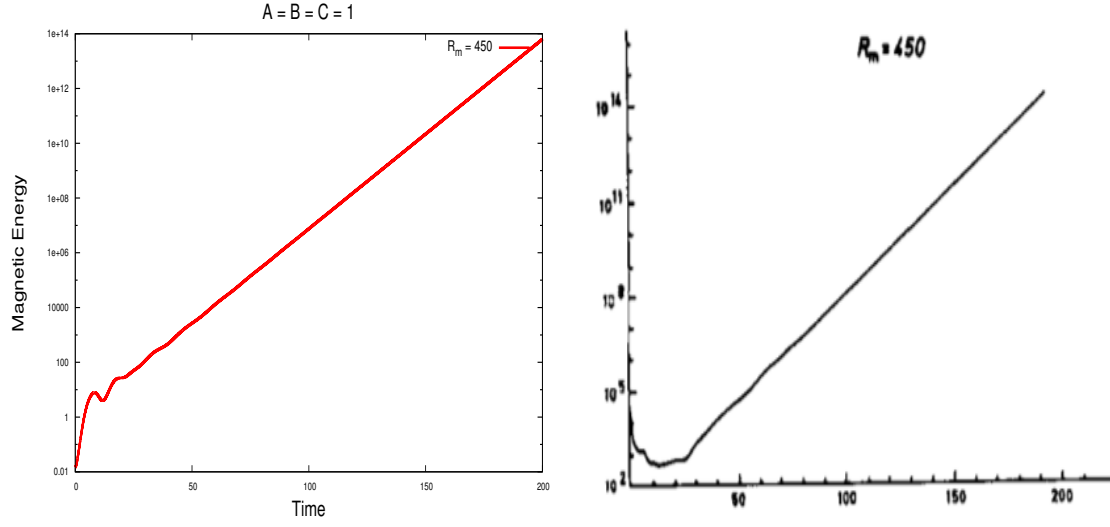


Figure 2.20: Growth of magnetic energy  $[= \sum_{x,y,z} B^2(x,y,z,t)]$  in the form of kinematic dynamo benchmarked with Galloway and Frisch [58] with  $R_m = 450$ . Figure reproduced from Galloway and Frisch [58] with  $R_m = 450$ . The initial time evolution and the star-up of dynamo action is different in the two figures because of the difference between the initial random number seeds used in the simulation.

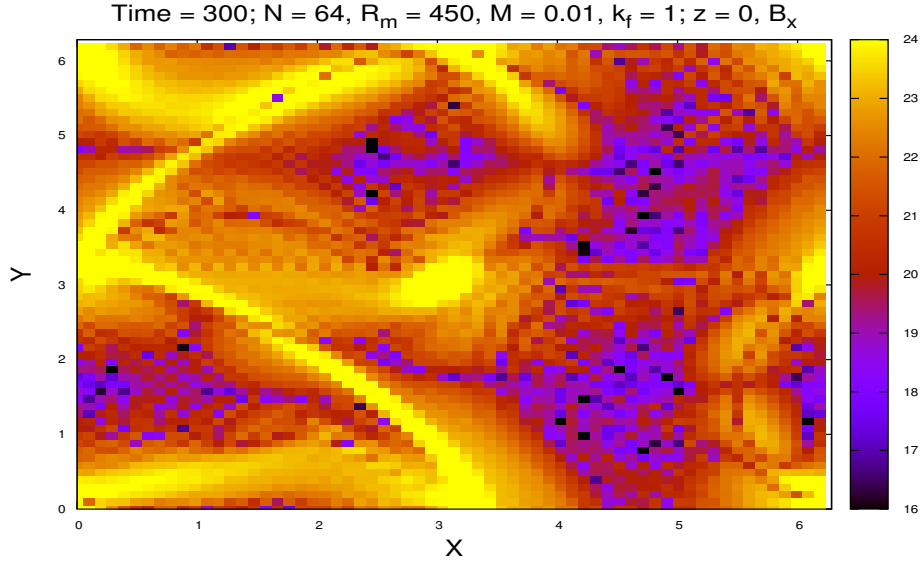


Figure 2.21: x-component of magnetic field ( $B_x(x,y,0)$ ) at time  $t = 300$  at identical parameter of Galloway and Frisch [58] with  $R_m = 450$

I choose  $M_A = 1$  such that, the initial kinetic and magnetic energies are equal. The kinetic and magnetic energy oscillates by transferring energies between kinetic and magnetic modes keeping the total energy conserved. In Fig.2.25 the fall of total energy is solely due to viscous and resistive effects. The  $\delta KE$ ,  $\delta ME$ ,  $\delta TE$

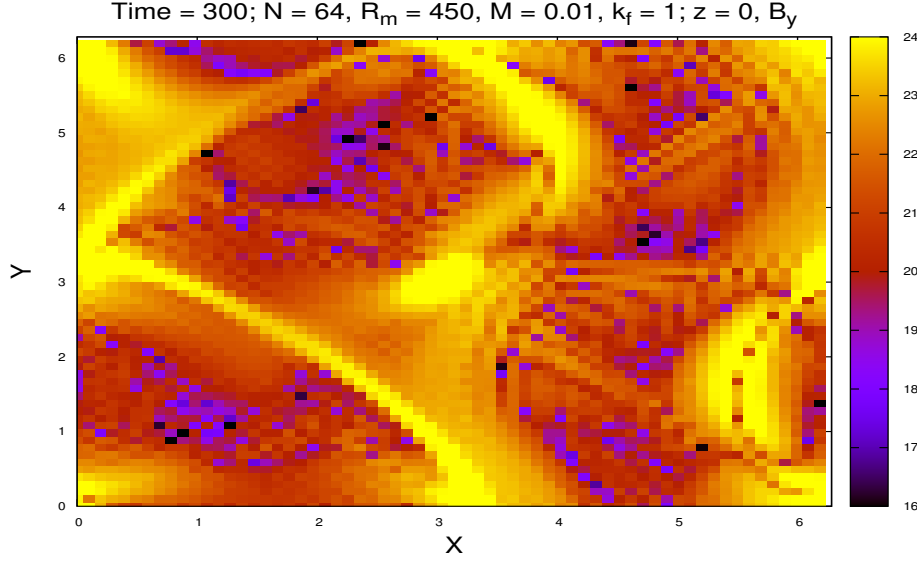


Figure 2.22:  $y$ -component of magnetic field ( $B_y(x, y, 0)$ ) at time  $t = 300$  at identical parameter of Galloway and Frisch [58] with  $R_m = 450$

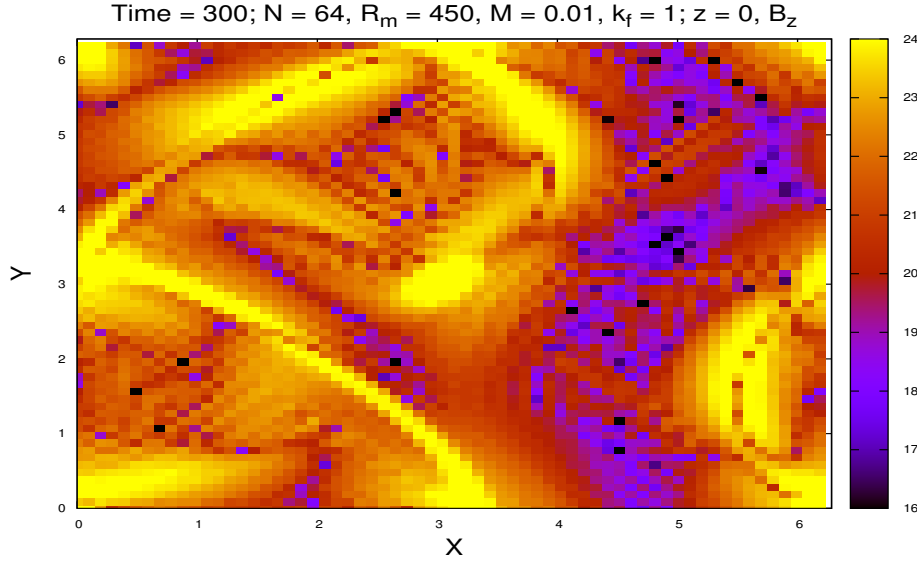


Figure 2.23:  $z$ -component of magnetic field ( $B_z(x, y, 0)$ ) at time  $t = 300$  at identical parameter of Galloway and Frisch [58] with  $R_m = 450$

denote the shifted Kinetic, Magnetic and Total energy respectively, where, the shift is calculated with respect to the initial corresponding value at the beginning of the simulation. For further check of the accuracy I increase the Alfvén Mach number ( $M_A$ ) such that the frequency of the Alfvén waves increase leaving its signature in the oscillations of the kinetic and magnetic energy. I choose  $M_A = 0.1$  and still found consistent decay of total energy, though some oscillations of tiny amplitude

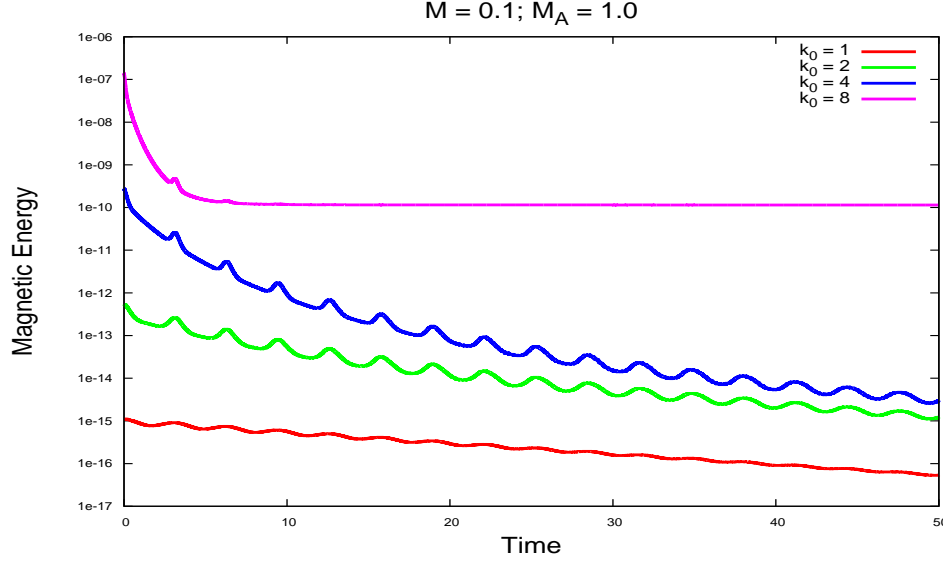


Figure 2.24: Multiple frequencies observed in the magnetic energy  $[= B^2(t)]$  of the MHD version of the DNS of decaying hydrodynamic turbulence earlier observed by Santaney *et al.* [59]

appears.

I also reproduce the kinetic and magnetic energy spectra for an incompressible three dimensional magnetohydrodynamic ABC flow where the backreaction of magnetic field on the velocity fields are not considered. The results were obtained earlier by Sadek *et al* [87].

In order to develop some diagnostics of the 3D MHD code, the density and velocity structure functions for a initially random velocity and magnetic field is calculated. Similar structure functions as earlier found by Yang *et al* [88] is also obtained.

I have developed modules for wavenumber based forcing and gaussian white noise implementation algorithms. I have also incorporated a dynamical wave-number dependent turbulent viscosity model in my code. The coupling in the above set of equations can be altered easily to suit specific purposes.

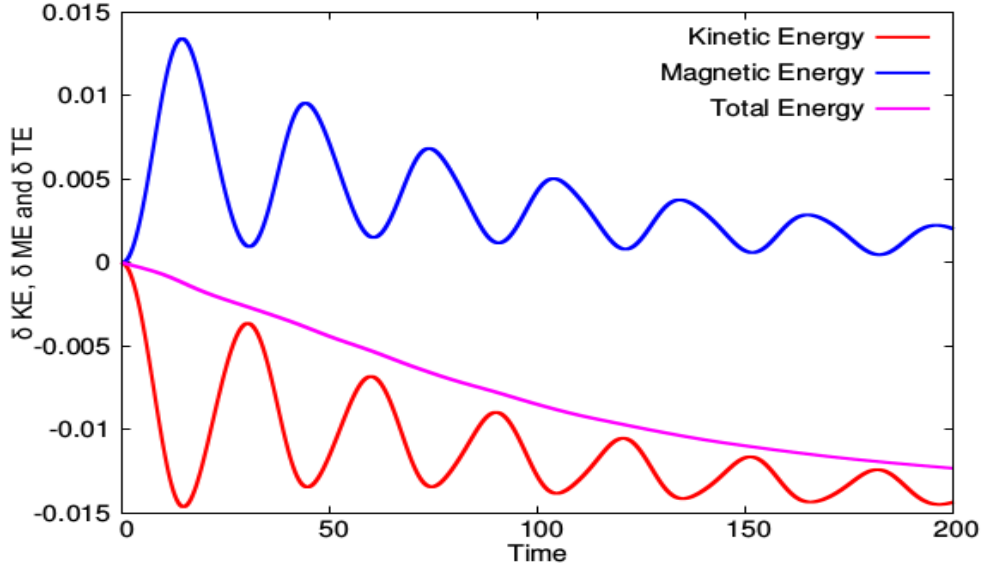


Figure 2.25: Conservation of shifted total energy  $[\delta TE = \sum_{x,y,z} u^2(x,y,z,t) - \sum_{x,y,z} u^2(x,y,z,0) + \sum_{x,y,z} B^2(x,y,z,t) - \sum_{x,y,z} B^2(x,y,z,0)]$  and time evolution of shifted kinetic  $[\delta KE = \sum_{x,y,z} u^2(x,y,z,t) - \sum_{x,y,z} u^2(x,y,z,0)]$  and shifted magnetic  $[\delta ME = B^2(t) - B^2(0)]$  energy for Arnold-Beltrami-Childress flow with  $M_A = 1$  and  $M = 0.1$  and  $Re = Rm = 450$  with  $k_0 = 1$ .

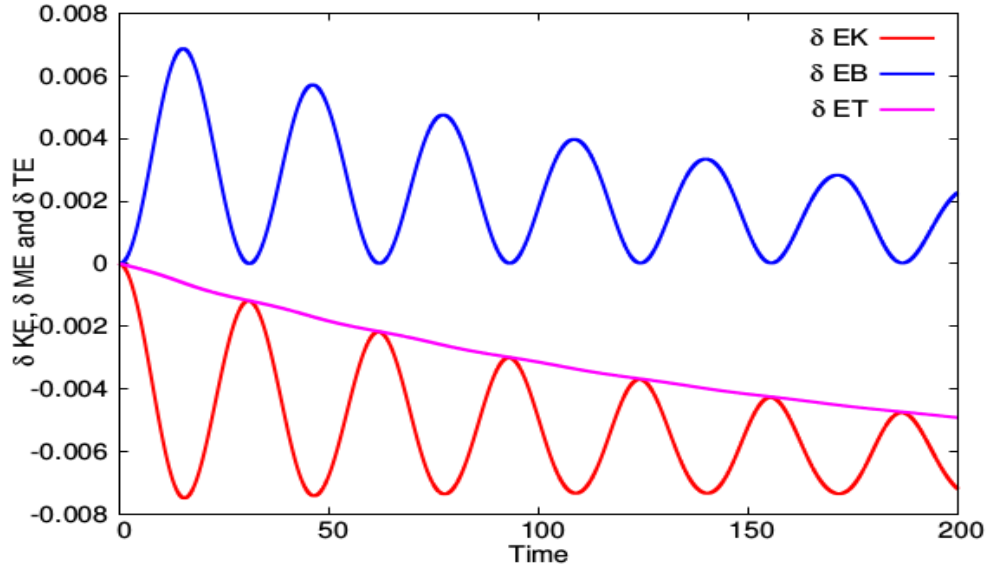


Figure 2.26: Time evolution of shifted kinetic  $[\delta KE = \sum_{x,y,z} u^2(x,y,z,t) - \sum_{x,y,z} u^2(x,y,z,0)]$  and shifted magnetic  $[\delta ME = \sum_{x,y,z} B^2(x,y,z,t) - \sum_{x,y,z} B^2(x,y,z,0)]$  energy for Taylor-Green flow with  $M_A = 1$  and  $M = 0.1$  and  $Re = Rm = 450$  with  $k_0 = 1$ .

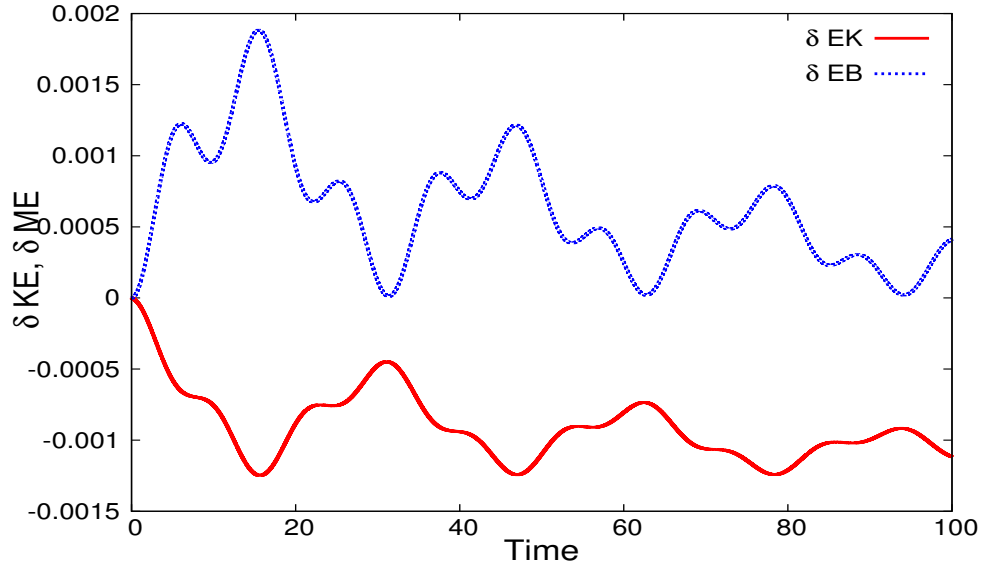


Figure 2.27: Time evolution of shifted kinetic [ $\delta KE = \sum_{x,y,z} u^2(x,y,z,t) - \sum_{x,y,z} u^2(x,y,z,0)$ ] and shifted magnetic [ $\delta ME = \sum_{x,y,z} B^2(x,y,z,t) - \sum_{x,y,z} B^2(x,y,z,0)$ ] energy for Roberts flow with  $M_A = 1$  and  $M = 0.1$  and  $Re = Rm = 450$  with  $k_0 = 1$ .

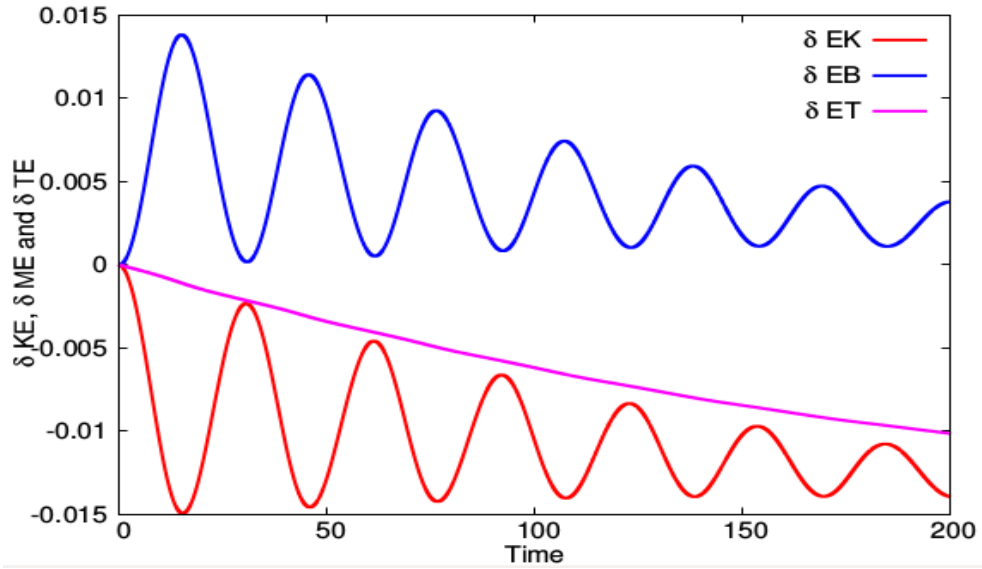


Figure 2.28: Time evolution of shifted kinetic [ $\delta KE = \sum_{x,y,z} u^2(x,y,z,t) - \sum_{x,y,z} u^2(x,y,z,0)$ ] and shifted magnetic [ $\delta ME = \sum_{x,y,z} B^2(x,y,z,t) - \sum_{x,y,z} B^2(x,y,z,0)$ ] energy for Cat's Eye flow with  $M_A = 1$  and  $M = 0.1$  and  $Re = Rm = 450$  with  $k_0 = 1$ .

## 2.6 Tracer Particles

Tracer particles act as a very important diagnostics for any fluid code as the correlation between any two fluid elements can be best described using this diagnostics. It gives us the information on the motion of the fluid elements in a turbulent plasma and one can follow the deterministic path of a tracer which may reveal more information about the underlying symmetries of the fluid / plasma flow. In MHD3D code also, tracer particles are added to discover the nature of turbulence that appears in a MHD plasma. The code evaluates the density, velocity and magnetic fields at the grid points using the MHD description of a plasma. The tracer particles are randomly sprinkled in the simulation domain at the beginning of the simulation. They can be placed anywhere in between the grids or at the grid location. These particles are considered to be passive elements of the code. Thus, they do not contribute to the time evolution of any of the fields that are calculated at the grid location from the MHD equations mentioned in the previous section. But the fields do affect the tracers and determine their motion within the simulation box. The initial velocity of the tracers are evaluated from the velocity at the grid. Next, the time evolution of the tracers are fully governed by the magnetic fields at the grids. The grid magnetic field is interpolated at the position of the tracers in between the grids and the Lorentz force acting on them is evaluated. This force pushes the particles to their new positions. The interpolation of the grid magnetic field is done again at the new positions of the tracers and the new force is evaluated. This procedure is repeated to follow the trajectory of the tracer particles in the plasma. Following I describe the interpolation scheme and the particle pusher algorithm in detail.



### 2.6.1 Interpolation Scheme for Test Particle Transport

In order to calculate the magnetic force acting on a tracer particle, I use the following Cloud-In-Cell (CIC) scheme. In this scheme, the magnetic field of eight grid points are interpolated at the particle position. In Fig. 2.29, I show the volume weighting scheme. The magnetic field is known at all the grid points at the simulation domain. The tracer particle divides the unit cube, into eight subshells. One of them (the bottom-left-front) are shown in dark colors (Fig. 2.29) with blue filled and hollow circles at the corners for better identification. The magnetic field at eight corner-grids (blue and black hollow circles at Fig. 2.29) are then interpolated at the particle location ( $\vec{B}_p$ ) (yellow filled circle at Fig. 2.29) using the below scheme.

If the  $m^{th}$  particle is placed within an unit cube whose bottom-left-front corner has a grid index  $(i, j, k)$ , the magnetic field acting on the  $m^{th}$  particle ( $= \vec{B}_p^m$ ) will be given by,

$$\begin{aligned}
 \vec{B}_p^m = & \vec{B}_g^{i,j,k} \left[ (x_g^{i+1} - x_p^m) \cdot (y_g^{j+1} - y_p^m) \cdot (z_g^{k+1} - z_p^m) \right] dt \\
 & + \vec{B}_g^{i+1,j,k} \left[ (x_p^m - x_g^i) \cdot (y_g^{j+1} - y_p^m) \cdot (z_g^{k+1} - z_p^m) \right] dt \\
 & + \vec{B}_g^{i,j+1,k} \left[ (x_g^{i+1} - x_p^m) \cdot (y_p^m - y_g^j) \cdot (z_g^{k+1} - z_p^m) \right] dt \\
 & + \vec{B}_g^{i+1,j+1,k} \left[ (x_p^m - x_g^i) \cdot (y_p^m - y_g^j) \cdot (z_g^{k+1} - z_p^m) \right] dt \\
 & + \vec{B}_g^{i,j,k+1} \left[ (x_g^{i+1} - x_p^m) \cdot (y_g^{j+1} - y_p^m) \cdot (z_p^m - z_g^k) \right] dt \\
 & + \vec{B}_g^{i+1,j,k+1} \left[ (x_p^m - x_g^i) \cdot (y_g^{j+1} - y_p^m) \cdot (z_p^m - z_g^k) \right] dt \\
 & + \vec{B}_g^{i,j+1,k+1} \left[ (x_g^{i+1} - x_p^m) \cdot (y_p^m - y_g^j) \cdot (z_p^m - z_g^k) \right] dt \\
 & + \vec{B}_g^{i+1,j+1,k+1} \left[ (x_p^m - x_g^i) \cdot (y_p^m - y_g^j) \cdot (z_p^m - z_g^k) \right] dt
 \end{aligned} \tag{2.20}$$

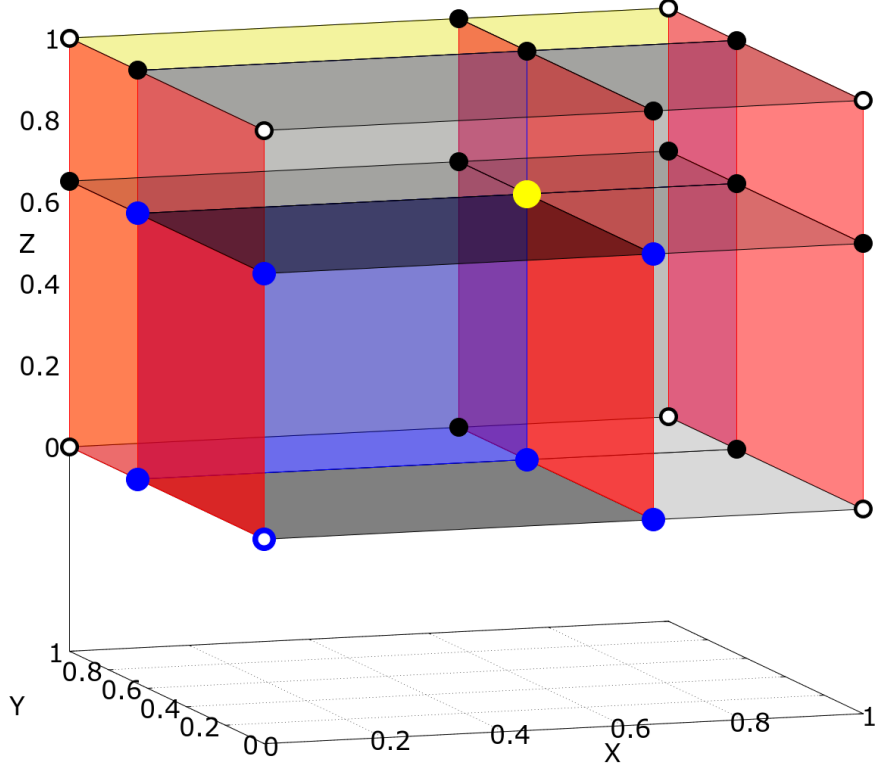


Figure 2.29: CIC scheme for volume weighting for the evaluation of magnetic fields on the location of the tracer particles. The tracer particle (yellow filled circle) is located within the unit shell. It divides the unit shell into 8 subshells, one of them are shown in dark colors with blue circles at the edges. The magnetic field at the tracer particle location ( $\vec{B}_p$ ) is interpolated from the grid magnetic field ( $\vec{B}_g$ ) of the outer corner grids (black hollow circles). The weights of interpolation is given in Eq. 2.20

where, the subscript  $p$  denotes the particle and subscript  $g$  denotes the grid.  $x_g^i, y_g^j, z_g^k$  denote the coordinate of the  $(i, j, k)^{th}$  grid. Periodic boundary condition (PBC) has been used such that the tracer particle present at one boundary can feel the magnetic field from the opposite boundary.

### 2.6.2 Particle Pusher Scheme

I use Boris Algorithm [89] for pushing the particles from its old to new position due to the effect of Lorentz force acting on the particles. This Lorentz force is evaluated by interpolating the grid magnetic fields to the tracer particle location using the CIC scheme mentioned above. If  $\vec{x}_t^m$  and  $\vec{v}_t^m$  are the position and velocity of  $m^{th}$  tracer particle respectively at time  $t$ , I use the following steps to calculate  $\vec{x}_{t+dt}^m$  and  $\vec{v}_{t+dt}^m$  at time  $t + dt$ .

$$\begin{aligned}\vec{t} &= \frac{q\vec{B}_p^m}{M} \frac{dt}{2} \\ \vec{s} &= \frac{2\vec{t}}{1 + t^2} \\ \vec{v}_d &= \vec{v}_t + \vec{v}_t \times \vec{t} \\ \vec{v}_{t+dt} &= \vec{v}_t + \vec{v}_d \times \vec{s}\end{aligned}\tag{2.21}$$

$$\vec{x}_{t+dt} = \vec{x}_t + \vec{v}_{t+dt} \cdot dt\tag{2.22}$$

where,  $q$  and  $M$  are the charge and mass of the tracer particle respectively. In this code I work in the normalisations where I assume  $q = M = 1$ . The particles are guranteed to stay inside the simulation domain by enforcing periodic boundary condition in the position of the tracers.

Thus the following steps are executed to determine the dynamics of the tracers in the code.

1. Determine the grid index  $(i, j, k)$  of the bottom-left-front corner grid point of the unit cell in which the  $m^{th}$  tracer particle is situated.
2. Use Eq. 2.20 to evaluate the magnetic field at the particle position.
3. Calculate the Lorentz force on the  $m^{th}$  tracer particle using Eq. 2.21.

4. Determine the new position of the tracer particle using Eq. [2.22](#)

## 2.7 GPU Acceleration

The long-time simulation of the OpenMP code falls short to cater to the need of the physics issues addressed in this Thesis. Specifically the runs with higher grid resolution takes large time and thus restricting us to look into the physics results. Hence in order to increase the performance of the code I choose parallelise the code in graphics processing units (GPU).

Over the last decade, there has been an increasing use of graphics processing units (GPUs) as general-purpose highly parallel computing units. The GPU is a massively parallel computing device consisting of a large number of streaming multiprocessors (SM), each of which is a set of computing cores. Each SM has a fixed number of registers and a fast on-chip memory that is shared among its cores. The different SMs share a slower off-chip memory called the device memory, which is much larger in capacity. For example, the Tesla P100 GPU has 56 SMs each with 64 cores, resulting in a total of 3584 cores [\[90\]](#). Each SM of the Tesla P100 has a 256 KB register file size and 64 KB of fast on-chip memory. All SMs share a 4 MB L2 cache and 16 GB of device memory [\[90\]](#).

In a general purpose computing on graphics processing units (GPUs), a GPU is typically called a device, while the CPU is called a host. A kernel refers to a program that is executed on the GPU device using a large number of threads.

In order to port the code to GPU I face two basic challenges - the first one is the parallelisation procedure has been changed from OpenMP to OpenACC and the second one is the Fourier transform is taken using the available library cuFFT which is a library written in CUDA apart from FFTW. I describe the concept of OpenACC in brief and then in another section discuss about the usage of cuFFT

library.

OpenACC [75] is an approach for quick and easy porting of existing applications from CPU to GPU. The next section introduces the OpenACC programming paradigm and describes how the MHD3D code was accelerated using the OpenACC pragmas.

### 2.7.1 OpenACC Acceleration of MHD3D

OpenACC is a compiler directive-based programming model, designed to facilitate quick porting of existing applications to accelerators like GPUs, without significant programming effort [75]. OpenACC directives, which are pragmas in C/C++ and specialized comments in Fortran, provide the compiler with additional information, enabling them to optimize the code within the directives for a specific accelerator. With openACC, the same code can be compiled for different accelerators, thereby providing performance portability.

OpenACC provides two types of directives broadly - data directives and compute directives. The data directives provide hints to the compiler on movement of data between the host memory and accelerator memory. The compute directives define regions of the host program that need to be compiled as accelerator code. More details on the OpenACC directives can be found in the OpenACC Programming and Best Practices Guide [91] and the OpenACC specifications document [92].

The MHD3D code has triply nested loops interspersed with Fourier transforms. To port the triply nested loop regions to the GPU, I use the OpenACC parallel and loop constructs coupled with the collapse clause [92]. Figure 2.30 shows how the OpenMP loop regions are mapped to OpenACC parallel regions.

The compiler that supports OpenACC, compiles the loop region into a GPU kernel and distributes the iteration space of the triply nested loop between threads on the

<b>CPU code</b> (OpenMP - parallel)	<b>GPU code</b> (OpenACC - parallel)
<pre> call omp_set_num_threads (thread_num) !\$omp parallel shared(Lx,...) private(i,...) !\$omp do do k = 1,Nz do j = 1,Ny do i = 1,Nx/2+1 .... enddo enddo enddo !\$omp end do !\$omp end parallel </pre>	<pre> !\$acc parallel firstprivate(Lx,...) present(ux, ...) !\$acc loop collapse(3) do k = 1, Nz do j = 1, Ny do i = 1, Nx/2+1 .... enddo enddo enddo !\$acc end parallel </pre>

Figure 2.30: Mapping of OpenMP loops in MHD3D to OpenACC parallel loops in G-MHD3D.

GPU. There are clauses that the programmer can use to tune how the loops are distributed amongst the threads.

Figure 2.31 is a snapshot of the compile command and the compiler output. The `-acc` flag tells the compiler to process the openACC directives, `-ta=tesla:XX` specifies the architecture for which the accelerator code should be compiled and `-Minfo=accel` makes the compiler output information corresponding to all the accelerator regions in the code. The compiler output tells the user which loops are transformed into GPU kernels and how the threads are organized. Information about what data is copied into or out of the accelerator is also dumped.

## 2.7.2 cuFFT Library

The MHD3D code, as mentioned earlier, has loop regions interspersed with Fourier transforms. To accelerate the fourier transforms on the GPU, I call routines of the cuFFT library. The NVIDIA cuFFT library [74] APIs operate on data in the GPU device memory. Hence, before calling the cuFFT routines, I need to move the relevant data to the GPU, if not already present, and pass the device pointers to the API calls. The cuFFT plan creation (this is needed for initializing some

```

$pgf95 -acc -c -Minfo=accel -ta=tesla:cc60 -lm psmhd3.f95

Generating copyout(b2(:,:,:))
    Generating create(z(:))
    714, Generating
present(omega_z(:,:,:),ux(:,:,:),uy(:,:,:),uz(:,:,:),omega_x(:,:,:),omega_y(:,:,:))
    Accelerator kernel generated
    Generating Tesla code
    716, !$acc loop gang, vector(128) collapse(3) ! blockidx%x threadidx%x
    717, ! blockidx%x threadidx%x collapsed
    718, ! blockidx%x threadidx%x collapsed

```

Figure 2.31: OpenACC Compilation of G-MHD3D.

```

stream = acc_get_cuda_stream(acc_async_sync)
call createCUFFTPlan3D(fftPlanD2Z, Nz, Ny, Nx, CUFFT_D2Z, stream) //create plan once
!$acc data copy(rho, ux) //openACC pragma: data clause to copy in and out
!$acc host_data use_device(rho,ux) //openACC pragma: using device pointers in host code
call executeCUFFT3D(fftPlanD2Z, C_LOC(rho), C_LOC(rho), CUFFT_D2Z) //execute multiple in-place FFTs (re-use plan)
call executeCUFFT3D(fftPlanD2Z, C_LOC(ux), C_LOC(ux), CUFFT_D2Z)
!$acc end host_data
!$acc end data
call destroyCUFFTPlan3D(fftPlanD2ZMain) // destroy plan at the end

```

Figure 2.32: Steps to call cuFFT routines in G-MHD3D.

state information that is necessary before calling the fft routines) is done once in the beginning and destroyed at the end. Figure 2.32 shows the steps needed to call the cuFFT routines. To call the cuFFT library routines from my OpenACC Fortran application, I create C wrapper modules as shown in Figure 2.34. In-place transforms are used, i.e the output transforms are written to the input arrays. This reduces the memory footprint (amount of memory used by the application).

### 2.7.3 Out-of-core Processing

While computing the MHD3D equations for large 3D grids of size  $512 \times 512 \times 512$ , I observe that the data operated on within the triply nested loops (aka working set)

<pre> !Module for invoking cufft  module cufft3D    integer, public:: CUFFT_FORWARD = -1   integer, public:: CUFFT_INVERSE = 1   integer, public:: CUFFT_R2C = Z'2a' ! Real to Complex (interleaved)   integer, public:: CUFFT_C2R = Z'2c' ! Complex (interleaved) to Real   integer, public:: CUFFT_C2C = Z'29' ! Complex to Complex, interleaved   integer, public:: CUFFT_D2Z = Z'6a' ! Double to Double-Complex   integer, public:: CUFFT_Z2D = Z'6c' ! Double-Complex to Double   integer, public:: CUFFT_Z2Z = Z'69' ! Double-Complex to Double-Complex    interface     subroutine createCUFFTPlan3D(plan, nx, ny, nz, planType, stream) bind(C, name = 'createCUFFTPlan3D')       use iso_c_binding       use openacc       implicit none       type (c_ptr) :: plan       integer (c_int), value:: nx, ny, nz, planType       integer (acc_handle_kind), value:: stream     end subroutine createCUFFTPlan3D   end interface </pre>	<pre> interface   subroutine executeCUFFT3D(plan, iData, oData, planType) bind(C, name = 'executeCUFFT3D')     use iso_c_binding     use openacc     implicit none     type (c_ptr) :: plan     type (c_ptr), value:: iData     type (c_ptr), value:: oData     integer (c_int), value:: planType   end subroutine executeCUFFT3D end interface  interface   subroutine destroyCUFFTPlan3D(plan) bind(C, name = 'destroyCUFFTPlan3D')     use iso_c_binding     use openacc     implicit none     type (c_ptr) :: plan   end subroutine destroyCUFFTPlan3D end interface  end module cufft3D </pre>
--	---

Figure 2.33: Calling cuFFT routines through C wrapper modules in G-MHD3D.

```

extern "C" void createCUFFTPlan3D(void *plan, int nx, int ny, int nz, int planType, void *stream)
{
  cufftHandle *cPlan = (cufftHandle *)plan;
  CHECK_CUFFT(cufftPlan3d(cPlan, nx, ny, nz, (cufftType)planType));
  CHECK_CUFFT(cufftSetStream(*cPlan, (cudaStream_t)stream));
}

extern "C" void executeCUFFT3D(void *plan, void *iData, void *oData, int planType)
{
  cufftHandle *cPlan = (cufftHandle *)plan;
  switch (planType)
  {
    case CUFFT_D2Z: CHECK_CUFFT(cufftExecD2Z(*cPlan, (cufftDoubleReal *)iData,
      (cufftDoubleComplex *)oData));
      break;
    case CUFFT_Z2D: CHECK_CUFFT(cufftExecZ2D(*cPlan, (cufftDoubleComplex *)iData,
      (cufftDoubleReal *)oData));
      break;
  }
}

extern "C" void destroyCUFFTPlan3D(void *plan)
{
  cufftHandle *cPlan = (cufftHandle *)plan;
  CHECK_CUFFT(cufftDestroy(*cPlan));
}

```

Figure 2.34: Calling cuFFT routines through C wrapper modules in G-MHD3D.



exceeds the device memory capacity of the GPU. Each variable array in this case is 1 GB in size. This results in the need for efficient out-of-core processing. Out-of-core processing refers to processing of data that does not completely fit within the memory of a computing system. One approach to out-of-core processing is to split the data into blocks (also called tiles), move one tile to the GPU memory and completely process it before moving it back to the host memory. However, since the solver code is interspersed with fourier transforms that need the complete data, it is not possible to do a tile-by-tile processing.

For seamless out-of-core processing without programmer intervention, in G-MHD3D, NVIDIA's unified memory [38] is leveraged. Unified memory is a component of NVIDIA's GPU programming model that defines a managed memory space in which all processors (CPU and GPU) see a single coherent memory image with a common address space. This means that there is no need to explicitly move and manage data between the host memory and GPU [38]. For example, when a variable is accessed on the GPU within a kernel and the page that holds the variable is not present on the GPU device, (a page is a contiguous block of virtual memory), a page fault occurs. The system transparently handles this and moves the page to the GPU device if necessary. This is called on-demand page migration.

Unified memory also facilitates over-subscription of the GPU memory. This means that you can use variables whose sizes exceed the physical memory capacity of the GPU and the system transparently manages moving parts of data between host and GPU memory as needed.

To enable unified memory, one needs to compile and link your application with the `-ta:tesla=managed` flag.

### 2.7.4 Performance Results

In this Section, the performance analysis of the GPU accelerated 3D compressible magnetohydrodynamic code on different GPU architectures is presented. The accelerated code, as specified in Section 2.7, uses OpenACC [75] for GPU parallelization. In-place fourier transforms are computed on the GPU using the cuFFT library [74]. Computing the transforms in-place reduces the memory footprint, resulting in reduced data transfers between the host and GPU and improved performance. For seamless out-of-core processing of large grids that do not fit in the GPU memory, I leverage NVIDIA's unified memory [38].

Experiments are run on a Intel Xeon E5-2698 v3 16 core, dual socket CPU @2.3 GHz, 256 GB RAM and the NVIDIA Tesla K80 (Kepler) GPU, NVIDIA Tesla P100 (Pascal) and NVIDIA Tesla V100 (Volta) GPUs. I use CUDA toolkit 9.0.176 and PGI 17.9. Table 2.2 shows the execution time of the solver per timestep for grid sizes of  $64 \times 64 \times 64$  and  $128 \times 128 \times 128$  on the CPU and the Kepler, Pascal and Volta GPUs. The CPU version of the code is developed using OpenMP parallelization and the FFTW library. I see that the GPU code is about two orders of magnitude faster than the CPU code.

Across GPU architectures, I see that Tesla P100 is  $2\times$  to  $3\times$  faster than the Tesla K80. This is due to the difference in the memory bandwidth between the two architectures. Tesla P100 has a theoretical peak memory bandwidth of 720 GB/s which is  $3\times$  that of Tesla K80 whose peak memory bandwidth is 240 GB/s. As the MHD3D code is memory intensive, I can see  $2\times$ - $3\times$  performance difference between the two architectures. Performance results over the Pascal and Volta architecture are quite similar (within 30%) as there is not a great difference in their memory bandwidths (720 GB/s vs 900 GB/s). To verify the correctness of the GPU accelerated solver, I compared the CPU and GPU outputs and computed the mean square error. This was found to be of the order of  $5.89\text{E-}15$ .

Grid Size	CPU	Kepler K80	Tesla P100	Tesla V100
$64 \times 64 \times 64$	0.4	0.02	0.01	0.01
$128 \times 128 \times 128$	5.89	0.12	0.04	0.03

Table 2.2: Execution time per timestep in seconds over CPU and Kepler, Pascal and Volta GPUs.

For larger grid sizes which do not fit in GPU memory, I use unified memory. On demand page migration and over-subscription features of unified memory are not supported on the Kepler K80 architecture. Hence, my analysis is restricted to the Pascal and Volta architectures.

Grid Size	CPU	Tesla P100	Tesla V100
$256 \times 256 \times 256$	65.82	0.32	0.22
$512 \times 512 \times 512$	566.12	80.97	92.81

Table 2.3: Execution time per timestep in seconds over CPU, Pascal and Volta GPUs for large grids.

Table 2.3 shows the execution time per timestep for large grids. For  $256 \times 256 \times 256$  grid size, the total memory footprint of the solver exceeds the GPU device memory of 16 GB. However, the working set of each kernel is within the GPU memory capacity. When the grid size becomes  $512 \times 512 \times 512$ , the working set of the GPU kernels is in some cases 40GB and does not fit completely within the GPU memory. As mentioned in Section 2.7.3, tiling the data typically helps in such a scenario, but since the solver code is interspersed with fourier transforms that need the complete data, it is not possible to do a tile-by-tile processing.

Therefore, in this case, there is frequent movement of pages back and forth between the CPU and GPU and a large number of page faults on the GPU. To reduce the page faults on the GPU (GPU page fault handling is expensive), I ensure that the data arrays on the CPU are pre-mapped on the GPU. This avoids a page fault on the first access. Eventually the page may migrate to the GPU (based on the unified memory system heuristics), but the mappings on the GPU page tables are kept updated.

Even with the above optimizations, the out-of-core solver is an order magnitude slower than the in-core solver, largely due to movement of pages between host and GPU and handling of the GPU page faults. Even with this additional overhead, the GPU accelerated code is able to show a speedup of 7x over the OpenMP version.

## 2.8 Future Scope

The implementation of some diagnostics viz. field line tracer, poincare section, modo-mode energy transfer in a triad [93] is in progress. The performance of the code can be improved by implementing implicit time solvers. In order to further enhance the speed of the code, the GPGPU parallel CUDA version of the code is being developed. At present the code can handle only periodic boundaries. The simulation of plasma flows in bounded domains with upgraded version of the code is under development.

## 2.9 Acknowledgements

The development as well as benchmarking of MHD3D has been done at Udbhav and Uday clusters at IPR. For benchmarking and performance results of G-MHD3D, K80, P100 and V100 GPU cards of NVIDIA has been used. I thank Samriddhi Sankar Ray, Akanksha Gupta, P N Maya for several helpful discussions. I acknowledge the support from ICTS program: ICTS/Prog-dcs/2016/05. The code has been ported to GPU by Nagavijayalakshmi Vydyanathan and Bharat Kumar from NVIDIA, Bengaluru. Porting the code G-MHD3D to IPR cluster Uday was done with Udaya Maurya. Also, I am thankful to Vinod Saini for helping me to develop the Particle Tracer subroutine from scratch which is based on the Cloud-In-Cell technique and the Boris Algorithm as particle pusher. I am also thankful

to Meghraj Sengupta for an illuminating discussion on particle pusher schemes in Particle-In-Cell method.



# Chapter 3

## Nonlinear Coherent Oscillation

### 3.1 Introduction

In the current Chapter, I describe one of the physics problems addressed in this Thesis using the code G-MHD3D described in the previous Chapter.

The fundamental problem of hydrodynamics that renders the long time scale prediction still open is the nonlinear interaction of modes. Consequently understanding energy cascades from different initial spectrum has been a longstanding challenge in the field of fluid dynamics. Recently, several direct numerical simulation (DNS) techniques have been developed to simulate fluid turbulence and have helped to analyse the shell to shell kinetic energy transfer in spectral space with the time evolution of any fluid governed by Navier-Stokes equation. The fluid equations traces the dynamics of *fluid elements*, which are collection of large number of interacting particles. Thus fluid picture inherently represents an infinite dimensional continuum system. This poses several fundamental challenging problems like time reversibility and entropy in the context of particle motion. Such problem is hard to solve analytically and has been addressed since long ago [94]. The complexity increases

manifold when the fluid is electrically conducting and hence becomes susceptible to magnetic field. The self generated magnetic field dynamically affects the fluid flows through the Lorentz force term in the momentum equation. Simultaneously, the flow of electrically charged fluid generates (and thereby sometimes cancels) magnetic field. Thus the energy accumulated in any mode may be expected to find new route via nonlinear cascade to other modes through transformation of kinetic to magnetic energy and vice versa. Thus the transformation of energy between kinetic and magnetic modes within the premise of single fluid magnetohydrodynamic (MHD) description of any magnetised fluid poses several novel fundamental problems that need to be addressed.

In the presence of weak resistivity, the MHD model is known to predict irreversible conversion of magnetic energy into fluid kinetic energy (i.e. reconnection) as well as conversion of kinetic energy into mean large scale magnetic field (i.e. dynamo). Therefore it is interesting to ask, for a given fluid type and magnetic field strength, are there fluid flow profiles which neither generate mean magnetic field nor the magnetic field energy converts to flow energy; instead there are nearly “reversible” coherent nonlinear oscillations? I have found that in both two and three dimensions there are ample examples of flows which at some typical parameter shows such oscillation of energy between two modes. For a wide range of initial flow speeds or Alfvén Mach number I have shown that the coherent nonlinear oscillation persists. As the Alfvén Mach number is increased further, a tendency to mean field dynamo (generation of large scale magnetic energy from kinetic energy) is also noticed.

However, the linearised MHD equations having a thermal gradient with free boundary conditions, is known to show overstability. In particular, overstability appears when  $\kappa > \eta$ , where  $\kappa$  and  $\eta$  are the co-efficient of thermal conductivity and resis-



tivity. Here in this work the system of equations considered, does not incorporate any thermal gradient and the full non-linearity of the equations are retained during the time evolution within a spatially periodic domain. Thus the oscillations I have observed, are not the case of overstability explored earlier in detail.

In this work, I find numerical observation of interplay of kinetic and magnetic energy in two as well as three dimensional single fluid MHD simulation for different sets of initial flow profiles. A finite mode representation of the field variables resulting in a set of nonlinear coupled ordinary differential equations has been presented in support of the pseudo-spectral DNS results. My numerical as well as analytical observations indicates that nonlinear reciprocity of kinetic and magnetic energy can take place within the frame-work of single fluid MHD representation of plasma and strongly depending on the  $M_A$ .

I start with a set of well known velocity flows as initial conditions and numerically time evolve the fluid as well as the magnetic variables self-consistently as an initial value problem. The magnetic field I choose is uniform in space to start with. I look into the regime where the Alfvén speed is equal to the sound speed of the system such that the energy transfer between the fluid and the magnetic variables are most efficient. This choice facilitates most efficient coupling between magnetic and kinetic variables through the Lorentz force term i.e.  $\vec{J} \times \vec{B}$ . I find a continuous nonlinear exchange of energy between fluid and magnetic variables. The key results that I obtain from my DNS study are:

- For decaying divergence-free two dimensional Orszag-Tang (OT) flow and Cat's Eye flow at Alfvén resonance ( $M_A = 1$ ), an initial uniform magnetic field profile leads to nonlinear coherent oscillation between kinetic and magnetic modes. (Section: 1.4.1, 1.4.2)

- For decaying divergence-free three dimensional Roberts flow, Cat's Eye flow and Arnold-Beltrami-Childress (ABC) flow at Alfvén resonance ( $M_A = 1$ ), an initial uniform magnetic field profile leads to nonlinear coherent oscillation between kinetic and magnetic modes. (Section: 1.4.4, 1.4.5, 1.4.6)
- The parameter dependency (Alfvén Mach number) of this oscillation for three dimensional ABC flow is studied indicating continuous transition between two nonlinear events - coherent nonlinear oscillation and dynamo effect. (Section: 1.4.7)
- These results are qualitatively supported by finite dimensional Galerkin truncated series expansion of the MHD equations. (Section: 1.5)
- For externally forced OT and ABC flows, the nearly ideal magnetohydrodynamic plasma acts as a forced-relaxed system. (Section: 1.4.8)

This work has been reported to arXiv and published recently [24, 25].

This Chapter is organised as follows. Section 3.2 summarises the equations that are time evolved in the code G-MHD3D described in Chapter 2. In Section 5.3, I provide all the parameters in which the code is run and section 3.4 provides all the direct numerical simulation (DNS) results I have obtained in two and three dimensions. Section 3.5 describes an analytical two dimensional finite mode representation of the DNS results and Section 4.6 summarises all the results and analysis performed in this work.

## 3.2 Governing Equations

The basic equations governing the dynamics of a magnetohydrodynamic fluid are as follows:

$$\frac{\partial \rho}{\partial t} + \vec{\nabla} \cdot (\rho \vec{u}) = 0 \quad (3.1)$$

$$\begin{aligned} \frac{\partial(\rho \vec{u})}{\partial t} + \vec{\nabla} \cdot \left[ \rho \vec{u} \otimes \vec{u} + \left( P + \frac{B^2}{2} \right) \mathbf{I} - \vec{B} \otimes \vec{B} \right] \\ = \mu \nabla^2 \vec{u} + \rho \vec{f} \end{aligned} \quad (3.2)$$

$$\frac{\partial \vec{B}}{\partial t} + \vec{\nabla} \cdot (\vec{u} \otimes \vec{B} - \vec{B} \otimes \vec{u}) = \eta \nabla^2 \vec{B} \quad (3.3)$$

$$P = C_s^2 \rho \quad (3.4)$$

In this system of equations,  $\rho$ ,  $\vec{u}$ ,  $P$  and  $\vec{B}$  are the density, velocity, kinetic pressure and magnetic field of a fluid element respectively.  $\mu$  and  $\eta$  denote the coefficient of kinematic viscosity and magnetic resistivity. I assume  $\mu$  and  $\eta$  are constants over space and time. The symbol “ $\otimes$ ” represents the dyadic between two vector quantities (see Chapter 2).

The kinetic Reynolds number ( $Re$ ) and magnetic Reynolds number ( $Rm$ ) are defined as  $Re = \frac{U_0 L}{\mu}$  and  $Rm = \frac{U_0 L}{\eta}$  where  $U_0$  is the maximum velocity of the fluid system to start with and  $L$  is the system length.

I also define the sound speed of the fluid as  $C_s = \frac{U_0}{M_s}$ , where,  $M_s$  is the sonic Mach number of the fluid. The Alfvén speed is determined from  $V_A = \frac{U_0}{M_A}$  where  $M_A$  is the Alfvén Mach number of the plasma. The initial magnetic field present in the plasma is determined from the relation  $B_0 = V_A \sqrt{\rho_0}$ , where,  $\rho_0$  is the initial density profile of the fluid.

### 3.3 Parameter Details

I choose  $L = 2\pi$  periodic box as my simulation domain and fix  $\rho_0 = 1$  and keep these parameters identical throughout my simulation. The initial magnitude of density ( $\rho_0$ ) is known to affect the dynamics and growth rate of an instability in a compressible neutral fluid [95, 96]. However, in this work the initial density is kept fixed ( $\rho_0 = 1$ ) for all the runs unless stated otherwise. It is also found that, in the long run in the incompressible limits, the density does not vary with space and time.

For two dimensional runs I choose a grid resolution of  $N_x = N_y = 128$  and a time stepping interval  $\delta t = 10^{-5}$ . The kinetic and magnetic Reynolds numbers are chosen as  $Re = Rm = 10^{-4}$ . My code is run for the incompressible limit ( $M_s = 0.01$ ).

For three dimensional runs I choose a grid resolution of  $N_x = N_y = N_z = 64$  and a time stepping interval  $\delta t = 10^{-4}$ . The kinetic and magnetic Reynolds numbers are chosen as  $Re = Rm = 450$ . For all cases I run my code for the incompressible limit ( $M_s = 0.1$ ).

For both two and three dimensional runs my results are checked with higher grid resolution ( $N$ ) and smaller time stepping ( $\delta t$ ) and no significant variation in the results of my test runs are found.

I choose  $M_A = 1$  i.e. the mean velocity ( $U_0$ ) is equal to the Alfvén speed of the system ( $V_A$ ) (i.e. Alfvén resonance) for both the two as well as the three dimensional runs.

For two dimensional flows the initial magnetic field profile is chosen as  $B_x = B_y = B_0$  and that for three dimensional flows as  $B_x = B_y = B_z = B_0$ .

## 3.4 Simulation Results

Orszag-Tang, Cat's eye, Roberts and Arnold-Beltrami-Childress flows are known to be the divergence-free flows. However, they are not stable solutions of single fluid MHD equations. In this section these flows are time evolved obeying the equations mentioned in Section 3.2 and the energy exchange between the fluid and magnetic modes are observed.

### 3.4.1 Results for Decaying 2D Orszag-Tang Flow

For two dimensional Orszag-Tang flow the velocity profile is chosen as

$$\begin{aligned} u_x &= -A \sin(k_0 y) \\ u_y &= +A \sin(k_0 x) \end{aligned} \tag{3.5}$$

with  $A = 1$  and  $k_0 = 1$ . The interchange of energy between kinetic and magnetic variables is plotted in Fig. 3.1. The x-axis represents the time evolution and the y-axis represents the shifted kinetic and magnetic energy where the shift indicates that the initial values of the corresponding variables are subtracted from the time evolution data. A long time evolution of the system with several cycles of oscillations with  $N = 256^2$ ,  $\delta t = 10^{-6}$ ,  $U_0 = 1$ ,  $k_0 = 1$ ,  $M_s = 0.01$ ,  $M_A = 1$  and  $Re = Rm = 10^{-5}$  are found to show numerical convergence. From figure in it evident that the time period of oscillation is  $T = 2.971$ .

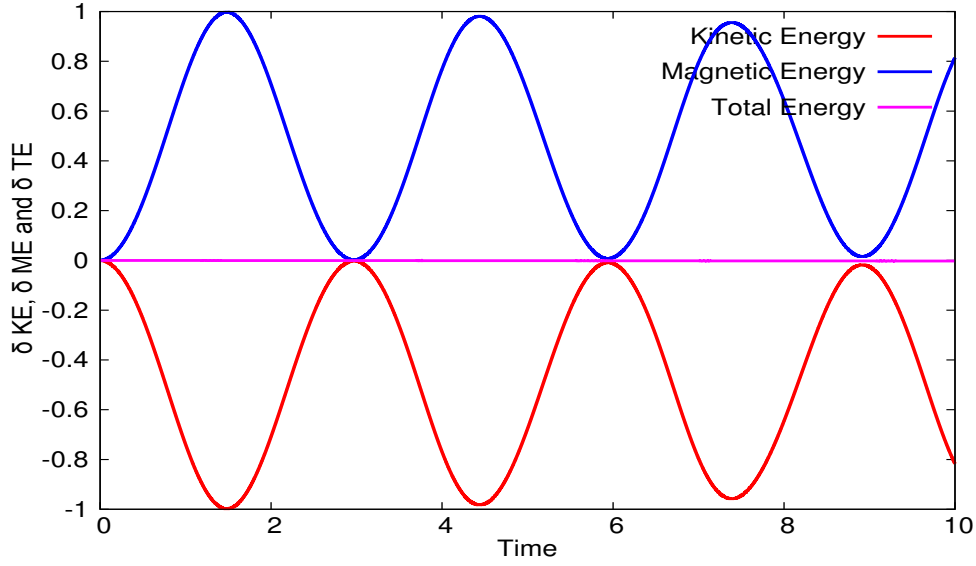


Figure 3.1: Time evolution of shifted kinetic  $[\delta KE = u^2(t) - u^2(0)]$ , magnetic  $[\delta ME = B^2(t) - B^2(0)]$  and total  $[\delta TE = u^2(t) - u^2(0) + B^2(t) - B^2(0)]$  energy per grid for two dimensional Orszag-Tang flow with  $N = 128^2$ ,  $U_0 = 1$ ,  $k_0 = 1$ ,  $M_s = 0.01$ ,  $M_A = 1$  and  $Re = Rm = 10^{-4}$  in the absence of external forcing. The energy keeps on switching between kinetic and magnetic modes keeping the total energy conserved. It is found that the time period of oscillation is  $T = 2.971$

### 3.4.2 Results for Decaying 2D Cat's Eye Flow

For two dimensional Cat's Eye flow the velocity profile is chosen as

$$\begin{aligned} u_x &= +\sin(k_0 x) \cos(k_0 y) - A \cos(k_0 x) \sin(k_0 y) \\ u_y &= -\cos(k_0 x) \sin(k_0 y) + A \sin(k_0 x) \cos(k_0 y) \end{aligned} \quad (3.6)$$

with  $A = 0.5$ ,  $k_0 = 1$ . The interchange of energy between kinetic and magnetic variables is plotted in Fig. 3.2. It is found that the time period of oscillation is  $T = 1.659$ .

### 3.4.3 Results for Forced 2D Orszag-Tang Flow

$$\vec{f} = \alpha \begin{bmatrix} -A \sin(k_f y) \\ +A \sin(k_f x) \end{bmatrix} \quad (3.7)$$

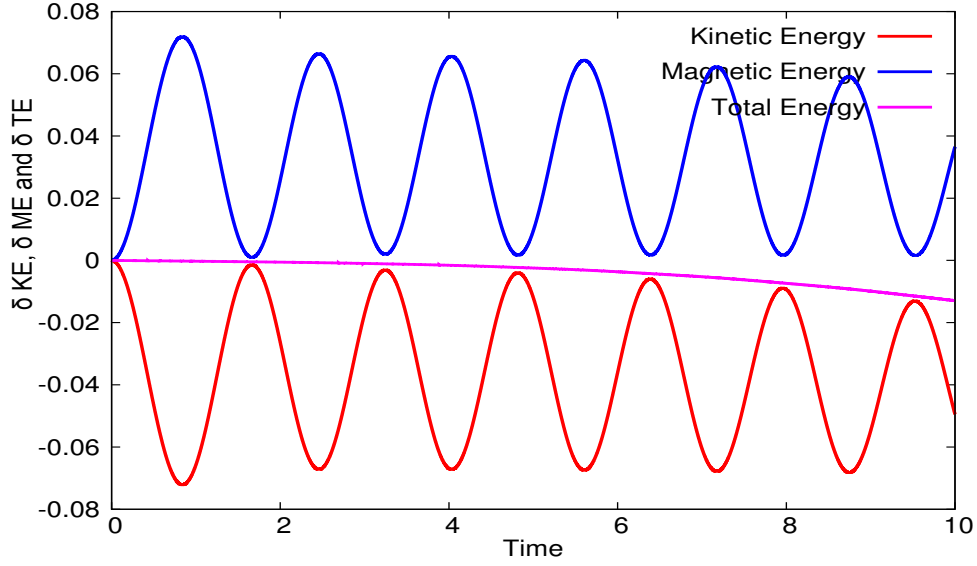


Figure 3.2: Time evolution of shifted kinetic [ $\delta KE = u^2(t) - u^2(0)$ ], magnetic [ $\delta ME = B^2(t) - B^2(0)$ ] and total energy [ $\delta TE = u^2(t) - u^2(0) + B^2(t) - B^2(0)$ ] per grid for two dimensional Cat's Eye flow with  $N = 128^2$ ,  $U_0 = 1$ ,  $A = 0.5$ ,  $k_0 = 1$ ,  $M_s = 0.01$ ,  $M_A = 1$  and  $Re = Rm = 10^{-4}$  in the absence of external forcing. The energy keeps on switching between kinetic and magnetic modes keeping the total energy conserved. The decay of total energy can be detrended by the multiplying the data by  $\exp(-2Dt)$  implying that it is solely due to viscous and resistive effects. The shift denotes the initial values of the kinetic and magnetic energies (at time  $t = 0$ ) are subtracted from the time evolution data of the corresponding variables. The time period of oscillation is  $T = 1.659$

I choose,  $\alpha = 0.1$ ,  $A = 1$  and  $k_f = 1$ . The kinetic and magnetic energy continue to oscillate but the magnitudes of the peaks vary with time. The total (kinetic + magnetic) energy for the decaying cases was constant and the decay can be detrended by the multiplying the data by  $\exp(-2Dt)$  implying that it is solely due to viscous and resistive effects. But for the forced case though the forcing acts for all the time over the whole system, the total energy oscillates with half the frequency of oscillation of the kinetic and magnetic energy [Fig. 3.3].

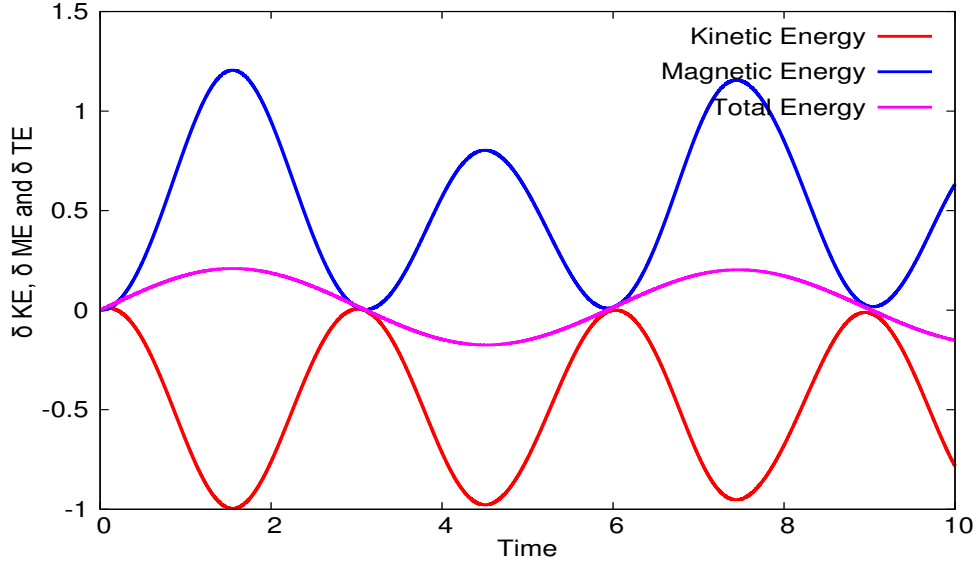


Figure 3.3: Time evolution of shifted kinetic  $[\delta KE = u^2(t) - u^2(0)]$ , magnetic  $[\delta ME = B^2(t) - B^2(0)]$  and total energy  $[\delta TE = u^2(t) - u^2(0) + B^2(t) - B^2(0)]$  per grid for two dimensional Orszag-Tang flow with  $N = 128^2$ ,  $U_0 = 1$ ,  $k_0 = 1$ ,  $M_s = 0.01$ ,  $M_A = 1$  and  $Re = Rm = 10^{-4}$  in the presence of external forcing. The energy keeps on switching between kinetic and magnetic modes. The total energy also oscillates around the same frequency and the whole system acts as a forced-relaxed system. The shift denotes the initial values of the kinetic and magnetic energies (at time  $t = 0$ ) are subtracted from the time evolution data of the corresponding variables.

### 3.4.4 Results for Decaying 3D Roberts Flow

For three dimensional Roberts flow the velocity profile is chosen as

$$\begin{aligned} u_x &= U_0[A \sin(k_0 z)] \\ u_y &= U_0[B \sin(k_0 x)] \\ u_z &= U_0[C \sin(k_0 y)] \end{aligned} \tag{3.8}$$

with  $A = B = C = 1$ ,  $k_0 = 1$ . The interchange of energy between kinetic and magnetic variables is plotted in Fig. 3.4. It is found that the time period of oscillation is  $T = 30.680$ .



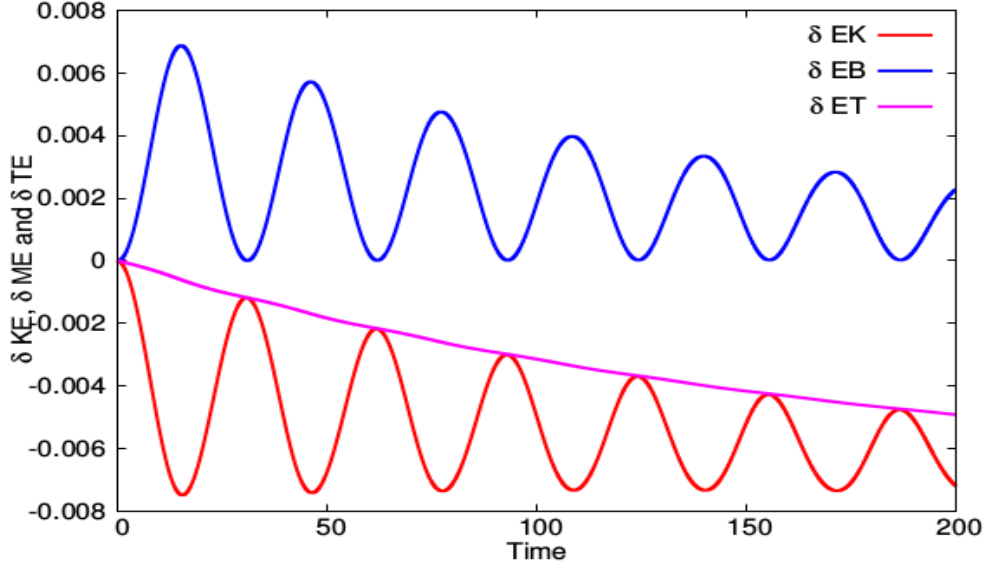


Figure 3.4: Time evolution of shifted kinetic  $[\delta KE = u^2(t) - u^2(0)]$ , magnetic  $[\delta ME = B^2(t) - B^2(0)]$  and total energy  $[\delta TE = u^2(t) - u^2(0) + B^2(t) - B^2(0)]$  per grid for three dimensional Roberts flow with  $N = 64^3$ ,  $U_0 = 0.1$ ,  $A = B = C = 1$ ,  $k_0 = 1$ ,  $M_s = 0.1$ ,  $M_A = 1$  and  $Re = Rm = 450$  in the absence of external forcing. The energy keeps on switching between kinetic and magnetic modes keeping the total energy conserved. The decay of total energy can be detrended by the multiplying the data by  $\exp(-2Dt)$  implying that it is solely due to viscous and resistive effects. The shift denotes the initial values of the kinetic and magnetic energies (at time  $t = 0$ ) are subtracted from the time evolution data of the corresponding variables. The time period of oscillation is  $T = 30.680$

### 3.4.5 Results for Decaying 3D Cat's Eye Flow

For three dimensional 3D Cat's Eye flow the velocity profile is chosen as

$$\begin{aligned} u_x &= U_0[B \sin(k_0 y)] \\ u_y &= U_0[A \sin(k_0 x)] \\ u_z &= U_0[A \cos(k_0 x) - B \cos(k_0 y)] \end{aligned} \tag{3.9}$$

with  $A = \sqrt{\frac{3}{5}}$ ,  $B = 2A$ . The interchange of energy between kinetic and magnetic variables is plotted in Fig. 3.5. It is found that the time period of oscillation is  $T = 30.510$ .

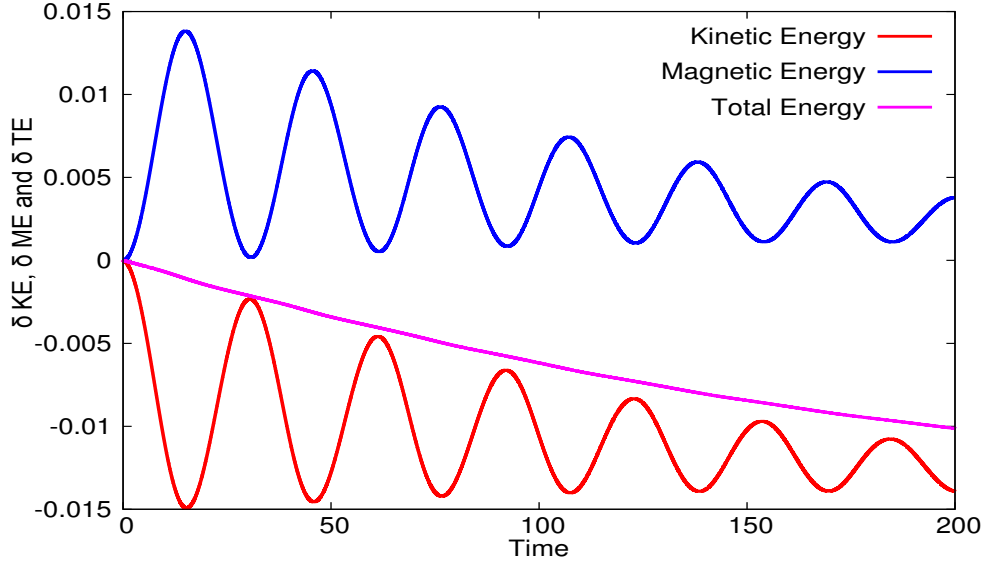


Figure 3.5: Time evolution of shifted kinetic [ $\delta KE = u^2(t) - u^2(0)$ ], magnetic [ $\delta ME = B^2(t) - B^2(0)$ ] and total energy [ $\delta TE = u^2(t) - u^2(0) + B^2(t) - B^2(0)$ ] per grid for three dimensional Cat's Eye flow with  $N = 64^3$ ,  $U_0 = 0.1$ ,  $A = \sqrt{\frac{3}{5}}$ ,  $B = 2A$ ,  $k_0 = 1$ ,  $M_s = 0.1$ ,  $M_A = 1$  and  $Re = Rm = 450$  in the absence of external forcing. The energy keeps on switching between kinetic and magnetic modes keeping the total energy conserved. The decay of total energy can be detrended by the multiplying the data by  $\exp(-2Dt)$  implying that it is solely due to viscous and resistive effects. The shift denotes the initial values of the kinetic and magnetic energies (at time  $t = 0$ ) are subtracted from the time evolution data of the corresponding variables. The time period of oscillation is  $T = 30.510$

### 3.4.6 Results for Decaying 3D ABC Flow

For three dimensional Arnold-Beltrami-Childress flow I choose the velocity profile as

$$\begin{aligned} u_x &= U_0[A \sin(k_0 z) + C \cos(k_0 y)] \\ u_y &= U_0[B \sin(k_0 x) + A \cos(k_0 z)] \\ u_z &= U_0[C \sin(k_0 y) + B \cos(k_0 x)] \end{aligned} \tag{3.10}$$

with  $A = B = C = 1$ . The interchange of energy between kinetic and magnetic variables is plotted in Fig. 3.6. It is found that the time period of oscillation is  $T = 30.171$ .

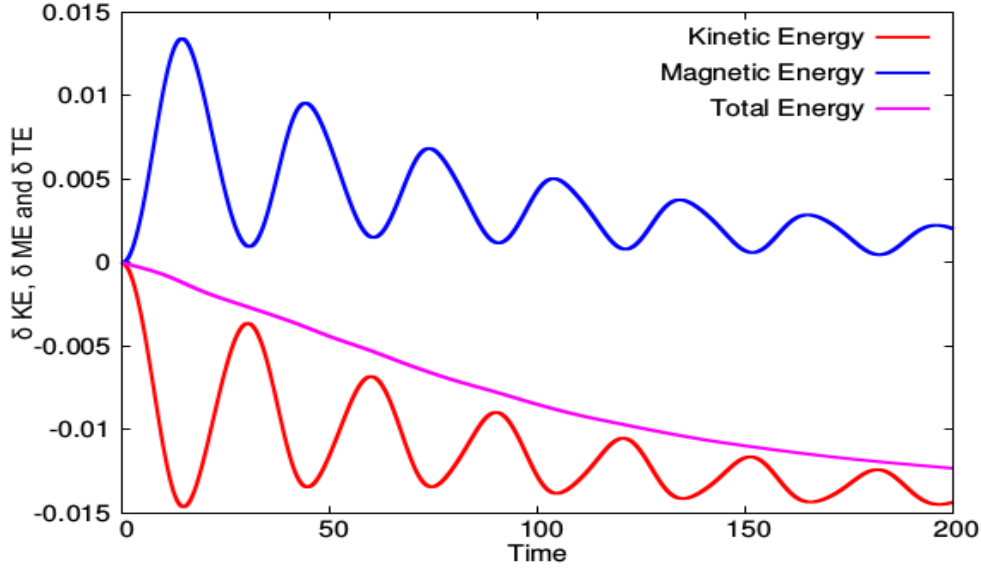


Figure 3.6: Time evolution of shifted kinetic  $[\delta KE = u^2(t) - u^2(0)]$ , magnetic  $[\delta ME = B^2(t) - B^2(0)]$  and total energy  $[\delta TE = u^2(t) - u^2(0) + B^2(t) - B^2(0)]$  per grid for three dimensional Arnold-Beltrami-Childress flow with  $N = 64^3$ ,  $U_0 = 0.1$ ,  $A = B = C = 1$ ,  $k_0 = 1$ ,  $M_s = 0.1$ ,  $M_A = 1$  and  $Re = Rm = 450$  in the absence of external forcing. The energy keeps on switching between kinetic and magnetic modes keeping the total energy conserved. The decay of total energy can be detrended by the multiplying the data by  $\exp(-2Dt)$  implying that it is solely due to viscous and resistive effects. The shift denotes the initial values of the kinetic and magnetic energies (at time  $t = 0$ ) are subtracted from the time evolution data of the corresponding variables. The time period of oscillation is  $T = 30.171$

### 3.4.7 Analysis of Decaying 3D ABC Flow

#### Effect of Initial Wave-number

I choose  $k_0 = 1, 2, 4, 8, 16$  keeping  $M_A = 1$ . The frequency of oscillation increases with the increase of  $k_0$  value. However the viscous  $(\mu \nabla^2 \vec{u})$  as well as the resistive terms  $(\eta \nabla^2 \vec{B})$  in Equation (5.2 and 5.3) affects the dynamics heavily when a higher wavenumber is excited. It is because the second derivative in the viscous and the resistive terms becomes more prominent when the velocity and magnetic field variables contain a higher magnitude of  $k_0$  [Table 3.1, Fig. 3.9].

$k_0$	Time Period of Oscillation (T)
1	30.171
2	15.001
4	7.410
8	3.620
16	1.749

Table 3.1: Frequency of oscillation ( $\omega$ ) of kinetic and magnetic energy with mode number of excitation ( $k_0$ )

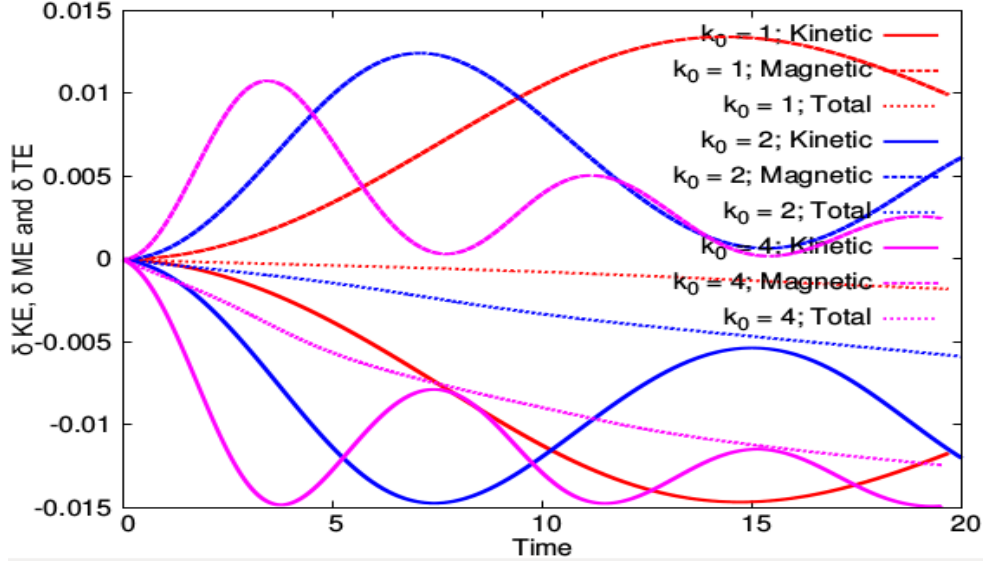


Figure 3.7: Time evolution of shifted kinetic (solid)  $[\delta KE = u^2(t) - u^2(0)]$ , magnetic (dashed)  $[\delta ME = B^2(t) - B^2(0)]$  and total (dotted)  $[\delta TE = u^2(t) - u^2(0) + B^2(t) - B^2(0)]$  energy per grid for three dimensional Arnold-Beltrami-Childress flow with  $N = 64^3$ ,  $U_0 = 0.1$ ,  $A = B = C = 1$ ,  $k_0 = 1$  (red), 2 (blue), 4 (magenta),  $M_s = 0.1$ ,  $M_A = 1$  and  $Re = Rm = 450$  in the absence of external forcing. Drag forces are found to affect the kinetic modes more than the magnetic modes as expected and explained in the text. The shift denotes the initial values of the kinetic and magnetic energies (at time  $t = 0$ ) are subtracted from the time evolution data of the corresponding variables.

### Effect of Alfven Speed

I study the effect of Alfven speed ( $V_A$ ) on the energy exchange process by changing the Alfven Mach number  $M_A$  for  $k_f = 1$ . Fig.(3.10) represents the oscillation of kinetic energy for  $M_A = 0.1, 0.2, 0.3, 0.4, 0.5$  and Fig.(3.11) represents the oscillation of kinetic energy for  $M_A = 0.5, 1.0, 1.5$ . From both the figures it is evident that the frequency of oscillation decreases linearly with the increase of  $M_A$ . However if I further increase  $M_A$  to 10, 100 and 1000 the oscillation vanishes and saturation of

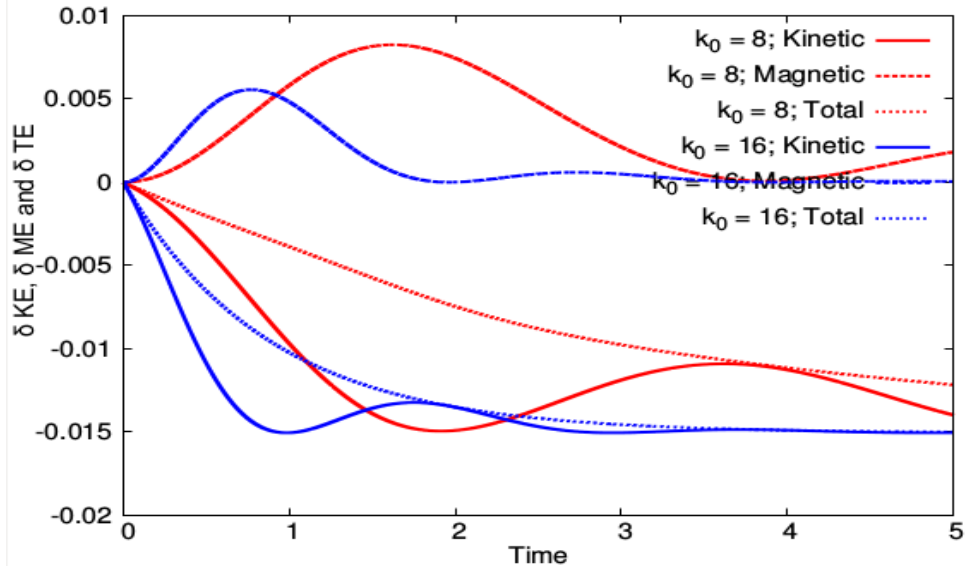


Figure 3.8: Time evolution of shifted kinetic (solid) [ $\delta KE = u^2(t) - u^2(0)$ ], magnetic (dashed) [ $\delta ME = B^2(t) - B^2(0)$ ] and total (dotted) [ $\delta TE = u^2(t) - u^2(0) + B^2(t) - B^2(0)$ ] energy per grid for three dimensional Arnold-Beltrami-Childress flow with  $N = 64^3$ ,  $U_0 = 0.1$ ,  $A = B = C = 1$ ,  $k_0 = 8$  (red), 16 (blue),  $M_s = 0.1$ ,  $M_A = 1$  and  $Re = Rm = 450$  in the absence of external forcing. Drag forces are found to affect the kinetic modes more than the magnetic modes as expected and explained in the text. The shift denotes the initial values of the kinetic and magnetic energies (at time  $t = 0$ ) are subtracted from the time evolution data of the corresponding variables.

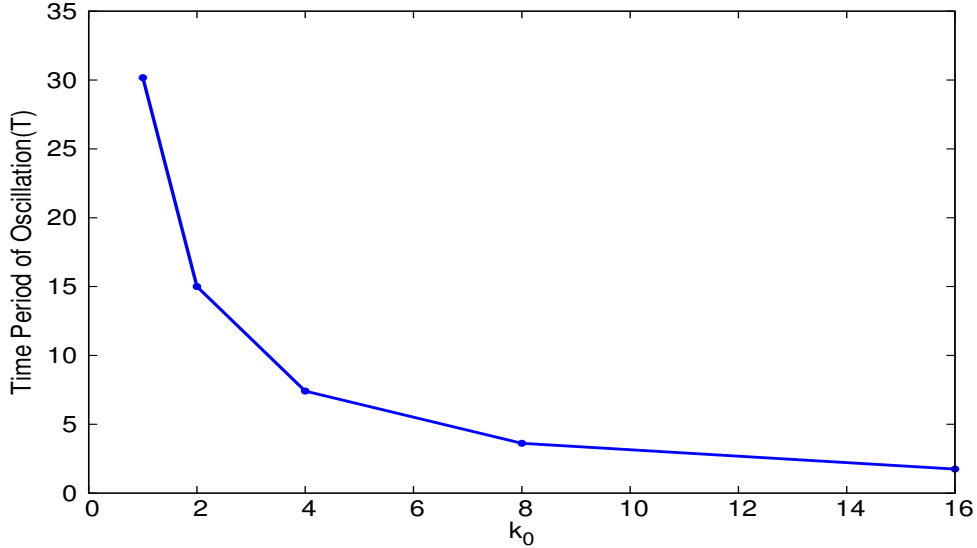


Figure 3.9: Variation of time period of oscillation ( $T$ ) of kinetic and magnetic energy with  $k_0$ . [see Table 3.1]

magnetic energy is observed after a linear growth of magnetic energy at the cost of kinetic energy indicating a dynamo effect taking place [Fig.3.13].

I primarily believe these oscillations are due to excitation of Alfvén waves. I know the time period of oscillation of Alfvén wave ( $T_{Alfvén}$ ) varies linearly with  $B_0$  which is directly proportional to  $V_A = \frac{U_0}{M_A}$ . Thus if,  $M_A$  is increased,  $T_{Alfvén}$  decreases linearly Fig.(3.10, 3.11). I analyse the frequency of oscillation for a series of  $M_A$  values and find good agreement with this linearity prediction [Table 3.2, Fig. 3.12].

$M_A$	Time Period of Oscillation (T)
0.1	3.150
0.2	6.268
0.3	9.364
0.4	12.428
0.5	15.461
1.0	30.171
1.5	43.238

Table 3.2: Time period of oscillation ( $T$ ) of kinetic and magnetic energy with  $M_A$ .

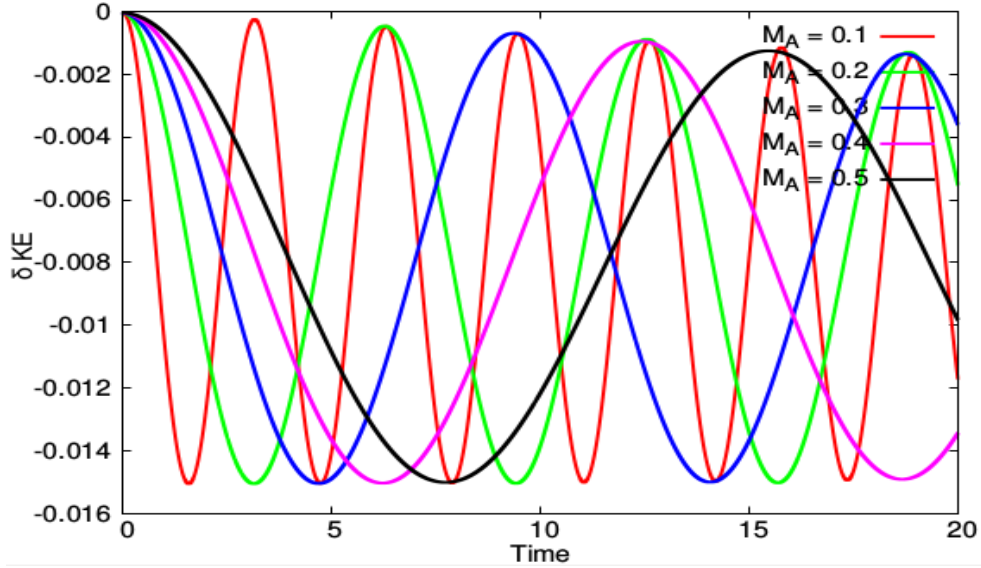


Figure 3.10: Time evolution of shifted kinetic energy [ $\delta KE = u^2(t) - u^2(0)$ ] per grid for three dimensional Arnold-Beltrami-Childress flow with  $N = 64^3$ ,  $U_0 = 0.1$ ,  $A = B = C = 1$ ,  $k_0 = 1$ ,  $M_s = 0.1$ ,  $M_A = 0.1$  (red), 0.2 (green), 0.3 (blue), 0.4 (magenta), 0.5 (black) and  $Re = Rm = 450$  in the absence of external forcing. The frequency of oscillation decreases with the increase of  $M_A$ . The shift denotes the initial values of the kinetic and magnetic energies (at time  $t = 0$ ) are subtracted from the time evolution data of the corresponding variables.

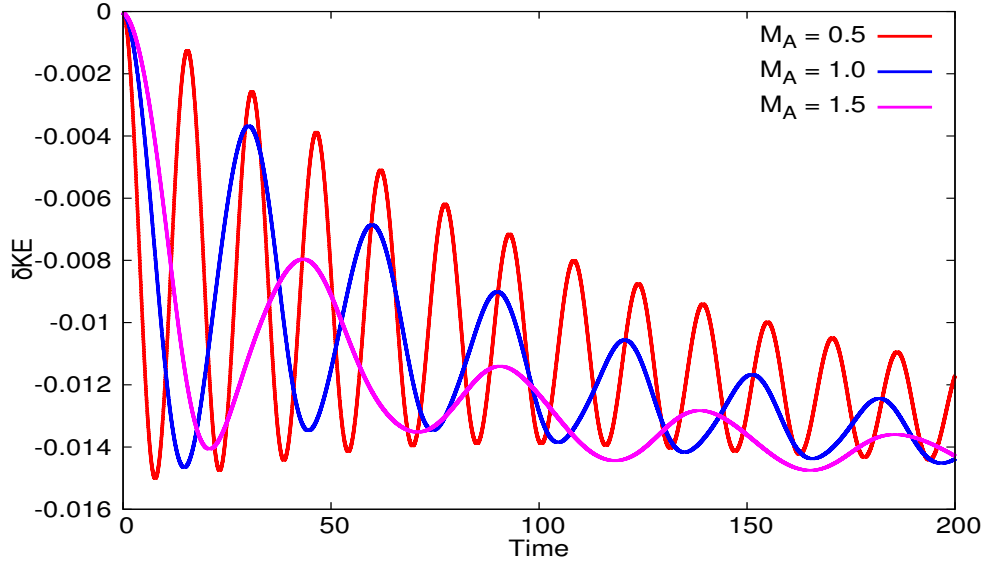


Figure 3.11: Time evolution of shifted kinetic energy [ $\delta KE = u^2(t) - u^2(0)$ ] per grid for three dimensional Arnold-Beltrami-Childress flow with  $N = 64^3$ ,  $U_0 = 0.1$ ,  $A = B = C = 1$ ,  $k_0 = 1$ ,  $M_s = 0.1$ ,  $M_A = 0.5$  (red), 1 (blue), 1.5 (magenta) and  $Re = Rm = 450$  in the absence of external forcing. The frequency of oscillation decreases with the increase of  $M_A$ . The shift denotes the initial values of the kinetic and magnetic energies (at time  $t = 0$ ) are subtracted from the time evolution data of the corresponding variables.

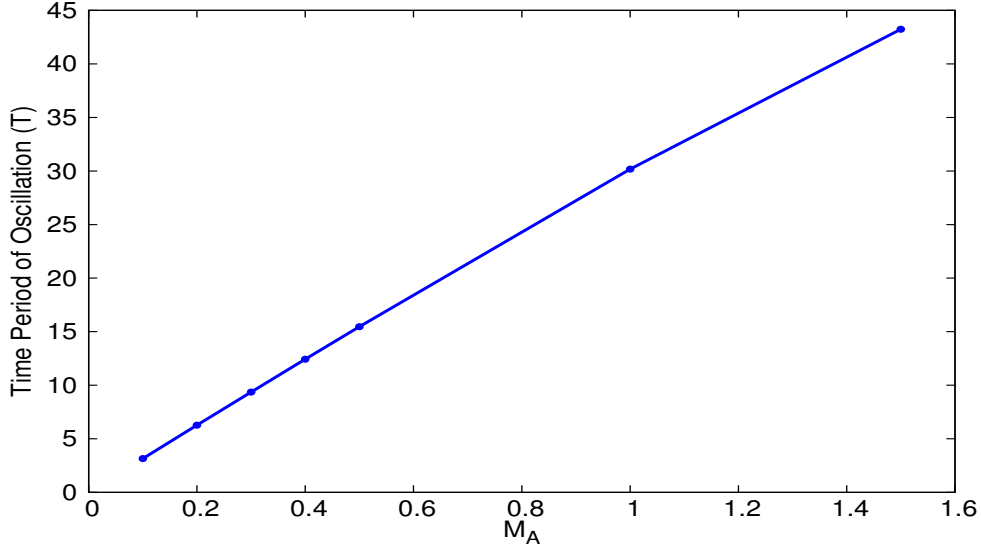


Figure 3.12: Variation of time period of oscillation ( $T$ ) of kinetic and magnetic energy with  $M_A$ . [see Table 3.2]

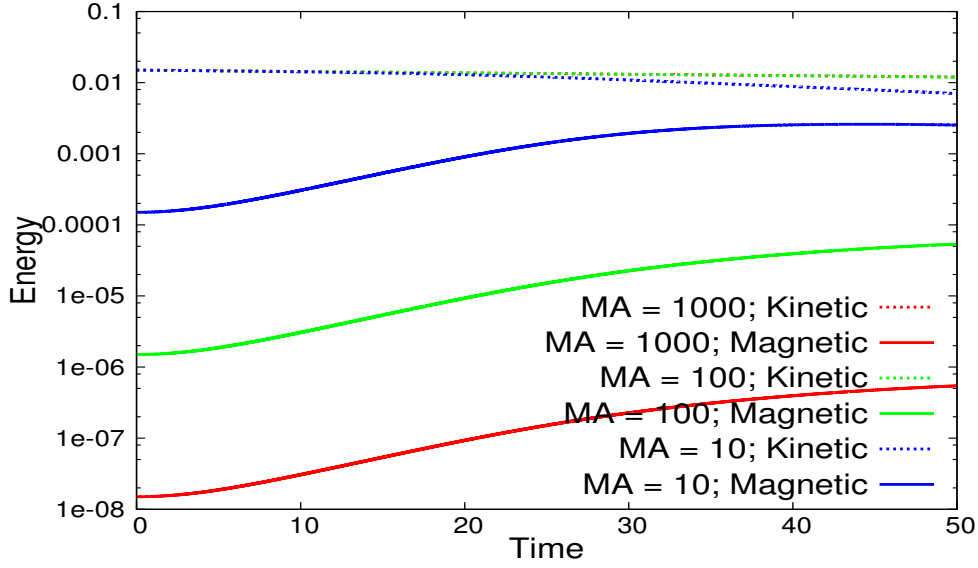


Figure 3.13: Saturation of magnetic energy with higher values of  $M_A$  indicating “dynamo effect”.

### 3.4.8 Results for Forced ABC Flow

Now I turn on the forcing on the velocity field. The forcing term I apply for all the time in the system is as follows:

$$\vec{f} = \alpha \begin{bmatrix} A \sin(k_f z) + C \cos(k_f y) \\ B \sin(k_f x) + A \cos(k_f z) \\ C \sin(k_f y) + B \cos(k_f x) \end{bmatrix} \quad (3.11)$$

I choose,  $\alpha = 0.1$ ,  $A = B = C = 1$  and  $k_f = 1$ .

Similar to the externally forced two dimensional system [Fig.(3.3)], the total energy oscillates with time Fig.(3.14). Initially [Fig.(3.15)] the frequency of oscillation of kinetic and magnetic energy were same though every second peak of magnetic energy had much lesser amplitude. The frequency of total energy is half of the frequency of kinetic energy. In intermediate time of evolution [Fig.(3.16)], the every second weak peak of magnetic energy smoothes out and in the late time evolution [Fig.(3.17)] I observe that the frequency of oscillation of magnetic energy becomes



half of that of kinetic energy thereby becoming similar to that of total energy. I also plot the Lissajous curve of Kinetic and magnetic energy for the forced system in Fig. (3.18).

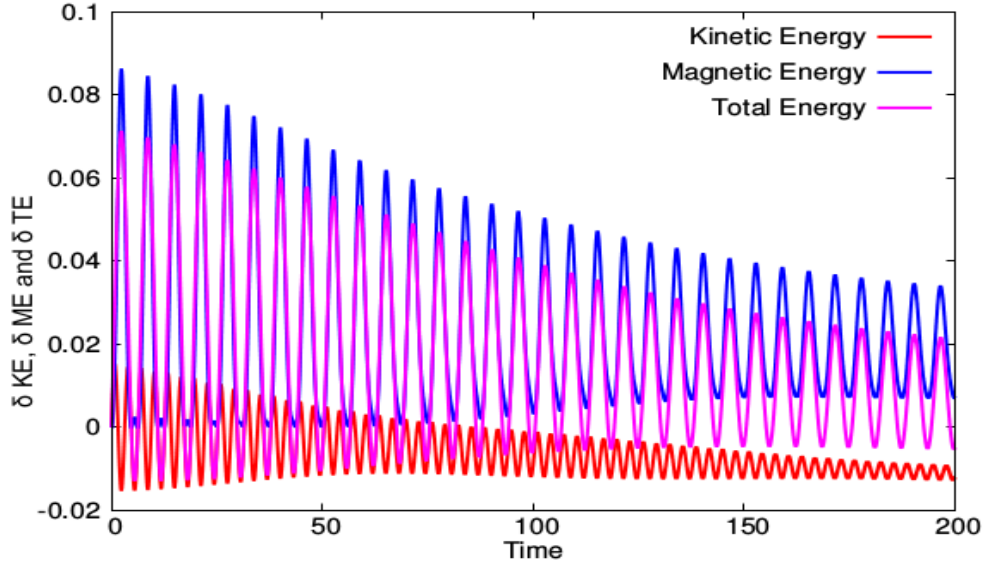


Figure 3.14: Time evolution of shifted kinetic  $[\delta KE = u^2(t) - u^2(0)]$ , magnetic  $[\delta ME = B^2(t) - B^2(0)]$  and total energy  $[\delta TE = u^2(t) - u^2(0) + B^2(t) - B^2(0)]$  per grid for three dimensional Arnold-Beltrami-Childress flow with  $N = 64^3$ ,  $U_0 = 0.1$ ,  $A = B = C = 1$ ,  $k_0 = 1$ ,  $M_s = 0.1$ ,  $M_A = 1$  and  $Re = Rm = 450$  in the presence of external forcing. The energy keeps on switching between kinetic and magnetic modes. The total energy also oscillates around the same frequency and the whole system acts as a forced-relaxed system. The shift denotes the initial values of the kinetic and magnetic energies (at time  $t = 0$ ) are subtracted from the time evolution data of the corresponding variables.

### 3.5 Galerkin Representation in Two dimensions

In order to gain further understanding of the process, I resort to the finite mode or Galerkin representation for the field variables. The analytical theory is constructed for two dimensional decaying cases and is believed to hold for three dimensional decaying phenomena also. In two dimensions, I construct stream function ( $\psi$ ) defined as  $\vec{u} = \hat{z} \times \vec{\nabla} \psi$  and magnetic vector potential ( $\vec{A}$ ), defined as,  $\vec{B} = \vec{\nabla} \times \vec{A}$ . In two

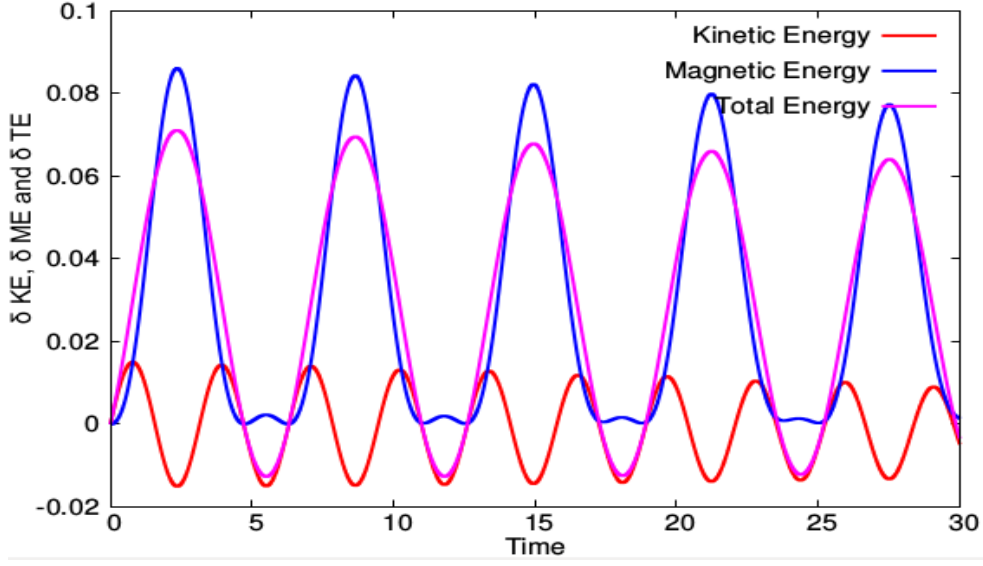


Figure 3.15: Initial time evolution obtained from Fig. 3.14.

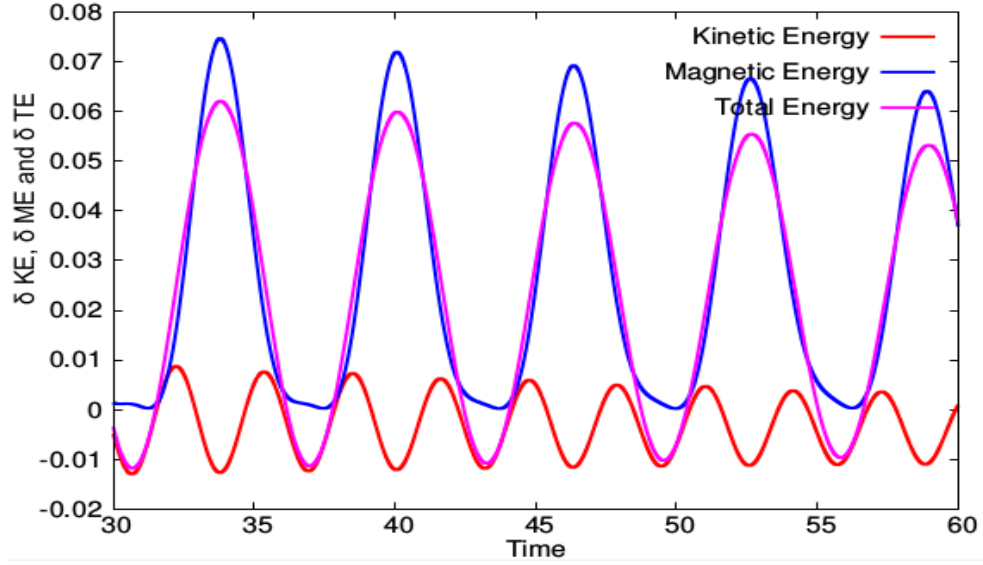


Figure 3.16: Intermediate time evolution obtained from Fig. 3.14.

dimensions the normalised incompressible MHD equations turns out as

$$\begin{aligned} \frac{\partial}{\partial t} \nabla^2 \psi + (\hat{z} \times \vec{\nabla} \psi \cdot \vec{\nabla}) \nabla^2 \psi \\ = -\vec{\nabla} \times ((\vec{\nabla} \times \vec{B}) \times \vec{B}) \end{aligned} \quad (3.12)$$

$$\frac{\partial A}{\partial t} + (\hat{z} \times \vec{\nabla} \psi \cdot \vec{\nabla}) A = 0 \quad (3.13)$$

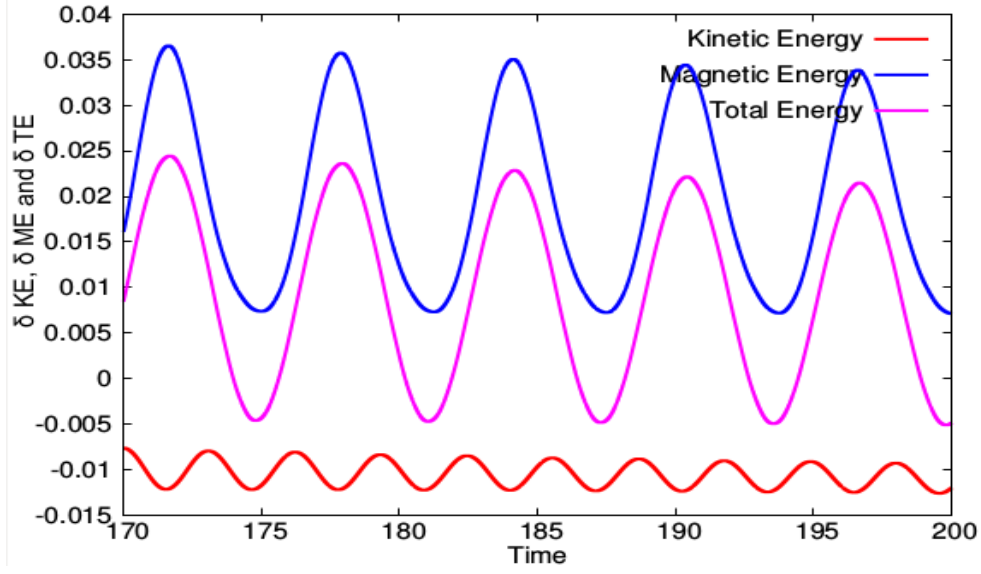


Figure 3.17: Late time evolution obtained from Fig. 3.14.

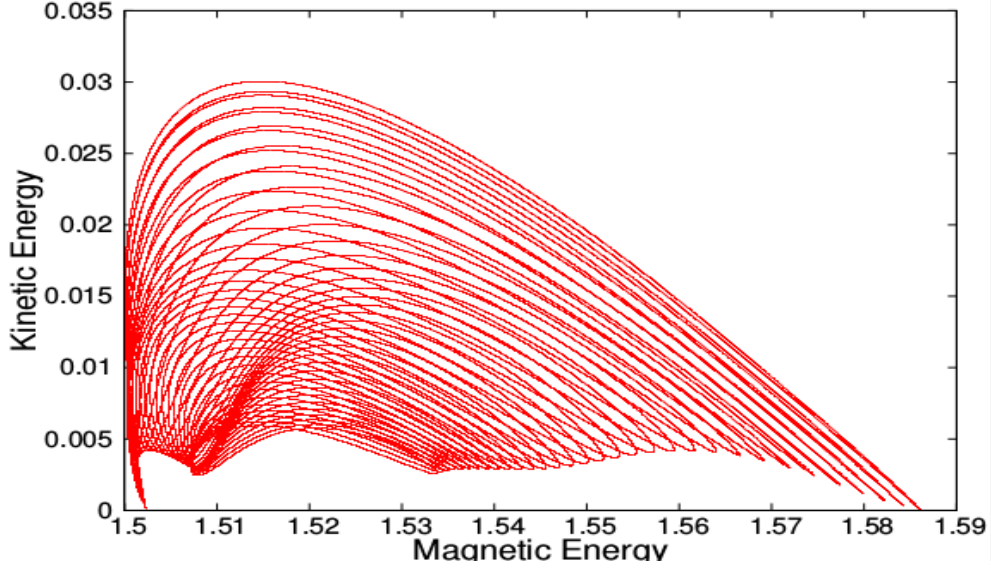


Figure 3.18: Time evolution of kinetic and magnetic energy per grid for three dimensional Arnold-Beltrami-Childress flow with  $N = 64^3$ ,  $U_0 = 0.1$ ,  $A = B = C = 1$ ,  $k_0 = 1$ ,  $M_s = 0.1$ ,  $M_A = 0.1$  and  $Re = Rm = 450$  in the presence of external forcing. The shift denotes the initial values of the kinetic and magnetic energies (at time  $t = 0$ ) are subtracted from the time evolution data of the corresponding variables.

I represent the finite mode expansion as,

$$\begin{aligned} \psi(x, y) = & \psi_0 \sin kx + e^{iky}(\psi_1 + \psi_3 \cos kx) \\ & + e^{-iky}(\psi_1^* + \psi_3^* \cos kx) \end{aligned} \quad (3.14)$$

$$\begin{aligned} A(x, y) = & A_0 \sin kx + e^{iky}(A_1 + A_3 \cos kx) \\ & + e^{-iky}(A_1^* + A_3^* \cos kx) \end{aligned} \quad (3.15)$$

where  $k$  is the wave vector corresponding to the largest scale length of the system. Substituting Equation 3.14 and 3.15 into Equation 5.2 and 3.13 I obtain the time evolution of the galerkin truncated modes. The evolution of various modes of stream function and magnetic vector potential can thus be written as,

$$\frac{d\psi_0}{dt} = ik^2(\psi_3^*\psi_1 - \psi_3\psi_1^*) \quad (3.16)$$

$$\frac{d\psi_1}{dt} = \frac{i}{2}k^2(\psi_0\psi_3 + A_0A_3) \quad (3.17)$$

$$\frac{d\psi_3}{dt} = 0 \quad (3.18)$$

$$\frac{d\psi_0^*}{dt} = -ik^2(\psi_3\psi_1^* - \psi_3^*\psi_1) \quad (3.19)$$

$$\frac{d\psi_1^*}{dt} = -\frac{i}{2}k^2(\psi_0^*\psi_3^* + A_0^*A_3^*) \quad (3.20)$$

$$\frac{d\psi_3^*}{dt} = 0 \quad (3.21)$$

$$\frac{dA_0}{dt} = ik^2(A_3\psi_1^* - A_3^*\psi_1 + A_1\psi_3^* - A_1^*\psi_3) \quad (3.22)$$

$$\frac{dA_1}{dt} = \frac{i}{2}k^2(A_0\psi_3 - A_3\psi_0) \quad (3.23)$$

$$\frac{dA_3}{dt} = ik^2(A_0\psi_1 - A_1\psi_0) \quad (3.24)$$

$$\frac{dA_0^*}{dt} = -ik^2(A_3^*\psi_1 - A_3\psi_1^* + A_1^*\psi_3 - A_1\psi_3^*) \quad (3.25)$$

$$\frac{dA_1^*}{dt} = -\frac{i}{2}k^2(A_0^*\psi_3^* - A_3^*\psi_0^*) \quad (3.26)$$

$$\frac{dA_3^*}{dt} = -ik^2(A_0^*\psi_1^* - A_1^*\psi_0^*) \quad (3.27)$$

I start with a case similar to that of my initial condition used for the DNS code ( $\psi_0 = 1, \psi_1 = 0 = \psi_3, \psi_0^* = \psi_1^* = \psi_3^* = 0, A_0 = A_1 = A_3 = 1, A_0^* = A_1^* = A_3^* = 0$ )

and  $k = 1$ ) and time evolve the above set of ordinary differential equations using RK4 method. In Fig. 3.19 I show the time evolution of real part of  $\psi_1$  and  $A_1$ . The variables ( $\psi_1$  and  $A_1$ ) are found to keep exchanging their values as the time evolves.

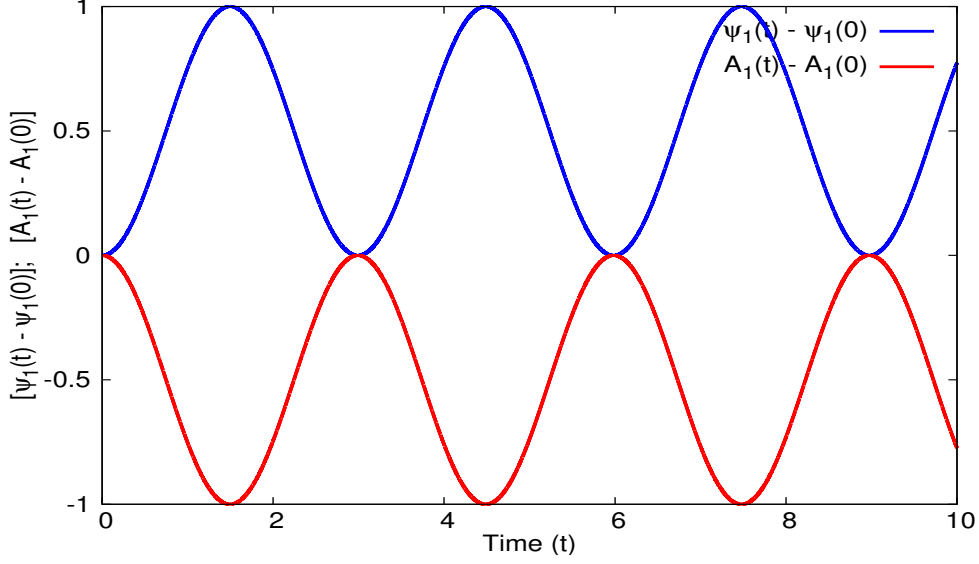


Figure 3.19: Galerkin truncated two dimensional MHD equations representing similar nonlinear coherent oscillations observed in DNS results with  $k = 1$ .

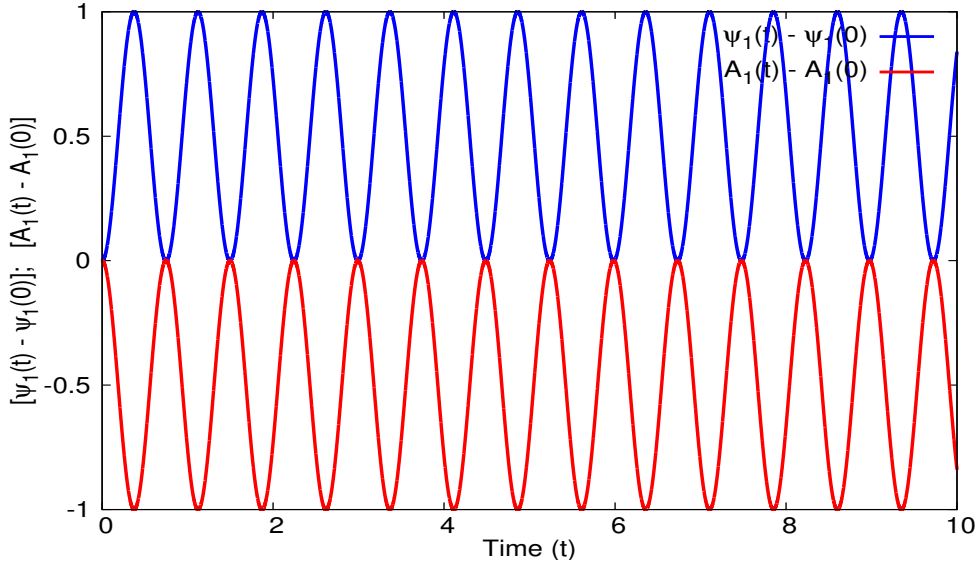


Figure 3.20: Galerkin truncated two dimensional MHD equations representing similar nonlinear coherent oscillations observed in DNS results with  $k = 2$ .

I also find the increment of frequency with the increase of  $k_0$  in two dimensional system similar to that in three dimensional system [Fig 3.20,3.21].

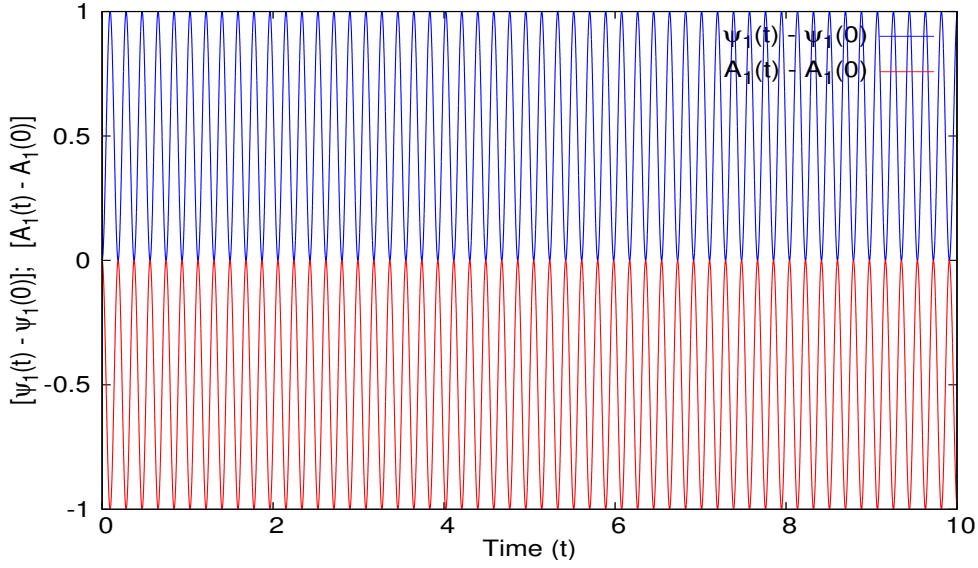


Figure 3.21: Galerkin truncated two dimensional MHD equations representing similar nonlinear coherent oscillations observed in DNS results with  $k = 4$ .

I further explore the parameter space by choosing lower values of  $A$  indicating the higher  $M_A$  cases where the “dynamo effect” happened in the 3D DNS runs. No saturation of magnetic energy is observed in the low degree of freedom model, indicating that the dynamo effect requires more number of modes to occur which is beyond the scope of the present analytical model.

### 3.6 Summary and Future Work

In this chapter I have shown the single fluid magnetohydrodynamic equations support energy exchange between kinetic and magnetic variables over a long enough period in both two and three dimensions. Thus it is shown that the energy exchange phenomena takes place for both non-chaotic as well as chaotic flow fields. The time period of oscillation of the energy exchange is found to vary linearly with Alfvén Mach number ( $M_A$ ). Also frequency is seen to increase with the initial wave-number ( $k$ ) excited within the flow. In presence of an external forcing identical to the initial velocity field, the system is found to act as a forced-relaxed system showing the periodic variation of the total energy of the system as well as exchange

of energy between kinetic and magnetic modes.

The three dimensional calculations are performed over  $64^3$  grid resolution. A better spatial resolution is expected to be capable of simulating higher fluid and magnetic Reynolds number runs. Thus the periodicity of energy exchange in three dimensional flows could be observed for larger number of cycles for high resolution runs. However, it is expected that, the higher resolution runs will not qualitatively change the basic findings discovered in this Chapter and only improve the results in terms of numbers of cycles of oscillations.





# Chapter 4

## Recurrence

### 4.1 Introduction

In Chapter 3, I have demonstrated coherent nonlinear oscillation between kinetic and magnetic energies within the premise of single fluid MHD model. In the current Chapter I delve into the structures of the fluid and magnetic variables in three dimensions for various flow fields mentioned in the previous Chapter. This clearly brings out distinctions between flows that appear to show two opposite behaviours mediated through energy exchange mentioned in the previous Chapter. Flows of one type that reconstructs the initial condition, I call “Recurrence” type and the other “Non-recurrence” type. It is found that, though recurrence is quite common in nature, it is not studied in detail in electromagnetic simulations earlier.

Recurrence phenomenon implies a repeated occurrence of a ‘state’ in a dynamical system including the spatial structures involved. However the observation of recurrence and its criterion critically depend on the dimensionality of the system. For example, a spring pendulum keeps the energy back and forth almost completely between the spring and the pendulum for several oscillation periods [97]. A non-linear interaction leading to the recurrence for a spring-pendulum system has been invoked

to explain many such ideas [98, 99]. The first approach to solve the problem from the point of view of effective degrees of freedom is due to Falk [100, 101].

Reconstruction of the vibrations of molecules in an one dimensional string was first numerically observed by Fermi *et al* (commonly known as ‘Fermi-Pasta-Ulam-Tsingou (FPUT) Problem’ [78]). The excitation of a fundamental mode in a string generates further higher modes with time - a natural expectation from statistical mechanics point of view. However, the authors observed, the energy comes back to the fundamental mode after further time evolution - a completely counter-intuitive phenomena. Such surprising results of periodic reconstruction of the initial condition showed the existence of a high wave-number cut-off in the instability and confirmed that the active participants in the energy sharing process are limited to a finite range of wave-numbers even though infinite degrees of freedom is available to the system. This indicated that the system will never “*thermalise*”. Zabusky and Kruskal [79] were the first to explain it from the aspect of interaction of solitons. Later Chirikov [102] explained the FPUT (or FPU) problem from *dynamical chaos* approach, insisting on the dimensionality of the problem.

Yuen and Ferguson [80] observed FPUT recurrence in two spatial dimensions for a fluid system and Thyagaraja [70] explained their findings using one-dimensional nonlinear Schrodinger equations from the point of view of number of conserved quantities stressing on the possibility of recurrence in dissipative open systems. Thyagaraja [70] also commented on the possibility of solutions of Navier-Stokes equation having finite number of effective degrees of freedom in Benard and Couette flow extending a conjecture by Landau, expecting a quasi-periodic motion [103]. It was suggested that “Stable, recurrent motions are common to all physical systems which can be characterized as having, effectively, a finite number of degrees of freedom” [70]. However, it was found that in more than one dimension, the criteria for observing a non-collapsing recurrent dynamics was complicated and no general criteria

was found in the Lagrange and Poisson stability approach [81, 104]. Later on such phenomena was observed in shallow water waves [48], ocean waves [49], Couette turbulence [50] and in quantum dynamics [105]. A detailed picture of recurrence in dynamical system is captured in the sense of Poincare recurrence by Katok and Hasselblatt [47].

Tajima *et al* [106] had observed a complete reconstruction of Langmuir wave packets following its initial break-up in two spatial dimensional electrostatic particle simulation including ion and electron dynamics. Kaw *et al* [107] identified the reconstruction as the spatial density dependence of the plasma frequency that causes in and out of phase oscillations.

To the best of my knowledge recurrence phenomena has never been observed in simple 3D electromagnetic simulations of magnetised plasmas. The solutions of Navier-Stokes equation having lower number of effective degrees of freedom was conjectured by Landau [103]. In the presence of Maxwell's equations in a magnetohydrodynamic (MHD) fluid, where the degrees of freedom increases by several times, the criteria for observation of recurrence get more involved and the possibility of happening of recurrence phenomena in MHD systems may be expected to get reduced because of the extra dimensionality in the system as compared to hydrodynamic system.

In this Chapter, I describe an observation of a near complete structural reconstruction of certain initial flow profiles in time - a recurrence phenomena - in three dimensional MHD plasma. It is demonstrated that Rayleigh Quotient [70] (defined later) plays a key role in identifying "recurrence" class as earlier shown by Thyagaraja for two dimensional fluid flows. I start with some typical well studied chaotic flows (also studied in Chapter 3) and let the plasma system time evolve. The initial flow structure is disrupted by the dynamics of the physical quantities with time. Upon further time evolution the initial flow profile is found to get nearly recon-

structed back including its spectral structures. The cycle goes on until the viscous and resistive effects bring the magnitudes of each of the energies (kinetic and magnetic) down by certain fraction. This indicates that the motion in the phase space is quasi-periodic even though the higher dimensionality of the phase space apparently does not constrain the dynamics of the field quantities to be chaotic. I invoke an analytical framework by Thyagaraja [70] to explain the phenomenon observed and comment on the validity of such a model.

In particular, I make the following observations from my direct numerical simulation (DNS) code - G-MHD3D and provide the analytical description of MHD plasma based on my DNS results.

- The recurrence of flow and magnetic field structures are found for the first time in 3D MHD plasma.
- I identify zero Rayleigh Quotient flows that exhibit recurrence phenomena in 3D MHD plasma.
- I provide a numerical diagnostics to identify the recurrence event.
- An analytical interpretation of the phenomena has been attempted.
- The possible directions to improve the study are pointed out.

The governing equations of 3D MHD plasma whose DNS results are analysed are explicitly provided again in the next Section apart from Chapter 2 for convenience. The initial profiles of density, velocity and magnetic field, the boundary conditions and the parameters in which the code G-MHD3D is run are mentioned in Section 4.3. Section 4.4 deals with the numerical results obtained from the code for four different initial flow profiles. The detailed analytical analysis of the numerical results are provided in Section 4.5 and the flow profiles leading to recurrence phenomenon

are isolated. Section 4.6 summarises the results and analysis I have done. This Section also depicts the limitations of my numerical and analytical surveys and outlines the future directions of this study.

This work has been reported to arXiv [23] and published recently in Physics of Plasmas [108].

## 4.2 Governing Equations

The basic equations governing the dynamics of the single fluid MHD plasma are as follows:

$$\frac{\partial \rho}{\partial t} + \vec{\nabla} \cdot (\rho \vec{u}) = 0 \quad (4.1)$$

$$\begin{aligned} \frac{\partial(\rho \vec{u})}{\partial t} + \vec{\nabla} \cdot \left[ \rho \vec{u} \otimes \vec{u} + \left( P + \frac{B^2}{2} \right) \mathbf{I} - \vec{B} \otimes \vec{B} \right] \\ = \mu \nabla^2 \vec{u} \end{aligned} \quad (4.2)$$

$$P = C_s^2 \rho \quad (4.3)$$

$$\frac{\partial \vec{B}}{\partial t} + \vec{\nabla} \cdot (\vec{u} \otimes \vec{B} - \vec{B} \otimes \vec{u}) = \eta \nabla^2 \vec{B} \quad (4.4)$$

In this system of equations,  $\rho$ ,  $\vec{u}$ ,  $P$  and  $\vec{B}$  are the density, velocity, kinetic pressure and magnetic field of a fluid element respectively.  $\mu$  and  $\eta$  denote the coefficient of kinematic viscosity and magnetic resistivity. I assume  $\mu$  and  $\eta$  are constants over space and time. The symbol “ $\otimes$ ” represents the dyadic between two vector quantities (See Chapter 2 for more details).

The kinetic Reynolds number ( $Re$ ) and magnetic Reynolds number ( $Rm$ ) are defined as  $Re = \frac{U_0 L}{\mu}$  and  $Rm = \frac{U_0 L}{\eta}$  where  $U_0$  is the maximum velocity of the fluid system to start with and  $L$  is the system length.

I also define the sound speed of the fluid as  $C_s = \frac{U_0}{M_s}$ , where,  $M_s$  is the sonic Mach number of the fluid. The Alfven speed is determined from  $V_A = \frac{U_0}{M_A}$  where  $M_A$  is the Alfven Mach number of the plasma. The initial magnetic field present in the plasma is determined from the relation  $B_0 = V_A \sqrt{\rho_0}$ , where,  $\rho_0$  is the initial density profile of the fluid. For iso-surface plots I use the open-source 3D scientific data visualization and plotting application of Python named “*MayaVi*” [109].

### 4.3 Initial and boundary conditions

The choice of initial velocity profile is very crucial for the recurrence of the initial flow structure. The identification of the class of velocity profiles giving rise to recurrence phenomenon is described at length in Section 4.5. I take four examples of the four flows, two showing recurrence and two other which do not show recurrence and perform my numerical analysis. The flows I take up, are quite well known and well discussed in previous literatures and in the previous Chapter also. The first two I consider are Taylor-Green (TG) flow and Roberts flow for which I report the recurrence phenomena. The next two are Arnold-Beltrami-Childress (ABC) flow and Cat’s Eye flow which show the absence of recurrence, as expected from my analytical insight discussed later.

The initial density profile is chosen to be uniform throughout the simulation domain. The initial magnetic field profile is chosen as  $B_x = B_y = B_z = B_0$  throughout the space. My simulation domain is periodic in all the three spatial directions and thus may be considered to represent a part of an infinitely large plasma system.

#### 4.3.1 Parameter details

The parameters for which I run my code G-MHD3D are given in Table 4.1. The

$N$	$L$	$dt$	$\rho_0$	$U_0$	$Re$	$Rm$	$M_s$	$M_A$
64	$2\pi$	$10^{-5}$	1	0.1	450	450	0.1	1

Table 4.1: Parameter details for the results mentioned in this Chapter. These parameters are kept identical throughout this thesis unless stated otherwise.

OpenMP parallel G-MHD3D code is run on 20 cores for 9600 CPU hours for a single set of parameters. From my energy spectra calculation I find that most of the energies are accumulated within the large scales and hence a grid resolution of  $64^3$  is believed to be good enough to resolve the phenomena of interest. For some test runs, I have increased the grid resolution to  $128^3$  and found no significant variation from the results of  $64^3$  in the kinetic and magnetic energy evolution at least till one cycle of oscillation. Similarly a single run with grid resolution  $64^3$  and time stepping width  $dt = 10^{-6}$  produced identical result as  $dt = 10^{-5}$ . It is well known that the magnitude of initial density affects the dynamics of compressible fluid [95, 96]. However, the effect of variation of the magnitude of initial density is beyond the scope of this present work and is kept as a future study (see Chapter 6).

## 4.4 3D DNS Results from G-MHD3D

I time evolve the above-mentioned initial density profile, velocity and magnetic field profiles according to the equations mentioned in Section 4.2 using my DNS code - G-MHD3D, described in Chapter 2. Results are described below.

### 4.4.1 Taylor-Green flow

The velocity profile of MHD plasma subjected to divergence-free Taylor-Green (TG) flow is

$$\begin{aligned} u_x &= A U_0 [\cos(kx) \sin(ky) \cos(kz)] \\ u_y &= -A U_0 [\sin(kx) \cos(ky) \cos(kz)] \\ u_z &= 0 \end{aligned} \tag{4.5}$$

I choose  $A = 1$  and  $k = 1$  in this study. The fluid and magnetic helicities ( $H_f = \int_V \vec{u} \cdot \vec{\omega} dV$  and  $H_m = \int_V \vec{A} \cdot \vec{B} dV$  with  $\vec{\omega} = \vec{\nabla} \times \vec{u}$  and  $\vec{B} = \vec{\nabla} \times \vec{A}$ ) (Fig. 4.1) are found to remain conserved over time. The kinetic and magnetic energies oscillate as a result of continuous conversion and exchange of energy between the two modes (Fig. 4.2). The decay in the total energy is solely due to viscous and resistive effects.

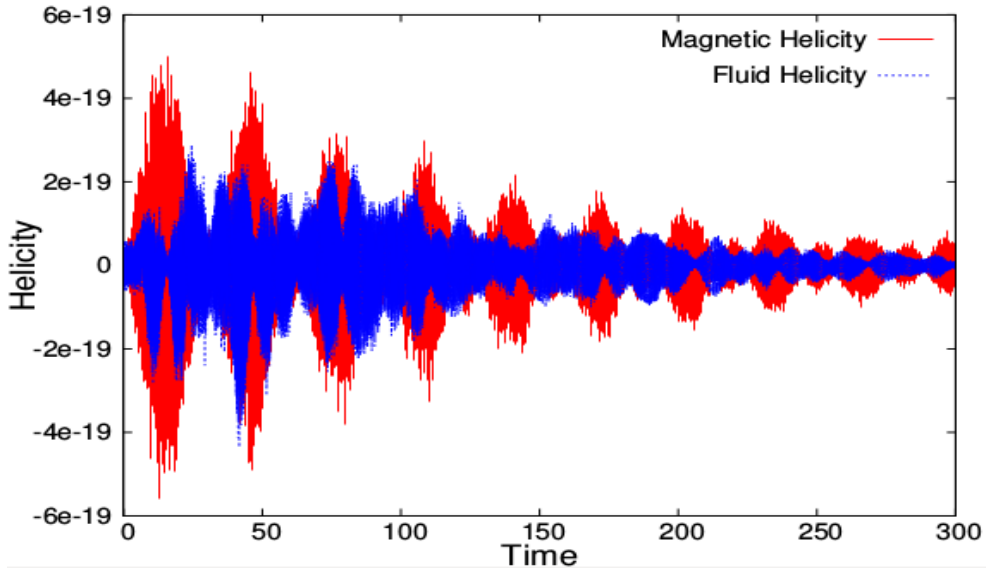


Figure 4.1: Conservation of magnetic (red solid) and fluid (blue dotted) helicity over a long time for Taylor - Green flow.

I plot the energy spectra for Taylor-Green flow and found that most of the energies are contained in first 5 modes [Fig.4.3, 4.4] only. It is also noticeable that a two orders of magnitude energy difference exists within the first 5 modes. In Fig.[4.3], the kinetic energy spectra [ $E_k(= \sum \frac{u_k^2}{2})$  vs  $k$ ] is plotted at times  $t = 31.2, 62.4, 93.6$



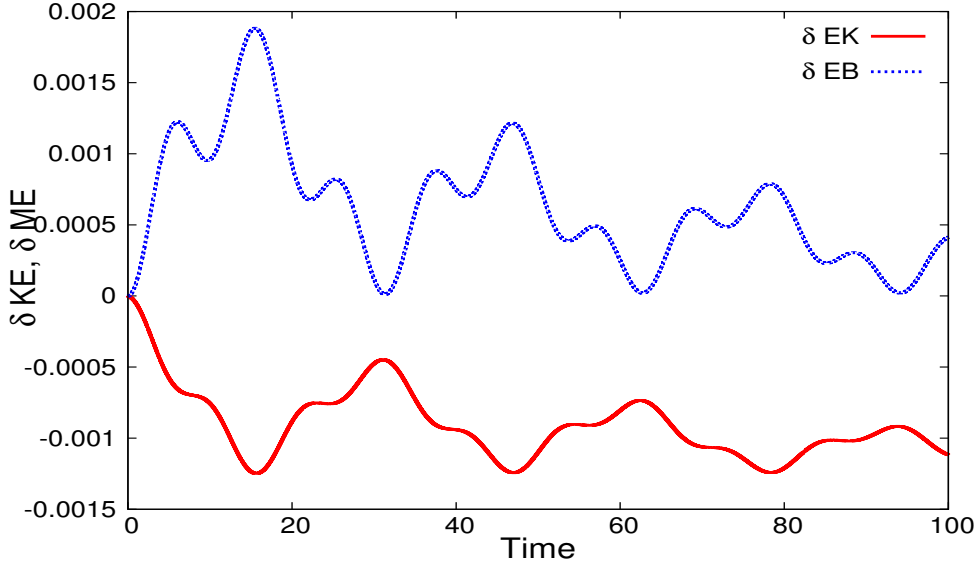


Figure 4.2: The shifted kinetic  $[\delta KE = \frac{1}{2} \iiint_V \vec{u}^2(x, y, z, t) - \frac{1}{2} \iiint_V \vec{u}^2(x, y, z, 0)]$  (red solid) and magnetic  $[\delta ME = \frac{1}{2} \iiint_V \vec{B}^2(x, y, z, t) - \frac{1}{2} \iiint_V \vec{B}^2(x, y, z, 0)]$  (blue dotted) energies of Taylor - Green flow oscillate with time exchanging energy between their respective modes. The shift is measured by the removal of the initial magnitude of kinetic and magnetic energy respectively.

which signifies the recurrence as observed in Fig.[4.26] as well as in the global maxima of Fig.[4.2]. I also plot the energy spectra at half times between the recurrence i.e.  $t = 46.8, 78.0, 109.2$ . It is evident that the kinetic energy contained in the first 5 modes oscillate with time with identical frequency of recurrence. Also, the magnetic energy spectra  $[B_k (= \sum \frac{B_k^2}{2}) \text{ vs } k]$  oscillate antiphase with the kinetic energy spectra [4.4]. It is interesting to note that the difference of energy in the fundamental mode oscillates with a magnitude of two orders of magnitude.

The kinetic and magnetic energy contained in the fundamental mode ( $E_{k=1}$  and  $B_{k=1}$ ) is plotted with time in Fig.4.5. Fig.4.6 shows the same for first 5 relevant modes which contribute to recurrence. I notice that all these modes contribute in equal manner to the energy exchange process.

The velocity and magnetic field isosurfaces are plotted in Fig 4.26 and 4.27 respectively. In Fig. 4.26 the blue, sky and green isosurfaces are plotted for the values

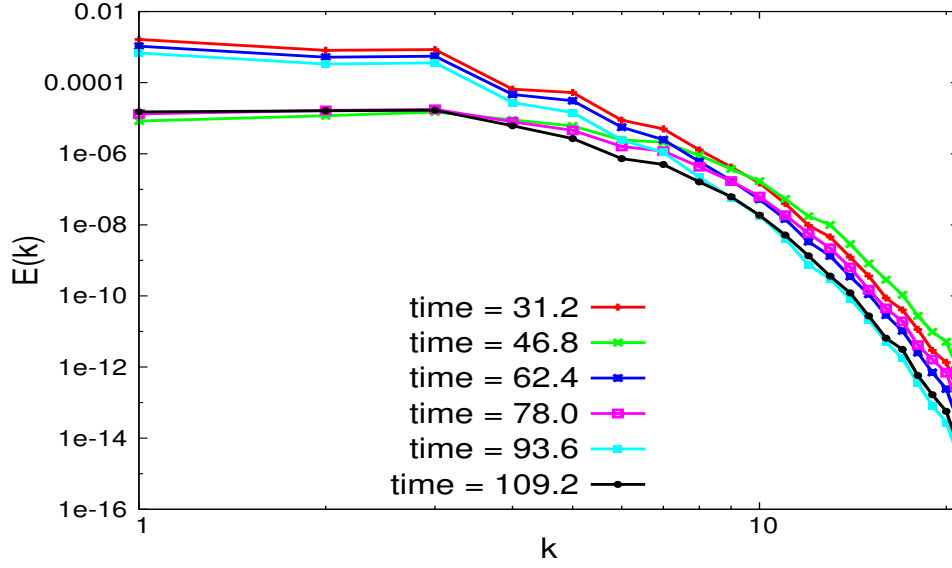


Figure 4.3: The kinetic energy spectra  $[E_k(= \sum \frac{u_k^2}{2})$  vs  $k$ ] from long time evolution of the Taylor-Green velocity profile. Even after several recurrence cycles, the energies are found to be contained in the large spatial scales only. The oscillation of the first five modes with time indicates a recurrence phenomena. The difference of energy in the fundamental mode oscillates with a magnitude of two orders of magnitude.

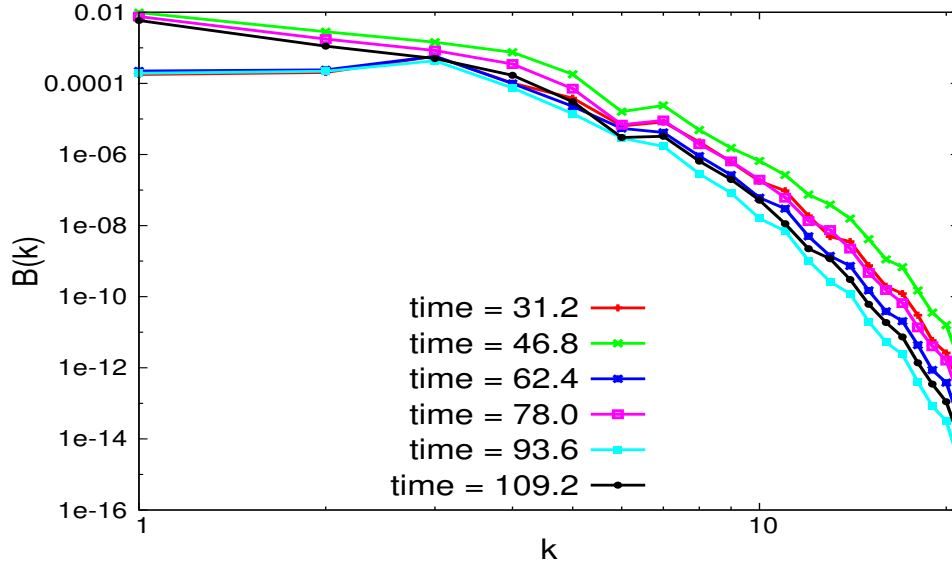


Figure 4.4: The magnetic energy spectra  $[B_k(= \sum \frac{B_k^2}{2})$  vs  $k$ ] from long time evolution of the Taylor-Green velocity profile. Even after several recurrence cycles, the energies are found to be contained in the large spatial scales only. The oscillation of the first five modes with time indicates a recurrence phenomena. The difference of energy in the fundamental mode oscillates with a magnitude of two orders of magnitude.

0.001, 0.05, 0.01 and similarly in Fig. 4.27 for 0.13, 0.16, 0.2 respectively. From Fig. 4.26 I observe that the flow profile is repeated after a time  $t = 31.2$ . It can be easily noted that in Fig. 4.26 [(a), (f) and (k)] show similar flow profiles. Similarly, [(b),

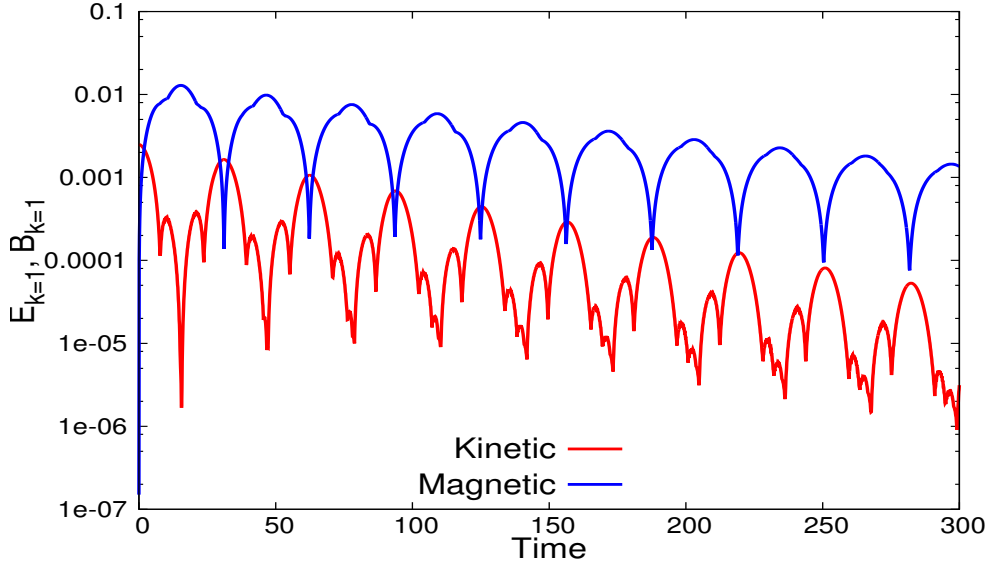


Figure 4.5: The time evolution of kinetic and magnetic energy contained in fundamental mode for the Taylor-Green velocity profile. Energy is continuously exchanged between kinetic and magnetic variables for several cycles.

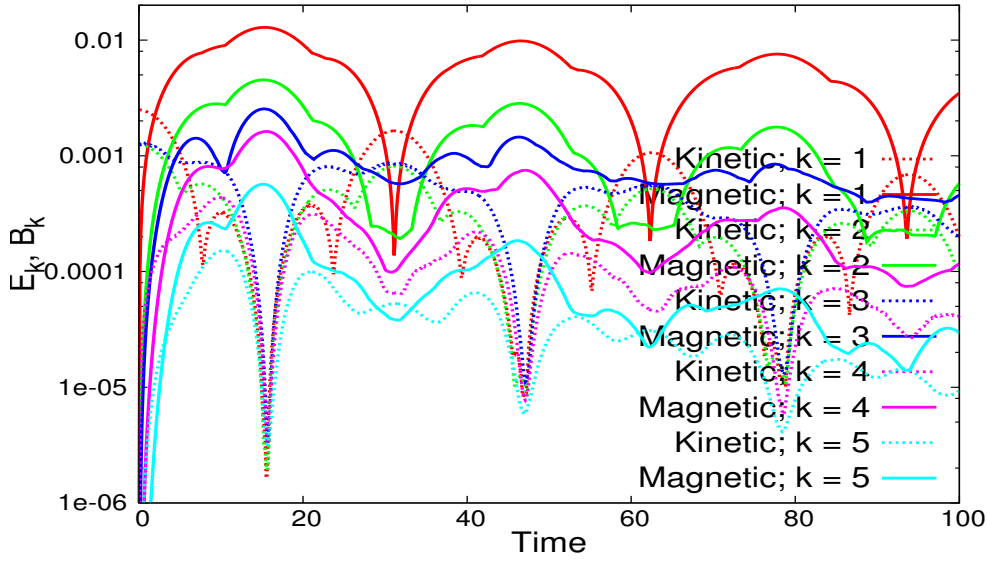


Figure 4.6: The time evolution of kinetic and magnetic energy contained in first five modes for the Taylor-Green velocity profile. All the five modes efficiently exchange energy between kinetic and magnetic variables leading to the happening of recurrence phenomena.

(g), (l)], [(c), (h), (m)], [(d), (i), (n)] and [(e), (j), (o)] show similar flow structures though some of the isosurfaces present in (b) or (e) do not appear in (g) or (j) and (l) or (o) because of viscous and resistive effects. After the third cycle, the initial condition is not exactly reproduced. However the structures of the flow profile continues to remain same. This repeated nonlinear re-occurrence of the structural details

of the initial profile is called “recurrence” phenomena. Similar to velocity profiles, magnetic field profiles also show the recurrence phenomena. At  $t = 0$  the magnetic field is uniform and hence, no flow structure remains, thus no isosurface is observed for several distinct values of magnitudes mentioned above. The uniform field profile comes back after the same time  $t = 31.2$  as observed for velocity profiles. Identical to velocity profiles in Fig. 4.27 the same corresponding subfigures show the similar profiles of isosurfaces after time interval 31.2 unit. The viscous and resistive effects are quite prominent and show the disappearance of some profiles at late time of evolution. A run with much lesser  $\mu$  and  $\eta$  with better grid resolution and smaller time stepping ( $dt$ ) interval will make the results more convenient to look at.

#### 4.4.2 Roberts flow

The velocity profile of MHD plasma subjected to divergence-free Roberts flow is

$$\begin{aligned}u_x &= A U_0 \sin(kz) \\u_y &= B U_0 \sin(kx) \\u_z &= C U_0 \sin(ky)\end{aligned}\tag{4.6}$$

I choose  $A = B = C = 1$  and  $k = 1$  in this study. The fluid and magnetic helicities (Fig. 4.7) are found to remain conserved over time. The kinetic and magnetic energies oscillate as a result of continuous conversion and exchange of energy between the two modes (Fig. 4.8). The decay in the total energy is solely due to viscous and resistive effects.

I plot the energy spectra for Roberts flow and find that most of the energies are contained in large scales [Fig.4.9, 4.10] only. In Fig.[4.9] the energy spectra is plotted

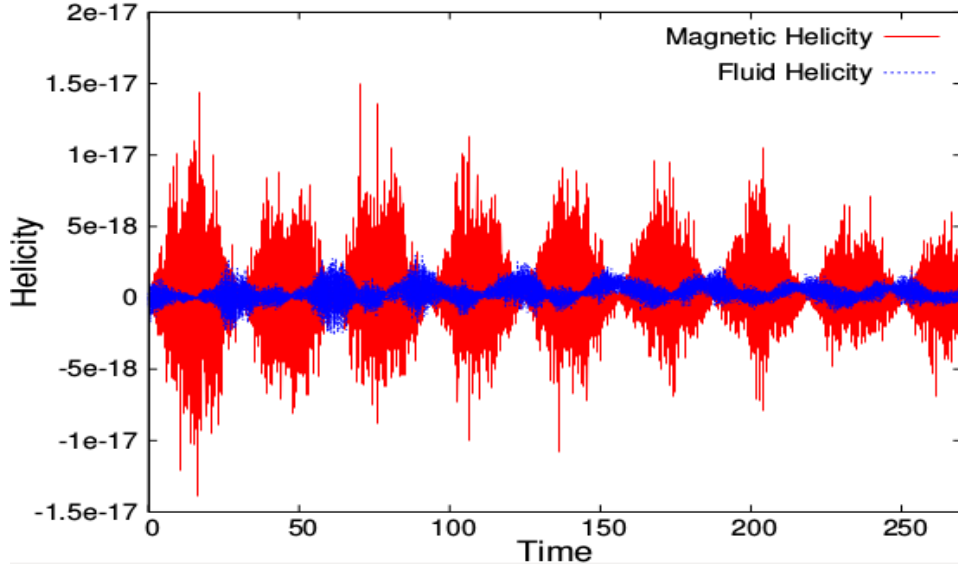


Figure 4.7: Conservation of magnetic (red solid) and fluid (blue dotted) helicity over a long time for Roberts flow.

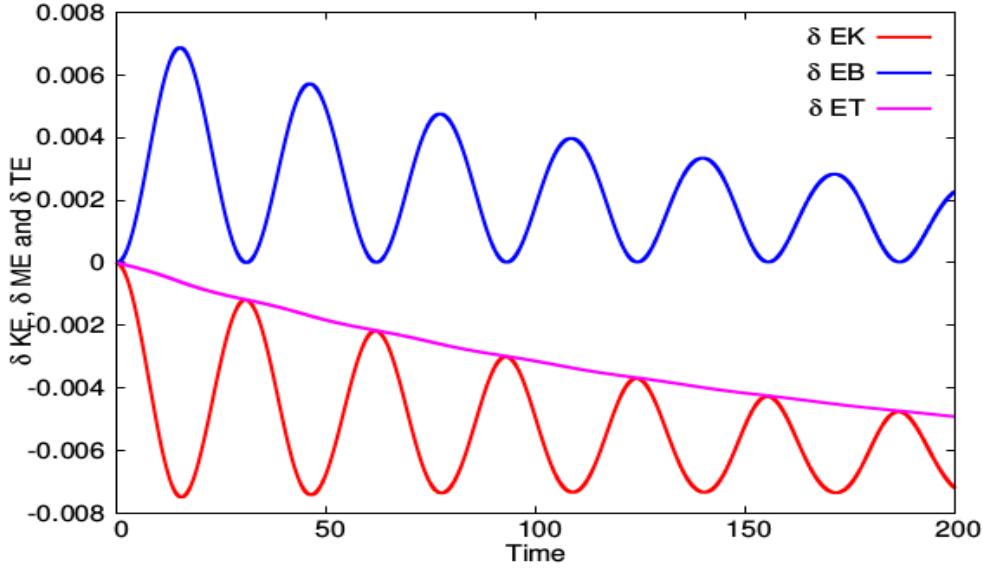


Figure 4.8: The shifted kinetic  $[\delta KE = \frac{1}{2} \iiint_V \vec{u}^2(x, y, z, t) - \frac{1}{2} \iiint_V \vec{u}^2(x, y, z, 0)]$  (red solid) and magnetic  $[\delta ME = \frac{1}{2} \iiint_V \vec{B}^2(x, y, z, t) - \frac{1}{2} \iiint_V \vec{B}^2(x, y, z, 0)]$  (blue dotted) energies of Roberts flow oscillate with time exchanging energy between their respective modes. The shift is measured by the removal of the initial magnitude of kinetic and magnetic energy respectively.

for times  $t = 31.2, 62.4, 93.6$  which signifies the global maximas of Fig.[4.8]. I also plot the energy spectra at half times between the recurrence i.e.  $t = 46.8, 78.0, 109.2$ . It is evident that the kinetic energy contained in the first 5 modes oscillate with time with identical frequency of recurrence. Also, the magnetic energy spectra oscillate

antiphase with the kinetic energy spectra [4.10]. Again, it is interesting to note that the difference of energy in the fundamental mode oscillates with a magnitude of two orders of magnitude.

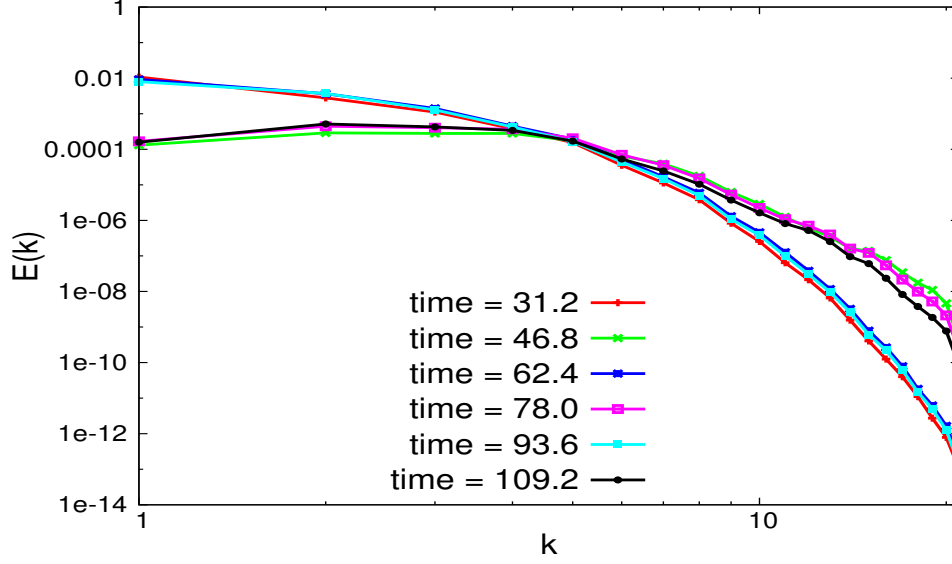


Figure 4.9: The kinetic and magnetic energy spectra from long time evolution of the Roberts velocity profile. Even after several recurrence cycles, the energies are found to be contained in the large spatial scales only.

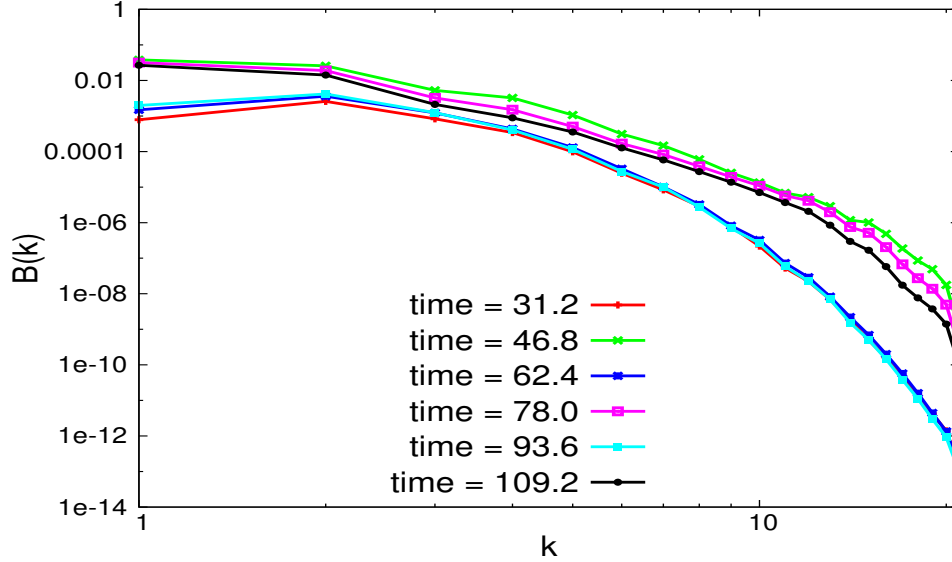


Figure 4.10: The kinetic and magnetic energy spectra from long time evolution of the Roberts velocity profile. Even after several recurrence cycles, the energies are found to be contained in the large spatial scales only.

The kinetic and magnetic energy contained in the fundamental mode is plotted

with time in Fig.4.11. Fig.4.12 shows the same for first 5 relevant modes which contribute to recurrence. I notice that all these modes contribute in equal manner to the energy exchange process.

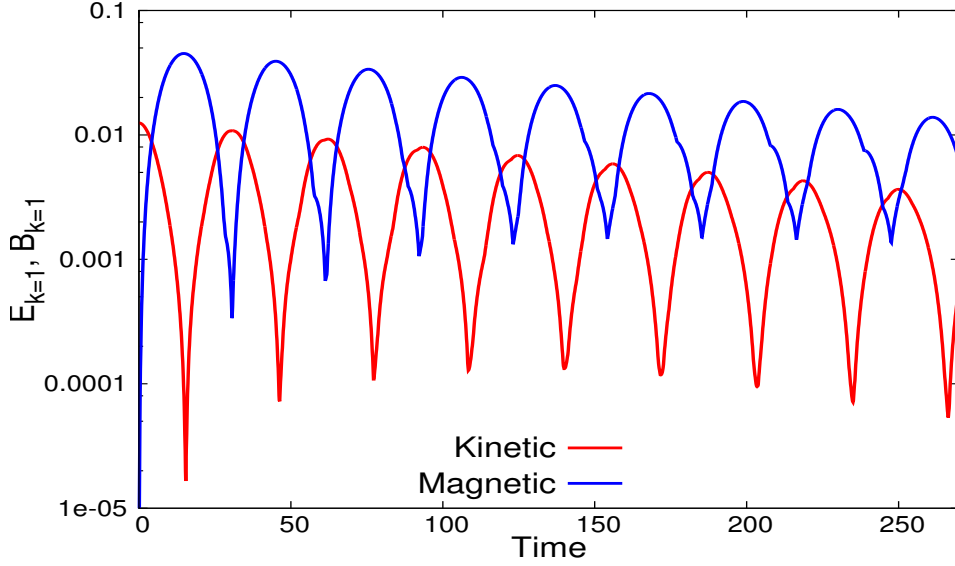


Figure 4.11: The kinetic and magnetic energy spectra from long time evolution of the Roberts velocity profile. Even after several recurrence cycles, the energies are found to be contained in the large spatial scales only.

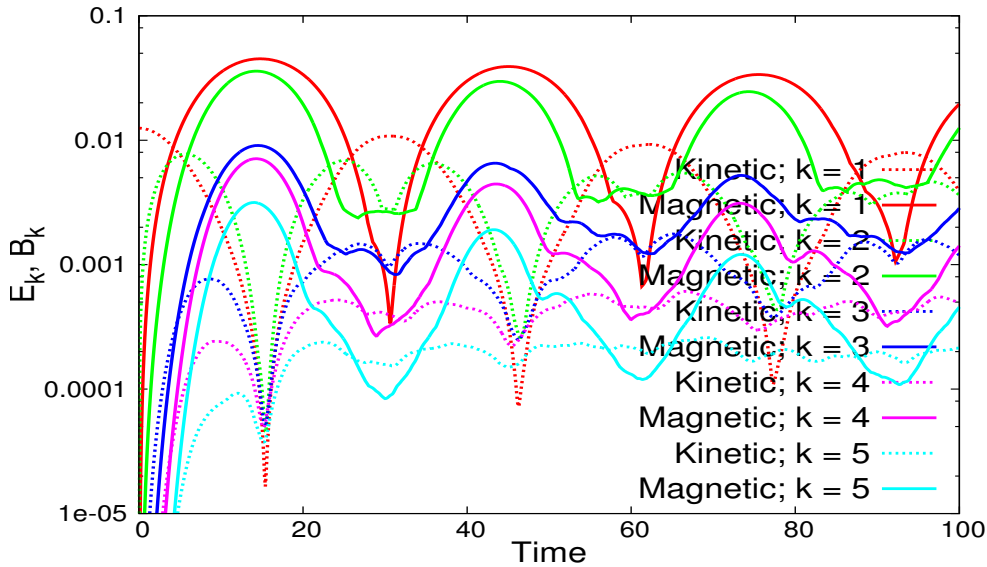


Figure 4.12: The kinetic and magnetic energy spectra from long time evolution of the Roberts velocity profile. Even after several recurrence cycles, the energies are found to be contained in the large spatial scales only.

### 4.4.3 Arnold-Beltrami-Childress flow

I choose another velocity profile of MHD plasma subjected to divergence-free Arnold-Beltrami-Childress (ABC) flow as

$$\begin{aligned} u_x &= U_0[A \sin(kz) + C \cos(ky)] \\ u_y &= U_0[B \sin(kx) + A \cos(kz)] \\ u_z &= U_0[C \sin(ky) + B \cos(kx)] \end{aligned} \quad (4.7)$$

$A = B = C = 1$  and  $k = 1$  are chosen for this study. The fluid and the magnetic helicity are found to oscillate (Fig. 4.13) during the time evolution of the MHD plasma. The kinetic and magnetic energies oscillate as a result of continuous conversion and exchange of energy between the two modes (Fig. 4.14). The decay in the total energy is solely due to viscous and resistive effects.

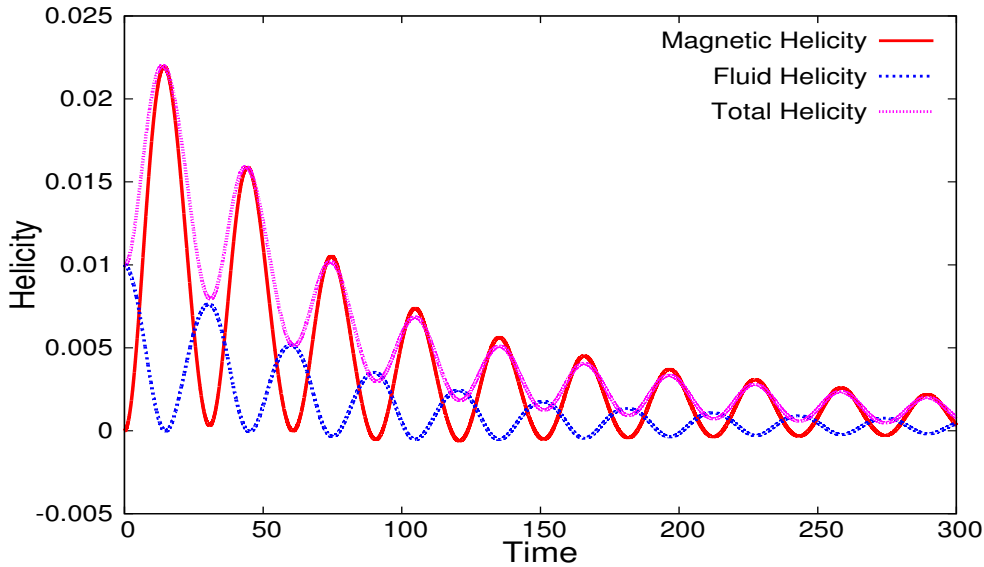


Figure 4.13: Time evolution of magnetic (red solid), fluid (blue dotted) and total (magenta dashed) helicity over a long time for Arnold-Beltrami-Childress flow.

I plot the energy spectra for Arnold-Beltrami-Childress flow and found that most of the energies are contained in first 5 modes [Fig.4.15, 4.16] only. In Fig.[4.15] the energy spectra is plotted at times  $t = 31.2, 62.4, 93.6$  which signifies the recurrence as observed in Fig.[4.28] as well as in the global maximas of Fig.[4.14]. I also plot the



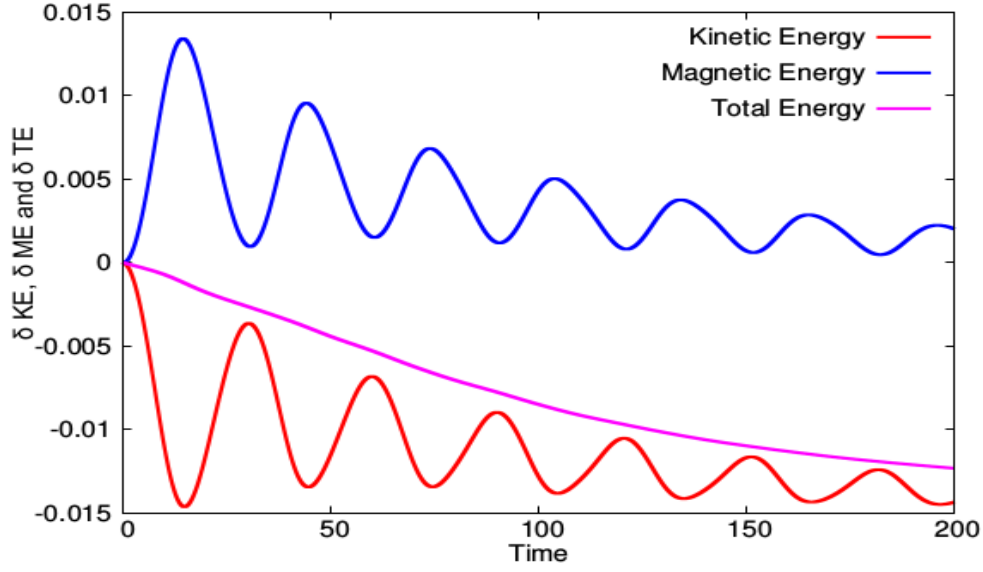


Figure 4.14: The shifted kinetic  $[\delta KE = \frac{1}{2} \iiint_V \vec{u}^2(x, y, z, t) - \frac{1}{2} \iiint_V \vec{u}^2(x, y, z, 0)]$  (red solid) and magnetic  $[\delta ME = \frac{1}{2} \iiint_V \vec{B}^2(x, y, z, t) - \frac{1}{2} \iiint_V \vec{B}^2(x, y, z, 0)]$  (blue dotted) energies for Arnold-Beltrami-Childress flow oscillate with time exchanging energy between their respective modes. The shift is measured by the removal of the initial magnitude of kinetic and magnetic energy respectively.

energy spectra at half times between the recurrence i.e.  $t = 46.8, 78.0, 109.2$ . From Fig.4.15 is evident that the oscillation of kinetic energy in the first 5 modes takes place with much weaker amplitude. Similarly the magnetic energy spectra [Fig.4.16] shows no oscillation with time. Thus I infer an absence of recurrence phenomena.

The kinetic and magnetic energy contained in the fundamental mode is plotted with time in Fig.4.17. Fig.4.18 shows the same for first 5 relevant modes which contains energy. I notice apart from the first mode, the other modes do not show the efficient transfer of energy between the kinetic and magnetic field variables.

The velocity and magnetic field isosurfaces are plotted in Fig. 4.28 and 4.29 respectively. In Fig. 4.28 the blue, sky, yellow and green isosurfaces are plotted for the values 0.03, 0.05, 0.08, 0.1 and similarly in Fig. 4.29 for 0.1, 0.133, 0.166, 0.2 respectively. After time  $t = 31.2$  the velocity profile tries to reconstruct due to oscillatory (and bounded) nature of total helicity (as described in section 4.5) but

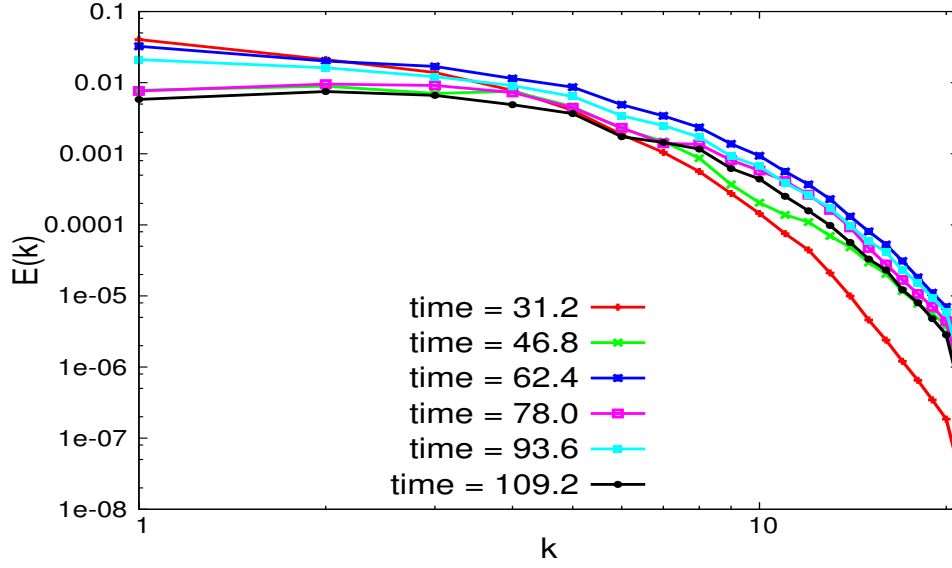


Figure 4.15: The kinetic and magnetic energy spectra from long time evolution of the Arnold-Beltrami-Childress velocity profile. Even after several recurrence cycles, the energies are found to be contained in the large spatial scales only.

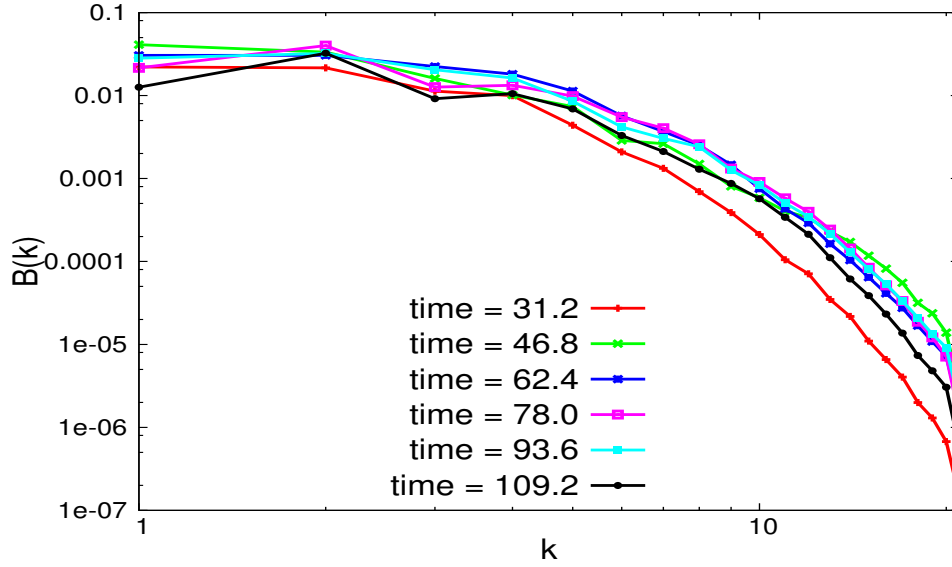


Figure 4.16: The kinetic and magnetic energy spectra from long time evolution of the Arnold-Beltrami-Childress velocity profile. Even after several recurrence cycles, the energies are found to be contained in the large spatial scales only.

significantly misses the initial flow profile. This deviation is not due to viscous and resistive effects and that can be verified from the profiles of other time instants for example in Fig. 4.28 subfigures [(b), (g), (l), (q), (v)], [(c), (h), (m), (r), (w)], [(d), (i), (n), (s), (x)] and [(e), (j), (o), (t), (y)]. The significant deviation can be well observed from the magnetic field profiles listed in Fig. 4.29

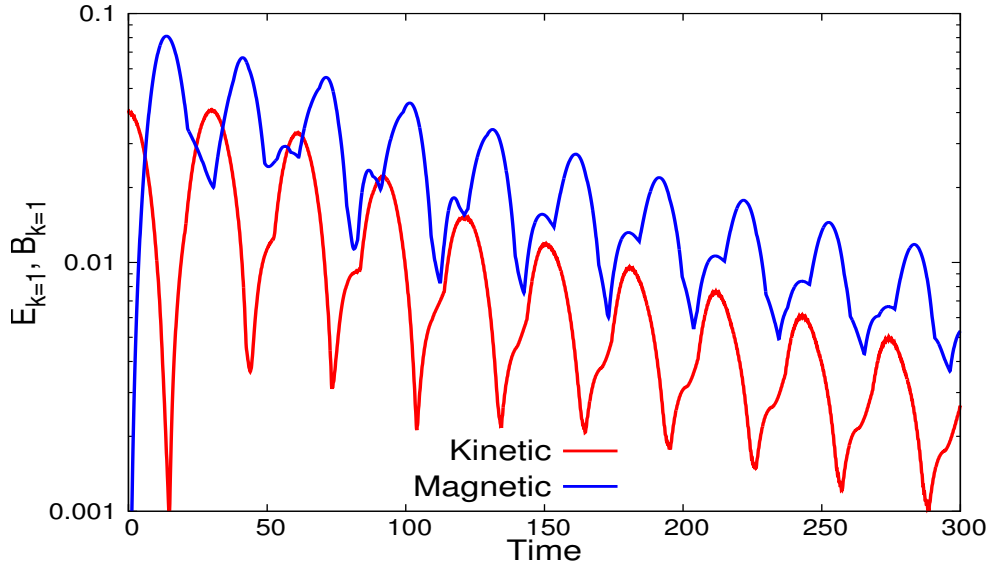


Figure 4.17: The kinetic and magnetic energy spectra from long time evolution of the Arnold-Beltrami-Childress velocity profile. Even after several recurrence cycles, the energies are found to be contained in the large spatial scales only.

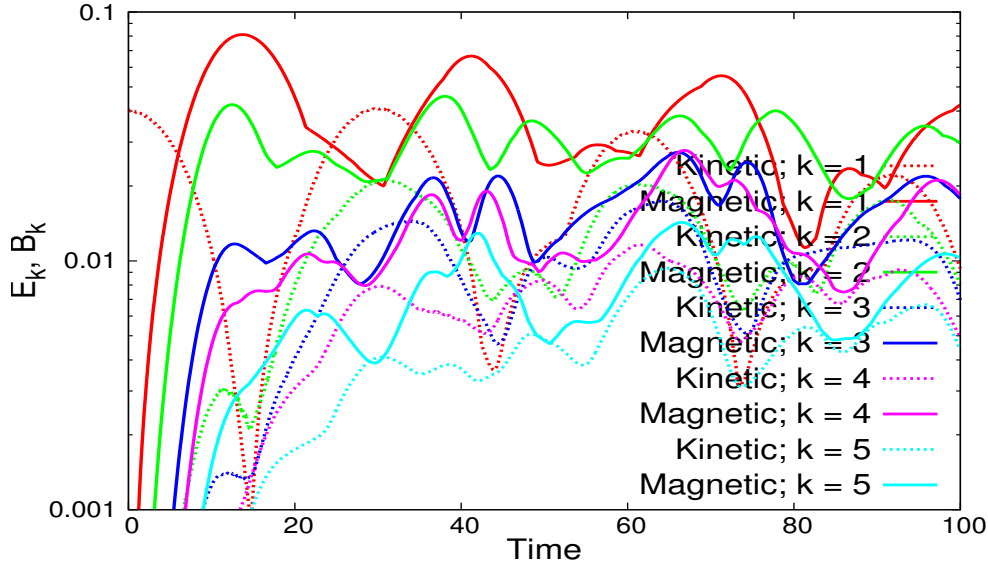


Figure 4.18: The kinetic and magnetic energy spectra from long time evolution of the Arnold-Beltrami-Childress velocity profile. Even after several recurrence cycles, the energies are found to be contained in the large spatial scales only.

#### 4.4.4 Cats Eye flow

I choose another velocity profile of MHD plasma subjected to divergence-free Cat's Eye flow as

$$\begin{aligned} u_x &= U_0 B \sin(ky) \\ u_y &= U_0 A \sin(kx) \\ u_z &= U_0 [A \cos(kx) - B \sin(ky)] \end{aligned} \quad (4.8)$$

$A = B = C = 1$  and  $k = 1$  are chosen for this study. The fluid and the magnetic helicity are found to oscillate (Fig. 4.19) during the time evolution of the MHD plasma. The kinetic and magnetic energies oscillate as a result of continuous conversion and exchange of energy between the two modes (Fig. 4.20). The decay in the total energy is solely due to viscous and resistive effects.

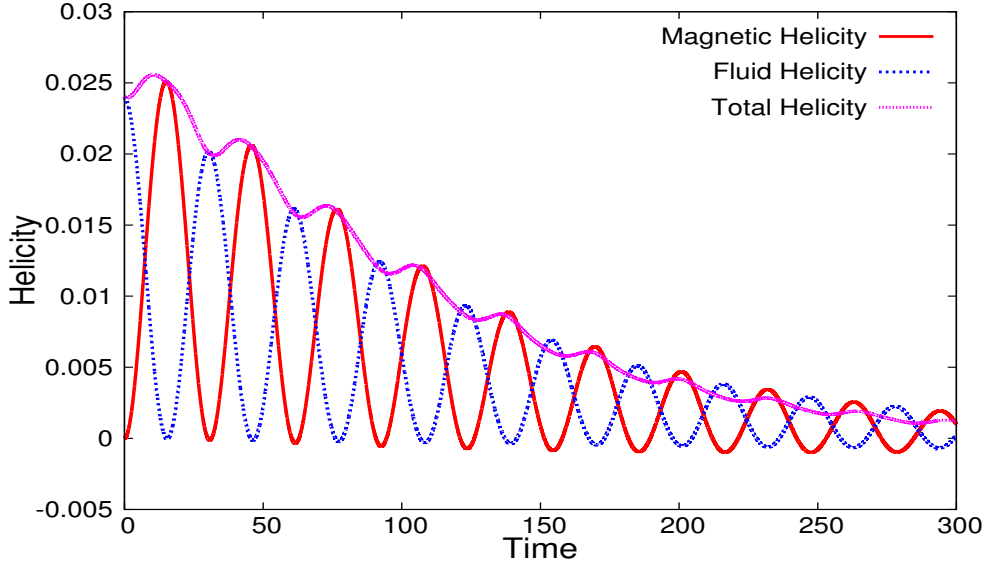


Figure 4.19: Time evolution of magnetic (red solid), fluid (blue dotted) and total (magenta dashed) helicity over a long time for Cat's Eye flow.

I plot the energy spectra for Cat's Eye flow and found that most of the energies are contained in first 5 modes [Fig.4.21, 4.22] only. In Fig.[4.21] the energy spectra is plotted at times  $t = 31.2, 62.4, 93.6$  which signifies the global maximas of Fig.[4.20]. I also plot the energy spectra at half times between the recurrence i.e.  $t = 46.8, 78.0, 109.2$ . From Fig.4.21 is is evident that the oscillation of kinetic

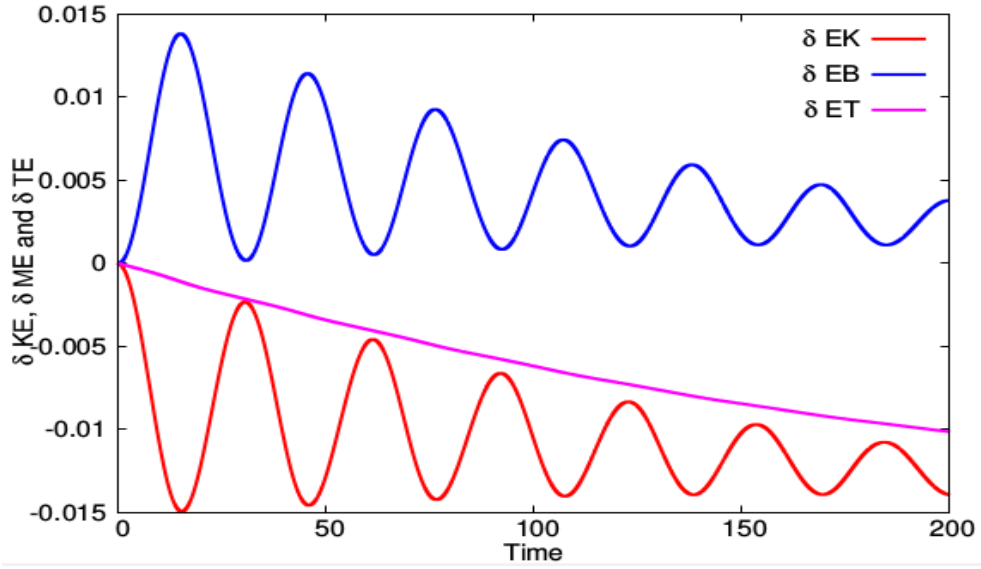


Figure 4.20: The shifted kinetic  $[\delta KE = \frac{1}{2} \iiint_V \vec{u}^2(x, y, z, t) - \frac{1}{2} \iiint_V \vec{u}^2(x, y, z, 0)]$  (red solid) and magnetic  $[\delta ME = \frac{1}{2} \iiint_V \vec{B}^2(x, y, z, t) - \frac{1}{2} \iiint_V \vec{B}^2(x, y, z, 0)]$  (blue dotted) energies for Cat's Eye flow oscillate with time exchanging energy between their respective modes. The shift is measured by the removal of the initial magnitude of kinetic and magnetic energy respectively.

energy in the first 5 modes takes place with much weaker amplitude. Similarly the magnetic energy spectra [Fig.4.22] shows no oscillation with time. Thus I infer an absence of recurrence phenomena.

## 4.5 Analytical description of DNS results

The numerical results in Section 4.4 show that, there exists a certain class of flows that iteratively reproduces the initial flow profile (4.26). Simultaneously the magnetic field structures are also reproduced in cycles (4.27). In order to gain a physical understanding of this phenomena I examine the Rayleigh Quotient which effectively analyses the “active number of degrees of freedom” of the system.

I generalise the earlier definition of Rayleigh Quotient [70] for MHD systems and

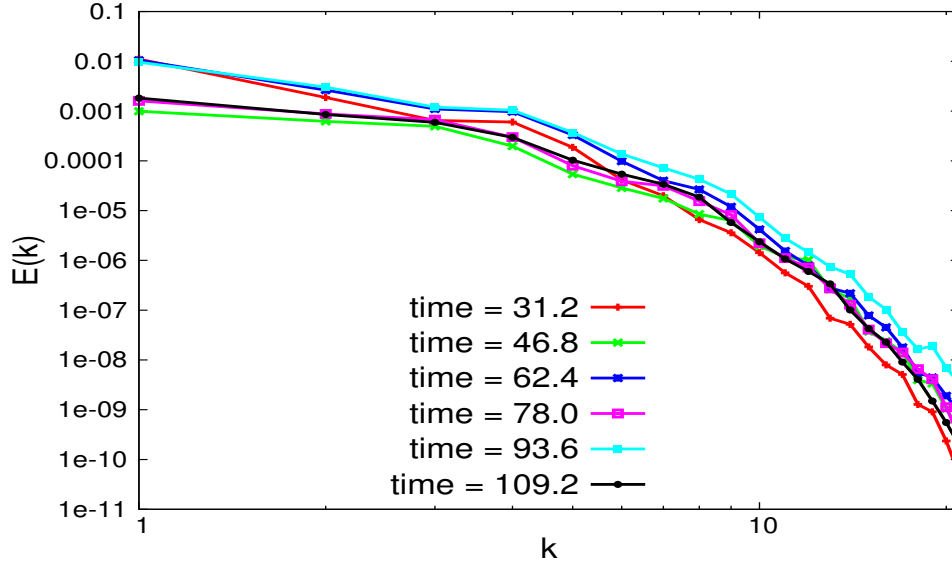


Figure 4.21: The kinetic and magnetic energy spectra from long time evolution of the Cat's Eye velocity profile. Even after several recurrence cycles, the energies are found to be contained in the large spatial scales only.

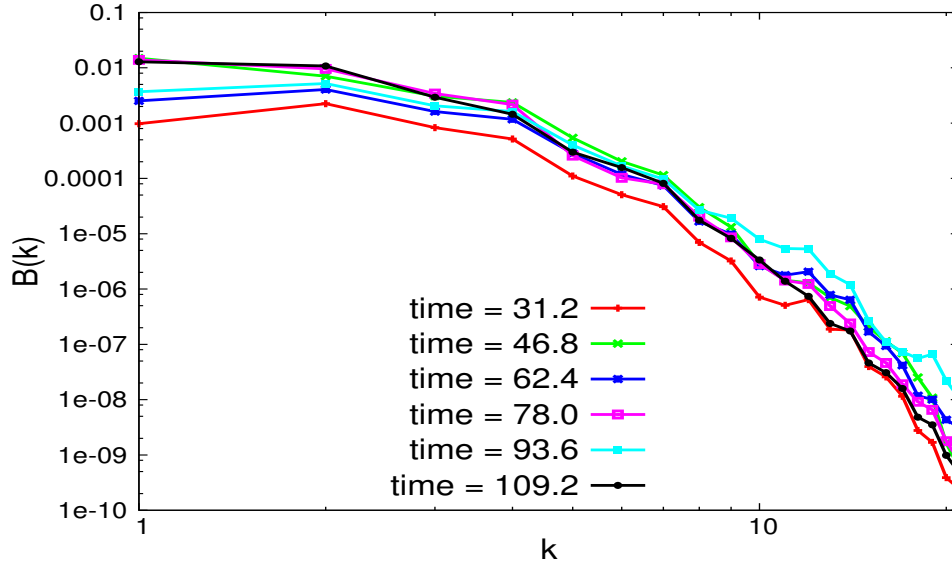


Figure 4.22: The kinetic and magnetic energy spectra from long time evolution of the Cat's Eye velocity profile. Even after several recurrence cycles, the energies are found to be contained in the large spatial scales only.

define the same as,

$$Q(t) = \frac{\int_V \left[ (\vec{\nabla} \times \vec{u})^2 + \frac{1}{2} (\vec{\nabla} \times \vec{B})^2 \right] dV}{\int_V \left( |\vec{u}|^2 + \frac{1}{2} |\vec{B}|^2 \right) dV} = \frac{\sum_k k^2 |c_k|^2}{\sum_k |c_k|^2}$$

where, where,  $u$  &  $B$  are expanded in a Fourier series and  $V$  is the volume of the

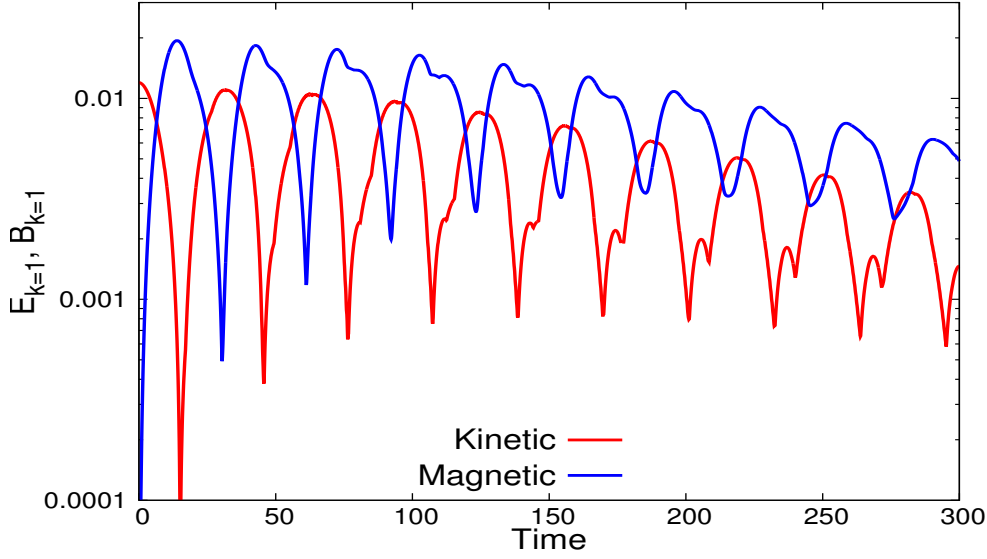


Figure 4.23: The kinetic and magnetic energy spectra from long time evolution of the Cat's Eye velocity profile. Even after several recurrence cycles, the energies are found to be contained in the large spatial scales only.

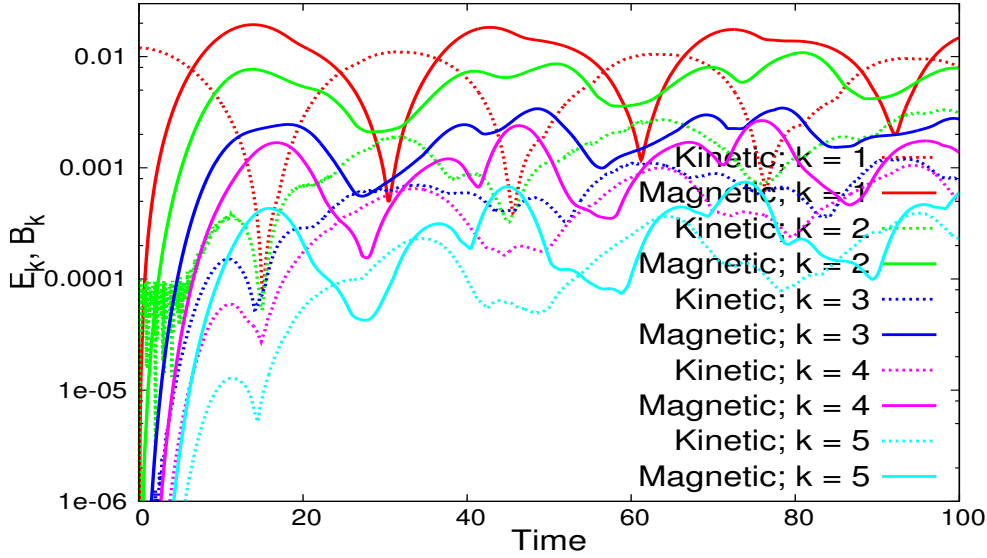


Figure 4.24: The kinetic and magnetic energy spectra from long time evolution of the Cat's Eye velocity profile. Even after several recurrence cycles, the energies are found to be contained in the large spatial scales only.

three dimensional space and evaluate the same for both Taylor-Green and Arnold-Beltrami-Childress flows. From Fig. 4.25, it is evident that for Taylor-Green flow the Rayleigh Quotient ( $Q(t)$ ) is bounded while for Arnold-Beltrami-Childress flow the Rayleigh Quotient ( $Q(t)$ ) increases as the time evolves. It is already known that [70, 110], typical hydrodynamic flows with bounded Rayleigh Quotient has the property to execute recurrence phenomena. Also it is commented by Thyagaraja

[81] that “...whereas the situation is more complicated in higher dimensions, and no general criterion is as yet available for deciding which initial data lead to noncollapsing recurrent motion”. From my numerical simulation it is found that analytical description applied to hydrodynamic flows is well capable of describing the MHD flows.

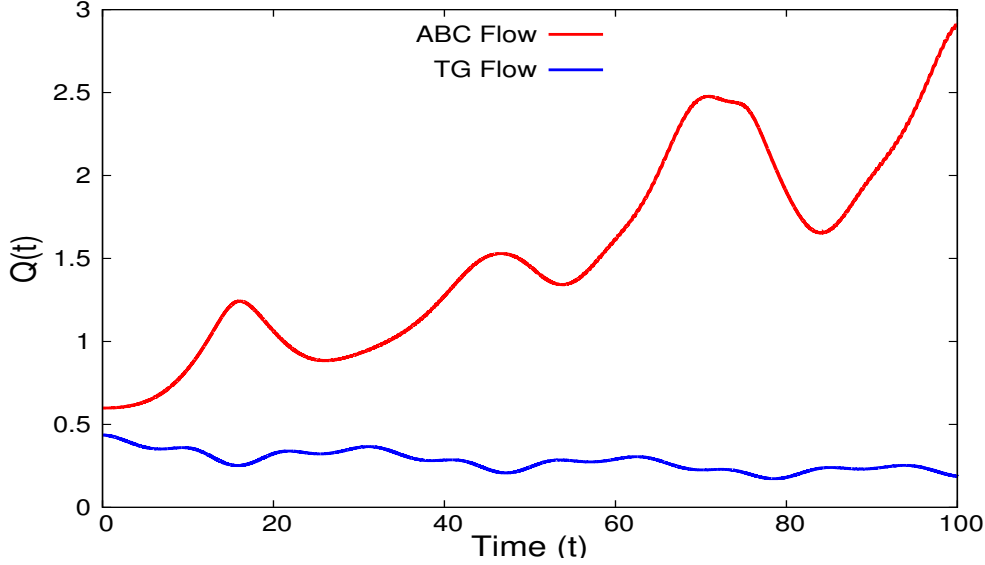


Figure 4.25: The time evolution of Rayleigh Quotient  $[Q(t)]$  for Taylor-Green (TG) and Arnold-Beltrami-Childress (ABC) flow.

In my numerical simulation, the equations are not ideal i.e. the co-efficient of viscosity ( $\mu$ ) and resistivity ( $\eta$ ) are non-zero. Thus the system under consideration is not exactly Hamiltonian. This prevents the dynamics to be exactly repetitive. Also, in my simulation, I see that, after few recurrence cycles, the initial flow profiles start slowly deviating from the exact initial structure.

The kinetic as well as the magnetic energy is primarily contained in the large spatial scales of the spectrum (Fig. 4.3, 4.4). Hence, a better grid resolution with a smaller time-stepping will not change the fundamental nature of the results obtained. However lesser values of  $\mu$  and  $\eta$  might show larger number of repeatative cycles, though the computational cost of the runs to resolve the tiny length-scales will be



much higher than the present runs.

## 4.6 Summary and conclusion

I report the observation of recurrence of velocity and magnetic field isosurfaces for a three dimensional nearly ideal magnetohydrodynamic plasma. The initial flow profile plays a crucial role in the recurrence phenomenon. I observe that, only those flow profiles which shows the conservation of Rayleigh Quotient ( $Q(t)$ ) over time, are the suitable candidates for the happening of the recurrence [70]. As an example I choose Taylor-Green flow and observe the periodic reconstruction of isosurfaces. I also consider Arnold-Beltrami-Childress flow profile that does not keep the total helicity conserved and find significant deviation from the reconstruction phenomena.

A numerical study with better resolution and smaller time stepping width and lesser viscous and resistive effects is expected to enhance the quality of the results and worth performing. Since viscous regularisation of three dimensional MHD system does not provide a Hamiltonian description, a conservative regularisation [111, 112, 113, 114] may help to provide the recurrence phenomena with better accuracy. Detailed simulation on such regularisation is an interesting problem to perform. A study on the effect of density, compressibility will make the understanding of the recurrence phenomena more complete.

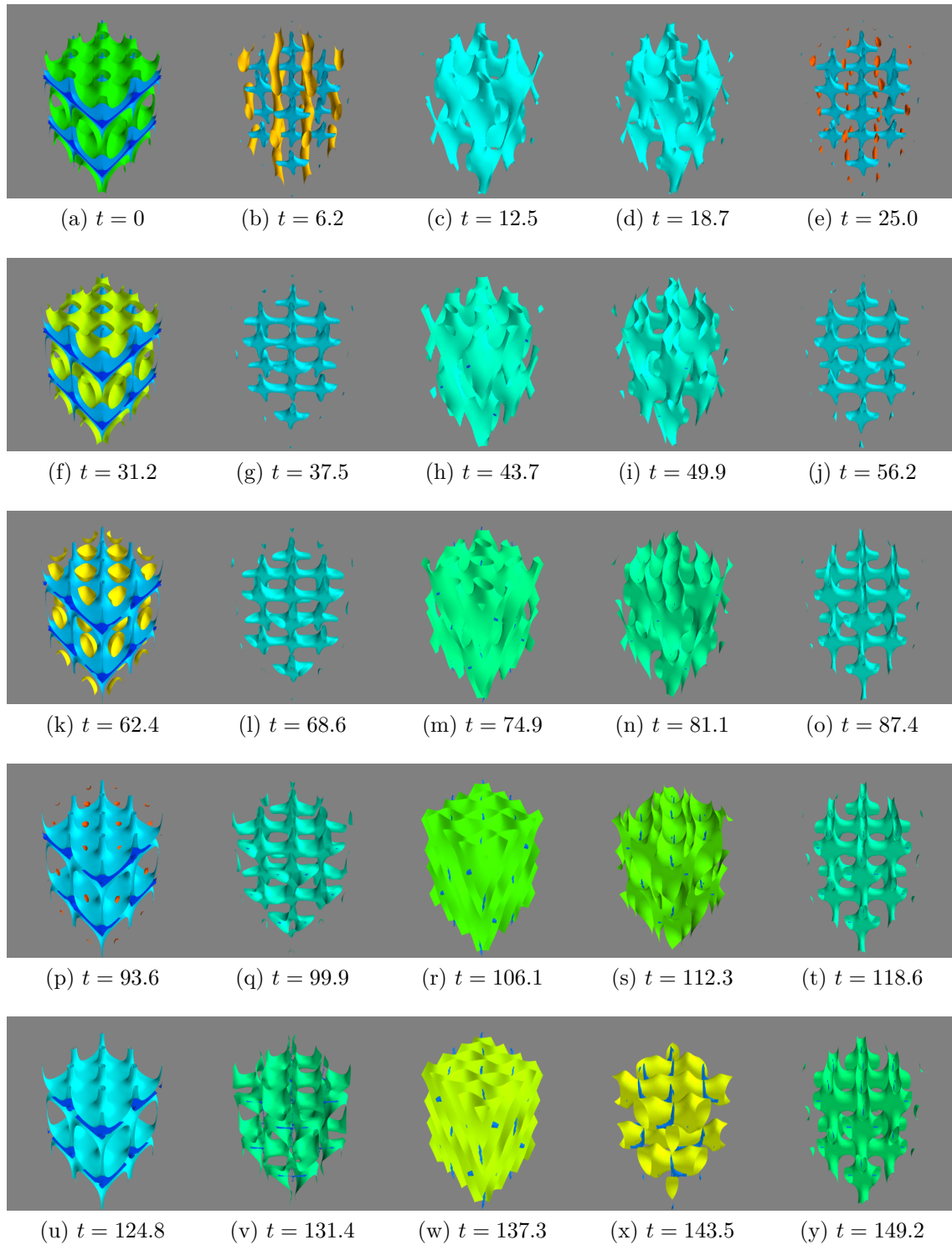


Figure 4.26: Recurrence of velocity isosurfaces for Taylor-Green flow [Eq. 4.5] for the magnitudes 0.001, 0.05, 0.01.

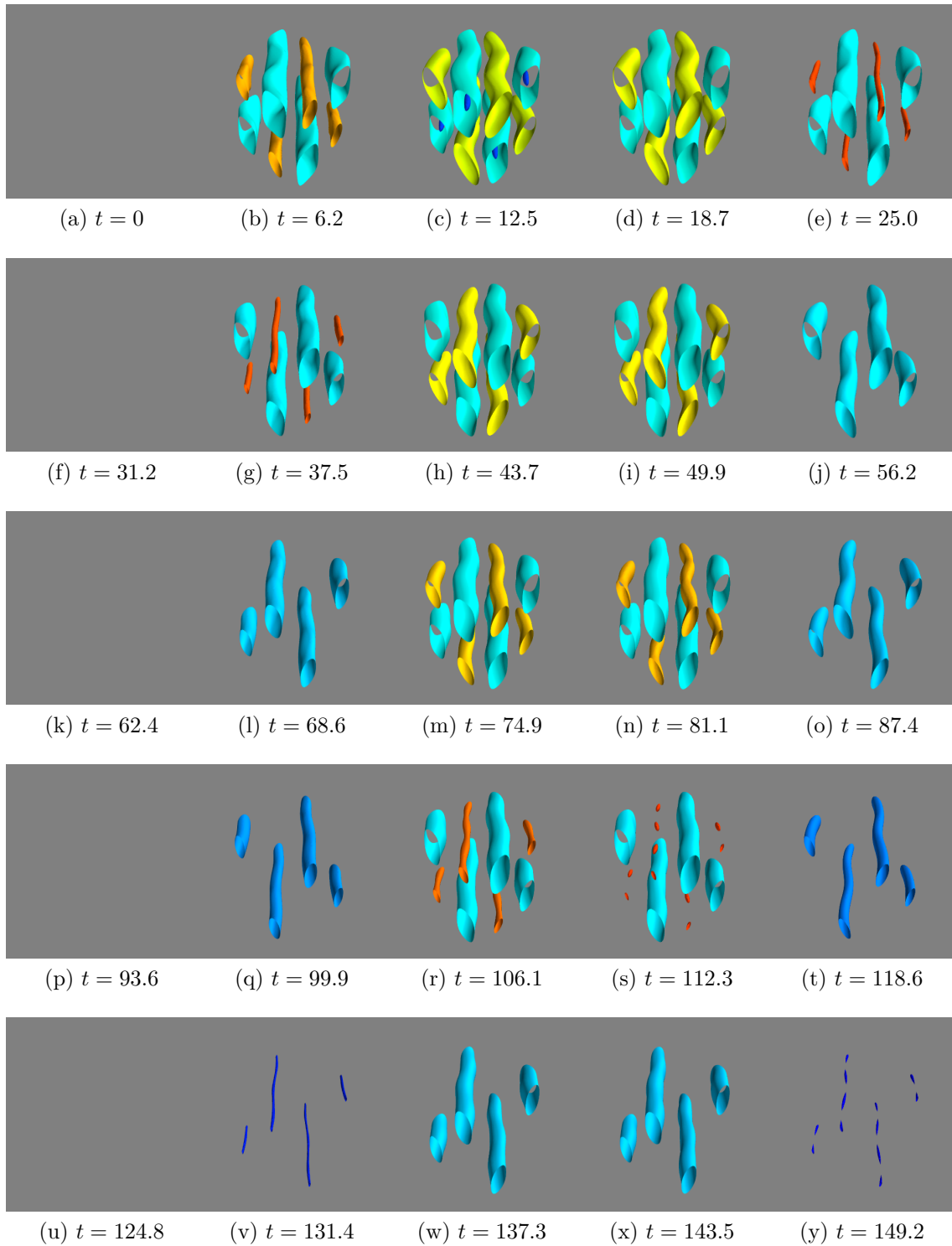


Figure 4.27: Recurrence of magnetic field isosurfaces for Taylor-Green flow for the magnitudes 0.13, 0.16, 0.2.

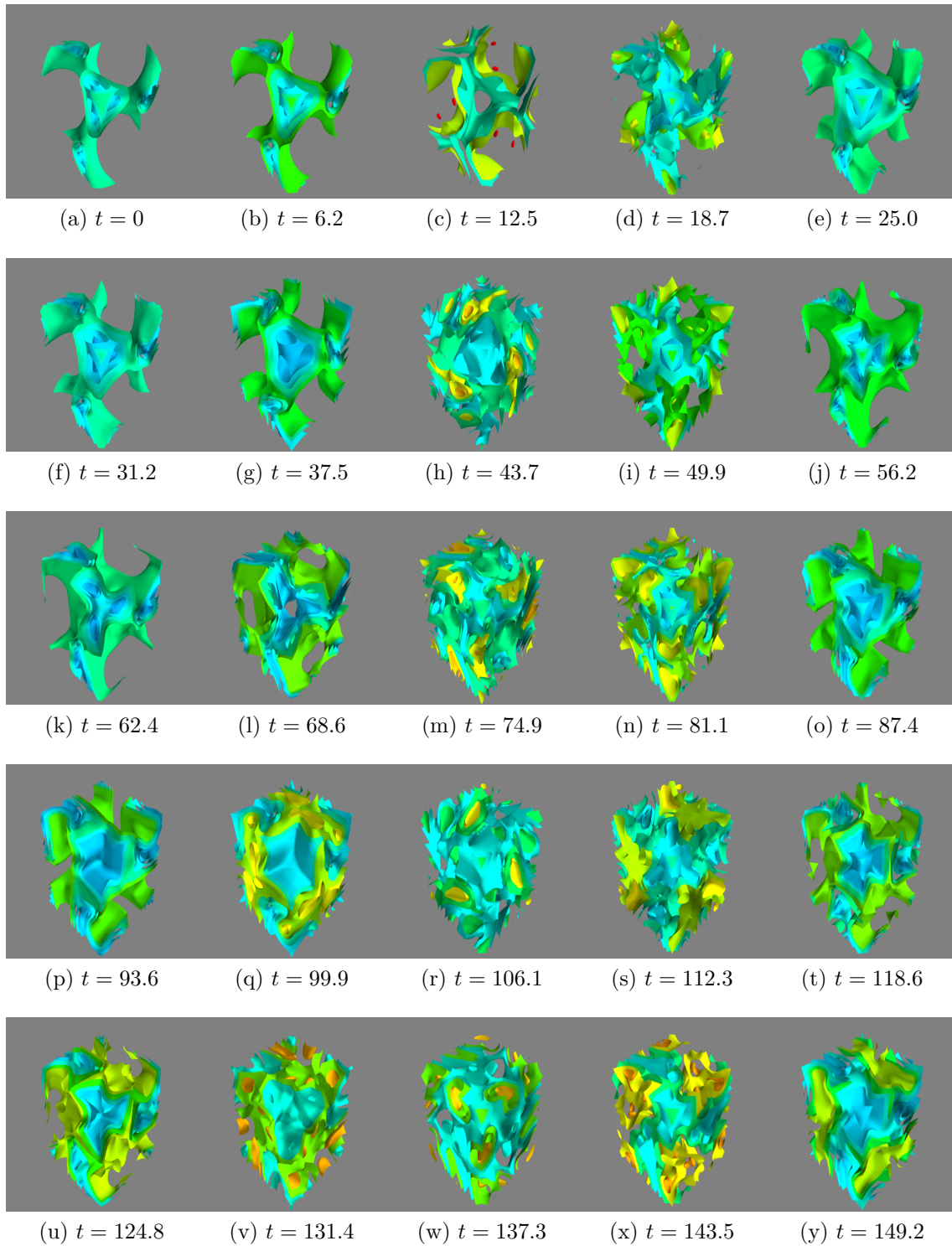


Figure 4.28: Time evolution of velocity isosurfaces for Arnold-Beltrami-Childress flow [Eq.4.8] for the magnitudes 0.03, 0.05, 0.08, 0.1.

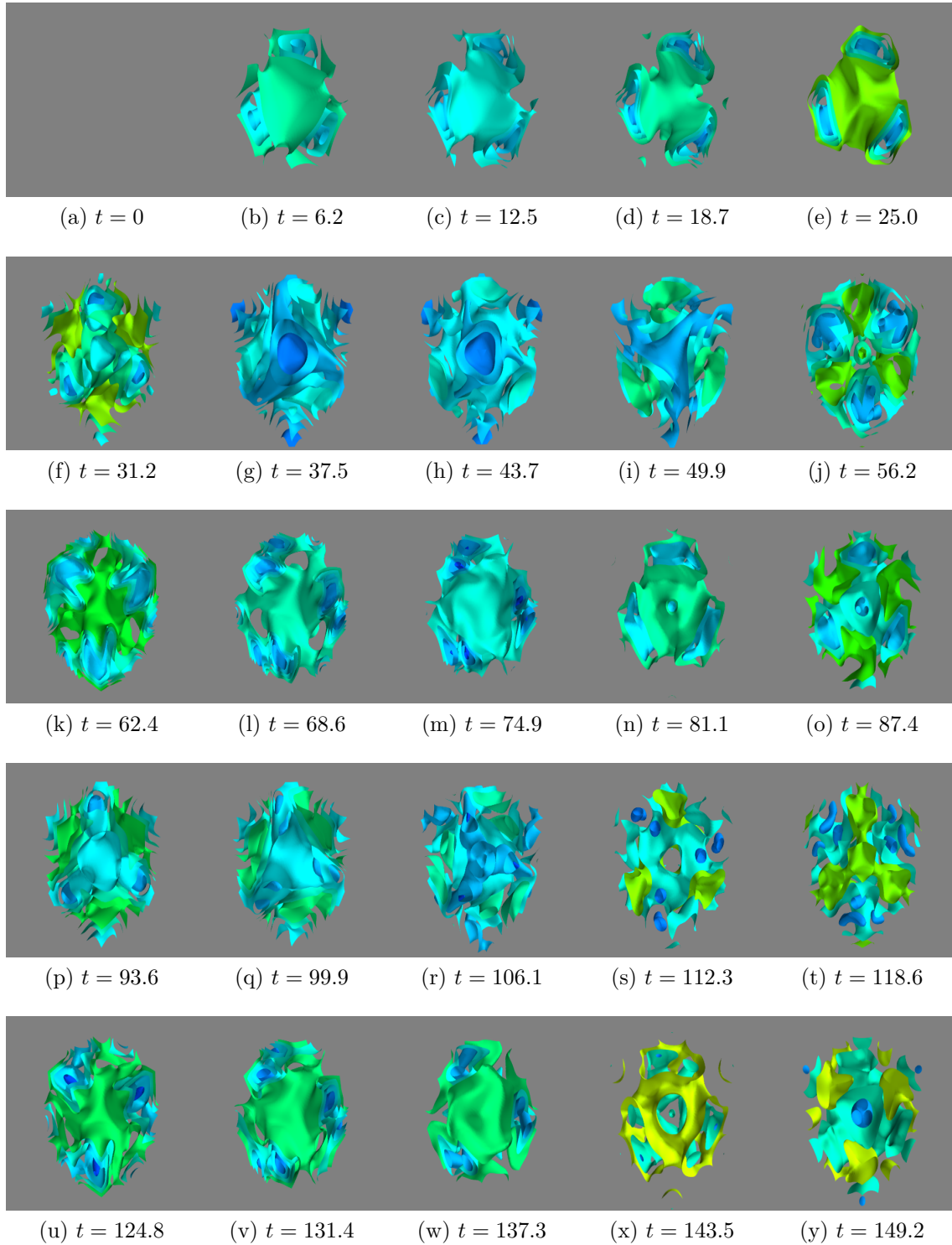


Figure 4.29: Time evolution of magnetic field isosurfaces for Arnold-Beltrami-Childress flow for the magnitudes 0.1, 0.133, 0.166, 0.2.



# Chapter 5

## Self Consistent Dynamo

### 5.1 Introduction

The last two Chapters (Chapter 3 & 4) described in detail the nature of energy transport amongst different scales where the short scales were not excited. Chapter 3 showed how nonlinear coherent oscillations appear in the single fluid Magnetohydrodynamics model where only a few modes are energetically dominant. In Chapter 4, I have shown that such large amplitude oscillations lead to a novel phenomena called “Recurrence”, where for some typical flow fields, the initial flow structures are periodically recovered even after complete spatial destruction because of nonlinear interaction between the modes. Thus in examples considered in the previous Chapters, energy was primarily contained in the large scales of the system and very little energy was contained within short scales. On the contrary in the current Chapter, I shall discuss about a controlled excitation of the short scales and then further comment on the energy sharing between all the scales thereby leading to a turbulent phenomena in the context of dynamo studies relevant for several laboratory as well as astrophysical scenario. A key parameter has been identified namely Alfvén Mach number, and is widely varied to explore such controlled excitation of the short scales

in the system.

One of the most interesting open questions of astrophysics is the birth of mean or large scale magnetic field in the Cosmos. There are several theoretical models [115, 116], some of them have been put to test in laboratory [117, 118, 119, 120], which mimic some aspects of the astrophysical plasma. Amongst the large number of theoretical models, E N Parker’s [28] theory of *dynamo action* is one widely celebrated model. The large-scale magnetic field generation in the ‘Sun’ or in galaxies are mostly attributed to mean-field-dynamo - a process of generating large scale magnetic fields out of the flow fields. On the other hand, there are astrophysical evidences of small scale magnetic field generation through turbulent fluctuation dynamo [121, 29, 122, 123, 124, 125, 126]. Even though it is well known that by virtue of Cowling’s theorem [127], origin of dynamo in two dimensions are ruled out, the behaviour and growth rates of three dimensional dynamos on Reynolds number and forcing length scale is still poorly understood and is a matter of debate [128, 129, 33, 130]. In general, most of the theoretical models employed in this study use the basic equations of MagnetoHydroDynamics (MHD). The model governs the dynamics of each ‘*fluid element*’ - a “collisional enough” fundamental block of the medium. However, MHD equations describing the plasma in the continuum limit offer fundamental challenges and analytical demonstration of the dynamo phenomena from basic equations [22] have been very few, if at all. Hence it is interesting to ask whether there exists any finite dimensional description of the subject?

In Chapter 3, it is shown that in two spatial dimensions for incompressible flows a finite dimensional approach exists and the analytical results were found to fit well with the numerical results obtained earlier [36]. However, in this current Chapter, I also delineate the regimes where the analytical description does not hold good



[24, 25]. In three spatial dimensions, the problem becomes more critical to analyse analytically. The phase space of the system being infinite dimensional, in three dimensions, long time prediction of the chaotic trajectories are extremely challenging. But, it is shown in the previous Chapter, that for some typical chaotic flows in three spatial dimensions, the flow and the magnetic field variables are found to reconstruct back to their initial condition - thereby getting trapped in the phase space of the system [23]. The cause of such *recurrence* is believed to be the low dimensional behaviour of the single fluid plasma medium for some typical parameters. Most of the short scales were not excited in the system and thus the continuum was acting like a low degree of freedom medium. Thus in this Chapter, we carefully choose those flows which do not ‘recur’ even in the low dimension to facilitate dynamo phenomena to occur. However, controlled sharing of energy between the short scales is a challenging problem and to the best of our knowledge has not been reported so far.

I ask myself the following questions:

1. Is there any way to excite the short scales in a regulated manner as I continuously move up in the parameter scale (more specifically Alfven Mach number)?
2. What happens when all the scales are excited for an initial flow which is known (from results of Chapter 3) not to recur? Does it lead to a dynamo?

In the first part of this Chapter, I address the above questions. A model distinctly showing a continuous transition to self-consistent dynamo from a non-linear coherent oscillation is proposed [24]. Though, an analytical description identifying the exact process is still lacking, the direct numerical simulation studies of three dimensional

chaotic flows supports the model mentioned above. It is known that, in case of a fluctuation / short-scale dynamo (where the small wave-numbers ( $k$ ), possesses considerable amount of energy), the magnetic field lines frozen to the plasma flows get first stretched along the chaotic velocity flows - then get twisted and folded back [53]. Such processes introduce generation of short scales into the system giving birth of dynamos classified as STF (Stretch-Twist-Fold) dynamo [131, 132]. Though it is well known that a small but non-zero resistivity affects the plasma relaxation because of reconnection process [40, 41, 133, 42, 43, 45], I choose flows with finite viscosity and resistivity showing the robustness of my results. A continuous growth of magnetic energy at the cost of kinetic energy is found and thereafter the magnetic energy decreases through reconnection process and converts back to kinetic energy. I move in parameter space and find the reconnection to occur with less probability and growth of magnetic energy for some specific parameter discussed at length in Section 1.4 of this Chapter. Thus by varying a single parameter, in one limit I observe coherent nonlinear oscillation of kinetic and magnetic energy within the premise of single fluid magnetohydrodynamics and in the other limit observe dynamo action to occur.

As discussed earlier, based on the results of previous Chapter (Chapter 4), I choose flows that do not recur and thus even though there is an energy exchange between the kinetic and the magnetic modes, the trapping in phase space does not occur even in the opposite limit of the dynamo.

I choose Arnold-Beltrami-Childress (ABC) flow which is non-recurrent (as shown in Chapter 4). Also, it is already known to produce fastest dynamos in the kinematic regimes [33] and is non-recurrent [23].

In the second part of the Chapter, I mostly focus on the growth of magnetic en-

ergy (dynamo action) under the action of externally driven flows. As mentioned earlier, the process of systematic and sustained generation of large and intermediate scale magnetic fields via the nonlinear energy transfer from kinetic to magnetic modes through continuously stretching and refolding the magnetic field lines [115, 116, 28] is known as *dynamo action* [127, 116, 133]. It is believed to be the fundamental mechanism behind the growth of magnetic energy in intergalactic and interstellar medium, accretion disks, interiors of stars or planets and in geomagnetism [134]. For example in order to understand the order of magnitude of the strength of intergalactic magnetic fields [135, 136], one often resorts to the primordial seed fields at small spatial scales, below the co-moving Hubble radius of the early Universe. It is believed that the energy of these seed fields has cascaded to different scales via magnetohydrodynamic (MHD) turbulence through dynamo process [137, 138, 139, 140, 141, 142, 143]. Of late, such processes have been attempted to be reproduced in laboratory experiments as well [117, 118, 119, 120].

For most astrophysical objects (larger than a small star) the resistive timescale is much larger than the advection timescale. Thus, if the dynamo action takes place in a resistive timescale (also called “slow” dynamo), an approximate growth time of the large scale magnetic field in the astrophysical objects against the laminar magnetic diffusivity (or resistivity) can be estimated from the Spitzer formula. As is well-known, the time-scale one obtains for the development of such magnetic fields is found to be longer than the age of the universe [144]. Thus slow dynamos prove to be inefficient candidate to explain the strength of magnetic fields in the cosmos. This situation created a pressing need to find dynamos which grow on the largest eddy turnover timescale rather than diffusive timescale. In 1972, Vainshtein and Zeldovich [145] proposed “fast” dynamo, whose growth rate remains finite for sufficiently large magnetic Reynolds number ( $Rm$ ) (the ratio of large scale velocity time scale to the large scale resistive time scale). The result was obtained ignoring the

resistivity ( $\eta$ ) while a small but non-zero resistivity is known to affect the plasma relaxation to a great extent [133, 40].

For a fast dynamo to set in, the line elements of the chaotic magnetic field are expected to grow exponentially fast to preserve the positivity of the flow of topological entropy [146]. Thus chaotic flows were believed to be potential candidates to show fast dynamo action in intermediate scales. Several flows having this chaotic nature (e.g. Ponomarenko [147], Roberts [148, 149], Arnold-Beltrami-Childress [150, 151, 152], Taylor-Green [153], Cat's eye [154], Archontis [155]) have been studied analytically and numerically both in laminar and in the turbulent regimes and have been found to display fast dynamo action. Amongst such flows, search for the dynamo that gives the fastest growth of magnetic energy was also performed. For example, Alexakis [33] identified that the kinematic dynamo effect is fastest for laminar Arnold-Beltrami-Childress (ABC) flow. In this present chapter we focus on ABC flow only and study some characteristics of the flow that shows even faster generation of magnetic energy.

The suitability of ABC flow for dynamo studies from the point of view of dynamical systems theory was studied by Arnold and Korkina [150]. This was followed by the seminal study of Galloway and Frisch [82] which revealed that, above a critical value of magnetic Reynolds number ( $Rm_c$ ), the flow shows a fast dynamo. Soon after, ABC flow was studied in detail and has been found to be quite accessible analytically [156, 157, 158, 159, 160, 161, 162, 163, 164, 165, 166, 167, 168, 169, 170]. ABC flow is a steady solution of Euler equations for a steady incompressible hydrodynamic flow. Also, if the external forcing is compensated by the viscous dissipation, it can be considered as a solution of Navier-Stokes equation. The *kinematic dynamo* study with given velocity field has proven to be quite efficient to produce fast dynamo phe-

nomena for a wide range of parameters, when the back-reaction of the magnetic field on the velocity field is ignored. This phenomena has been well studied by several authors [171, 172, 173, 82, 58, 174, 175, 144, 129, 176, 177, 178, 179, 51, 52, 180]. For the case when velocity field contains a higher wave-number, Galanti *et al* [181] obtained a slow growth of magnetic energy below  $Rm_c$ . One of the major findings of this Chapter is that, at the same wave-numbers we get a faster kinematic dynamo action with  $Rm$  above  $Rm_c$ . I explore the parameter regime further in search of other fast kinematic dynamos.

The growth of magnetic energy under the action of any such chaotic flow can be divided into two parts, *i*) the kinematic regime where the plasma flow stretches the magnetic field lines giving rise to an exponential growth of magnetic field and *ii*) the nonlinear, self-consistent regime where the magnetic field generates Lorentz force strong enough to modify the topology of the background plasma flow, resulting in a saturation of the growth rate of the magnetic field [182, 183]. There exists a huge literature about the back-reaction of magnetic field on velocity field and a very popular model called  $\alpha$  and  $\beta$  dynamos exist [184, 185]. However, these models are perturbative models and does not consider the complete nonlinear back-coupling to the full extent when the magnetic energy is of the order of kinetic energy. In this DNS simulation, I do not assume any such perturbative ordering and treat the complete nonlinear back-reaction of the magnetic field to the flow field.

In the kinematic regime, the growth of magnetic field is found to exponentially rise without bound after crossing a critical threshold Reynolds number ( $Rm_c$ ). When the backreaction is not negligible, (I dub this case as *self-consistent dynamo* as against *kinematic dynamo*) the dynamo saturates when it enters the nonlinear regime. At very low magnetic Prandtl number ( $P_m \ll 1$ ), the self-consistent dynamo has been

studied in detail [186, 187, 188, 189, 190, 182, 181, 191, 192, 193]. A detailed review of the ABC flow leading to kinematic dynamo action is due to Galloway [144]. However, in the solar convection zone, unprecedentedly high resolution simulation with Prandtl number unity ( $P_m = 1$ ) has been shown to produce global-scale magnetic field even in the regime of large Reynolds numbers [46]. For  $P_m = 1$  and Reynolds number  $Rm > Rm_c$ , I extend my search for faster self-consistent dynamos when the initial velocity and forcing scales contain higher wave-number. I also address the cases where the Alfven speed and sonic speed differ significantly. I see that the backreaction of the magnetic field alters the ABC flow profile and thereby the growth of magnetic energy itself gets affected. I notice three distinct growth rates in the magnetic energy solely because of the inclusion of the backreaction of the magnetic field on the velocity field.

In the present Chapter, I analyse both kinematic and self-consistent dynamo phenomena using a 3D weakly compressible MHD spectral solver MHD3D in Cartesian co-ordinate with periodic boundary condition at  $P_m = 1$ . In particular, the following aspects of dynamo action under ABC flow have been studied in detail:

- Above threshold or critical Reynolds number (say,  $Rm_c$ ), the growth rate of kinematic dynamo process increases with velocity scale containing higher wave numbers.
- Above threshold or critical Reynolds number ( $Rm_c$ ), the growth rate of self-consistent dynamo also increases, with velocity and forcing scales containing higher wave numbers.
- For super Alfvenic flows, when strong self-consistent dynamo action occurs, the effect of interplay of energy between magnetic and kinetic modes leads to saturation of the growth of magnetic energy at late times.



## 5.2 Governing Equations

The basic equations governing the dynamics of the magnetohydrodynamic fluid are as follows:

$$\frac{\partial \rho}{\partial t} + \vec{\nabla} \cdot (\rho \vec{u}) = 0 \quad (5.1)$$

$$\begin{aligned} \frac{\partial(\rho \vec{u})}{\partial t} + \vec{\nabla} \cdot \left[ \rho \vec{u} \otimes \vec{u} + \left( P + \frac{B^2}{2} \right) \mathbf{I} - \vec{B} \otimes \vec{B} \right] \\ = \mu \nabla^2 \vec{u} + \rho \vec{f} \end{aligned} \quad (5.2)$$

$$\frac{\partial \vec{B}}{\partial t} + \vec{\nabla} \cdot (\vec{u} \otimes \vec{B} - \vec{B} \otimes \vec{u}) = \eta \nabla^2 \vec{B} \quad (5.3)$$

$$\text{where } P = C_s^2 \rho \text{ and } \vec{f} = \begin{pmatrix} A \sin(k_f z) + C \cos(k_f y) \\ B \sin(k_f x) + A \cos(k_f z) \\ C \sin(k_f y) + B \cos(k_f x) \end{pmatrix}.$$

In this system of equations,  $\rho$ ,  $\vec{u}$ ,  $P$  and  $\vec{B}$  are the density, velocity, kinetic pressure and magnetic field of a fluid element respectively.  $\mu$  and  $\eta$  denote the coefficient of kinematic viscosity and magnetic resistivity. As mentioned in Chapter 2,  $\mu$  and  $\eta$  are assumed to be independent of space. However the effect of spatial variation can be incorporated in the Code and is discussed at length in the Chapter 6.  $\mathbf{I}$  represents the unit matrix and the symbol ' $\otimes$ ', the tensor product between two vector quantities (see Chapter 2). The kinetic Reynolds number ( $Re$ ) and magnetic Reynolds number ( $Rm$ ) are defined as  $Re = \frac{U_0 L}{\mu}$  and  $Rm = \frac{U_0 L}{\eta}$  where  $U_0$  is the maximum velocity of the fluid system to start with and  $L$  is the system length.  $\vec{f}$  represents the external forcing applied to the system through velocity perturbations where  $A, B, C$  governs the magnitude of the forcing and  $k_f$  indicates the length-scale at which the fluid is perturbed. I also define the sound speed of the fluid as  $C_s = \frac{U_0}{M_s}$ , where,  $M_s$  is the sonic Mach number of the fluid. The Alfven speed is determined from  $V_A = \frac{U_0}{M_A}$  where  $M_A$  is the Alfven Mach number of the plasma. The initial seed magnetic field present in the plasma is determined from the relation  $B_0 = V_A \sqrt{\rho_0}$ ,



where,  $\rho_0$  is the initial density profile of the fluid which is known to be uniform.

### 5.3 Parameter Details

Galloway and Frisch [82] showed for the first time that a critical dependency on the magnitude of magnetic resistivity ( $Rm$ ) for kinematic dynamos. Later this result was further tested and reproduced with much greater accuracy and resolution in several other independent studies [129, 180]. The observation that, within a  $2\pi$  periodic box, for algorithms depending on spectral solvers, the smallest features in magnetic field appear at scales of order  $Rm^{-1/2}$ , indicates that the grid size required to resolve a given  $Rm$  scales like  $Rm^{1/2}$  [58]. I choose,  $N = 64$  which resolves  $Rm$  values upto  $64^2 = 4096$  and keep my parameters fixed at  $Rm = 450$  (where the growth rate of dynamo was found to get saturated [58]) well within the resolution threshold. Also the result of Sadek *et al* [87] confirms that most of the kinetic and magnetic energy content remains within the large scales, even when the driving wave-number is kept at intermediate scales (at least upto  $k_f = 16$ ). This sets limit to my choice of maximum driving wave number ( $k_f = 16$ ) at the grid resolution  $N = 64$ .

Throughout my simulation, I set  $N = 64$ ,  $L = 2\pi$ ,  $\delta t = 10^{-4}$ ,  $\rho_0 = 1$ . For some test runs the grid resolution is increased from  $N = 64$  to  $N = 128$  for both kinematic and self-consistent cases, but I found no significant variation of the physics results. The initial magnitude of density ( $\rho_0$ ) is known to affect the dynamics and growth rate of an instability in a compressible neutral fluid [95, 96]. However, in present case I start with the constant initial density, fixed at  $\rho_0 = 1$  for all the runs. I find that the density remains the same with time as the simulation evolves. Effect of variation of density over the space is a future study and is addressed in Chapter 6.

I check my code with smaller time stepping ( $\delta t$ ) keeping the grid resolution  $N = 64$ . No deviation from the results were observed with such test runs.

The kinematic viscosity is controlled through the parameters  $Re$  and to guarantee similar decay of kinetic and magnetic energy, I set  $Re = Rm$  everywhere. Next I vary the Alfven speed through  $M_A$  and observe the effect of these parameters on the dynamo action. I also change the magnitude of forcing by controlling the values of  $A, B, C$  and the length-scale of forcing through  $k_f$ .

The OpenMP parallel MHD3D code is run on 20 cores for 9600 CPU hours for a single run with parameters mentioned above and got the following results.

## 5.4 Simulation Results

In this Section I start with the initial values chosen for the simulation and then identify the critical parameter to excite the short scales in the plasma leading to a self-consistent dynamo. Finally I comment of the parameter dependency of the growth rates of both kinematic as well as the self-consistent dynamo.

### 5.4.1 Initial Profile of Density, Velocity and Magnetic Field

I start with the initial condition  $\rho = \rho_0$  as a uniform density fluid, the initial velocity profile as  $u_x = U_0[A \sin(k_f z) + C \cos(k_f y)]$ ,  $u_y = U_0[B \sin(k_f x) + A \cos(k_f z)]$ ,  $u_z = U_0[C \sin(k_f y) + B \cos(k_f x)]$  and the initial magnetic field as  $B_x = B_y = B_z = B_0$ . I keep the initial profiles of all the fields identical throughout this Chapter unless otherwise stated.

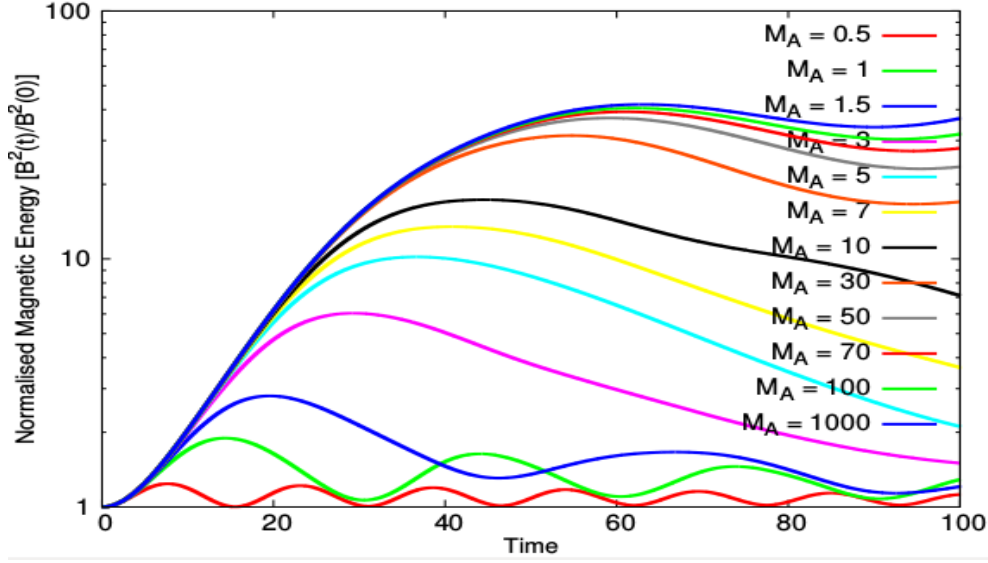


Figure 5.1: (Color online) Transition to dynamo like regime with the increase of  $M_A$  from coherent nonlinear oscillation regime.  $B^2(t)/B^2(0)$  shows the normalised magnetic energy as the Alfvén velocity changes with variation of  $M_A$ . Thus a growth in normalised magnetic energy indicates a dynamo like phenomena to occur. However, at large  $M_A$ , a saturation is found.

#### 5.4.2 Transition to Self-Consistent Dynamo: Initial value problem

For  $M_A \sim 1$ , a coherent nonlinear oscillation is reproduced as reported earlier [36]. As  $M_A$  is moved up from unity, the oscillation persists alongwith the generation of other modes into the system. Thus as can be found from Fig. 5.1, the magnetic energy does not come back to its initial value after one period of oscillation. Upon further increment of Alfvén Mach number, the linear dependency of the frequency of oscillation breaks down and persistent magnetic field starts to generate. Finally, the growth of magnetic energy reaches a maximum. From Fig. 5.1, it can be seen that, the normalised magnetic energy at  $M_A = 10^2$  &  $10^3$  does not differ significantly, indicating a saturation of the growth. However, such saturation does not occur in the driven cases where, the plasma is driven continuously using an external drive which pumps in kinetic energy to the system. Such phenomena is further explored in the next section of the Chapter.

### 5.4.3 Kinematic Dynamo: Driven velocity field

The phenomenon of magnetic energy growing exponentially with time for a statistically steady flow, where the velocity field is held fixed in time or driven, is called, kinematic dynamo action. Arnold-Beltrami-Childress (ABC) flow being a steady solution of Euler equation, sets the premise to study the kinematic dynamo problem. For ABC flow, kinematic dynamo was first addressed by Arnold *et al* [194] at magnetic Reynolds number ( $Rm$ ) between 9 and 17.5. Galloway *et al* [82] found a more efficient dynamo effect with much higher growth rate after  $Rm = 27$  breaking certain symmetries of the flow. Later on, the study had been extended for the parameters where  $A, B, C$  are not equal [58]. The threshold  $Rm$  for a kinematic dynamo has been well explored [195, 189, 196, 197]. The real part of the growth rate of the magnetic energy for increasing  $Rm$  is found to increase while the imaginary part decreases continuously [58]. ABC flows with different forcing scales ( $k_f \neq 1$ ) providing kinematic dynamo has been explored by Galanti *et al* [181] and more recently by Archontis *et al* [192] and M Sadek *et al* [130].

First I reproduce the previous results and then choose an optimal set of working parameters. The motivation behind choosing the parameters are explained in the previous Section i.e. motivation is to generate short scales in our results. I give the following runs (Table 5.1) to explore the parameter regime of a kinematic dynamo problem.

#### Effect of Magnetic Resistivity [KR Series]

Effect of magnetic resistivity ( $\eta$ ) through the magnetic Reynolds number ( $Rm$ ) has been widely studied in past [58, 58, 181] and in recent years [129]. First I reproduce the previous results by Galloway *et al* [58] using my code [Runs: KR1, KR2, KR3]. Similar to the previous study [58] I choose  $U_0 = 1$ ,  $A = B = C = 1$ ,  $k_f = 1$ . I

Name	$k_f$	$M_A$	$Rm$
KF1	1	1000	450
KF2	2	1000	450
KF3	4	1000	450
KF4	8	1000	450
KF5	16	1000	450
KM1	1	100	450
KM2	1	1	450
KM3	1	0.1	450
KR1	1	10	450
KR2	1	10	200
KR3	1	10	120

Table 5.1: Parameter details with which the simulation has been run for kinematic dynamo problem.

time evolve only Eq. 5.3 for the initial time data mentioned above for magnetic Reynolds number  $Rm = 120, 200, 450$  and obtain the identical growth of magnetic field as Galloway *et al* [58]. This result is shown in Fig 5.2. I also reproduce the real and imaginary part of the eigenvalue obtained previously [58]. The critical value of onset of kinetic dynamo action is found to be  $Rm = 27$  (See Chapter 2, Section 1.5.2, Fig. 1.18-20).

I obtain the energy spectra of the kinematic dynamo from ABC flow [Fig.(5.3)] and observe energy is not only contained in large scales rather, the energy contained in the intermediate scales are quite large. I observe a  $k^{\frac{7}{10}}$  scaling of magnetic energy at the resolution used here.

### Effect of Forcing Scale [KF Series]

The effect of forcing scale on the growth rate of magnetic energy has been earlier studied by Galanti *et al* [181] for  $k_f = 1$  to 10 for  $Rm$  values upto  $Rm = 45$ . For the kinematic dynamo case, Galloway and Frisch ([58]) have shown that, even though the critical value of  $Rm$  for kinematic dynamo action for ABC flow is  $Rm_c = 27$ , the growth rate monotonically increases until  $Rm = 350$ . In the past work of Galanti *et*

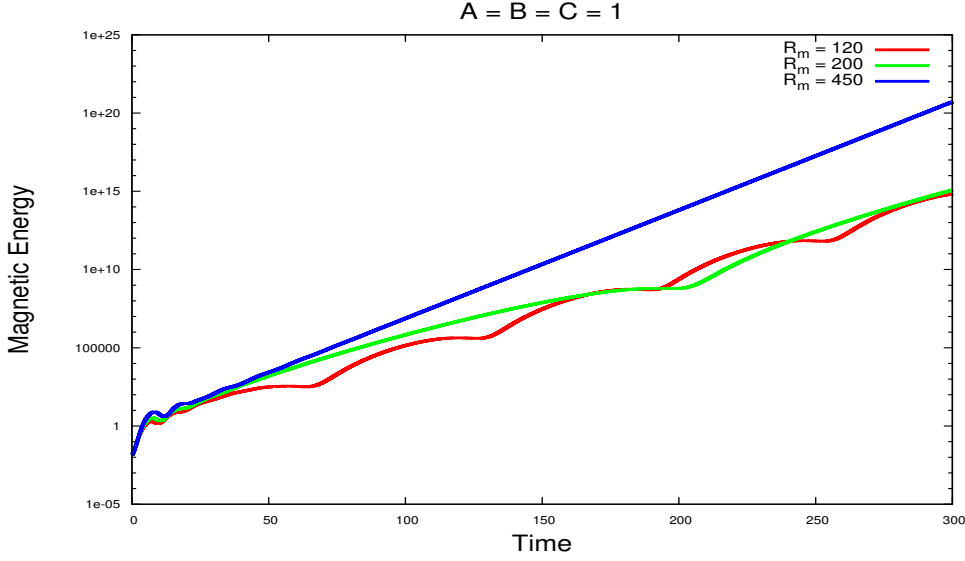


Figure 5.2: Kinematic Dynamo effect reproduced using the identical parameter regime ( $A = B = C = 1$ ,  $k_f = 1$ ) by Galloway *et al* [58]. The grid resolution is  $64^3$  which is close to the value  $60^3$  that was taken by Galloway *et al* [58]. The growth rates of magnetic energy  $\left(\sum_V \frac{B^2(x,y,z)}{2}\right)$  of kinematic dynamo are found to increase as  $Rm$  is increased. The oscillation frequency of the magnetic energy is also found to be similar as Galloway *et al* [58]

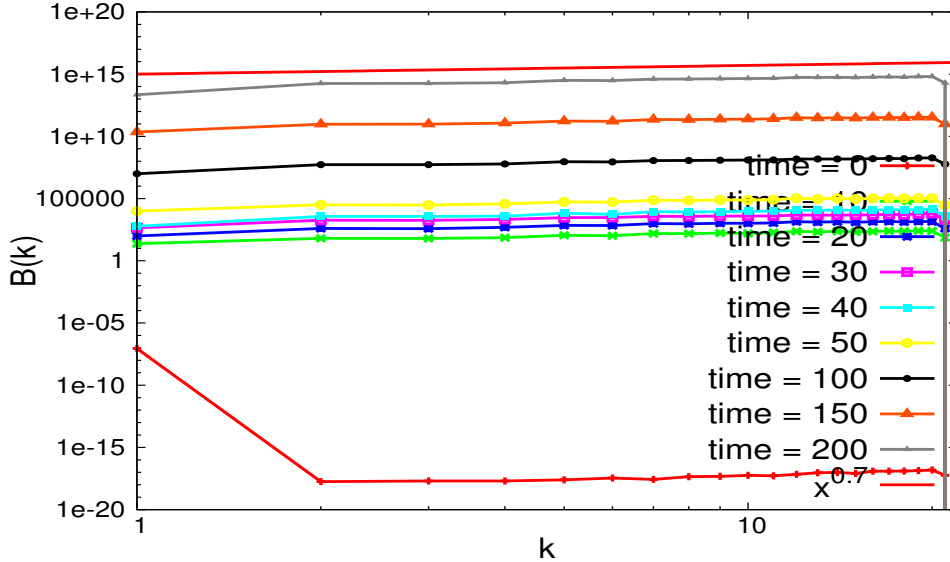


Figure 5.3: Magnetic energy spectra at different times for ABC flow with the identical parameter described in Fig. (5.2) with  $Rm = 450$ . The energy content in the large scales at late times shows that the short scales are equally important for a kinematic dynamo obtained from ABC flow.

al [181] it was found that  $k_f = 2$  has higher growth rate than  $k_f = 1$  for  $Rm = 45$ . Also changing  $Rm$  from 12 to 20 did not affect the growth rate for different  $k_f$  much. In my case, I keep the forcing length scale at  $k_f = 1, 2, 4, 8, 16$  holding the  $Rm = 450$  much above the critical value ( $Rm_{crit} = 27$ ) of onset of kinetic dynamo for  $k_f = 1$  (where imaginary part of the eigenvalue ( $2\gamma$ ) is undetectably small) and in the regime where the growth rate does not vary much with the further increase of  $Rm$ . [Runs: KF1, KF2, KF3, KF4, KF5] The growth rate of normalised magnetic energy,  $\frac{B^2}{B_0^2}$ , is found to increase as  $k_f$  is increased [Fig.5.4, 5.5]. However, the growth rate ( $2\gamma$ ) saturates as  $k_f$  is increased for  $U_0 = 0.1$ [5.5]. A similar saturation was also observed earlier at  $Rm = 12$  and 20 [181].

The late time dynamics is found to be widely different for different driving frequencies ( $k_f$ ) [Fig.5.4,5.5]. For a kinetic dynamo problem similar transient behaviour ( $k_f = 16$  and 8 in Fig. 5.5) starting from a typical initial condition has been addressed previously in detail [129]. It was found that when the fastest growing eigenmode is not excited, it takes some time for the fastest eigenmode to overcome the initially excited mode and hence the crossover happens at a later time. Even for a self-consistent dynamo under external forcing, similar result was earlier obtained by Galanti *et al* [181] for  $A = B = C = 1$ ,  $k_f = 1$  and  $Re = Rm = 12$ .

### Effect of Alfven Speed [KM Series]

The Alfven speed is defined as  $V_A = \frac{U_0}{M_A}$ . If  $M_A < 1$ ;  $V_A < U_0$  and the plasma is called Sub-Alfvenic. Similarly if  $M_A > 1$ , the plasma is Super-Alfvenic. For kinetic dynamo problem, the growth rate of magnetic energy is found to be independent of the magnitude of  $M_A$ . [Runs: KF1, KM1, KR1, KM2, KM3] I check the growth rate for  $M_A = 0.1, 1, 10, 100, 1000$  and for every case the growth rate of dynamo is found to be identical as shown in Fig. 5.6 and 5.7 unlike the self-consistent case discussed in the next subsection.

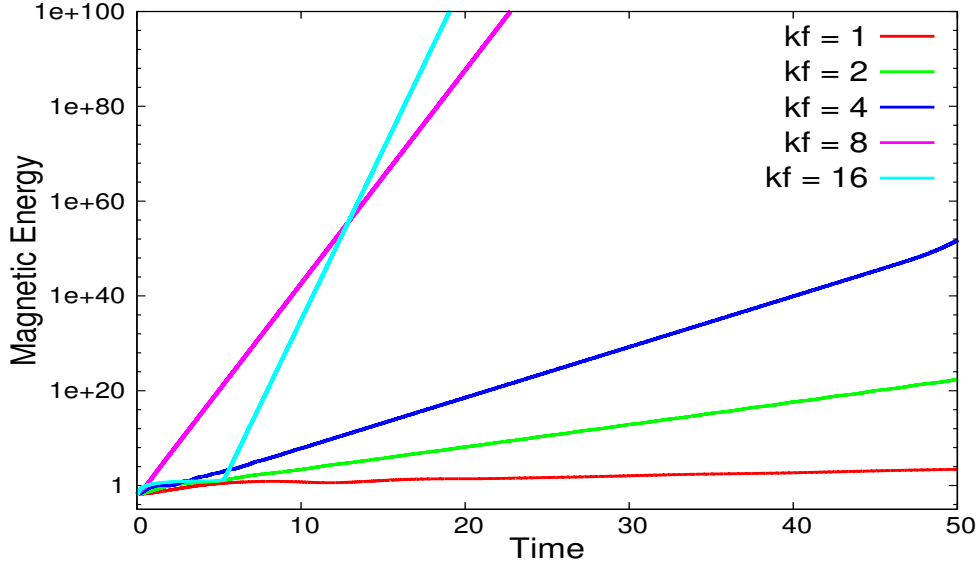


Figure 5.4: Kinematic Dynamo effect for different driving frequency ( $k_f$ ). The magnetic energy is normalised with the initial magnitude at time  $t = 0$ . The parameters chosen are  $A = B = C = 1$  and  $Re = Rm = 450$  with  $U_0 = 1$  and  $M_A = 1000$ . The initial growth rates are found to grow as  $k_f$  is increased.

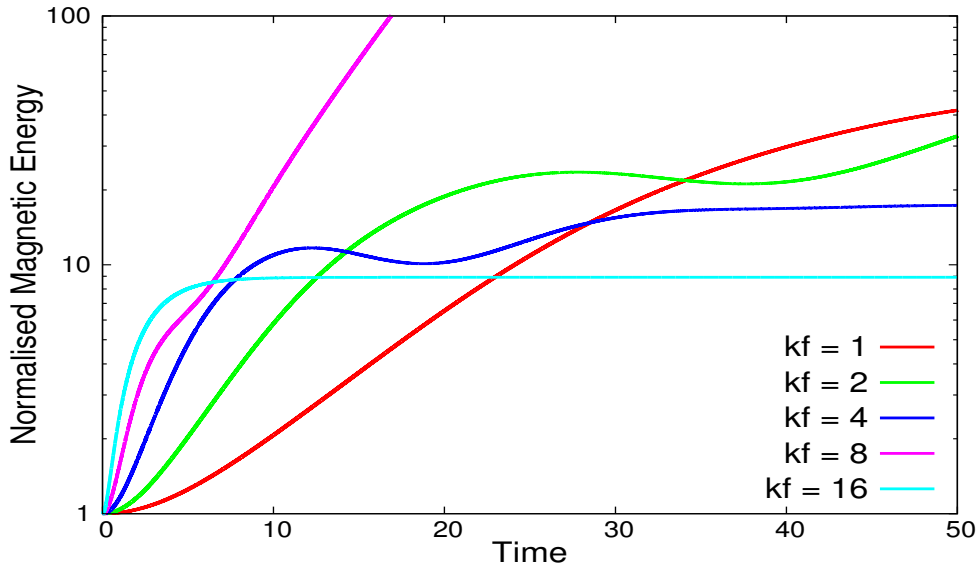


Figure 5.5: Kinematic Dynamo effect for different driving frequency ( $k_f$ ). The normalised magnetic energy is defined as  $\left( \sum_V \frac{B^2(x,y,z,t)}{2} - \sum_V \frac{B^2(x,y,z,0)}{2} \right)$ . The parameters chosen are  $A = B = C = 1$  and  $Re = Rm = 450$  with  $U_0 = 0.1$  and  $M_A = 1000$ . The initial growth rates are found to grow and saturate as the  $k_f$  is increased.



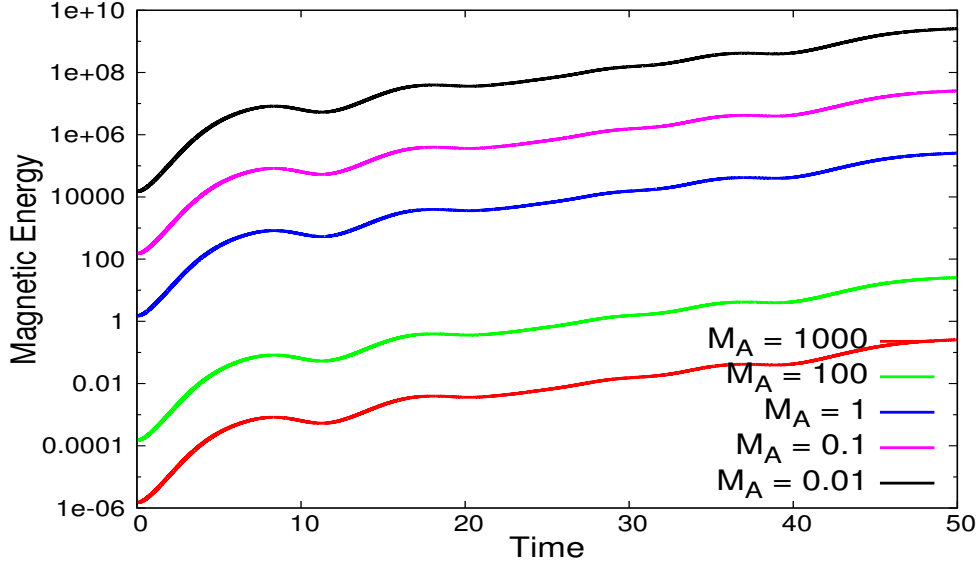


Figure 5.6: Kinematic Dynamo effect for different driving frequency ( $M_A$ ). The parameters chosen are  $A = B = C = 1$  and  $Re = Rm = 450$  with  $U_0 = 1$ . The growth rates are found to be identical for different  $M_A$  values.

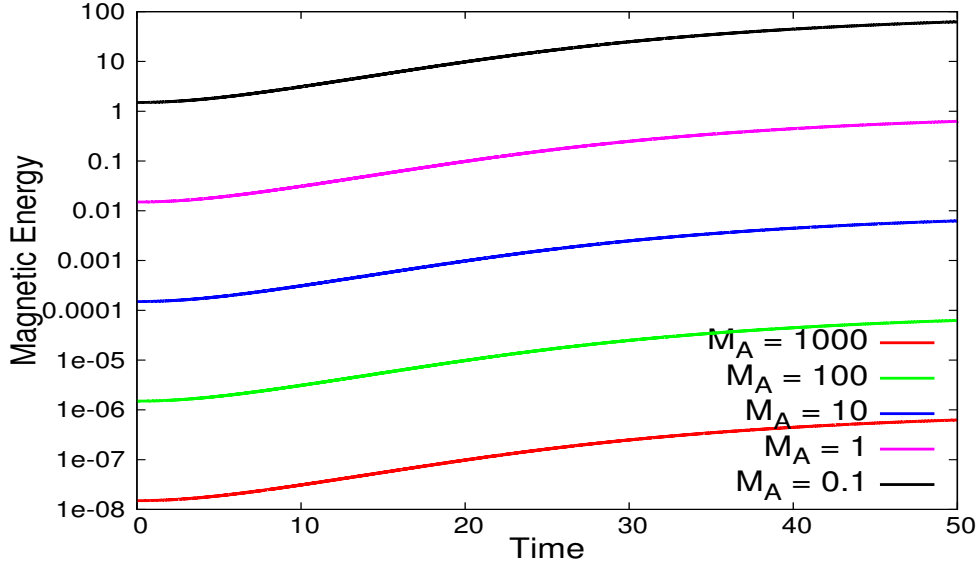


Figure 5.7: Kinematic Dynamo effect for different driving frequency ( $M_A$ ). The parameters chosen are  $A = B = C = 1$  and  $Re = Rm = 450$  with  $U_0 = 0.1$ . The growth rates are found to be identical for different  $M_A$  values.

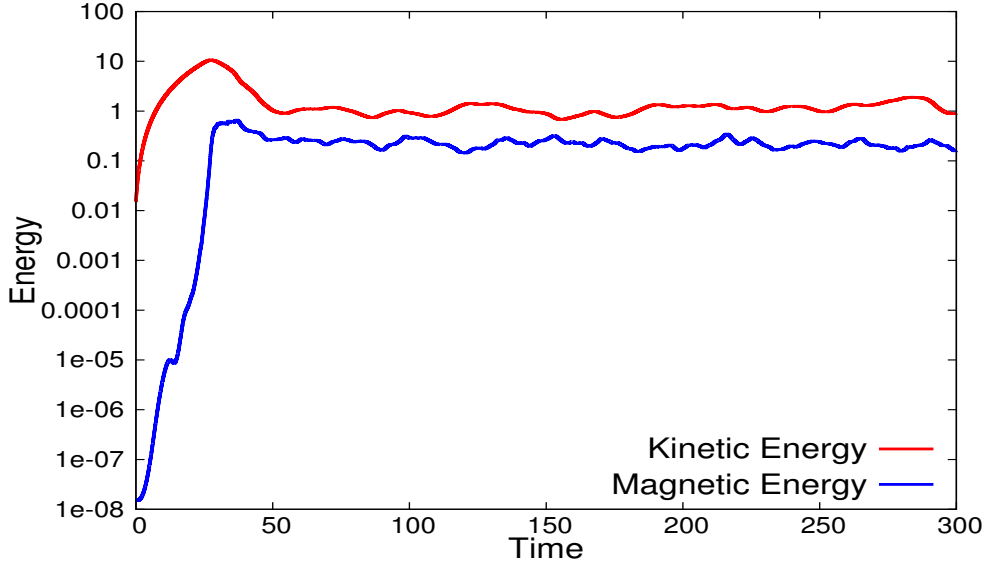


Figure 5.8: Self-consistent dynamo growth of kinetic  $\left(\sum_V \frac{U^2(x,y,z)}{2}\right)$  and magnetic  $\left(\sum_V \frac{B^2(x,y,z)}{2}\right)$  energy for ABC flow with  $M_A = 1000$  and  $k_f = 1$  for a long time with initial flow profile as ABC flow.

#### 5.4.4 Dynamo with Back-Reaction or Self-Consistent Dynamo

A self-consistent dynamo represents a situation where the magnetic energy grows exponentially for a plasma where the plasma itself evolves in time. Hence the velocity field is not externally imposed like a kinematic dynamo, rather it has a dynamical nature. The time evolution of the velocity field is generally governed by the Navier-Stokes equation including the magnetic feedback on the velocity field. In order to simulate such a scenario, I time evolve all the three equations, viz. Eq. 5.1, 5.2, 5.3. A result for parameters  $M_A = 1000$  and  $k_f = 1$  for initial flow profile ABC is given in Fig. 5.8.

I change the forcing scale, Alfven velocity and compressibility to observe the effect on the dynamics of the fields.

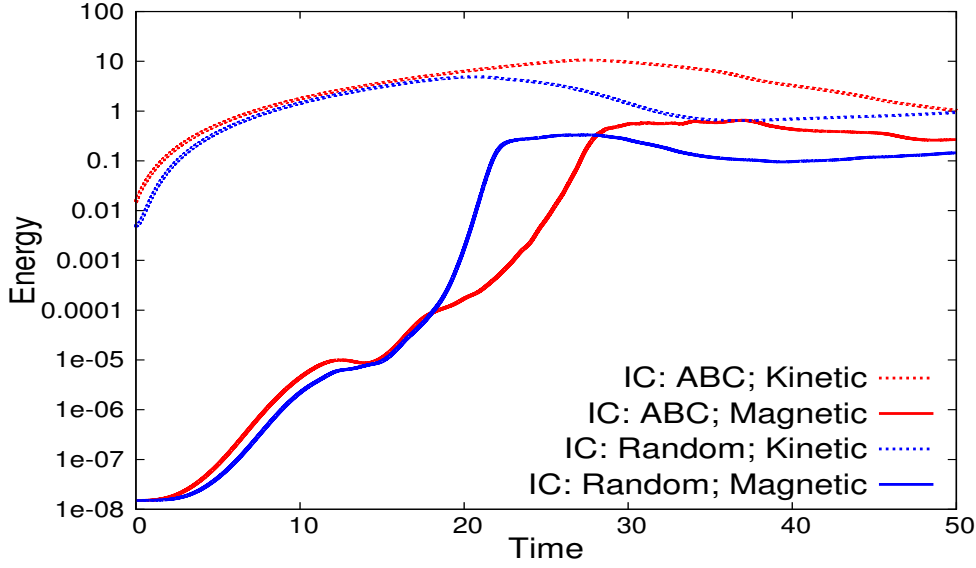


Figure 5.9: Self-consistent dynamo growth of kinetic and magnetic energy for two different initial conditions with  $M_A = 1000$  and  $k_f = 1$ . The initial growth rate of magnetic energy for ABC initial flow profile is found to be identical with that of random field profile.

I turn on external forcing to the velocity field. I keep the nature of forcing as  $f_x = A \sin(k_f z) + C \cos(k_f y)$ ,  $f_y = B \sin(k_f x) + A \cos(k_f z)$ ,  $f_z = C \sin(k_f y) + B \cos(k_f x)$ . I keep  $A = B = C = 0.1$  and  $U_0 = 1$  throughout all the calculations and fix  $Re = Rm = 450$ . In case of an external forcing the initial memory is lost and hence the sensitivity to the initial condition is expected to be lost. I redo my numerical calculations for an initial random velocity field profile and find that the basic nature of dynamo effect does not get affected as shown in Fig. 5.9. The saturation regime for both the kinetic (sum over all velocity modes) and magnetic (sum over all magnetic modes) energies remain the same though the two systems are evolved from different initial conditions. I perform the following runs (Table. 5.2) using my code to understand the externally forced ABC flow dynamo process.

Now I vary  $U_0$  and the magnitude of  $A, B, C$  keeping  $A = B = C$  for all the cases. I run my simulation for  $U_0 = 0.1, 0.2, 0.3, 0.4, 0.5$  keeping  $A = B = C = 0.1$  and see the trend of dynamo action is identical for all values of  $U_0$  [Fig. 5.10]. Next I vary the values of  $A = 0.1, 0.1, 0.3$  keeping  $A = B = C$  and  $U_0 = 0.1$ . I see faster

Name	$k_f$	$M_A$	$M_s$
FDF1	1	1000	0.1
FDF2	2	1000	0.1
FDF3	4	1000	0.1
FDF4	8	1000	0.1
FDF5	16	1000	0.1
FDMA1	1	100	0.1
FDMA2	1	10	0.1
FDMA3	1	1	0.1
FDMA4	1	0.1	0.1
FDMS1	1	100	0.2
FDMS2	1	100	0.3
FDMS3	1	100	0.4
FDMS4	1	100	0.5

Table 5.2: Parameter details with which the simulation has been run for the externally forced self-consistent dynamo problem.

growth of dynamo with higher values of forcing through the magnitudes of  $A$ ,  $B$  and  $C$  [Fig. 5.11].

### Effect of Forcing scale

A self-consistent dynamo with external forcing has been studied earlier by Galanti *et al* [181] for incompressible plasma with  $U_0 = 1$ ,  $A = B = C = 0.1$ ,  $Re$  &  $Rm$  upto 20 (below  $Rm_c = 27$ ), and  $k_f = 1, 2, 4$ . I change the length scale of forcing ( $k_f$ ) on the velocity field keeping  $U_0 = 0.1$ ,  $A = B = C = 0.1$ ,  $Re = Rm = 450$ ,  $M_s = 0.1$  and  $M_A = 1000$  as fixed parameters. [Runs: FDF1, FDF2, FDF3, FDF4, FDF5] From Fig. 5.12 I find, the growth rate of magnetic energy increases while that of kinetic energy decreases as  $k_f$  is increased. The case  $k_f = 16$  in Fig. 5.12 shows a delayed dynamo action. A possible explanation of this late time dynamo action is the excitation of a slow eigenmode to start with, which gets overpowered by the fastest eigenmode excited later. The identical phenomena I have seen in the kinematic dynamo section [Fig. 5.5]. From Fig. 5.12 I also note that though externally forced, the saturation regime of both kinetic and magnetic energies goes downwards as  $k_f$  is increased. This is so, because the forcing scale also has a wave

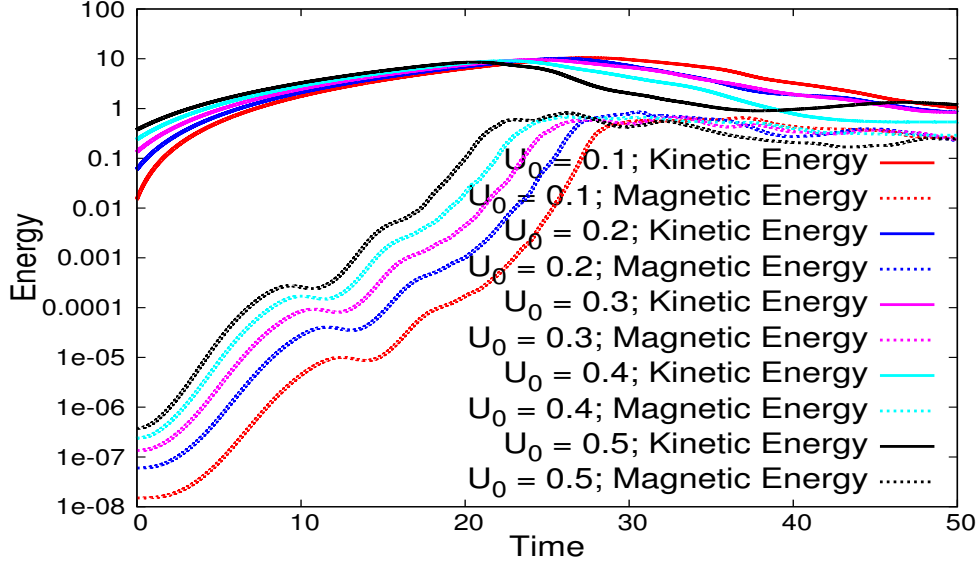


Figure 5.10: Self-Consistent dynamo growth of kinetic and magnetic energy for five different initial velocities viz.  $U_0 = 0.1, 0.2, 0.3, 0.4, 0.5$ , with  $M_A = 1000$ ,  $A = B = C = 0.1$  and  $k_f = 1$ . The initial growth rate of magnetic energy for ABC initial flow profile is found to be identical for all initial magnitude of velocities.

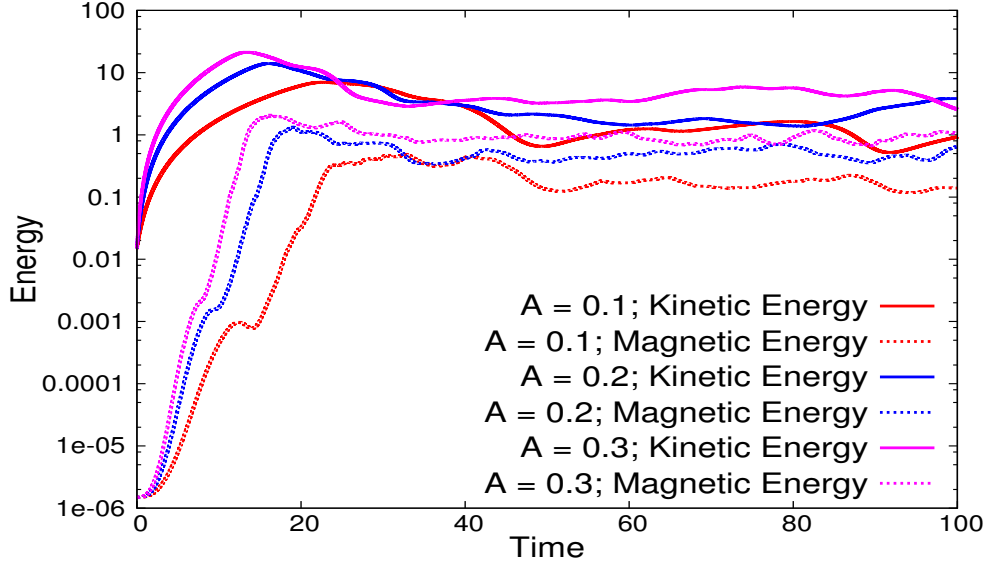


Figure 5.11: Self-Consistent dynamo growth of kinetic and magnetic energy for three different forcing magnitudes  $A = 0.1, 0.2, 0.3$  having  $A = B = C$ , with  $M_A = 1000$  and  $k_f = 1$ . The initial growth rate of magnetic energy for ABC initial flow profile is found to increase with the increment of magnitude of forcing.

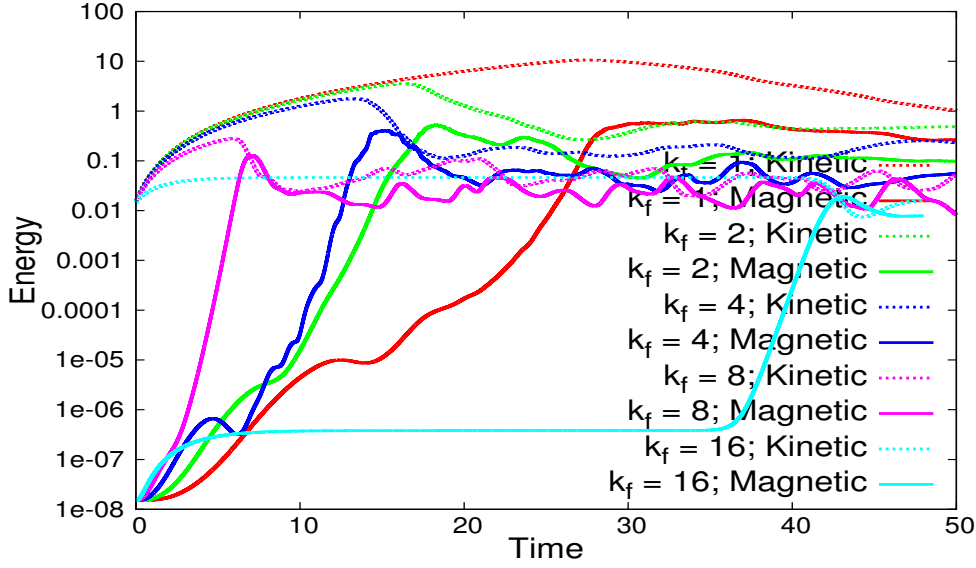


Figure 5.12: Self-Consistent dynamo growth of kinetic and magnetic energy for  $k_f = 1, 2, 4, 8, 16$  with  $M_A = 1000$ . The growth rate of magnetic energy is found to be steeper with the increase of  $k_f$ . The growth rate of kinetic energy due to external forcing decreases as  $k_f$  is increased.

number term within it which helps to drain out energy through viscous dissipation, if a higher wavenumber ( $k_f$ ) is excited.

### Effect of Alfven Speed

I change the Alfven Mach number ( $M_A$ ) of the plasma, keeping  $U_0 = 0.1$   $A = B = C = 0.1$ ,  $Re = Rm = 450$ ,  $M_s = 0.1$  and  $k_f = 1$ .

I analyse the runs: FDF1, FDMA1, FDMA2, FDMA3. By choosing  $M_A = 1, 10, 100$  and  $1000$  I set the Alfven Velocity  $V_A = \frac{U_0}{M_A} = 10^{-1}, 10^{-2}, 10^{-3}$  and  $10^{-4}$  respectively. For  $\rho_0 = 1$ ,  $V_A = B_0$ , the initial magnitude of the seed magnetic field profile. As I start from a lower value of  $B_0$ , the growth rate of the magnetic energy increases rapidly. This is quite similar to the kinematic dynamo action with a distinct difference. In kinematic dynamo there was no saturation of magnetic energy. On the other hand, in forced self-consistent dynamo, there is a saturation value of the magnetic field. This saturation is believed to be due to the backreaction of

the magnetic field on the velocity field through the Lorentz force term. The strong magnetic field generated through the dynamo process, starts affecting the topology of the velocity field in turn affecting its dynamics. Thus the modified velocity field no longer remains a ABC flow and finally the dynamo saturates. The effect of such magnetic feedback on the velocity field is shown in Fig 5.13 for  $M_A = 1, 100, 1000$ .

I make the following observations from Fig 5.13.

- I notice that, for both the cases  $M_A = 100$  and  $1000$  there exists three distinct slopes. At the beginning, the magnetic energy starts exponentially increasing with time. Once it gets amplified by around four orders of magnitude, the exponent of increment suddenly falls down for both the cases  $M_A = 100$  and  $1000$ . After that, the magnetic energy again starts increasing with higher exponent.
- It is also note-worthy that, the initial growth rate of the magnetic energy for  $M_A = 100$  and  $1000$  are identical though they differ later on. Thus I understand it as similar to Kinematic dynamo (5.7) where the backreaction is negligible. However, at later time because of the difference in the strength of the backreaction, the slopes of increment of the magnetic energy in logarithmic scale differ.
- I also find that when the growth of the dynamo is of several orders of magnitude (for higher values of  $M_A$ ) the kinetic energy also grows faster though ultimately both kinetic and magnetic energies saturate at the same value.
- I see that, independent of the strength of the seed magnetic field, the saturation regime of the kinetic and magnetic energies are the same.

Thus I conclude from the above observations that, if the velocity field is ABC forced, whatever be the seed magnetic field, the dynamo effect becomes possible in super Alfvenic systems and the dynamo action is quite strong leading the final magnetic energy comparable to the kinetic energy.

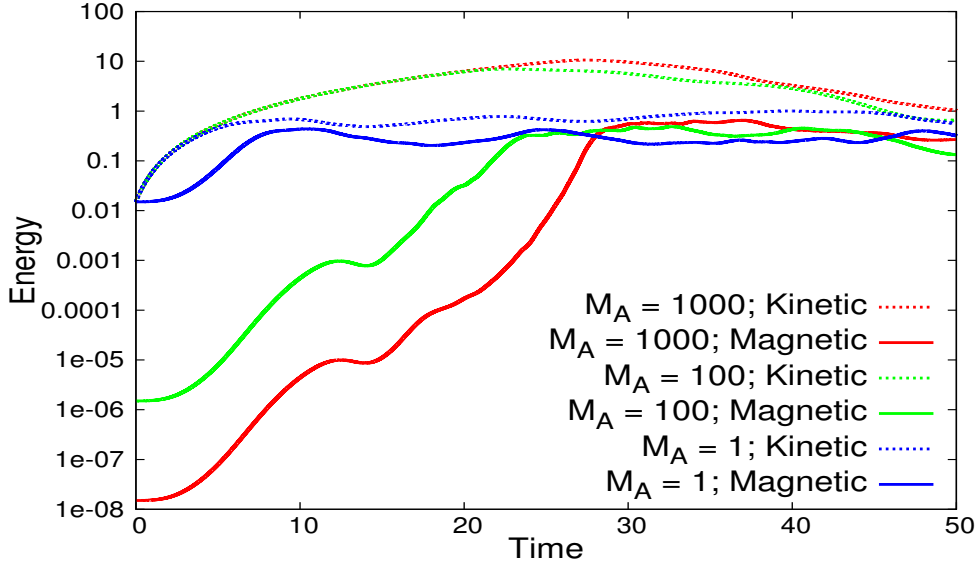


Figure 5.13: Self-Consistent dynamo growth of kinetic and magnetic energy for  $M_A = 1, 100, 1000$ . The back-reaction of magnetic field on velocity field is found to affect the growth rate and dynamics of velocity field. This effect is captured in the time evolution of kinetic energy for different  $M_A$ .

### Energy Spectra

Now I analyse the kinetic and magnetic energy spectra of the self-consistent dynamo action at different times for  $U_0 = 0.1$ ,  $A = B = C = 0.1$ ,  $k_f = 1$ ,  $M_A = 1000$ ,  $Re = Rm = 450$ . Initially the energy content was limited to the fundamental mode only. But in course of time the kinetic energy shows a  $k^{-5/3}$  spectra while the magnetic energy shows a  $k^{0.7}$  spectra identical to the kinematic dynamo phenomena. However it is worth notable that the growth of magnetic energy in intermediate scales is much slower than that of the kinematic dynamo as can be found in Fig. 5.3

### Effect of Compressibility

I start with a initial profile  $\vec{\nabla} \cdot \vec{u} = 0 = \vec{\nabla} \cdot \vec{B}$  and set the forcing term which also leads divergence-free velocity profile. However I nowhere impose the incompressibility cri-



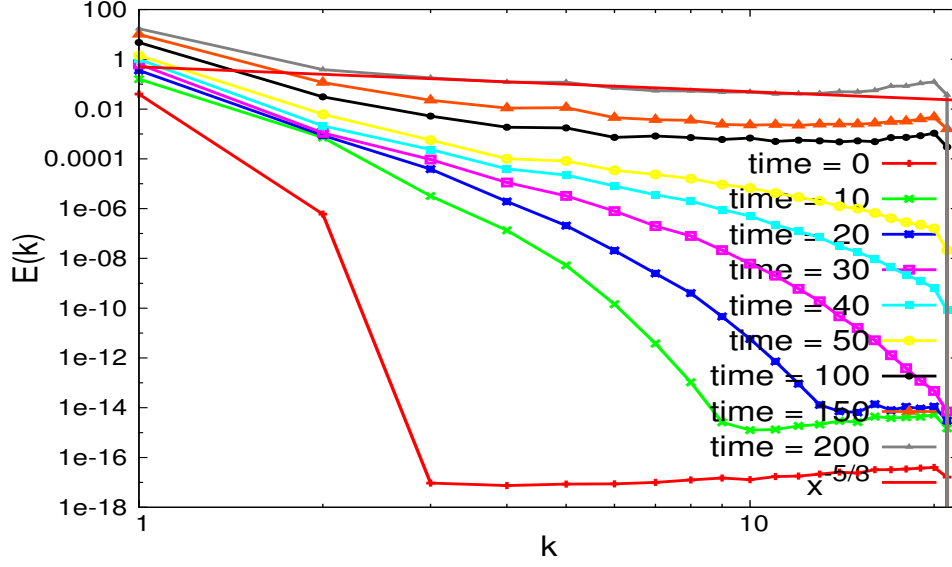


Figure 5.14: Kinetic energy spectra for self-consistent dynamo with  $U_0 = 0.1$ ,  $A = B = C = 0.1$ ,  $k_f = 1$ ,  $M_A = 1000$ ,  $Re = Rm = 450$ .

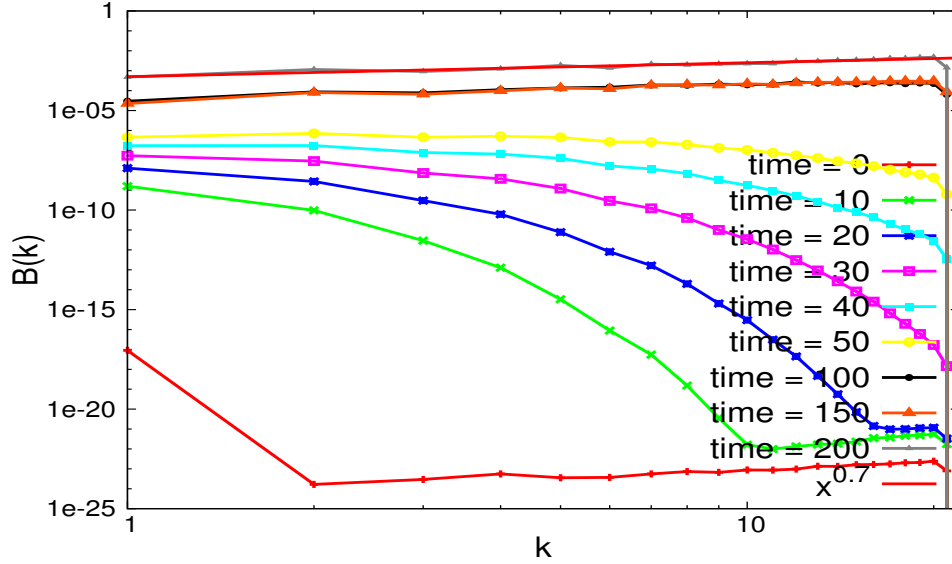


Figure 5.15: Kinetic energy spectra for self-consistent dynamo with  $U_0 = 0.1$ ,  $A = B = C = 0.1$ ,  $k_f = 1$ ,  $M_A = 1000$ ,  $Re = Rm = 450$ .

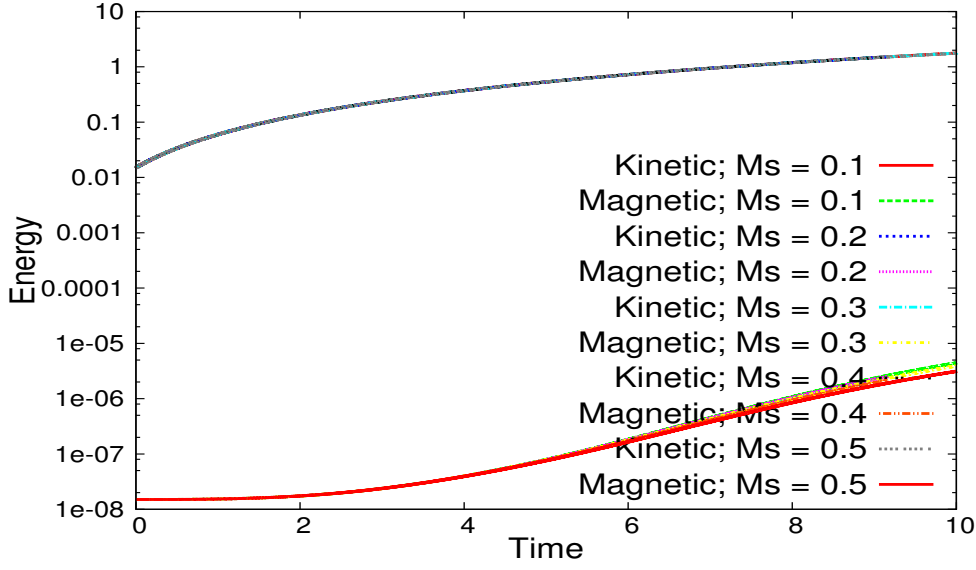


Figure 5.16: Growth of kinetic and magnetic energy for  $M_s = 0.1, 0.2, 0.3, 0.4, 0.5$  at  $M_A = 100$ . The growth rate does not get much affected with the change of compressibility.

teria for the mhd plasma during the time evolution. Thus, I change the compressibility of the plasma by changing the sonic Mach number ( $M_s$ ), keeping the parameters identical to section 5.3. I keep  $U_0 = 1$ ,  $A = B = C = 0.1$ ,  $Re = Rm = 450$ ,  $M_A = 100$  and  $k_f = 1$ . [Runs: FDMA1, FDMS1, FDMS2, FDMS3, FDMS4] I run my simulation in incompressible  $M_s = 0.1, 0.2, 0.3$  limits first. In two dimensions for a hydrodynamic problem I check my results for a Kelvin-Helmholtz like problem and found good agreement upto at least  $M_s = 0.8$ . Here, I run My code for some weakly compressible  $M_s = 0.4, 0.5$  cases. I do not find any distinguishable change in the growth rate of the dynamo process (Fig. 5.16) at least in the primary evolution phase.

## 5.5 Summary and Future Works

In this Chapter I have analysed several phenomena of a magnetohydrodynamic plasma under ABC flow. Mostly, I have concentrated on parameter space that

reveals the transition to self-consistent dynamo phenomena. I have found parameter namely Alfven Mach number, which leads to self-consistent dynamo action at very high values and in the other limit, gives rise to nonlinear coherent oscillations in the form of large amplitude Alfven waves discussed at length in Chapter 3. Rest of the Chapter is dedicated to parameter search for ‘Fast’ dynamos using Arnold-Beltrami-Childress flow, since this flow is well-known to produce ‘fast’ kinematic dynamos. In particular, the following observations are made out of this Chapter.

- First I study the kinematic dynamo effects where the velocity field is the ABC flow - a known solution of Euler equation. At different wave-numbers of the flow, I see that the growth rate of the magnetic energy in the kinematic dynamo case increases as  $k_f$  is increased.
- In case of an ABC forced velocity field for the self-consistent dynamo problem seems to show similar variation with  $k_f$ , though now the dynamo action becomes very prominent. The magnetic energy grows upto the order of kinetic energy when I remain in the super Alfvenic regime.
- The magnetic energy is found to be contained primarily in the intermediate scales in wave-number.

The compressibility however has not been found to affect the results for the weakly compressible cases. From the energy spectra for kinetic and self-consistent dynamos, it is rather obvious that the resolution  $64^3$  and the corresponding  $k_{max}$  is not sufficient to see a numerically converged spectra at all  $k$ 's, asymptotically speaking. Convergence at high  $k$  values meaning reduced power in high  $k$ -modes asymptotically in time contributing to magnetic and kinetic energies is desirable. It would

be pertinent to give large  $N$  runs, larger than  $64^3$ . The effect of variation of initial density ( $\rho_0$ ) on the dynamo effect can be an interesting piece of study and will be discussed in Chapter 6.

# Chapter 6

## Conclusion

### 6.1 Introduction

In this Chapter, I summarize the major findings and future scope of present Thesis. Starting from the development of a new code GMHD3D from scratch all the details are provided in Chapter 2 of this Thesis. Next in Chapter 3, I discuss issues when only a few large scales are excited. I observe large amplitude coherent oscillations of energy between kinetic and magnetic modes due to the excitation of dispersionless nonlinear Alfvén waves in the medium. Further in Chapter 4, I discuss cases within the premise of single fluid magneto-hydrodynamics model, when only the short scales are excited, how does some flows recur periodically after going through a complete nonlinear destruction. In Chapter 5, I go into the other limit where, large as well as the short scales are excited. I identify a parameter, namely Alfvén Mach number, that acts as a control parameter to excite such short scales in the medium. In the later part of the Chapter, I delve into identifying parameters which gives rise to ‘fast’ dynamos.

It is to be noted that, all the phenomena studied in this Thesis are the outcome

of a few coupled fundamental equations of hydrodynamics and Maxwell's equations, capable of modelling plasmas. The non-linear coupled partial differential equations are known to be hard to solve analytically. Thus the long time prediction of any given initial state of such plasma has been found to become increasingly challenging to study through analytical approaches. The linear approximations of these set of equations are well studied over several decades. However the nonlinear evolution has been found to be quite difficult to study analytically. Over the time, the progress of computer simulation techniques, enabled people to extensively study the approximate solutions of such coupled nonlinear equations. In course of time, the need for first principle simulation of plasma has become increasingly important and with the improvement of computer hardwares and softwares, new algorithms has been developed to study the same. Such study has opened a new era in the area of plasma physics enabling us to probe nearer to the problems faced in the experimental projects of plasma science.

Here in this Thesis development of one of such codes from scratch is discussed in detail and the trial to improve the performance of the code is also discussed. After that, using the code, several non-linear problems are addressed and some of them are solved. The individual problems are addressed in Chapter 3, 4 & 5. Finally I end with the limitation of my code. It has been found that, as we increase the value of  $M_A$ , the generation of short scales become prominent and thus the need for a code that is capable of high resolution runs is highly essential.

## 6.2 Summary

The Thesis describes the details of the development of a numerical solver G-MHD3D capable of solving single fluid Magnetohydrodynamic equations in three spatial di-

mensions with periodic boundary. The benchmarking details of the code at different limits have been well explained and the normalisation of the basic equations used are also distinctly identified in the first part of Chapter 2. The basic spatial discretisation technique used in the code is a spectral one. The finite-difference based schemes fall short to fit the purpose of long time simulation that is needed to address the physics issues mentioned above. Thus in this thesis, stress is given on the judicious choice of schemes that fit to the long time accurate simulation purpose. That is why I choose pseudo-spectral method which is fast and give low phase or dispersion error in the long time simulation of the code [35]. Also the time discretisation is checked by several schemes like Runge-Kutta 4, Predictor-corrector, Adams-Bashforth technique. It is found that all the schemes give identical result upto the toleration limit of the precesion used in the code. Because of the pressing demand of the physics results, the code has to be parallalised in graphics processing unit for better performance. The parallelisation and compilation procedure, performance results are also described in detail towards the end of the Chapter 2.

In Chapter 3, energy exchange phenomena has been studied for a wide range of parameters using this code - G-MHD3D. Using direct numerical simulation of the MHD equations the energy has been found to cascade through both kinetic as well as magnetic channels giving rise to coherent nonlinear oscillation. Such oscillation is found to exist for both two dimensional and three dimensional cases. An analytical study has been carried out using the finite mode expansion of the incompressible two dimensional MHD equations and similar observation is found for the identical parameter. A criticism of the analytical study is also delineated pointing out the limitation of the theory. The parameters for which the analytical study fails are identified. The failure of the analytical approach and the extensive parameter study has actually motivated the detailed discussion of the problems addressed in Chapter 5 of this thesis.

Chapter 4 is dedicated to look into the structures of the magnetic and kinetic iso-surfaces generated from the coherent nonlinear oscillation described in Chapter 3. It is shown that, even though, coherent nonlinear oscillation persists for several flows, some flows reconstructs back the initial condition and some not. The reconstruction of the initial condition is named as “Recurrence”. In past recurrence has been observed in many electrostatic systems in both one and two dimensions. However, I demonstrate recurrence in electromagnetic systems in three dimensions and find that the cause of recurrence in a single fluid MHD model is fundamentally different from the previous studies. An analytical study is employed to study the number of effective active degrees of freedom of the system. The quantity measured is known as Rayleigh Quotient. For flows that recur, it is found that the Rayleigh Quotient is bounded as expected from the theory developed by Birkhoff in his book, “Dynamical Systems” [71]. On the other hand, it is found that the Rayleigh Quotient is unbounded for the other flows that does not recur.

In Chapter 5, I describe the opposite limit of the study described in earlier Chapters. Chapter 3 & 4 were dedicated to simulations where the high wave numbers were not excited. In this Chapter, a suitable parameter is found that excites short scales in the plasma in a controlled manner. Alfven Mach number ( $M_A$ ) is found to be the key parameter. Starting with the identical flows described in the previous chapters, only the single parameter  $M_A$ , is varied and mean magnetic field generation is found. For driven flows, the energy spectra of both the kinetic as well as magnetic energy is studied. The kinetic energy spectra is found to have a slope of  $-5/3$ , as predicted by A. N. Kolmogorov in 1941 [54]. Surprisingly for MHD plasma driven with chaotic fields, is found to show a 0.7 scaling indicating prominancy of small scale structures. Finally, the growth rate of the magnetic field generation is



also studied for a wide range of parameters. Key parameters are identified what causes rapid growth rate of such small scale turbulent dynamo action. However, it has to be stressed that, as I increase the Alfvén Mach number ( $M_A$ ), the tendency to dynamo action appear and consistently the short scales starts getting generated. Thus, the present code with  $64^3$  resolution fails to resolve the effect and the scaling of kinetic and magnetic energy spectra gets severely truncated. Thus a new version of the code that can handle high resolution runs is very important to generate which is expected to throw more light into the large scale simulation of such problem and will help to identify the physics issues happening in such problems in a better way.

### 6.3 Future Work

The further development of the code to increase the performance results is itself a challenging task. However, as described in Chapter 5, the problems addressed need further resolution of the code for which the performance of the code needs to be increased. Below, the future works of this project is described.

- In Chapter 2, the single fluid equations are derived and the approximations are specifically mentioned. I assume that, the electrons, due to their high mobility, always form a Boltzmann distribution around the ions. Thus there is no large scale electric field is produced due to charge separation. However, implementing ions and electrons as two different fluids will make the observations more robust. As can be expected, the computational cost will be very high for the case and needs even smarter parallelisation.
- $\mu$  &  $\eta$  are assumed to be space independent in the code MHD3D. However, it can be implemented in code as space-dependent variable. However, in that case, the spatial derivatives will also appear in the governing equations and thus the computation will consume more time to perform.

- Initial density is known to affect the dynamics of the plasma [96, 95]. Both in Chapter 3 & 4 I for all the cases considered, I have assumed the initial density is uniform and thus it is interesting to perform a study with different initial density which is not uniform. A detailed study can be a subject of future study.
- The single fluid equations mentioned in Chapter 2 does not incorporate the effect of spatial gradient of temperature. Such a term can be added in the RHS of Navier-Stokes equation mentioned in Chapter 2. However, the closure will have to be chosen carefully and hence some more spatial derivatives in the system of equations will hamper the performance of the code.
- A source term added to the continuity equation solved in G-MHD3D may help in involving driven-dissipative limits of MHD. It should not affect the performance of the code since, such calculation will not cause any extra Fourier transform to evaluate. Thus such term can be readily added into the code and its effect can be checked in the results obtained in Chapter 3, 4 and 5.
- A suitable theory that can be used to explain the three dimensional incompressible MHD equations needs to be developed. Also the approximate theory I use in Chapter 3 only addresses the incompressible equations. Apart from that, the critical limitation of the theory is also described in the same Chapter. It would be helpful if a theory can be developed which can handle cases at different Alfvén Mach numbers as required in the dynamo problems mentioned in Chapter 5.
- A better quantitative measure for recurrence phenomena would have been perfect. Also the viscous regularisation of the 3D MHD equations show a deviation of the isosurfaces from its initial condition. Thus a direct numerical simulation using the conservative regularisation as mentioned in Chapter 4 would have been more appropriate to study recurrence phenomena.

- The optimisation of the multi-GPU code is very essential. In Chapter 5, I identify that the kinetic and magnetic energy spectra showed a severe truncation. Thus an optimised multi-GPU code is expected to perform better than the present one and should be able to solve the problem. Currently a multi-GPU code is developed in collaboration with NVIDIA, Bengaluru. However, its performance does not allow us to fit our purpose. The out-of-place Fourier transforms should be changed to in-place Fourier transform such that the memory requirement of the code gets reduced and hence it is expected to make the code faster at large grid size consequently.



# Bibliography

- [1] Ronald Davidson. *Methods in nonlinear plasma theory*. Elsevier, 2012.
- [2] JH Malmberg et al. Properties of nonneutral plasma. *Physical Review Letters*, 35(9):577, 1975.
- [3] Arnab Rai Choudhuri. *Astrophysics for physicists*. Cambridge university press, 2010.
- [4] Subrahmanyan Chandrasekhar. On stars, their evolution and their stability. *Reviews of modern physics*, 56(2):137, 1984.
- [5] Richard C Tolman. Static solutions of einstein’s field equations for spheres of fluid. *Physical Review*, 55(4):364, 1939.
- [6] J Robert Oppenheimer and George M Volkoff. On massive neutron cores. *Physical Review*, 55(4):374, 1939.
- [7] Demetrios Christodoulou. Reversible and irreversible transformations in black-hole physics. *Physical Review Letters*, 25(22):1596, 1970.
- [8] Arnab Rai Choudhuri. *The physics of fluids and plasmas: an introduction for astrophysicists*. Cambridge University Press, 1998.
- [9] John Wesson and David J Campbell. *Tokamaks*, volume 149. Oxford University Press, 2011.

- [10] SB Bhatt, D Bora, BN Buch, CN Gupta, KK Jain, R Jha, PI John, PK Kaw, Ajay Kumar, SK Mattoo, et al. Aditya: The first indian tokamak. *Indian J. Pure Appl. Phys*, 27(9-10):710–742, 1989.
- [11] Y.C Saxena. Sst-1 commissioning and first plasma results. *Proceedings of the 21st IAEA conference*, 38(17):1991–2374, 2007.
- [12] K Ikeda. Progress in the iter physics basis. *Nuclear Fusion*, 47(6), 2007.
- [13] C Bourdelle, JF Artaud, Vbulandi Basiuk, M Bécoulet, S Brémond, J Bucalossi, H Bufferand, G Ciruolo, L Colas, Y Corre, et al. West physics basis. *Nuclear Fusion*, 55(6):063017, 2015.
- [14] J Pamela, Emilia R Solano, and JET EFDA Contributors. Overview of jet results. *Nuclear fusion*, 43(12):1540, 2003.
- [15] DJ Battaglia, MD Boyer, S Gerhardt, D Mueller, CE Myers, W Guttenfelder, JE Menard, SA Sabbagh, F Scotti, F Bedoya, et al. Scenario development during commissioning operations on the national spherical torus experiment upgrade. *Nuclear Fusion*, 58(4):046010, 2018.
- [16] RJ Buttery, B Covele, J Ferron, A Garofalo, CT Holcomb, T Leonard, JM Park, T Petrie, C Petty, G Staebler, et al. Diii-d research to prepare for steady state advanced tokamak power plants. *Journal of Fusion Energy*, pages 1–40, 2018.
- [17] YX Wan, ST Wu, PD Weng, JG Li, and DM Gao. Progress of the east project in china. Technical report, EAST Team, 2005.
- [18] Dieter Biskamp. *Nonlinear magnetohydrodynamics*, volume 1. Cambridge University Press, 1997.
- [19] Cathie Clarke, Bob Carswell, and RF Carswell. *Principles of astrophysical fluid dynamics*. Cambridge University Press, 2007.

- [20] Dieter Biskamp. *Magnetohydrodynamic turbulence*. Cambridge University Press, 2003.
- [21] A Frenkel, E Levich, and L Stilman. Hamiltonian description of ideal mhd revealing new invariants of motion. *Physics Letters A*, 88(9):461–465, 1982.
- [22] Philip J Morrison. Hamiltonian description of the ideal fluid. *Reviews of modern physics*, 70(2):467, 1998.
- [23] Rupak Mukherjee, Rajaraman Ganesh, and Abhijit Sen. Recurrence in three dimensional magnetohydrodynamic plasma. *arXiv preprint arXiv:1811.00754*, 2018.
- [24] Rupak Mukherjee, Rajaraman Ganesh, and Abhijit Sen. Coherent nonlinear oscillations in magnetohydrodynamic plasma at  $\text{alfv}\backslash\text{'en}$  resonance. *arXiv preprint arXiv:1811.00744*, 2018.
- [25] Rupak Mukherjee, Rajaraman Ganesh, and Abhijit Sen. Coherent nonlinear oscillations in magnetohydrodynamic plasma at  $\text{alfv}\backslash\text{'en}$  resonance. *Physics of Plasmas*, 26(4):042121, 2019.
- [26] Vasily Semenovich Beskin. Magnetohydrodynamic models of astrophysical jets. *Physics-Uspekhi*, 53(12):1199–1233, 2010.
- [27] Prateek Sharma. Kinetic effects on turbulence driven by the magnetorotational instability in black hole accretion. *arXiv preprint astro-ph/0703542*, 2007.
- [28] Eugene N Parker. Hydromagnetic dynamo models. *The Astrophysical Journal*, 122:293, 1955.
- [29] Rainer Moll, J Pietarila Graham, J Pratt, RH Cameron, W-C Müller, and M Schüssler. Universality of the small-scale dynamo mechanism. *The Astrophysical Journal*, 736(1):36, 2011.

- [30] Jonathan Squire and Amitava Bhattacharjee. Nonmodal growth of the magnetorotational instability. *Physical review letters*, 113(2):025006, 2014.
- [31] Jonathan Squire and Amitava Bhattacharjee. Magnetorotational instability: nonmodal growth and the relationship of global modes to the shearing box. *The Astrophysical Journal*, 797(1):67, 2014.
- [32] Jonathan Squire and Amitava Bhattacharjee. Coherent nonhelical shear dynamos driven by magnetic fluctuations at low reynolds numbers. *The Astrophysical Journal*, 813(1):52, 2015.
- [33] Alexandros Alexakis. Searching for the fastest dynamo: Laminar abc flows. *Physical Review E*, 84(2):026321, 2011.
- [34] Wikipedia contributors. Direct numerical simulation — Wikipedia, the free encyclopedia, 2018. [Online; accessed 28-December-2018].
- [35] David A Kopriva. *Implementing spectral methods for partial differential equations: Algorithms for scientists and engineers*. Springer Science & Business Media, 2009.
- [36] Rupak Mukherjee, Rajaraman Ganesh, Vinod Saini, Udaya Maurya, Nagavijayalakshmi Vydyanathan, and Bharatkumar Sharma. Three dimensional pseudo-spectral compressible magnetohydrodynamic gpu code for astrophysical plasma simulation. *Conference Proceedings of 25th IEEE International Conference on High Performance Computing Workshops*, 2018.
- [37] Wikipedia contributors. Openmp — Wikipedia, the free encyclopedia, 2018. [Online; accessed 28-December-2018].
- [38] Unified memory programming, cuda programming guide. <http://docs.nvidia.com/cuda/cuda-c-programming-guide/index.html>. [Online].



- [39] Wikipedia contributors. Graphics processing unit — Wikipedia, the free encyclopedia, 2018. [Online; accessed 28-December-2018].
- [40] Lodewijk Woltjer. A theorem on force-free magnetic fields. *Proceedings of the National Academy of Sciences*, 44(6):489–491, 1958.
- [41] J Brian Taylor. Relaxation of toroidal plasma and generation of reverse magnetic fields. *Physical Review Letters*, 33(19):1139, 1974.
- [42] JBJ Taylor. Relaxation and magnetic reconnection in plasmas. *Reviews of Modern Physics*, 58(3):741, 1986.
- [43] Hong Qin, Wandong Liu, Hong Li, and Jonathan Squire. Woltjer-taylor state without taylor’s conjecture: Plasma relaxation at all wavelengths. *Physical review letters*, 109(23):235001, 2012.
- [44] SR Hudson, RL Dewar, G Dennis, MJ Hole, M McGann, G Von Nessi, and S Lazerson. Computation of multi-region relaxed magnetohydrodynamic equilibria. *Physics of Plasmas*, 19(11):112502, 2012.
- [45] Rupak Mukherjee and Rajaraman Ganesh. Numerical relaxation of a 3d mhd taylor-woltjer state subject to abrupt expansion. *Conference Proceedings of 27th IAEA Fusion Energy Conference*, page 476, 2018.
- [46] H Hotta, M Rempel, and T Yokoyama. Large-scale magnetic fields at high reynolds numbers in magnetohydrodynamic simulations. *Science*, 351(6280):1427–1430, 2016.
- [47] Anatole Katok and Boris Hasselblatt. *Introduction to the modern theory of dynamical systems*, volume 54. Cambridge university press, 1997.
- [48] Elgar Steve, Freilich M. H., and Guza R. T. Recurrence in truncated boussinesq models for nonlinear waves in shallow water. *Journal of Geophysical Research: Oceans*, 95(C7):11547, 1990.

- [49] Peter J Bryant. Cyclic recurrence in nonlinear unidirectional ocean waves. *Journal of Fluid Mechanics*, 192:329–337, 1988.
- [50] Divakar Viswanath. Recurrent motions within plane couette turbulence. *Journal of Fluid Mechanics*, 580:339–358, 2007.
- [51] John M Finn and Edward Ott. Chaotic flows and fast magnetic dynamos. *The Physics of fluids*, 31(10):2992–3011, 1988.
- [52] John M Finn and Edward Ott. Chaotic flows and magnetic dynamos. *Physical review letters*, 60(9):760, 1988.
- [53] Edward Ott. Chaotic flows and kinematic magnetic dynamos: A tutorial review. *Physics of Plasmas*, 5(5):1636–1646, 1998.
- [54] Andrey Nikolaevich Kolmogorov. The local structure of turbulence in incompressible viscous fluid for very large reynolds numbers. *Dokl. Akad. Nauk SSSR*, 30(4):299–303, 1941.
- [55] Rupak Mukherjee and Rajaraman Ganesh. Study of dynamo action in three dimensional magnetohydrodynamic plasma with arnold-beltrami-childress flow. *arXiv preprint arXiv:1901.09610*, 2019.
- [56] Akanksha Gupta. *Shear Flows in 2D Strongly Coupled Fluids - A Theoretical and Computational Study*. PhD thesis, Institute for Plasma Research, Homi Bhabha National Institute, 2017.
- [57] Rony Keppens, G Tóth, RHJ Westermann, and JP Goedbloed. Growth and saturation of the kelvin–helmholtz instability with parallel and antiparallel magnetic fields. *Journal of Plasma Physics*, 61(1):1–19, 1999.
- [58] D Galloway and Uriel Frisch. Dynamo action in a family of flows with chaotic streamlines. *Geophysical & Astrophysical Fluid Dynamics*, 36(1):53–83, 1986.

- [59] Ravi Samtaney, Dale I Pullin, and Branko Kosović. Direct numerical simulation of decaying compressible turbulence and shocklet statistics. *Physics of Fluids*, 13(5):1415–1430, 2001.
- [60] Patrick H Diamond, Uriel Frisch, and Yves Pomeau. Editorial introduction to the special issue “plasma physics in the 20th century as told by players”, 2018.
- [61] Russell M Kulsrud. *Plasma physics for astrophysics*. Princeton University Press, 2005.
- [62] Megh Nad Saha. Liii. ionization in the solar chromosphere. *The London, Edinburgh, and Dublin Philosophical Magazine and Journal of Science*, 40(238):472–488, 1920.
- [63] Meghnad N Saha. On a physical theory of stellar spectra. *Proc. R. Soc. Lond. A*, 99(697):135–153, 1921.
- [64] Ronald C Davidson. *Physics of nonneutral plasmas*. World Scientific Publishing Company, 2001.
- [65] Francis F Chen. *Introduction to plasma physics*. Springer Science & Business Media, 2012.
- [66] Bishwanath Chakraborty. *Principles of plasma mechanics*. New Age International, 2007.
- [67] Nicholas A Krall and Alvin W Trivelpiece. Principles of plasma physics. *American Journal of Physics*, 41(12):1380–1381, 1973.
- [68] Arnab Rai Choudhuri. *Nature’s third cycle: a story of sunspots*. OUP Oxford, 2015.
- [69] Uriel Frisch. *Turbulence: the legacy of AN Kolmogorov*. Cambridge university press, 1995.

- [70] A Thyagaraja. Recurrent motions in certain continuum dynamical systems. *The Physics of Fluids*, 22(11):2093–2096, 1979.
- [71] George David Birkhoff. *Dynamical systems*. American mathematical society, 1960.
- [72] Wikipedia contributors. Message passing interface — Wikipedia, the free encyclopedia, 2018. [Online; accessed 28-December-2018].
- [73] Matteo Frigo and Steven G. Johnson. The design and implementation of FFTW3. *Proceedings of the IEEE*, 93(2):216–231, 2005. Special issue on “Program Generation, Optimization, and Platform Adaptation”.
- [74] Nvidia cuda fft library. <https://developer.nvidia.com/cufft>. [Online].
- [75] Openacc. <https://www.openacc.org/>. [Online].
- [76] Amir Gholami, Judith Hill, Dhairya Malhotra, and George Biros. Accfft: A library for distributed-memory fft on cpu and gpu architectures. *arXiv preprint arXiv:1506.07933*, 2015.
- [77] Enrico Fermi, P Pasta, S Ulam, and M Tsingou. Studies of the nonlinear problems. Technical report, Los Alamos Scientific Lab., N. Mex., 1955.
- [78] Thierry Dauxois. Fermi, pasta, ulam and a mysterious lady. *arXiv preprint arXiv:0801.1590*, 2008.
- [79] Norman J Zabusky and Martin D Kruskal. Interaction of" solitons" in a collisionless plasma and the recurrence of initial states. *Physical review letters*, 15(6):240, 1965.
- [80] Henry C Yuen and Warren E Ferguson Jr. Fermi–pasta–ulam recurrence in the two-space dimensional nonlinear schrödinger equation. *The Physics of Fluids*, 21(11):2116–2118, 1978.

- [81] A Thyagaraja. Recurrence, dimensionality, and lagrange stability of solutions of the nonlinear schrödinger equation. *The Physics of Fluids*, 24(11):1973–1975, 1981.
- [82] David Galloway and Uriel Frisch. A numerical investigation of magnetic field generation in a flow with chaotic streamlines. *Geophysical & Astrophysical Fluid Dynamics*, 29(1-4):13–18, 1984.
- [83] PG Drazin. Discontinuous velocity profiles for the orr-sommerfeld equation. *Journal of Fluid Mechanics*, 10(4):571–583, 1961.
- [84] Thomas P Ray. The effects of a simple shear layer on the growth of kelvin–helmholtz instabilities. *Monthly Notices of the Royal Astronomical Society*, 198(3):617–625, 1982.
- [85] Rupak Mukherjee, Akanksha Gupta, and Rajaraman Ganesh. Compressibility effects on quasistationary vortex and transient hole patterns through vortex merger. *arXiv preprint arXiv:1802.03240*, 2018.
- [86] Rupak Mukherjee, Akanksha Gupta, and Rajaraman Ganesh. Compressibility effects on quasistationary vortex and transient hole patterns through vortex merger. *Physica Scripta*, 94(11):115005, 2019.
- [87] Mira Sadek, Alexandros Alexakis, and Stephan Fauve. Optimal length scale for a turbulent dynamo. *Physical review letters*, 116(7):074501, 2016.
- [88] Yan Yang, Minping Wan, Yipeng Shi, Kun Yang, and Shiyi Chen. A hybrid scheme for compressible magnetohydrodynamic turbulence. *Journal of Computational Physics*, 306:73–91, 2016.
- [89] Hong Qin, Shuangxi Zhang, Jianyuan Xiao, Jian Liu, Yajuan Sun, and William M Tang. Why is boris algorithm so good? *Physics of Plasmas*, 20(8):084503, 2013.

- [90] Tesla-p100-nvidia. <https://www.nvidia.com/en-us/data-center/tesla-p100/>. [Online].
- [91] Openacc programming and best practices guide. <https://www.openacc.org/>, June 2015. [Online].
- [92] The openacc application programming interface, version 2.6. <https://www.openacc.org/>, November 2017. [Online].
- [93] Mahendra K Verma. Statistical theory of magnetohydrodynamic turbulence: recent results. *Physics Reports*, 401(5-6):229–380, 2004.
- [94] PJ Morrison. Hamiltonian fluid dynamics. *Encyclopedia of mathematical physics*, pages 593–600, 2006.
- [95] BJ Bayly, CD Levermore, and T Passot. Density variations in weakly compressible flows. *Physics of Fluids A: Fluid Dynamics*, 4(5):945–954, 1992.
- [96] Daiki Terakado and Yuji Hattori. Density distribution in two-dimensional weakly compressible turbulence. *Physics of Fluids*, 26(8):085105, 2014.
- [97] MG Olsson. Why does a mass on a spring sometimes misbehave? *American Journal of Physics*, 44(12):1211–1212, 1976.
- [98] Thomas E Cayton. The laboratory spring–mass oscillator: an example of parametric instability. *American Journal of Physics*, 45(8):723–732, 1977.
- [99] HM Lai. On the recurrence phenomenon of a resonant spring pendulum. *American Journal of Physics*, 52(3):219–223, 1984.
- [100] Lars Falk. Recurrence effects in the parametric spring pendulum. *American Journal of Physics*, 46(11):1120–1123, 1978.
- [101] Lars Falk. Student experiments on parametric resonance. *American Journal of Physics*, 47(4):325–328, 1979.

- [102] Boris V Chirikov. A universal instability of many-dimensional oscillator systems. *Physics Reports*, 52(5):263 – 379, 1979.
- [103] LD Landau and EM Lifshitz. Fluid mechanics (chap. iii). *Course of Theoretical Physics, Pergamon Press, London*, 6, 1959.
- [104] A Thyagaraja. *Nonlinear Waves, Chapter 17*. CUP Archive, 1983.
- [105] T Hogg and BA Huberman. Recurrence phenomena in quantum dynamics. *Physical Review Letters*, 48(11):711, 1982.
- [106] T Tajima, Martin V Goldman, JN Leboeuf, and JM Dawson. Breakup and reconstitution of langmuir wave packets. *The Physics of Fluids*, 24(1):182–183, 1981.
- [107] Predhiman Krishan Kaw, AT Lin, and JM Dawson. Quasiresonant mode coupling of electron plasma waves. *The Physics of Fluids*, 16(11):1967–1975, 1973.
- [108] Rupak Mukherjee, Rajaraman Ganesh, and Abhijit Sen. Recurrence in three dimensional magnetohydrodynamic plasma. *Physics of Plasmas*, 26(2):022101, 2019.
- [109] P. Ramachandran and G. Varoquaux. Mayavi: 3D Visualization of Scientific Data. *Computing in Science & Engineering*, 13(2):40–51, 2011.
- [110] Abhijit Sen, Dilip P Ahalpara, Anantanarayanan Thyagaraja, and Govind S Krishnaswami. A kdv-like advection–dispersion equation with some remarkable properties. *Communications in Nonlinear Science and Numerical Simulation*, 17(11):4115–4124, 2012.
- [111] A Thyagaraja. Conservative regularization of ideal hydrodynamics and magnetohydrodynamics. *Physics of Plasmas*, 17(3):032503, 2010.

- [112] A Thyagaraja. Adjoint variational principles for regularised conservative systems. In *AIP Conference Proceedings*, volume 1582, pages 107–115. AIP, 2014.
- [113] Govind S Krishnaswami, Sonakshi Sachdev, and Anantanarayanan Thyagaraja. Local conservative regularizations of compressible magnetohydrodynamic and neutral flows. *Physics of Plasmas*, 23(2):022308, 2016.
- [114] Govind S Krishnaswami, Sonakshi Sachdev, and Anantanarayanan Thyagaraja. Conservative regularization of compressible dissipationless two-fluid plasmas. *Physics of Plasmas*, 25(2):022306, 2018.
- [115] Ia B Zeldovich, Aleksandr Andreevich Ruzmaikin, and Dmitriy Dmitrievič Sokolov. Magnetic fields in astrophysics. In *New York, Gordon and Breach Science Publishers (The Fluid Mechanics of Astrophysics and Geophysics. Volume 3), 1983, 381 p. Translation.*, volume 3, 1983.
- [116] Henry K Moffatt. Field generation in electrically conducting fluids. *Cambridge University Press, Cambridge, London, New York, Melbourne*, 1978.
- [117] Agris Gailitis, Olgerts Lielausis, Ernests Platacis, Sergej Dement’ev, Arnis Cifersons, Gunter Gerbeth, Thomas Gundrum, Frank Stefani, Michael Christen, and Gotthard Will. Magnetic field saturation in the riga dynamo experiment. *Physical Review Letters*, 86(14):3024, 2001.
- [118] Robert Stieglitz and Ulrich Müller. Experimental demonstration of a homogeneous two-scale dynamo. *Physics of Fluids*, 13(3):561–564, 2001.
- [119] Romain Monchaux, Michaël Berhanu, Mickaël Bourgoïn, Marc Moulin, Ph Odier, J-F Pinton, Romain Volk, Stéphan Fauve, Nicolas Mordant, François Pétrélis, et al. Generation of a magnetic field by dynamo action in a turbulent flow of liquid sodium. *Physical review letters*, 98(4):044502, 2007.



- [120] Florent Ravelet, Michaël Berhanu, Romain Monchaux, Sébastien Aumaître, Arnaud Chiffaudel, François Daviaud, Bérengère Dubrulle, Mickaël Bourgoin, Ph Odier, N Plihon, et al. Chaotic dynamos generated by a turbulent flow of liquid sodium. *Physical review letters*, 101(7):074502, 2008.
- [121] P Tzeferacos, A Rigby, AFA Bott, AR Bell, R Bingham, A Casner, F Cattaneo, EM Churazov, J Emig, F Fiuza, et al. Laboratory evidence of dynamo amplification of magnetic fields in a turbulent plasma. *Nature communications*, 9(1):591, 2018.
- [122] RVE Lovelace, MM Romanova, and WI Newman. Implosive accretion and outbursts of active galactic nuclei. *The Astrophysical Journal*, 437:136–143, 1994.
- [123] MA Latif, DRG Schleicher, W Schmidt, and J Niemeyer. The small-scale dynamo and the amplification of magnetic fields in massive primordial haloes. *Monthly Notices of the Royal Astronomical Society*, 432(1):668–678, 2013.
- [124] Amit Seta, Pallavi Bhat, and Kandaswamy Subramanian. Saturation of zeldovich stretch–twist–fold map dynamos. *Journal of Plasma Physics*, 81(5), 2015.
- [125] Rohit Kumar, Mahendra K Verma, and Ravi Samtaney. Energy transfers and magnetic energy growth in small-scale dynamo. *EPL (Europhysics Letters)*, 104(5):54001, 2014.
- [126] Denis A St-Onge and Matthew W Kunz. Small-scale turbulent dynamo in a collisionless, weakly magnetized plasma. *arXiv preprint arXiv:1806.11162*, 2018.
- [127] Thomas George Cowling. The magnetic field of sunspots. *Monthly Notices of the Royal Astronomical Society*, 94:39–48, 1933.

- [128] Axel Brandenburg, Dmitry Sokoloff, and Kandaswamy Subramanian. Current status of turbulent dynamo theory. *Space Science Reviews*, 169(1-4):123–157, 2012.
- [129] Ismaël Bouya and Emmanuel Dormy. Revisiting the abc flow dynamo. *Physics of Fluids*, 25(3):037103, 2013.
- [130] Mira Sadek, Alexandros Alexakis, and Stephan Fauve. Optimal length scale for a turbulent dynamo. *Physical review letters*, 116(7):074501, 2016.
- [131] Samuel I Vainshtein, Roald Z Sagdeev, Robert Rosner, and Eun-Jin Kim. Fractal properties of the stretch-twist-fold magnetic dynamo. *Physical Review E*, 53(5):4729, 1996.
- [132] Samuel I Vainshtein, Roald Z Sagdeev, and Robert Rosner. Stretch-twist-fold and abc nonlinear dynamos: restricted chaos. *Physical Review E*, 56(2):1605, 1997.
- [133] Eugene Newman Parker. Cosmical magnetic fields: Their origin and their activity. *Oxford, Clarendon Press; New York, Oxford University Press, 1979, 858 p.*, 1979.
- [134] François Pétrélis, Stéphan Fauve, Emmanuel Dormy, and Jean-Pierre Valet. Simple mechanism for reversals of earth’s magnetic field. *Physical review letters*, 102(14):144503, 2009.
- [135] Andrii Neronov and Ievgen Vovk. Evidence for strong extragalactic magnetic fields from fermi observations of tev blazars. *Science*, 328(5974):73–75, 2010.
- [136] Charles D Dermer, Massimo Cavadini, Soebur Razzaque, Justin D Finke, James Chiang, and Benoit Lott. Time delay of cascade radiation for tev blazars and the measurement of the intergalactic magnetic field. *The Astrophysical Journal Letters*, 733(2):L21, 2011.

- [137] Axel Brandenburg, Kari Enqvist, and Poul Olesen. Large-scale magnetic fields from hydromagnetic turbulence in the very early universe. *Physical Review D*, 54(2):1291, 1996.
- [138] Dieter Biskamp and Wolf-Christian Müller. Decay laws for three-dimensional magnetohydrodynamic turbulence. *Physical Review Letters*, 83(11):2195, 1999.
- [139] George B Field and Sean M Carroll. Cosmological magnetic fields from primordial helicity. *Physical Review D*, 62(10):103008, 2000.
- [140] Tina Kahniashvili, Alexander G Tevzadze, Axel Brandenburg, and Andrii Neronov. Evolution of primordial magnetic fields from phase transitions. *Physical Review D*, 87(8):083007, 2013.
- [141] Axel Brandenburg, Tina Kahniashvili, Sayan Mandal, Alberto Roper Pol, Alexander G Tevzadze, and Tanmay Vachaspati. Evolution of hydromagnetic turbulence from the electroweak phase transition. *Physical Review D*, 96(12):123528, 2017.
- [142] Axel Brandenburg, Tina Kahniashvili, and Alexander G Tevzadze. Nonhelical inverse transfer of a decaying turbulent magnetic field. *Physical review letters*, 114(7):075001, 2015.
- [143] Jonathan Zrake. Inverse cascade of nonhelical magnetic turbulence in a relativistic fluid. *The Astrophysical Journal Letters*, 794(2):L26, 2014.
- [144] David Galloway. Abc flows then and now. *Geophysical & Astrophysical Fluid Dynamics*, 106(4-5):450–467, 2012.
- [145] SI Vainshtein and Ya B Zel'Dovich. Reviews of topical problems: Origin of magnetic fields in astrophysics (turbulent" dynamo" mechanisms). *Soviet Physics Uspekhi*, 15:159–172, 1972.

- [146] Isaac Klapper and Lai-Sang Young. Rigorous bounds on the fast dynamo growth rate involving topological entropy. *Communications in mathematical physics*, 173(3):623–646, 1995.
- [147] Yu B Ponomarenko. Theory of the hydromagnetic generator. *Journal of Applied Mechanics and Technical Physics*, 14(6):775–778, 1973.
- [148] Gareth O Roberts. Spatially periodic dynamos. *Phil. Trans. R. Soc. Lond. A*, 266(1179):535–558, 1970.
- [149] Paul Harry Roberts. Kinematic dynamo models. *Phil. Trans. R. Soc. Lond. A*, 272(1230):663–698, 1972.
- [150] Vladimir Igorevich ARNOLD. Sur la topologie des écoulements stationnaires des fluides parfaits. *CR Acad. Sci Paris A*, 261:17–20, 1965.
- [151] E Beltrami. E. beltrami, opera matematiche 4, 304 (1889). *Opera Matematiche*, 4:304, 1889.
- [152] Stephen Childress. New solutions of the kinematic dynamo problem. *Journal of Mathematical Physics*, 11(10):3063–3076, 1970.
- [153] Yannick Ponty, Pablo D Mininni, Jean-Philippe Laval, Alexandros Alexakis, Julien Baerenzung, François Daviaud, Bérengère Dubrulle, Jean-François Pinton, Hélène Politano, and Annick Pouquet. Linear and non-linear features of the taylor–green dynamo. *Comptes Rendus Physique*, 9(7):749–756, 2008.
- [154] Alice Courvoisier, Andrew D Gilbert, and Yannick Ponty. Dynamo action in flows with cat’s eyes. *Geophysical and Astrophysical Fluid Dynamics*, 99(5):413–429, 2005.
- [155] Vasilis Archontis, Søren Bertil Fabricius Dorch, and Åke Nordlund. Non-linear mhd dynamo operating at equipartition. *Astronomy & Astrophysics*, 472(3):715–726, 2007.

- [156] Olga M Podvigina. Spatially-periodic steady solutions to the three-dimensional navier–stokes equation with the abc-force. *Physica D: Nonlinear Phenomena*, 128(2-4):250–272, 1999.
- [157] Xiao-Hua Zhao, Keng-Huat Kwek, Ji-Bin Li, and Ke-Lei Huang. Chaotic and resonant streamlines in the abc flow. *SIAM Journal on Applied Mathematics*, 53(1):71–77, 1993.
- [158] Viktor Kuz'mich Mel'nikov. On the stability of a center for time-periodic perturbations. *Trudy moskovskogo matematicheskogo obshchestva*, 12:3–52, 1963.
- [159] De-Bin Huang, Xiao-Hua Zhao, and Hui-Hui Dai. Invariant tori and chaotic streamlines in the abc flow. *Physics Letters A*, 237(3):136–140, 1998.
- [160] Sergei L'vovich Ziglin. An analytic proof of the nonintegrability of the abc-flow for  $a = b = c$ . *Functional Analysis and Its Applications*, 37(3):225–227, 2003.
- [161] Andrzej J Maciejewski and Maria Przybylska. Non-integrability of abc flow. *Physics Letters A*, 303(4):265–272, 2002.
- [162] Jaume Llibre and Clàudia Valls. A note on the first integrals of the abc system. *Journal of Mathematical Physics*, 53(2):023505, 2012.
- [163] Sergei L'vovich Ziglin. The abc-flow is not integrable for  $a = b$ . *Functional Analysis and Its Applications*, 30(2):137–138, 1996.
- [164] SL Ziglin. On the absence of a real-analytic first integral for abc flow when  $a = b$ . *Chaos: An Interdisciplinary Journal of Nonlinear Science*, 8(1):272–273, 1998.

- [165] NH Brummell, F Cattaneo, and SM Tobias. Linear and nonlinear dynamo properties of time-dependent abc flows. *Fluid Dynamics Research*, 28(4):237–265, 2001.
- [166] AA Didov and M Yu Uleysky. Nonlinear resonances in the abc-flow. *Chaos: An Interdisciplinary Journal of Nonlinear Science*, 28(1):013123, 2018.
- [167] AA Didov and M Yu Uleysky. Analysis of stationary points and their bifurcations in the abc-flow. *Applied Mathematics and Computation*, 330:56–64, 2018.
- [168] Henry K Moffatt and Michael RE Proctor. Topological constraints associated with fast dynamo action. *Journal of Fluid Mechanics*, 154:493–507, 1985.
- [169] Samuel E Jones and Andrew D Gilbert. Dynamo action in the abc flows using symmetries. *Geophysical & Astrophysical Fluid Dynamics*, 108(1):83–116, 2014.
- [170] Sergey V Ershkov. About existence of stationary points for the arnold-beltrami-childress (abc) flow. *arXiv preprint arXiv:1512.04367*, 2015.
- [171] Thierry Dombre, Uriel Frisch, John M Greene, Michel Hénon, A Mehr, and Andrew M Soward. Chaotic streamlines in the abc flows. *Journal of Fluid Mechanics*, 167:353–391, 1986.
- [172] VI Arnol’d, Ya B Zel’dovich, AA Ruzmalkin, and DD Sokolov. A magnetic field in riemannian space. *Zh. Eksp. Teor. Fiz*, 81:2052–2058, 1981.
- [173] Vladimir Igorevich Arnol’d. On the evolution of a magnetic field under the action of transport and diffusion. *Amer. Math. Soc. Transl*, 137(2):119–129, 1987.
- [174] D Galloway and Uriel Frisch. A note on the stability of a family of space-periodic beltrami flows. *Journal of Fluid Mechanics*, 180:557–564, 1987.

- [175] David J Galloway and Michael RE Proctor. Numerical calculations of fast dynamos in smooth velocity fields with realistic diffusion. *Nature*, 356(6371):691, 1992.
- [176] Misha Mikhail Vishik. Magnetic field generation by the motion of a highly conducting fluid. *Geophysical & Astrophysical Fluid Dynamics*, 48(1-3):151–167, 1989.
- [177] Yun-Tung Lau and John M Finn. Fast dynamos with finite resistivity in steady flows with stagnation points. *Physics of Fluids B: Plasma Physics*, 5(2):365–375, 1993.
- [178] Søren Bertil Fabricius Dorch. On the structure of the magnetic field in a kinematic abc flow dynamo. *Physica Scripta*, 61(6):717, 2000.
- [179] Andrew D Gilbert. Magnetic field evolution in steady chaotic flows. *Phil. Trans. R. Soc. Lond. A*, 339(1655):627–656, 1992.
- [180] Ismaël Bouya and Emmanuel Dormy. Toward an asymptotic behaviour of the abc dynamo. *EPL (Europhysics Letters)*, 110(1):14003, 2015.
- [181] Barak Galanti, Pierre-Louis Sulem, and Annick Pouquet. Linear and non-linear dynamos associated with abc flows. *Geophysical & Astrophysical Fluid Dynamics*, 66(1-4):183–208, 1992.
- [182] Stephen Childress and Andrew D Gilbert. *Stretch, twist, fold: the fast dynamo*, volume 37. Springer Science & Business Media, 2008.
- [183] Axel Brandenburg and Kandaswamy Subramanian. Astrophysical magnetic fields and nonlinear dynamo theory. *Physics Reports*, 417(1-4):1–209, 2005.
- [184] JB Taylor. Turbulent cascades and the alpha dynamo. *arXiv preprint arXiv:1210.3714*, 2012.

- [185] Alexandre Cameron and Alexandros Alexakis. Fate of alpha dynamos at large  $r$  m. *Physical review letters*, 117(20):205101, 2016.
- [186] Axel Brandenburg. The inverse cascade and nonlinear alpha-effect in simulations of isotropic helical hydromagnetic turbulence. *The Astrophysical Journal*, 550(2):824, 2001.
- [187] Max Steenbeck, F Krause, and K-H Rädler. Berechnung der mittleren lorentzfeldstärke für ein elektrisch leitendes medium in turbulenter, durch corioliskräfte beeinflusster bewegung. *Zeitschrift für Naturforschung A*, 21(4):369–376, 1966.
- [188] Fritz Krause and K-H Rädler. *Mean-field magnetohydrodynamics and dynamo theory*. Elsevier, 2016.
- [189] PD Mininni. Inverse cascades and  $\alpha$  effect at a low magnetic prandtl number. *Physical Review E*, 76(2):026316, 2007.
- [190] Pablo D Mininni, Yannick Ponty, David C Montgomery, Jean-Francois Pinton, Helene Politano, and Annick Pouquet. Dynamo regimes with a nonhelical forcing. *The Astrophysical Journal*, 626(2):853, 2005.
- [191] Y Ponty, A Pouquet, and PL Sulem. Dynamos in weakly chaotic two-dimensional flows. *Geophysical & Astrophysical Fluid Dynamics*, 79(1-4):239–257, 1995.
- [192] Vasilis Archontis, Søren Bertil Fabricius Dorch, and Åke Nordlund. Numerical simulations of kinematic dynamo action. *Astronomy & Astrophysics*, 397(2):393–399, 2003.
- [193] Peter Frick, Rodion Stepanov, and Dmitry Sokoloff. Large-and small-scale interactions and quenching in an  $\alpha$  2-dynamo. *Physical Review E*, 74(6):066310, 2006.



- [194] Vladimir Igorevich Arnold and Elena I Korkina. The growth of a magnetic field in the three-dimensional steady flow of an incompressible fluid. *Moskovskii Universitet Vestnik Serii Matematika Mekhanika*, pages 43–46, 1983.
- [195] Yannick Ponty, PD Mininni, DC Montgomery, J-F Pinton, Hélène Politano, and Annick Pouquet. Numerical study of dynamo action at low magnetic prandtl numbers. *Physical Review Letters*, 94(16):164502, 2005.
- [196] Alexander A Schekochihin, NEL Haugen, A Brandenburg, SC Cowley, JL Maron, and JC McWilliams. The onset of a small-scale turbulent dynamo at low magnetic prandtl numbers. *The Astrophysical Journal Letters*, 625(2):L115, 2005.
- [197] AB Iskakov, AA Schekochihin, SC Cowley, JC McWilliams, and MRE Proctor. Numerical demonstration of fluctuation dynamo at low magnetic prandtl numbers. *Physical review letters*, 98(20):208501, 2007.

*‘At this time of my parting, wish me good luck, my friends! The sky is flushed with  
the dawn and my path lies beautiful.*

*Ask not what I have with me to take there. I start on my journey with empty hands  
and expectant heart.*

*I shall put on my wedding garland. Mine is not the red-brown dress of the  
traveller, and though there are dangers on the way I have no fear in my mind.*

*The evening star will come out when my voyage is done and the plaintive notes of  
the twilight melodies be struck up from the King’s gateway.’*

*- Song Offerings (Gitanjali), Rabindranath Tagore.*